Climatic and tectonic controls on deep water sedimentary cyclicity : evidence from the Miocene to Pleistocene of Cyprus

Thesis

Climatic and tectonic controls on deep water sedimentary cyclicity; evidence from the Miocene to Pleistocene of Cyprus

A thesis submitted for the degree of

Doctor of Philosophy

by

Quintin James Davies
BSc (Hon) (Leicester)
MSc (Reading)

Department of Earth Sciences,
The Open University
2001

Abstract

Traditionally, sedimentation at active plate margins is thought to be dominantly controlled by tectonism, with any climatic cyclicity being overprinted. Since the early Miocene, Cyprus has been situated above an active subduction zone, which has strongly influenced the regional tectonics. Global climate change also occurred during the Miocene marking a transition from relative global warmth of the early-Miocene to the Neogene 'icehouse world'. Cyprus has extensive outcrops of Miocene to Pleistocene deep water sediments and provides an ideal setting to test the magnitude of climatic signals in tectonically active areas, and thus deduce the relative roles of climate and tectonics on sedimentation.

Detailed sedimentary logging and biostratigraphical dating of the Miocene-age pelagic Pakhna Formation reveals that the formation can be divided into depositional sequences, bounded by hardgrounds or erosion surfaces, and contains a distinct pattern of marl-chalk couplets. These sequences correlate, within the constraints of biostratigraphy to European and New Jersey Margin sequence chronostratigraphy. Three smaller scales of cyclicity are identified by stratigraphic time series analysis, and are likely to correspond to the 100 kyr, 41ky and ~20 ky Milankovitch cycles. Stable oxygen and carbon isotope analysis on pelagic foraminifera indicate the following climatic influences; (1) chalk-marl couplets probably record climatically controlled supply of terrigenous material; (2) a strong link between $\delta^{18}O$ maxima and sequence boundaries; and (3) the globally recognised $\delta^{13}C$ Monterey Excursion is present. The increasing abundance of tectonically derived Troodos material partially masks the climatically controlled sedimentation in the Pakhna Formation south of the Troodos massif.

Rapid Troodos uplift during the Pliocene-Pleistocene is demonstrated by the high abundance of ophiolite derived clasts in the Khirokitia-Psematismenos submarine fan-complex. Here,

graphic logging, and biostratigraphy suggests that the six cycles observed are likely to correlate to cycles identified in European sequence chronostratigraphy, though higher-frequency, climatic cyclicity is obscured by the overprint of tectonic activity.

Acknowledgements

Well here we are then, writing the acknowledgement, a sure sign that this Ph.D. malarkey is surely drawing to an end. It has been an interesting time, the Open University is a great place to conduct research in and very friendly, relaxed environment. Of course like all thesis there are many people to thank. So here goes....

I have to say a fantastic thank you to my supervisors Dr Angela Coe (OU) and Dr Howard Armstrong (Durham University) for all their patience, technical and moral support over the three and half years. Howard, I will remember you for your squeaky cheese and honey coated almond escapades while sitting at Kottaphi Hill and no I never want to see another calcareous nannoplankton again! Angela you have been a start, and well, I am just glad I found you note book.

I thank Professors Chris Wilson and Alastair Robertson who reviewed this NERC funded thesis and for our interesting discussions during my viva.

For helping me through the dark art of Time Series Analysis I thank Graham Weedon at Luton University, and Baruch Spiro and support staff at NIGL for assistance running the isotope analysis.

For field work assistance, and saving my sanity while in Cyprus I thank Steve Wills, Haggis, Ed, and Liz, for really making the trip far more enjoyable. I also thank Chris and Maria, my landlords in Cyprus for there friendliness, providing me with bizarre fruits, putting up with late night vodka drinking sessions, and reassuring me after escaping from the local fauna and military. Oh nearly forgot, thanks Stavros (the local taverna owner) for entertaining and supplying me with freebies while along in Cyprus.

As for life in Milton Keynes and at the OU, there are many folk I have encountered that need to be thanked. For being housemates at No.26, I could not go wrong with Gavin, Tubbs, Bruce, Lee, Chuck, Severine and Rob for times in the pub, late nights and getting me out of bed in the morning! As office buddies Lisa, Alison, Christophe, Marc and Stephen all proved to be good procrastination mates, and put up with my ranting (you know you liked it really!). As for the other friends I made in MK, thank you for being contemporaries and making life bearable in the land of concrete cows.

Well Mum, Dad and Julian, here is the bit where I thank you for you financial and moral support, through what had been a variable and indeed sometimes emotional 3 years or so, Cheers, you have been ace.

Contents

List of Figures

List of Tables

Table No. **Page**

Chapter 1

Introduction

1.1 Introduction

The island of Cyprus is the third largest island (9250 km^2) in the Mediterranean, and is situated 97 km west of Syria and 64 km south of Turkey. Anthropologically Cyprus has been populated since the Neolithic age (7000-3900 BC), and mainly due to its strategic position has had a turbulent history of invasion and conquest, which unfortunately continues to the present day. The principal topographic features of the island include the Troodos Mountains in the centre and the Kyrenia Range to the north. Mount Olympus in the Troodos Mountains rises to 1,952 meters, and forms the highest point on the island. Geologically, Cyprus is presently situated 25 km north of an active northward dipping subduction zone that marks the boundary of the African plate. The island is composed of three basement terranes (Troodos Ophiolite, Mamonia Complex and the Kyrenia Range) that were juxtaposed during tectonic events in the Late Cretaceous and Late Eocene. The summit of Mount Olympus is composed of rocks derived from the Earth's mantle, which testifies to the dramatic uplift Cyprus has experienced since the generation of the Ophiolite some ~90 million years ago. This thesis concentrates on cyclic sedimentation developed in the Miocene- to Pleistocene-aged sediments that form part of the cover succession of the Troodos Ophiolite.

1.2 Thesis Aims

This thesis has two main aims; firstly to investigate the nature of cyclicity developed in Miocene- to Pleistocene-age sediments, deposited on top of the Troodos Ophiolite, in order to assess the relative role of climate and tectonics on sedimentary deposition in Cyprus. Secondly, as the Miocene is a period of major climate change to investigate if this signal is present in a mid-latitude setting.

In order to establish the relative importance of tectonic and climatic controls on sedimentation this multidisciplinary study encompasses a variety of sedimentological and analytical techniques, which include detailed graphic logging, biostratigraphy, sequence stratigraphy, time series analysis and stable oxygen and carbon isotope analysis. The project aims to show how and when cycle development is climatically influenced, compared to periods and features controlled by tectonics associated with the uplift of the Troodos Ophiolite. Several sections of Miocene-aged, deep-water carbonates and Plio-Pleistocene-aged submarine-fan deposits are used to compare the influences on sedimentation in different depositional environments, at different periods in the geological evolution of Cyprus.

By acquiring the stable carbon and oxygen isotope record of the Miocene in Cyprus the project aims to deduce the relationship between the mid-Miocene climate transition and pelagic carbonate sedimentation, while gaining an insight to the inter-relationships between oceanographic state, the biosphere and climate.

This chapter provides a synopsis to the geological history of Cyprus. It also discusses the terminology and background knowledge to the techniques and issues addressed in this thesis.

1.3 A geological synopsis of the Troodos Ophiolite and adjacent units, Cyprus.

Cyprus has been an area of great interest to the geologist. The island's diverse and sometimes unique geology has provided geologists a field in which to test working hypotheses, particularly those concerning ophiolite genesis. The Troodos Ophiolite was the first attributed to be a fragment of oceanic crust by Ian Gass in 1968 (Robertson and Xenophontos, 1993). This finding triggered a phase of extensive investigation to determine the ophiolite's emplacement and genesis.

1.3.1 Basement terranes

Cyprus is sub-divided into three tectonic units that were juxtaposed during the northward migration of the African Plate. Firstly, and most famously, the Troodos ophiolite tectonic unit comprises a relatively undeformed ophiolite succession (deep-sea sediments, pillow lavas, sheeted dykes, gabbro, and ultramafic rocks). This complex was subsequently uplifted to expose ultramafic rocks towards the centre of the massif, with gabbro, sheeted dykes and finally extrusives forming roughly concentric outcrops away highest topographical point, Mount Olympus. Resting upon the ophiolite are Mesozoic to Recent sedimentary rocks, the deposition and lithology of which, have been influenced by the post-genesis structural movements of the Troodos Ophiolite. The second unit is located in south-west Cyprus, and is termed to Mamonia Complex (Robertson and Xenophontos 1993; Robertson *et al.*, 1998). This unit, which is composed of Triassic lavas, Mesozoic sediments and subordinate ophiolite rocks, is allochthonous, and separated from the Troodos massif by high angle faults. The sedimentary rocks of the Mamonia Complex are interpreted as deep-water base-of-slope facies of a Mesozoic passive margin (Robertson, 1998). The third and final tectonic

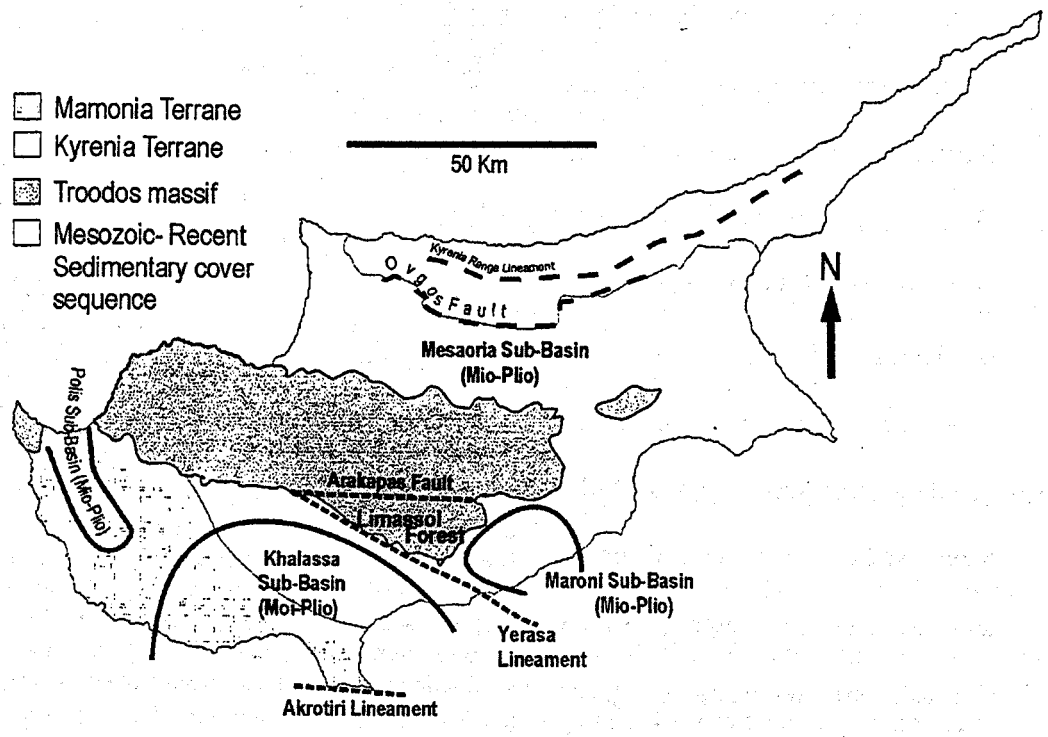

Figure 1.1.The main structural components of Cyprus.

unit, the Kyrenia Range, in the north of Cyprus, is analogous to an Alpine-type fold-and-thrust belt (Robertson and Xenophontos, 1993). It has a core of Mesozoic shallow-water carbonates surrounded by younger volcanics and sediments (Robertson, 1998).

1.3.2 Pre-Mesozoic history

Palaeomagnetic and stratigraphic data suggest an ocean (Tethys) existed between the super-continents of Gondwanaland and Laurasia during the Late Palaeozoic (Bullard *et al.*, 1965; Smith and Briden, 1977). The tectonic evolution of the Tethys can be divided into two – an essentially Palaeozoic "Palaeotethys" and a Mesozoic "Neotethys". By the Late Permian Palaeotethys was closing by northward subduction beneath Laurasia (Gass *et al.*, 1994).

1.3.3 Mesozoic Development of Cyprus.

Robertson (1998) provides a detailed Mesozoic-Tertiary tectonic reconstruction of the eastern Mediterranean. Rifting of the Gondwanan margin was complete by the mid- to late-Triassic, creating the Neotethyan ocean basin (Robertson, 1998). The Neotethys was bounded by Gondwana to the south and to the north by rifted Gonwanan micro-continents (Figure 1.2). The Mesozoic Mamonia Complex (south-west Cyprus, Figure 1.1), the Moni Mélange (southern Cyprus), and the Kyrenia Range (northern Cyprus), are remnants of these northerly micro-continents (Figure 1.2 and 1.3; Robertson, 1998). It is thought that within the southerly Neotethyan ocean basin that the Troodos and associated ophiolites were

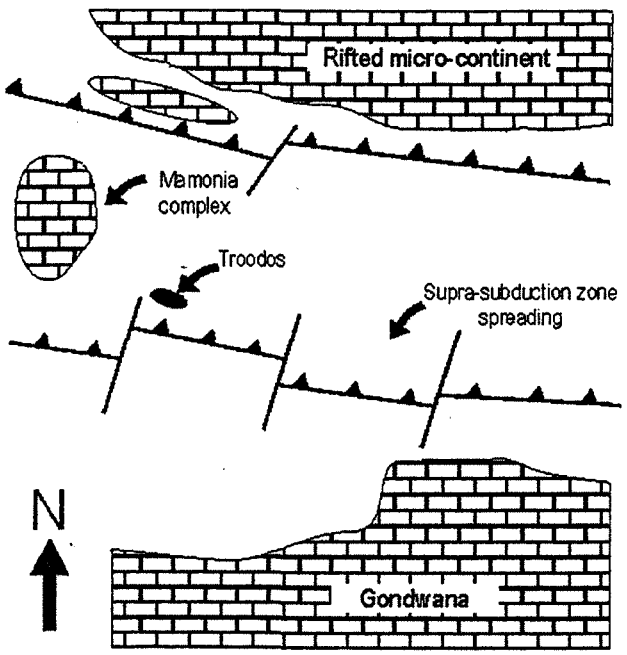

Figure 1.2 Map reconstructing the plate tectonic configuration of Cenomanian-Turonian Eastern Mediterranean. The easternmost Mediterranean oceanic basin is closing through the activity of two north-ward dipping subduction zones (Robertson, 1998). The Troodos Ophiolite formed above the southerly subduction zone. Redrawn from Robertson (1998)

generated above a northward dipping subduction zone during the late Cretaceous (Figure 1.2; Sengör and Yilmaz 1981; Robertson and Dixon, 1984; Robertson, 1998). Geochemical, tectonic, and isotopic studies suggest a late Cretaceous age, 91.6±1.4Ma (Gass 1994 *et al.*; Clube *et al.*, 1985) for the Troodos ophiolite. The attitude of subduction is controversial, Robertson and Dixon (1984) favour a northward dipping African plate based on field and kinematic evidence (Figure 1.3), but Dilek *et al.* (1990) prefer a southerly dipping plate model based on geochemical evidence. The intra-oceanic subduction zone (Figure 1.2) collided with the southerly continent during the Campanian to Maastrichtian, triggering the rotation of the Troodos micro-continent (Clube *et al.*, 1985; Clube and Robertson 1986; Robertson 1998). It was during this rotation that the Mamonia Complex was juxtaposed with the Troodos ophiolite. Palaeomagnetic data (Clube *et al.*, 1985; Clube and Robertson 1986) indicate an anticlockwise rotation of 90° for the Troodos massif, resulting in a north-south palaeo-spreading axis orientation. As a result of collision, the Troodos massif was tilted en masse to the south, producing a palaeoslope, which was then influential in the deposition of Lower Tertiary pelagic carbonates and, more importantly, calciturbidites Robertson 1976).

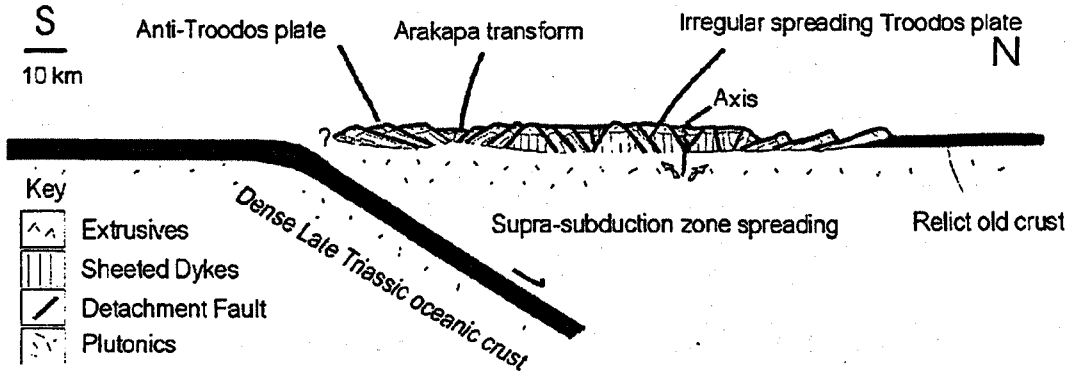

Figure 1.3 Reconstruction of the Troodos formed by spreading above a N-dipping subduction zone, cut by a transform fault. Modified from Robertson 1990.

Late Cretaceous (Campanian - Maastrichtian) deep-water pelagic sedimentation upon the newly formed oceanic crust shows that areas of the Troodos massif were already topographically elevated (Robertson 1977a). Figure 1.4 summarises the main features of the Campanian–Recent sedimentary cover of Cyprus. Sedimentation close to the spreading axis

consisted of chemical precipitates (umbers) leached from the underlying lavas by circulating hot sea-water (Shelton and Gass 1980) and radiolarian mudstones. These umbers and radiolarian mudstones (Robertson and Hudson, 1974; Pantazis 1980) were the first autochthonous sediments deposited on the newly created ocean floor (Figure 1.4; Perapedhi Formation). Overlying this are volcaniclastic sandstones and bentonitic clays of the Kannaviou Formation (Figure 1.4; Robertson, 1977a)

1.3.4 Lefkara Formation (Maastrichtian-Oligocene)

Kähler and Stow (1998) summarise Lefkara Formation deposition to be a result of pelagic, turbidity current and bottom-current processes. The Formation is split into three sub-groups, lower, middle and upper. The basal chalks and marls of the Lower Lefkara Formation in the north and east, represent deposition in broad hollows, close to the carbonate compensation depth (Robertson and Hudson 1974). The Lower Lefkara is comparable to the red to white biomicrites of the Upper Cretaceous in other areas of the Tethys, including the Southern Alps, Sicily and western Greece (Robertson 1976). To the south, the Lower Lefkara Formation attains a considerably greater thickness (>800 m) than that in the north (Morse, 1996). This is thought to be mainly due to the increased sediment supply from the eroding Moni Mélange emplaced earlier in the Maastrichtian. The Lower Lefkara thins and pinches out towards the west, where the Middle Lefkara (Palaeocene) lies directly on the ophiolitic rocks (Gass *et al.* 1994). During the Palaeocene through to the Early Eocene, the Lefkara Formation is interpreted to represent continued deposition in a gradually shallowing sea (Follows 1992; Robertson 1977a). The Middle Lefkara is composed of chalk with chert overlain by, massive-bedded chalks with cleaved marly chalk. Some beds contain Mamonia-derived clasts (<20mm) which are concentrated close to the bed bases (Robertson 1977a). Robertson also noted the presence of well-developed sedimentary structures, including normal grain-size grading, parallel lamination and cross-lamination. Robertson (1977) and later Gass (1994) interpreted these rocks as calciturbidites, which form incomplete Bouma sequences (C-D-E and D-E). Intraformational slumping within the Middle Lefkara is

commonplace, though the degree of deformation is reduced to broad anticlinal structures, east of the Limassol Forest Complex (Gass 1994). Palaeocurrent data indicates a transportation direction, for the calciturbidites, from the north to north-east (Robertson 1977a; Gass 1994). The Maastrichtian tilting of the southern Troodos margin was responsible for generating this palaeoslope dip direction.

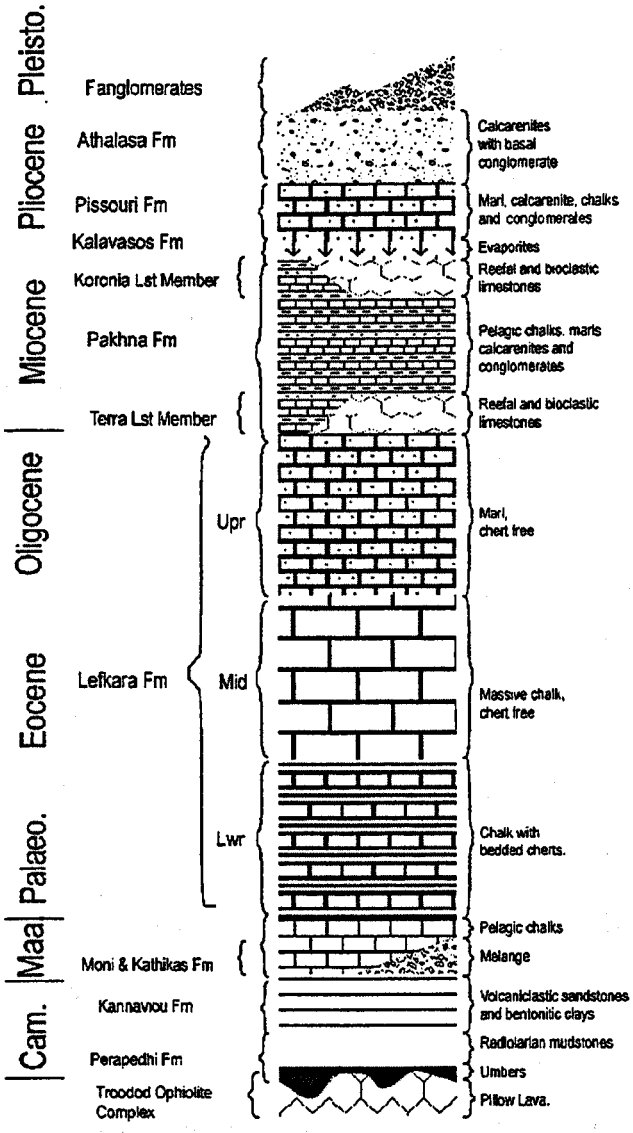

Figure 1.4 Geological vertical section of the Troodos sedimentary cover. Redrawn from Morse (1996).

The Upper Eocene to the earliest Miocene is represented by the Upper Lefkara Formation which comprises bedded marls intercalated with dark-coloured, thin (1-10cm) shale layers that in places contain sulphides (Gass 1994). Robertson (1977a) demonstrate that the marginal facies of the Upper Lefkara Formation contain an assemblage of autochthonous benthonic foraminifera, which suggest that by Palaeocene times, the seas around the Troodos margin were shallowing. Throughout the Middle and Upper Lefkara Formation (Oligocene) benthonic foraminifera are abundant and Lower Lefkara-derived clasts are absent. However, basic grains of volcanic composition suggest that erosion of the underlying Troodos was taking place (Gass 1994). Robertson (1977a) noted contemporaneous contrasting environments during this interval. Firstly, the northern, southern and eastern Troodos margins witnessed carbonate deposition in an open

shallow sea, though in the north deposits are thin, and in places discontinuous. Secondly, the north-west Troodos margin suffered erosion and the development of reefs during the early Miocene.

1.3.5 Pakhna Formation (Miocene)

Unconformably overlying the Lefkara Formation is the Pakhna Formation (Figure 4.3). The unconformity is interpreted to represent uplift, exposure and erosion prior to the deposition of the Terra Member (reef facies) and the chalks, marls and calcarenites of the Pakhna Formation (Figure 1.4; Robertson, 1977). This localised unconformity was caused by a pulse of north-south compression (Robertson, 1998). Robertson (1998) suggested that this change corresponds to the onset of the present phase of northward subduction beneath Cyprus, and the possible collision of a topographic high (such as a seamount) with the subduction trench. The uplift is thought to have terminated deposition of the Upper Lefkara, which it deformed (Robertson, 1977b), before an abrupt change to more localised, tectonically controlled deposition of the Pakhna Formation (Eaton and Robertson 1993). Early-Middle Miocene compression gave rise to the Yarasa Fold and Thrust Belt (Figure.1.1; Morel, 1960), where the Limassol Forest Block is thrust southward over earlier Tertiary sediments (Robertson 1977b; Eaton and Robertson 1993). Today in southern Cyprus the Pakhna Formation is bounded to the north by the Limassol Forest Block and to the south by the Akrotiri High, a ridge composed of exotic Mesozoic lithologies (Eaton and Robertson 1993). Tectonic compartmentalisation resulted in the development of three Miocene to Pliocene sub-basins, the Polis, the Khalassa, and the Maroni sub-basins (Figure 1.4).

The Pakhna Formation comprises a general shallowing upward succession, beginning with deep-water pelagic carbonates. Towards the top of the succession there is bioclastic and terrigenous material (Gass 1994; Eaton and Robertson 1993; Orszag-Sperber *et al.* 1989). In places, on the southern margin of the Troodos, the Pakhna Formation unconformably overlies the Moni Mélange, whereas in the north, where preserved, it is underlain by a

complete succession of the Lefkara Formation (Eaton and Robertson 1993). Debris flows are found both near the base and at the top of this formation (Gass 1994). Those at the base contain Mamonia-derived clasts, which are replaced by Troodos-derived clasts higher up. The ophiolite-derived clasts show the progressive unroofing of the Troodos massif from the supra-ophiolite cover to the sheeted dykes (Gass 1994). Farrell and Eaton (1988) noted the presence of southwards-verging slump folds within bioclastic sandstones of the Pakhna Formation. , Late mid Miocene sedimentary deposits are similar to the underlying Lefkara Formation and considerably thicker south of Troodos with ~350 metres of Pakhna Formation, whereas to the north they have an average thickness of ~15 metres (Robertson 1977b). Reefs are developed in two distinct phases, firstly the Aquitanian-Burdigalian (Terra Member) and secondly, the Tortonian (Koronia Member, Follows 1992). The Terra Member (reef and shelly limestones), rest on an oceanic crust erosion surface (Follows, 1992). The later, Koronia Member has fore-reef facies that comprises decimetre thick beds of bioclastic reef detritus (Follows 1992). In places, (northern Troodos margin, south of the Limassol Forest Block and Akamas) the Koronia Member grades into the Pakhna Formation, and is considered a member within the Pakhna Formation as it contains similar lithologies (Gass 1994, Follows and Robertson 1990). Gass (1994) suggested that the deposition of reefs within this formation was dominantly controlled by the Yerasa fold and thrust belt, which developed due to the uplift of the Limassol Forest Complex. Contemporaneous basin depocentres were also the sites of continued relatively deep-water pelagic foraminiferal chalks (Robertson 1977b). The upper part of the Pakhna Formation deposited during the Messinian, is more siliciclastic rich, due to a relative sea-level fall (Orszag-Sperber *et al.* 1989). The three sub-basins mentioned previously became progressively more restricted as evidenced by deposition of lagoonal calcareous and diatomitic laminites (Orszag-Sperber *et al.* 1989). The Kyrenia Range was emplaced, via movement along the Misis-Andirin strike-slip lineament during the late Miocene (Robertson, 1998).

The sediments of the Pakhna Formation provide the focus to this study, as they were deposited during a tectonically active regime and display a clearly developed cyclicity. Detailed facies descriptions for the Pakhna Formation based on outcrop localities are discussed in Chapter 2.

1.3.6 Kalavasos Formation (Messinian)

The Kalavasos Formation comprises gypsum evaporites that represent the continued shallowing trend seen at the top of the Pakhna deposition. The Kalavasos Formation is ~contemporaneous with other evaporite facies developed in the Mediterranean area during well-documented Messinian "salinity crisis". McClelland *et al.* (1996) note that the Messinian salinity crisis marked a dramatic climate change in the Mediterranean area, which resulted in widespread evaporite deposition in most Mediterranean basins. Magnetostratigraphy suggests that evaporite formation displays diachroneity across the Mediterranean (McClelland *et al.*, 1996). Müller and Mueller's (1991) show that the salt deposits in the centre of the Mediterranean formed later than those on the margins, suggesting gradual sea-level draw down. Orszag-Sperber *et al.* (1989) conducted a detailed study of evaporite distribution in Cyprus. They noted the occurrences of three phases of breccia formation: pre-evaporite, intra-evaporite and post evaporite. These breccias were attributed to three discrete pulses of compressional tectonic activity during the Miocene-Pliocene transition, prior to a Pliocene transgression. The Miocene-Pliocene "events" were, in reality, a series of tectonic pulsations that were recorded by sedimentary parameters (Orszag-Sperber *et al.*, 1989). Robertson (1998) attributes increased tectonic activity during the Messinian?- early Pliocene, to the initial collision of the Eratosthenes Seamount with the subducting margin to the south of Cyprus. The Eratosthenes Seamount is interpreted as a continental fragment with igneous intrusions at depth, which was rifted from the African margin probably in the Triassic (Ben-Avraham *et al.*, 1976; Kempler, 1998; Robertson, 1998).

1.3.7 Nicosia (Pissouri) and Athalasa Formations (Pliocene)

During the early Pliocene marine transgression caused a return to marine deposition in many areas of Cyprus (Robertson, 1977b). The Nicosia Formation (equivalent in-part to the Pissouri Formation) oversteps all older formations and is composed of homogenous grey marls, with occasional limestone and sandy beds to the north of the Troodos Massif (Wilson, 1959). To the south the formation comprises intercalated clay-rich carbonates and sandy rocks (Krasheninnikov and Kaleda, 1994). The formation represents marine sedimentation, fluctuating between deep water and shallower near-shore environments (Bear, 1960). McCallum and Robertson (1995) interpreted Pliocene sedimentation (Nicosia and Athalasa Formations) in the Mesaoria Basin (Figure 1.1 and 1.4) to have been from a series of isolated fan-delta systems that built out from the uplifting Troodos Massif. Borehole data indicate that the Pliocene is 950 m thick in the Mesaoria Basin. Stow *et al.* (1995) attribute fan-delta deposition to Pliocene deposits in the Pissouri Basin, to the south of the Troodos Massif (Figure 1.1.). They note the presents of gabbro clasts in this interval, indicating that the Troodos ophiolite plutonic series was acting as a source area.

1.3.8 Fanglomerates (Pleistocene)

The continued underthrusting of the Eratosthenes Seamount due to the northward migration of the African Plate beneath Troodos during the Quaternary resulted in the uplift of Cyprus (Poole and Robertson 1991). Associated with this the ultramafic rocks within the overiding slab were serpentinized and rose dramatically, resulting in updoming of the Troodos Massif, exposing serpentinite on Mt. Olympos (Robertson, 1998). The loci of Quaternary uplift was centred on the Troodos massif (Mount Olympus), and microfossil and radiometric dates suggest uplift initiated in the Early Pleistocene (Poole and Robertson 1991). Uplift of the Kyrenia Range also occurred during this time (Robertson, 1998). The renewed uplift of the Troodos ophiolite resulted in rapid erosion and deposition of immature sediments, termed the Fanglomerates (Robertson 1977b). These coarse-grained fans radiate away from the Troodos Massif and are mainly preserved in the Mesaoria Basin. Poole and Robertson

(1991) suggest that in the Late Pleistocene-Holocene, the rate of uplift reduced and eustatic sea-level changes dominated. This led to the local submergence of southern coastal areas.

1.4 Sequence stratigraphy

Sequence stratigraphy is a technique for dividing the sedimentary record into meaningful packages of genetically related sediments resulting from relative changes in sea-level (Walker and James, 1992). It is applied in this study to document cycle development and to assist correlation both locally and regionally. The technique was developed on passive margin siliciclastic successions (Mitchum, 1977; Vail *et al.*, 1977; van Wagoner *et al.*, 1988, Vail *et al.*, 1991), where relative sea-level change is defined as variation in water depth resulting from both tectonic and eustatic changes. This section introduces the concept of sequence stratigraphy and its terminology.

Sequence stratigraphy divides sedimentary successions into a number of sequences that are bounded by unconformities and their correlative conformities, termed sequence boundaries (SB; Mitchum *et al*, 1977; Walker and James, 1992). Sequence boundaries form during the maximum rate of relative sea-level fall (Figure 1.5), and are typically characterised by erosional surfaces, and in deeper-water areas continuos sedimentation and correlative conformities. A depositional sequence represents a package of sediments that relates to one cycle of relative sea-level change. Sequences are further subdivided into systems tracts, that

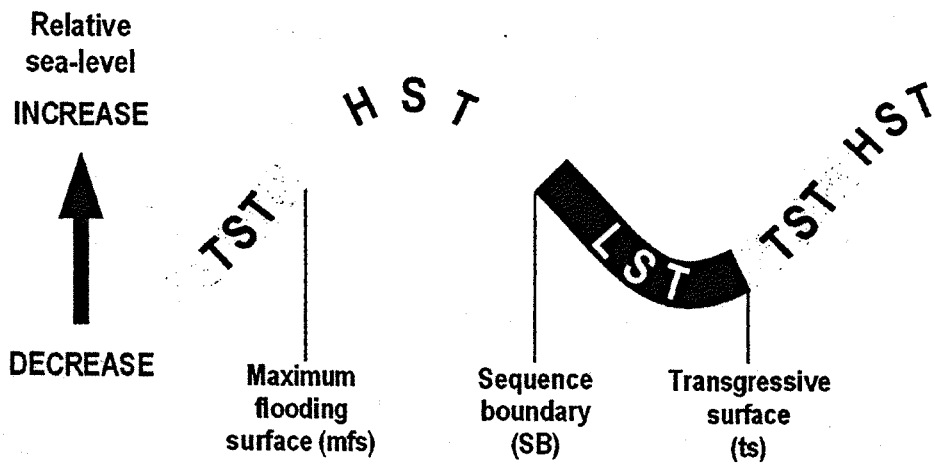

Figure 1.5 The position of systems tracts and key surfaces in relation to relative sea-level.

relate to particular portions of the relative sea-level cycle. Each systems tract is bounded unconformities or discontinuities (sequence boundary, transgressive and maximum flooding surfaces; Figure 1.5). These key surfaces relate to specific points on the sea-level curve and system tract boundaries (Figure 1.5).

A sequence boundary (SB) forms at the maximum rate of sea-level fall (Figure 1.5), and is marked by subaerial erosion in proximal areas and correlative conformities in distal areas (Walker, 1990). The lowstand system tract (LST) deposits follow development of a SB. These deposits form during continued relative sea-level fall to the point of initial significant transgression of the basin margins, the transgressive surface (ts). LST deposits typically relate to periods of increased terrigenous supply associated with a basinward shift in facies. Sediments deposited during the initial part of relative sea-level rise are grouped in to the transgressive systems tract (TST), and are bounded at the base by the ts and at the top by the maximum flooding surface (mfs), which denotes the maximum rate of relative sea-level rise. These deposits successively onlap on to the basin margins and show a landward migration of facies. Sediments deposited during the final stages of sea-level rise, the highest point of sea-level, and initial fall in relative sea-level (Figure 1.5) are grouped in the highstand systems tract (HST). These sediments mark the maximum extent of marine transgression and are therefore often characterised by the reduced influence of terrigenous derived material. The HST terminates with the development of at further SB, which forms at the maximum rate of sea-level fall associated with the next relative sea-level cycle.

A number of orders of cyclicity are recognised in sequence stratigraphy (Vail *et al.*, 1991). First-order cycles are the largest scale, and represent general sea-level variation over hundreds of millions of years. They are interpreted to be related to the accretion and subsequent splitting apart of supercontinents (Walker and James, 1992; Worsley, 1984). Second-order cycles spanning 10-100 million years are composed of a grouping of third-order cycles, and are widely accepted to relate to changes in the volume of oceanic ridges

(Hallam, 1963). Third-order cycles have durations of 1-10 million years, but are typically shorter than 3 million years (Plint *et al.*, 1992) and form the highest frequency cycles identified in the sequence chronostratigraphic schemes of Vail *et al.* (1991) and Hardenbol *et al.* (1998). Their control is problematical as they probably result from a variety of mechanisms operating through geological time. These cycles sometimes fall below the resolution of biostratigraphy, though are thought, by some, to be globally correlatable (Vail *et al.*, 1977; Haq *et al.*, 1998). Fourth- (500-200 kyr) and fifth-order (200-10 kyr) cyclicity represent the smallest scale of cyclicity and probably result from variations in the orbital parameters of the Earth (Milankovitch cycles, see discussion below).

The sequence stratigraphic model outlined above is refined in this study (Chapter 3) to suit the pelagic carbonate setting of the Pakhna Formation sediments discussed in this thesis.

1.5 Calcareous nannoplankton

Calcareous nannoplankton are used in this study to create a biostratigraphic framework to correlate sediments investigated in this study.

Coccoliths, together with small calcite bodies of organic, but otherwise unknown origin, organisms called nannoliths, constitute calcareous nannoplankton. Coccolithophores are predominantly autotrophic nannoplankton utilising the energy from sunlight to photosynthesise organic material from inorganic ones (Brasier, 1980). Living cells are therefore restricted to the photic zone of the water column (~0-200 m) with lighter, smaller cells living near the surface (Brasier, 1980). The oldest generally accepted fossil coccoliths are rare and reported from upper Triassic rocks, this was followed by major diversification during the Jurassic (Brasier, 1980). During the late Cretaceous a major marine transgression triggered a further explosive radiation of many planktonic groups (Brasier, 1980), which lead to the deposition of chalk over vast areas of the continental platforms. Regression at the end of the Cretaceous exterminated may coccolithophore genera, though a second resurgence of

forms occurred during the Eocene, including star-shaped the discoasters (Brasier, 1980). The minute calcite plates produced by planktonic unicellular marine algae, have proven extremely useful for the biostratigraphy of marine sediments of Jurassic through Pleistocene age (Perch-Nielsen, 1985). Their small size (1-25 μm) allows for age determinations of even very small samples, such as side wall cuttings. An introduction to calcareous nannoplankton is given by Reinhardt (1972) and Haq (1978), with detailed biological perspective provided by Tappan (1980). Biostratigraphic investigations were pioneered by Bramlette and Riedal (1954), Stradner (1959), Bramlette and Sullivan (1961), Bramlette and Wilcoxon (1967), Hey and Mohler (1967) and Hey *et al.*, (1967). The Cenozoic has been subdivided into some 46 zones by Martini and Worsley (1970) and Martini (1971), and into 34 zones and 45 subzones by Okada & Bukry (1980, based on earlier papers by Bukry (1993; 1995). Calcareous nannoplankton extinction and diversification events are widely accepted as useful biostratigraphical tools and are used extensively for dating sediment from the Deep Sea Drilling Project and the Ocean Drilling Program.

1.6 Orbital parameters and spectral analysis of stratigraphic time series analysis

The spectral analysis of stratigraphic time series is used in this study to identify regular cyclicity developed in bed thickness and lithological variation in the Pakhna Formation. In many modern and ancient pelagic sequences it has been postulated that variations in sediment composition record climatically controlled cycles linked to the variations in the Earth's orbital parameters - Milankovitch cycles (Fisher, 1991). Pleistocene studies have shown that orbital and climatic variations on a 10 kyr to 1 Ma time scale are dominated by a few regular components whose periods are known (Berger, 1984; Imbrie *et al.*, 1984). Milankovitch (1941) identified these components as related to variations in eccentricity (typically ~100-400 kyr), obliquity (41 kyr) and precession (~21 kyr) in the earth orbit and axial tilt (Figure 1.6). These vary over time according to the changing gravitational environment of the Earth as governed by the positions of the other planets, the Moon and the Sun (Berger, 1984). The eccentricity of the Earth's orbit determines the distance between

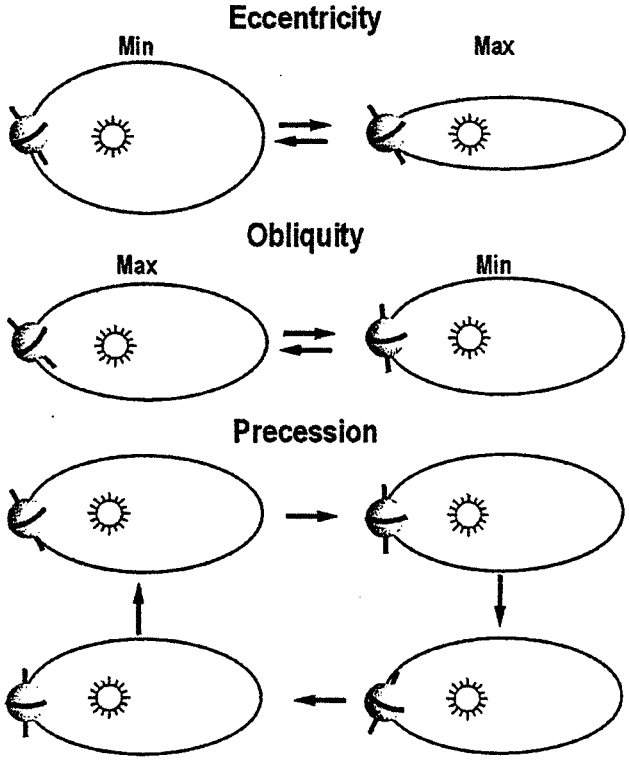

Figure 1.6 The three orbital parameters which cause orbital-climate cyclicity. All vary simultaneously, but here each is illustrated schematically at the extremes of variation with the other elements kept constant. Each illustration depicts the Earth at perihelion. Precession involves variation in both the direction of tilt of the Earth's axis and in the direction of the long axis of the orbital ellipse (not shown) which together determine the timing of perihelion relative to the seasons. Redrawn from Weedon (1993)

the Earth and the Sun (Figure 1.6). The most important wavelength of the eccentricity cycle is a ~400 kyr with further strong cycles at 128 and 95 kyr (Schwarzacher, 2000). The obliquity cycle relates to the inclination of the Earth's axis relative to the pole of the orbital ellipse (Figure 1.6), and has a period of between 54 and 41 kyr (Berger *et al.*, 1994). The precessional cycle is the variation in the direction of the Earth's axial tilt, and the direction of the long axis of the orbital ellipse (Figure 1.6), and has main periods of 19 and 23 kyr (Schwarzacher, 2000). The average annual insolation reaching the Earth is clearly the most important factor affecting climate (Valdes and Glover, 1999; Schwarzacher, 2000). It is now widely accepted that changes in the Earth orbital parameters have driven climate changes in the Quaternary and late Pliocene times, owing to their effect on the seasonal insolation (Pillans *et al.*, 1998; Valdes and Glover, 1999). Integrated distance variations (Earth to Sun) over a full year depend only on eccentricity and the resulting variations in isolation are extremely small (Schwarzacher, 2000). The eccentricity cycles have the effect of controlling the size of the precession effect, and only have a small control on total yearly radiative heating (Weedon, 1993; Wilson *et al.*, 2000). Despite this the eccentricity cycle has been the dominant cycle over the last 700 kyr (Valdes and Glover, 1999) and is thought to be related to land/lithosphere/ice feedbacks (Crowley and North, 1991). The obliquity cycle determines the degree of seasonality

(Weedon, 1993), the greater the angle of tilt the greater difference between summer and winter (Wilson *et al.*, 2000). The precession controls the timing of the seasons relative to perihelion and hence total radiative heating in each season (Weedon, 1993). The seasonal changes in the incoming solar radiation have a much more important effect on climate, particular summer insolation (Milankovitch, 1941). Cooler summer temperatures in northern high latitudes are suggested as a mechanism for initiating glaciations due to the preservation of winter snows (Maslin *et al.*, 1998). The relationship between changes in insolation and climate change is far from clear, particularly as climate conditions of the past are generally poorly understood (Schwarzacher, 2000).

1.6.1 Spectral analysis theory

The recognition of orbital variations or Milankovitch cycles rests on the regularity or time periodicity of such patterns (Schwarzacher, 2000). Spectral analysis is an objective, statistical method for detecting regular cyclicity in data called stratigraphic time series (Weedon, 1991). Stratigraphic time series, in this context also incorporates "length series", as bed thickness data can be attributed to a function of time. Regular cycles cannot explain why there is a connection between climatic variability and sedimentation, but can provide supporting evidence that such a connection existed (Weedon, 1991). A detailed mathematical explanation of the spectral analysis of stratigraphic time series is provided by Priestly (1981). Stratigraphic time series analysis is a well-established technique for identifying regular cyclicity in sedimentary strata, and has, for instance, been used on magnetic susceptibility data from Jurassic-aged British mudrock formations, to identify eccentricity, obliquity and precessional cycles (Weedon *et al.*, 1999). Reconstructing the chronology of orbital cycles through time is becoming an increasingly useful for astronomically calibrating geological sections (Clements, 1999), biostratigraphical zones (Raffi, 1999), and magnetostratigraphy (Kent, 1999). Currently astronomical time scale tuning is applicable back through the Miocene (Hilgen *et al.*, 1995; Shackleton *et al.*, 1999) to the Oligocene (Shackleton *et al.*, 1999), with implications that orbital-stratal calibrations

using the eccentricity cycle can extend back for several hundred million years (Hinnov, 2000).

Spectral analysis requires the generation of a stratigraphic time series gained from the rock record. A stratigraphic time series consists of measurements of some parameter at a constant interval of time or space (Weedon, 1991). Weedon (1991) stresses the importance of recognising the geological context when considering potential stratigraphic time series parameters. If regular cycles are sought then there must be a link between sedimentation and orbital parameters, however complex. Stratigraphic time series data can therefore be composed of a variety of geochemical (e.g. TOC, % $CaCO_3$, stable isotopes) or bed thickness data that are interpreted to vary with orbital parameters. When using bed thickness data the stratigraphic thickness is treated as a distorted time scale, and therefore event beds should be absent, or extracted, from the section (Weedon, 1991). The sampling interval for stratigraphic time series data should be equal to or less than the thickness of the thinnest bed present, to avoid "aliasing" the signal. To digitise a geological section each lithology is given a numeric code. The stratigraphic (length) time series is then a function of bed thickness and lithology. This results in the production of a square-wave time series, rather than a sine-wave series for geochemical data.

Any stratigraphic time series can be treated mathematically as the sum of many different components, each of which can have different amplitudes and phases (Weedon, 1991). The spectral analysis approach separates the different regular components (sine and cosine waves) of the stratigraphic time series, to produce power spectrum, where relative power is plotted against frequency (Weedon, 1991). The square of the average cosine amplitude plus the square of the average sine amplitude determine the relative power of peaks on the spectrum. Judging whether a peak is significant involves deciding whether it emerges above the general noise level (Weedon, 1991). A statistical comparison of spectra produced from real stratigraphic time series with those produced by an independent random process that

produces "red noise" (noise which gradually increases towards lower frequencies) enables peaks that emerge above this noise to be assessed in terms of percentile confidence levels.

Spectral analysis is designed for the analysis of stratigraphic time series that are "stationary", *i.e.* the mean and variance of the top halves are more or less the same as those of the bottom halves of the data (Weedon, 1991). When this is not the case (e.g. progressively higher values up section) the trend can be removed by linear regression and then subtracting the regression line point-by-point from the stratigraphic time series (Weedon, 1991). Trends in amplitude may also be accompanied by changes in average wavelength (e.g. successively thickening beds), which implies a changing trend in average sedimentation rates (Weedon, 1991). Such a wavelength trend is not removed with linear regression, as it requires a quantitative knowledge of the nature of the trend.

1.6.2 Geological complications and possible errors

Geological processes complicate spectra based on bed thickness data. The effect of sedimentation rates, hiatuses and differential compaction, often lead to one lithotype dominating the section. This produces an asymmetrical stratigraphic time series. Original regular spectral peaks are still preserved, in such instances, though asymmetry leads to harmonic peaks with frequencies that are integer multiples of the original peak (Weedon, 1991). Compaction also leads to a reduction in the thickness of all beds in the stratigraphic time series, which has the effect shifting original spectral peaks to higher frequencies (Weedon, 1991).

Variable sedimentation rates broaden and decrease the amplitude of spectral peaks. This effect can be minimised by splitting the stratigraphic time series into sections composed of approximately equal bed thickness, as each bed is inferred to represent a similar time (Weedon pers. com.). Hiatuses not related to rock type can seriously distort spectral shape (Weedon, 1991). Hiatuses develop at a variety of scales, and can be expected in all

geological sections and often remain undetected (Sadler 1981). The only way of minimising the effect to hiatuses in spectral analysis is to split the stratigraphic time series at locations where hiatuses are identified, such as hardgrounds (Weedon, pers. comm.).

The introduction of these "geological errors" in stratigraphic time series analysis is inevitable, and may partly explain why wavelength ratios commonly observed on spectra are not exactly those of the current orbital cycles (Weedon, 1991). Alternatively the periods of the orbital cycles are known to be slightly different in the geological past than that they are today (Walker and Zahnle, 1986). In the geological past the periods of the obliquity and precessional cycles have varied due to the faster rotation of the Earth, the Moon's closer orbit, and lengthening of the dynamical ellipticiy of the Earth's orbit (Reading and Levell, 1996). Together these forces shortened the periods of the precession cycles to 19 and 16 kyr (*c.f.* 23 and 19 kyr today), and the obliquity cycles to 30 and 37 kyr (*c.f.* 41 and 54 kyr today) in early Palaeozoic (Berger *et al.*, 1993). Eccentricity cycles do not appear to have changed through time (Reading and Levell, 1996).

1.7 Tectonics and climate: effects on relative sea-level and the sedimentary record

Sea-level changes are of two types. Eustatic sea-level change is a function of sea-surface movement relative to some fixed point, such as the centre of the Earth (Reading and Levell, 1996). Relative sea-level change is measured relative to some moving point in the underlying crust, or near the sea floor (Reading and Levell, 1996). Relative sea-level change is often restricted to local- to regional-scale tectonics that alters the accommodation space available for sedimentation. Eustatic sea-level changes result from a variety of mechanisms, that include: changing the volume of oceanic ridges (Hallam, 1963), thermal contraction and expansion of oceanic water (Donovan and Jones, 1979), and changes in the volume of ice. These various sea-level altering mechanisms operate synchronously but at different time scales. They are recorded by the distribution and composition of marine sedimentary

successions. Climatically induced changes in sea-level are generally recorded at a <1 million year time scale, and are the focus of this study. As sediments react to sea-level changes, isolating the individual tectonic and eustatic components from the sea-level deduced from the sediments is problematical.

The stratigraphic signature of tectonism results from a wide range of processes and has a profound effect on accommodation space (the area beneath the base level of erosion) available for sedimentary deposits (Vail *et al.*, 1991). Vail *et al.*, (1991) subdivide tectonic activity into a series of loose hierarchical scales. The evolution of a sedimentary basin is interpreted as a first-order tectonic event (thermal subsidence), where the basin itself is the stratigraphic signature (from initiation to subsequent infilling). Second-order tectonic events are indicated by changes in the rate of tectonic subsidence in the basin, or changes in the rate of uplift in the sediment source terrane. Major transgressive-regressive facies cycles are their stratigraphic signature (Zweigel *et al*, 1998). Third-order tectonism events include folding, faulting, magmatism and diapirism. These tend to make sequence boundaries easier to identify in areas of uplift and harder to identify in areas of subsidence (Vail *et al.*, 1991). At a local scale tectonic movements, such as faulting and uplift, result in changes in the type, thickness and distribution of sedimentary facies (Reading and Levell, 1996). Rapid uplift and faulting are partly responsible for supplying the necessary gradient and triggering mechanism for allochthonous, mass flow deposits. Tectonic processes operate on time scales from geologically instantaneous (individual fault movements and earthquakes) to protracted periods of time (subsidence or uplift). Though tectonics may be responsible for cyclic sedimentation, by repeated downthrow along a major fault for example, there is unlikely to be any long term, systematic regularity to it.

The climatic control on sea-level operates on regular basis, as glacioeustacy and thermal expansion/contraction is shown to be related to the quasi-periodic orbital parameters (or Milankovitch cycles) over the last 2.5 Ma (Tiedemann *et al.*, 1994). Increased average

global temperatures cause sea water expansion and therefore lead to a global sea-level rise. The converse occurs during period characterised by lowered global average temperatures. Orbital-forcing also has the effect of altering the distribution and intensity of climate zones (see section 1.6 for a detailed discussion), which will effect many variables related to sedimentation, such as precipitation and aridity. This will therefore, also operate on a quasi-periodic basis determined by orbital parameters.

1.8 Stable Isotopes

1.8.1 Oxygen Isotopes

^{16}O and ^{18}O are by far the most common of the oxygen isotopes and their relative abundance in an oxygen-bearing compound is dependent on a variety of fractionations (Faure, 1986). In this study we are concerned with the fractionation between ^{16}O and ^{18}O during; (1) the change in physio-chemical state of water and (2) the biogenic sequestration of CO_2 from seawater and the biomineralisation of calcite. By measuring the abundances of ^{16}O and ^{18}O in fossil marine organisms that precipitate calcite tests, the ratio of these two isotopes in seawater can determined through time. The $\delta^{18}O$ ratio of marine organisms has been used extensively as a palaeoclimate and temperature indicator (Emiliani, 1955; Shackelton, 1967; Shackelton and Opdyke, 1973; Shackelton and Kennet, 1975; Savin, 1977; Abreu, 1998; Miller *et al.*, 1991).

A general conceptual model for the behaviour of oxygen isotopes in natural systems is now widely accepted. As sea-water evaporates the lighter isotope (^{16}O) is preferentially partitioned into the vapour phase, resulting in the remaining liquid phase becoming isotopically enriched in the heavier isotope (^{18}O). Precipitation is therefore enriched in ^{16}O, and will replenish sea-water with the lighter isotope. Hence, the $^{18}O/^{16}O$ ($\delta^{18}O$) of calcite is also dependent on the temperature of the water it precipitates from. Warmer temperatures result in a more negative $\delta^{18}O$ and cooler temperatures have more positive $\delta^{18}O$ values.

The combined effects of climate and temperature on $\delta^{18}O$ have lead to their extensive use in determining the successive retreats and advances in Quaternary ice sheets, where glacials are marked by positive shifts in $\delta^{18}O$ and interglacials by negative shifts (Dansgaard, 1969; Abell, 2000; Alley, 2000;).

The oxygen isotope response, recorded in marine calcite precipitating organisms, is sensitive to climate, and can therefore be considered in terms of climate variability within two global climate states, icehouse and greenhouse, which act as two end member models, in a continuum of climatic states.

1.8.1.1 Icehouse periods

During icehouse periods the development of icecaps produces vigorous oceanic circulation. At high latitudes water in contact with the icecap is cooled and sinks to form cold deep bottom water. When this deep water impinges on a continental margin it upwells, warms and produces a surface return flow to the poles (Figure 1.7; Jacobs, 1978). Upwelling brings nutrients to the photic zone and hence increases bioproductivity in upwelling zones (Vincent and Berger, 1985). During icehouse periods, the quantity of ^{16}O returning to the oceanic reservoir is reduced, due to the development of large-scale continental ice-sheets (Figure 1.7). The storage of ^{16}O-enriched precipitation during glacials leads to a net increase of ^{18}O in the oceans. The cooler glacials are therefore, recorded as a positive shift $\delta^{18}O$. Periods of interglacial warming are characterised by retreating ice sheets and sea-level increases. The release of ice-bound ^{16}O, combined with relative warming will produce a negative shift in $\delta^{18}O$ (Figure 1.7).

High resolution $\delta^{18}O$ data sets have also be used as a proxy for sea-level during an icehouse state (Miller and Sugarman, 1995; Miller *et al.*, 1996) and has been tested against published

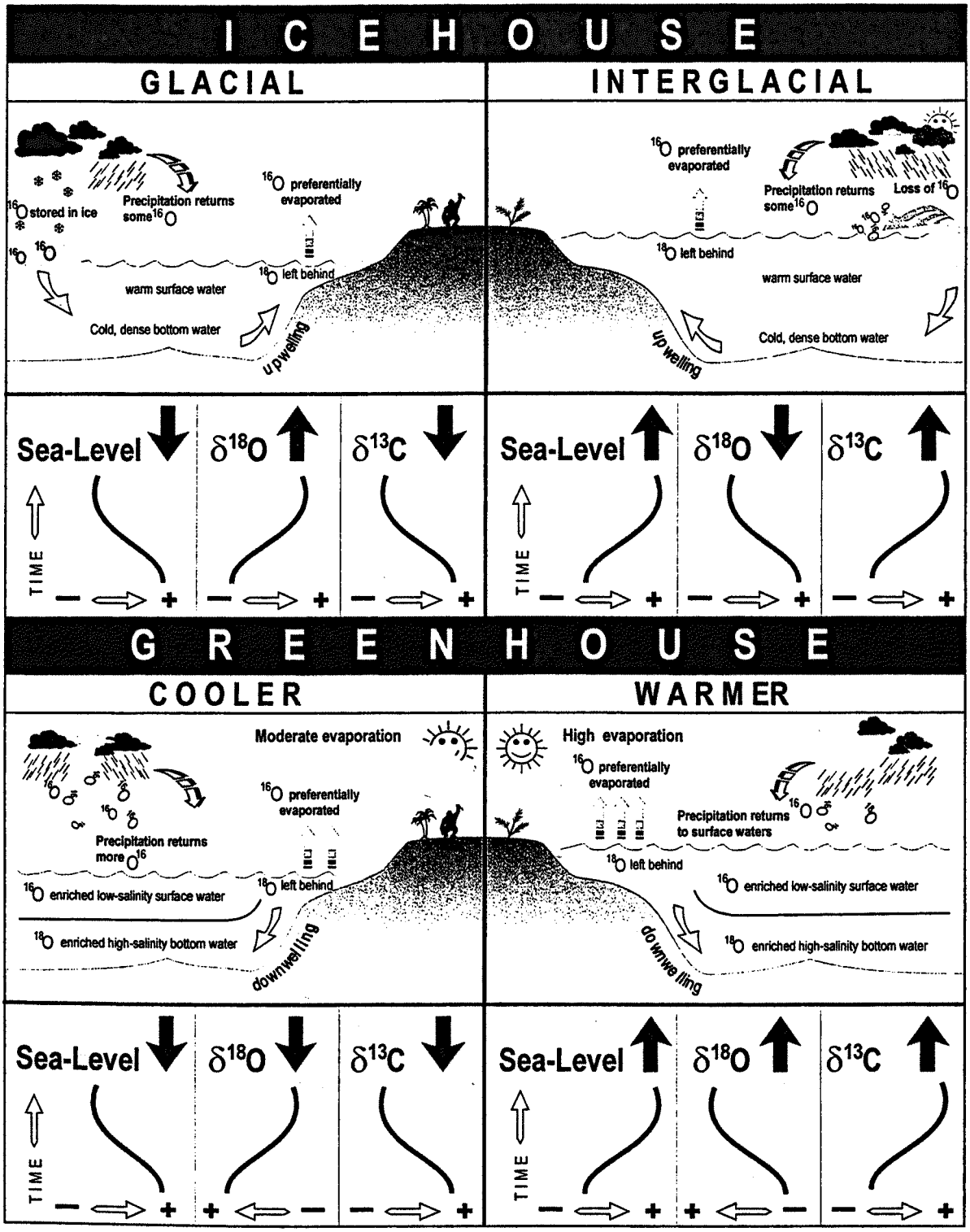

Figure 1.7. Diagram illustrating the predicted effects of climate variability on sea-level, ^{18}O and ^{13}C, within a greenhouse and icehouse world. In an icehouse world the relationship between ^{18}O and relative sea-level is inverse. During glacials and the build-up of ice, sea-level is lowered and ^{16}O is preferentially removed from the oceanic reservoir and stored in ice sheets, increasing ^{18}O (in the oceans). During warmer, interglacial periods, ice sheets retreat, sea-level rises and ^{16}O is returned to the ocean with a subsequent ^{18}O decrease. In greenhouse periods sea-level and ^{18}O have an in-phase relationship. In warmer greenhouse times sea-level rises due to thermal expansion, evaporation increases which, increases ^{18}O. During cooler greenhouse periods, sea-level lowers due to thermal contraction, and precipitation increases, returning more ^{16}O to the surface waters, decreasing ^{18}O. ^{13}C has an in-phase relationship with sea-level during icehouse and greenhouse states, as the removal of ^{12}C occurs mainly in shelf areas were marine productivity is highest. After (Abreu and Haddad 1998; Railsback, 1990).

eustatic sea-level curves and sequence stratigraphy (Haq *et al.*, 1987; Miller *et al.*, 1996; Abreu and Haddad, 1998; Hardenbol *et al.*, 1998).

More positive $\delta^{18}O$ values therefore, relate to periods of increased continental ice (glacio-eustatic sea-level fall) and colder temperatures (oceanic thermal contraction). Conversely, more negative $\delta^{18}O$ values relate to periods of sea-level rise via warmer temperatures (thermal expansion), and a reduction in the size of continental ice sheets. Figure 1.7 illustrates the inverse relationship between sea-level and $\delta^{18}O$ in response to the glacial and interglacial periods.

1.8.1.2 Greenhouse periods

During greenhouse periods, the breakdown of thermal stratification in the oceans and the development of salinity stratification further complicate the fractionation of ^{18}O and ^{16}O. Railsbeck (1990) proposed an alternative model for the $\delta^{18}O$ response during periods of salinity stratified oceans. High evaporation in low latitude basins produces warm saline water enriched in ^{18}O that sinks due to density contrasts and becomes trapped beneath the pycnocline (Figure 1.7). ^{16}O enriched precipitation returns fresh water to the surface of the oceans, reducing salinity and increasing the density contrast between the saline bottom waters. In this model, warmer periods with reduced precipitation result in less well-developed isotopically light surface waters, and a more positive shift in $\delta^{18}O$. Cooler times with more precipitation will result in more relatively negative $\delta^{18}O$ values. The Railsbeck (1990) model suggests that the inverse relationship observed between $\delta^{18}O$ and sea-level cannot function in a greenhouse world. In the greenhouse scenario the relationship between $\delta^{18}O$ and sea-level is in phase; $\delta^{18}O$ increases accompany warming and thermal expansion of the oceans.

1.8.2 Carbon Isotopes

The ratio of ^{12}C and ^{13}C in sea-water is a measure of global photosynthesis, especially marine productivity, as ^{12}C is concentrated preferentially into organic carbon. Positive shifts in $\delta^{13}C$ represent increased organic productivity, while negative shifts in $\delta^{13}C$ represent a reduction in organic productivity.

$\delta^{13}C$ has been suggested to be a proxy for sea-level during the Cretaceous, when there was larger scale flooding of the continental shelf (Scholle and Arthur, 1980; Weissert and Lini, 1991; Jenkyns *et al.* 1994; Voigt and Hilbrecht, 1997; Grant, 1998), though this may not be the case for other periods with less continental flooding. $\delta^{13}C$ will increase with the development of extensive shallow shelf seas during marine transgression and highstands times (Figure 1.7), as organic carbon is mainly synthesised in shelf areas (Jenkyns *et al.* 1994). A corresponding decrease in $\delta^{13}C$ will accompany sea-level fall as the size of the drowned shelf area reduces. This in-phase relationship with sea-level (Figure 1.7) will function in greenhouse and icehouse periods, as thermal contraction and expansion will occur in both climate states, and $\delta^{13}C$, unlike $\delta^{18}O$, is not fractionated by temperature or evaporation.

1.9 Cenozoic climate

Polar ice strongly influences the oceanic and atmospheric circulation (Flower and Kennett, 1994a; Lohmann, 1978). It's study is, therefore, of paramount importance when reconstructing palaeoclimates of the Cenozoic. Since Cenozoic deep-sea sediments are abundant and well preserved, they provide a useful palaeoclimatic record of this important period of the Earth's climate history. Detailed climatological research of the Cenozoic enables analogies to be made with other major cooling events where accessibility and preservation of sediments is more limited.

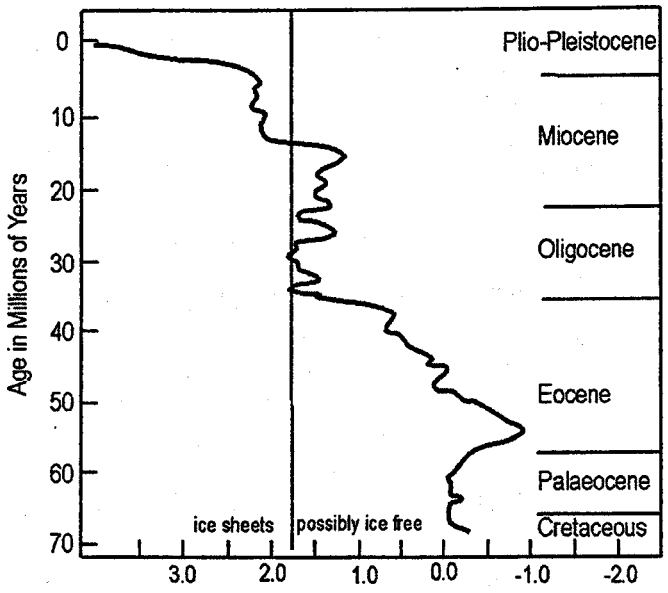

Figure 1.8 Summary of Cenozoic benthic foraminiferal oxygen isotopic records from the Atlantic Ocean. Note the Eocene-Oligocene boundary and mid-Miocene cooling phases. Modified from Miller (1987).

The Cenozoic witnessed a general climatic cooling, from the warm early Eocene optimum, culminating in the major ice advances of the Pliocene and Pleistocene (Kennet, 1995). Superimposed upon this protracted cooling event are several shorter episodes of cooling and warming, such as at the Eocene/Oligocene boundary (Figure 1.8; Flower and Kennett, 1994a; Frakes *et al.*, 1992). The mid-Miocene marks another major transition; between the relative warmth of the late Oligocene and lower Miocene to the "icehouse" state of the mid-Miocene to Recent (Kennet, 1995), and is the focus of this thesis. Evidence for the Cenozoic climate change comes principally from the isotopic record of calcareous foraminifera, and illustrates a decline in ocean temperatures from about 55 Ma onwards (Frakes *et al.*, 1992). Figure 1.8 summarises the Cenozoic benthic foraminiferal oxygen isotope record. The benthic foram $\delta^{18}O$ record depicts a general positive shift throughout the Cenozoic, suggesting cooling of deep water and greater ice volumes. Punctuating this trend are the Eocene-Oligocene and mid-Miocene relatively rapid cooling phases which are manifested as rapid positive increases in the $\delta^{18}O$ record (Figure 1.8).

Other, qualitative techniques of deducing Cenozoic climate include: plotting the amount of ice rafted deposits; the character of biogenic sediments, and the analysis of marine microfossils, pollen and spores deposited in oceanic sediments (Kennet, 1995).

It is widely accepted that ice accumulation began on East Antarctica during the early Oligocene (Kennet, 1995), with successive phases of development throughout the Neogene. Other evidence for Oligocene ice development comes from the record of glaciomarine ice rafted sediments from as far north as 58°S (Miller *et al.*, 1991). The development of the Earth's cryosphere caused fundamental changes in the global atmospheric and oceanic circulation which caused a latitudinal compression of climate zones and increased acidification (Frakes *et al.*, 1992) which, in turn affected biotic evolution through the Cenozoic. Since the storage of ice on land dramatically effects sea-level, coupled with the many waxing and waning events of the Oligocene to recent ice sheets, considerable changes in the distribution, and character of oceanic sediments have occurred (Miller *et al.*, 1991).

The causative mechanisms for the overall Cenozoic cooling are not totally understood. It is generally thought however, that the isolation of Antarctica and the Southern Ocean, due to the northward migration of Gondwanaland and the closure of oceanic gateways, led to the development of the Antarctic Circumpolar Current, which thermally isolated the Southern Ocean from warmer subtropic oceanic gyres (Frakes *et al.*, 1992). The step-wise cooling can be attributed to various feedback mechanisms that resulted from the development of the cryosphere itself (Kennet, 1995) that in turn heightened the cooling process (see section 1.10.2).

1.9.1 The character and causes of the mid-Miocene climate transition

Research on Miocene sediments reveals that this period hosts important changes in the oceanographic and climatic evolution of the Cenozoic (Flower and Kennett, 1994b). The mid-Miocene transition divides the Neogene into two distinct periods, a warm early Neogene and a cool late Neogene (Flower and Kennett, 1994a).

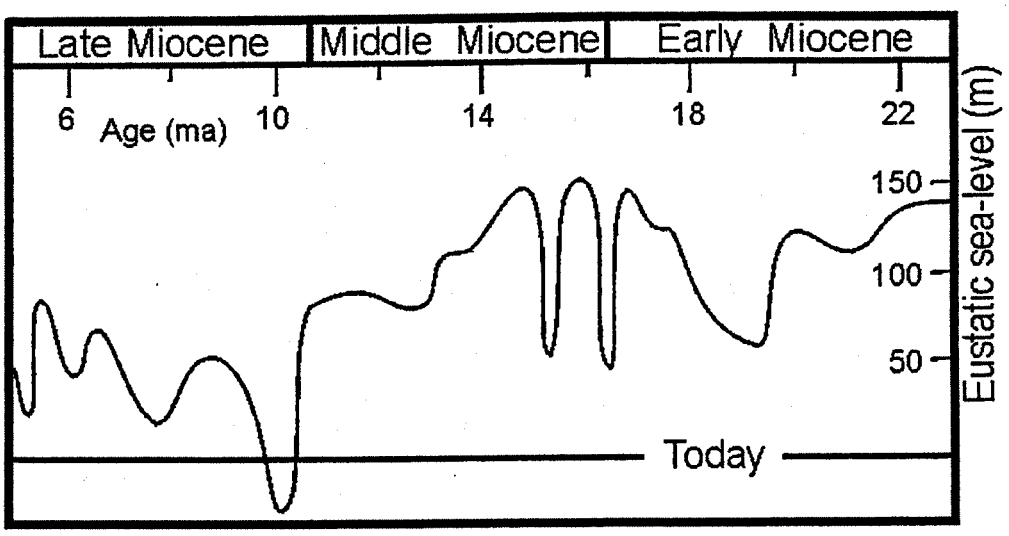

Figure 1.9 Miocene sea-level curve, relative to the present day. Note high frequency large amplitude variations in the early- to mid-Miocene, with two successive sea-level falls in the remainder of the Miocene. Redrawn from (Haq *et a.l*, 1987).

The early Miocene (23-16 Ma) was relatively warm with little ice stored on land, as exemplified by the $\delta^{18}O$ record, with the lowest $\delta^{18}O$ values for the entire Neogene in the late Early Miocene (Kennet, 1995). Palaeontological evidence also suggests relative climatic equity. A study of Early Miocene coal seam plant taxa, in Latrobe Valley, Southern Australia, suggest that mean annual temperatures may have been about 5°C higher than those of today (Kershaw, 1997). Early Neogene warmth was also expressed in the Northern Hemisphere, evidenced by laterized palaeosols in Japan, along with a marine molluscan assemblage, representing palaeotemperatures some 6°C higher than today (Itoigawa and Yamanoi, 1990). The extent of warming reached as far north as Eastern Siberia and Kamchatka, where subtropical palynofloras are present during the Early Miocene (Volkova *et al.*, 1986). However, the Northern Hemisphere lacked an ice sheet during this time due to the absence of a polar continent, on which a permanent continental ice sheet could be supported and preserved with relatively less temperature reduction compared to today (Thiede *et al.*, 1989).

The transition to a cooler climate is marked by a large increase in the benthic foraminiferal $\delta^{18}O$ of ~1.0-1.3‰ that occurred between ~16.5-12.5 Ma (Miller *et al.*, 1991; Shackleton and

Kennet, 1975; Vincent and Berger, 1985; Vincent *et al.*, 1985). The cooling is thought to be associated with the production of cold Antarctic deepwater caused by the growth of the East Antarctic Ice Sheet (EAIS). The EAIS was clearly not stable through its growth phase as high-amplitude eustatic sea-level fluctuations are noted from ~16-14 Ma followed by a two step, semi-permanent sea-level fall between ~14 and 12.5 Ma, see Figure 1.9 (Haq *et al.*, 1987). Ice rafted deposits were not present around the Antarctic during the Early Miocene, but appear during the mid-Miocene, and increase in frequency and abundance (in East Antarctica), to reach a climax in the late Miocene (Flower and Kennett, 1994a). The abrupt cooling led to a contraction of the tropical and subtropical provinces (Kennet, 1995), though low latitude warmth persisted contemporaneously with the East Antarctic Ice Sheet growth, as early Miocene tropical reef communities continued to grow through the mid-Miocene (Flower and Kennett, 1994a). Planktonic foraminiferal and calcareous nanofossil assemblages in Antarctica waters became essentially monospecific during the mid- to late-Miocene, reflecting high latitude cooling (Kennet, 1995). The cooling event heightened aridity in many continental areas. The assemblage of wind-blow clay off eastern Australia changed during this time recording a trend of increasing aridity (Kennet, 1995).

The newly developed ice house state strongly altered oceanic circulation. Cold, saline water produced at Antarctica sank and flowed away from polar areas, allowing a thermohaline stratification to develop with the warmer surface waters acting as a return flow from low latitude regions. This circulatory style, and the intensification of oceanic currents further developed nutrient rich upwelling zones, which in turn promoted deposition of siliceous biogenic sediments, as plankton with siliceous tests thrive in cooler nutrient rich waters (Kennet, 1995). Increased circulation invigorated the oceanic nutrient budget, which produced a rise in biogenic sedimentation. It also led to the redistribution of biogenic silica and carbonate deposition so that from ~18 to 12 Ma the locus of biosiliceous deposition moved from the North Atlantic Ocean to the North Pacific and Indian Oceans. This is termed the "silica switch" (Keller and Barron, 1983). Increased storage of organic material

acted as a feedback mechanism to perpetuate an icehouse state; this positive feedback is discussed further in the next section.

1.9.2 The Monterey Carbon Isotope Excursion

The middle to upper Miocene age Monterey Formation of California is composed of siliceous and organic-rich mudstones (Hornafius, 1991). It records the deep marine phase of a major late Cenozoic basin formation and infilling, associated with wrench faulting along the California margin (Isaacs *et al.*, 1983). The base of the Monterey Formation shows an upward decrease in clastic sedimentation rate, with the top defined by an upsection increase in detrital sedimentation (Hornafius, 1991). In general terms the formation can be sub-divided into three facies; a lower calcareous facies, a middle transitional phosphatic facies, and a thick upper siliceous facies composed of diatomaceous rocks and their diagenetic equivalents (Isaacs *et al.*, 1983). The Monterey Formation has an unusually high total organic carbon (TOC) level, especially in the mid-Miocene, where values can exceed 25% (Isaacs, 1998). For this reason scientific, research on the formation is considered important for both atmospheric CO_2 studies, and as a major oil source rock for southern California (Hornafius, 1991). There are many mid-Miocene, organic-rich deposits around the Pacific-rim, especially on the western margin of North America (Flower and Kennett, 1994b). The study

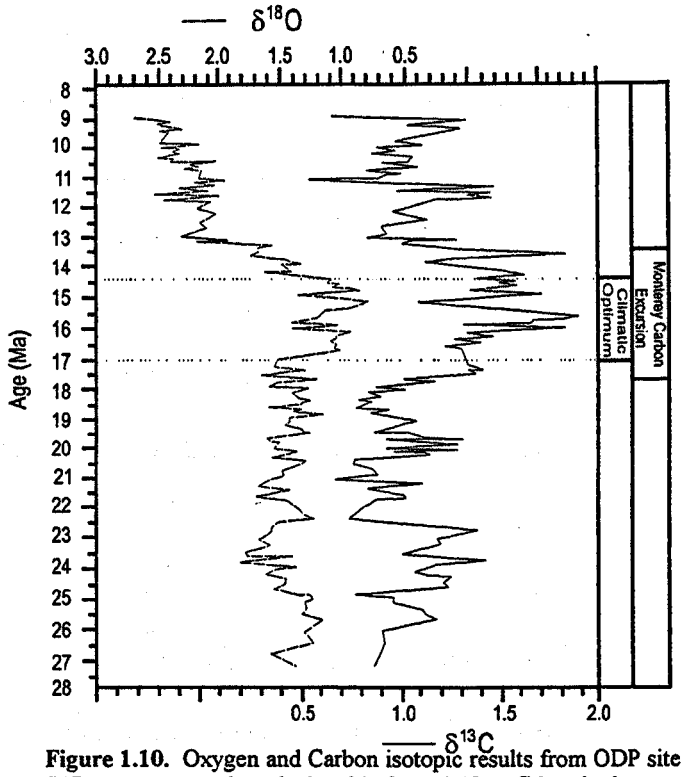

Figure 1.10. Oxygen and Carbon isotopic results from ODP site 747 measured on the benthic foraminifera *Cibicidoides* spp. by Wright, 1992. Note the early Miocene climatic optimum between 17 and 14.5 Ma shown by low $\delta^{18}O$ values. The Monterey Carbon Excursion is marked by high $\delta^{13}C$ values and slightly precedes the mid-Miocene cooling event. Modified from Hodell, (1994).

of the Monterey Formation, led to the recognition of similar sediments, and their link with global cooling events.

Penecontemporaneously with the deposition of the Monterey Formation there is a well-known substantial positive shift in the $\delta^{13}C$ in marine carbonates (Flower and Kennett, 1993b). The $\delta^{13}C$ of marine carbonate reflects the seawater $\delta^{13}C$ composition at the time of formation, so measuring the $\delta^{13}C$ of marine calcareous foraminifera will gauge palaeoceanic chemistry. Vincent and Berger (1985) termed this shift in $\delta^{13}C$ as the "Monterey Carbon Isotope Excursion" and attributed it to the deposition of organic-rich deposits, such as the Monterey Formation. The seawater $\delta^{13}C$ is related to the photosynthesis-respiration process, which results in the preferential removal of ^{12}C from surface waters by organic productivity (Frakes *et al.*, 1992). Consequently positive shifts in $\delta^{13}C$ relate to periods of high productivity, which leads (under the right circumstances) to the storage of carbon in deep-sea sediments. Flower and Kennet (1993a) demonstrated that sequestering ^{12}C in organic deposits raises $\delta^{13}C$ and lowers ΣCO_2 in the oceans, relatively increasing the carbonate ion content of the oceans. This has important implications for carbonate preservation. During periods of high organic productivity ($\delta^{13}C$ maxima) there is an increase in carbonate preservation. When organic-carbon is transferred back to the oceans ($\delta^{13}C$ minima) ΣCO_2 is raised and there is a carbonate ion deficit, resulting in an increase in carbonate dissolution.

Organic carbon ultimately originates from atmospheric CO_2 via the process of photosynthesis. This together with the storage of organic-carbon buried in oceanic sediments results in the reduction of atmospheric CO_2 levels (Flower and Kennet, 1993a). The ~1‰ shift in $\delta^{13}C$ during the Monterey $\delta^{13}C$ Excursion starts at ~17.5 Ma, and lasts for approximately 4 million years and is illustrated in Figure 1.10 (Vincent *et al.*, 1985). According to Vincent and Berger's (1985) Monterey hypothesis, intensification of the mid-Miocene cooling event was due a decrease in atmospheric CO_2, which resulted in a reverse

greenhouse feedback process. The reverse greenhouse process is heightened by increased oceanic circulation caused by polar cooling, which supplies more nutrients to upwelling areas, promoting increased productivity and further draw down CO_2 from the atmosphere. This positive feedback loop is broken when the supply of nutrients diminishes, or when the sea-level falls associated with ice growth limit shelf areas acting as sites of deposition.

Evidence for the "Monterey effect" is shown by both O and C isotopes. (Woodruff and Savin, 1991) observe that there is a positive correlation between $\delta^{18}O$ and $\delta^{13}C$ from 16 to 13.7 Ma (Figure 1.10), which terminates and the end of the Monterey Carbon Excursion. High resolution isotope analysis reveals that individual $\delta^{13}C$ maxima, within the excursion, are coincident with $\delta^{18}O$ increases and are inferred to result from deep water cooling associated with EAIS growth (Flower and Kennet, 1993a). The initiation of the Monterey Carbon Excursion precedes the mid-Miocene cooling event by some 1.5 Ma (Figure 1.10). It is thought (Flower and Kennet, 1993a; Flower and Kennett, 1993b) that this time lag relates a threshold level whereby the atmospheric partial CO_2 level had to be drawn down before significant cooling occurred. An alternative hypothesis for the time lag suggests that the eruption of the Columbia River Flood Basalt complex stalled the reduction of atmospheric CO_2 via an opposing greenhouse effect caused by the emission of large quantities of CO_2 during eruption (Hodell and Woodruff, 1994).

1.10 Thesis structure

This thesis is divided in to six other chapters. Chapters 2-5 deal with the deepwater facies of the Miocene-aged Pakhna Formation. As these chapters progressively characterise and interpret the Pakhna Formation, the main conclusions for the Miocene analysis are in Chapter 5. Chapter 6 documents the nature of Pliocene-Pleistocene sedimentation in southern Cyprus. Chapter 7 concludes the study, by reviewing the main findings and outlines views on possible further work.

Chapter 2

This chapter is divided into two subsections. This first section introduces the reader to the deepwater facies of the Pakhna Formation and discusses the geological processes that lead to their deposition. The second section places the study sections into a biostratigraphical (calcareous nannofossil) framework.

Chapter 3

Chapter 3 deals solely with the sequence stratigraphical interpretation of the Pakhna Formation. The sequence stratigraphical framework, constrained by biostratigraphy, forms the temporal scale for subsequent analysis.

Chapter 4

This chapter documents the statistical analysis of bed thickness and lithology data, and shows how regular cyclicity has been identified in the Pakhna Formation.

Chapter 5

This chapter combines data from Chapters 2-4 and places it in the context of stable carbon and oxygen isotope analysis. It documents the presence of the mid-Miocene Monterey carbon Excursion and associated cooling events in the Mediterranean.

Chapter 6

Chapter 6 investigates the facies, biostratigraphical and sequence stratigraphical interpretation of a Pliocene-Pleistocene-aged, deep-sea fan complex in southern Cyprus.

Chapter 7

Chapter 7 reviews the main conclusions of the thesis and places them in the context of the Miocene to Recent evolution of Cyprus.

Chapter 2

Deep Marine Miocene Sedimentation in Cyprus

2.1 The Troodos cover sequence

Since the emplacement of the Troodos Ophiolite in the late Cretaceous, (Gass 1994 *et al.*; (Clube and Robertson, 1986) thick (~200-1000m) deposits of sediments were deposited upon it. These sediments are termed the Tertiary Cover Sequence, though sedimentation actually commenced in the Campanian Maastrichtian (Robertson and Hudson 1974 (Kahler, 1998) with the metalliferous sediments and siliceous oozes of the Perapedhi and Kannaviou Formations deposited directly on pillow lava surface of the ophiolite. It is only relatively recently that more extensive research on the cover sequence has revealed its importance in terms of understanding the uplift history of the Troodos Ophiolite, the tectonic evolution of the Eastern Mediterranean (Robertson, 1977; Follows 1990; Eaton and Robertson, 1993; Morse 1996; Robertson 1998) and as a record of Miocene climate and oceanographical changes (this thesis).

The Lower Palaeocene to Upper Oligocene (Morse 1996) Lefkara Formation (Figure 2.1) is the lowest major laterally extensive division of the cover sequence and comprises deep marine chalk with secondary chert. The Lefkara chalks are diachronously overlain by the Pakhna Formation. The latter ranges in age from the lower Miocene (Aquitanain) to the Upper Miocene (Tortonian) and was first formally attributed to the Dahli Group by Henson *et al.*, (1949). The absence of chert and the presence of more terrigenous clay in the chalk of the Pakhna Formation is used to distinguish it from the underlying Lefkara Formation chalks. There are two sporadically distributed members within this formation (Terra and Koronia Members); both consist of reefal limestone facies and were extensively studied by Follows (1992). The remainder of the Pakhna Formation is composed of chalk and marl couplets,

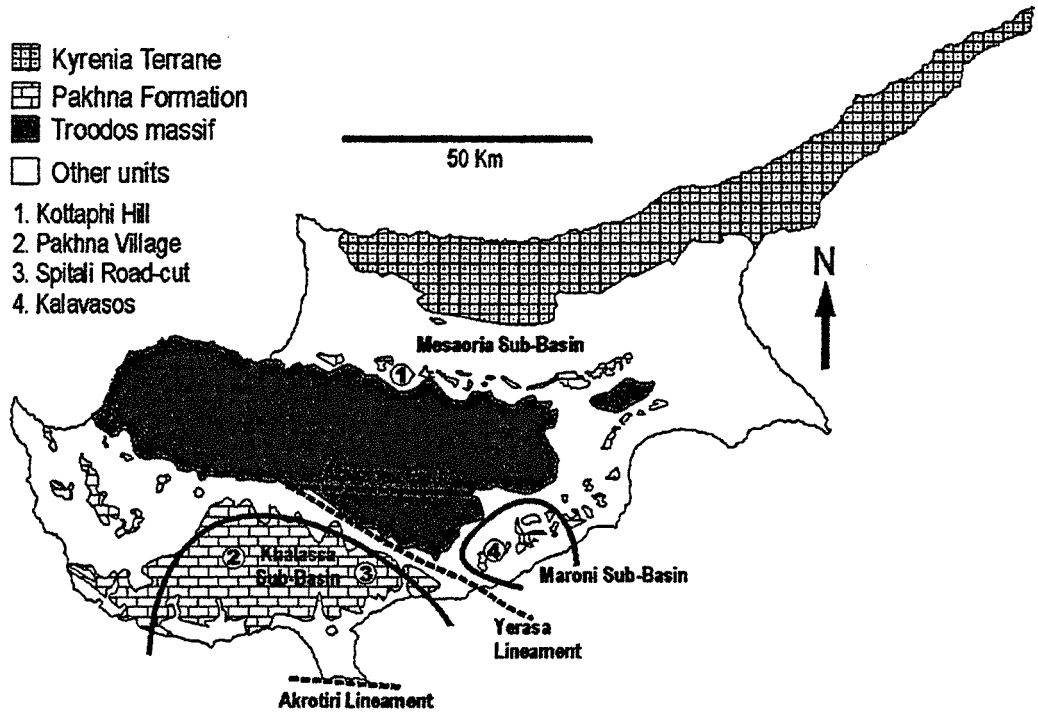

Figure 2.1 Map of Cyprus showing the Field Localities and the outcrop of the Pakhna Formation in relation to the Troodos and Kyrenia terrains. Note basin compartmentalisation and structural lineaments. (1) Kottaphi Hill, (2) Pakhna Village, (3) Spitali Road Cut, (4) Kalavasos. Redrawn form Eaton and Robertson (1993)

calcarenites and coarse-gained debrites. Eaton and Robertson (1993) provide a detailed study of the Pakhna Formation and recognise five facies associations. From proximal to distal, these are: (i) the Peripheral Sands Association; (ii) the Gullied-slope Association; (iii) the Channel-fill Association; (iv) the Basin-margin Association and (v) the Basin Plain Association. The Peripheral Sands Association comprises of amalgamated, massive coarse-grained bioclastic calcarenites. Provenance studies suggest clasts derived from three sources: (i) contemporaneous shallow water areas; (ii) the Troodos ophiolitic terrain and (iii) the Mamonia Complex. The Gullied-slope Association is split into: (i) fine grained successions composed of foraminiferal chalk, silt marlstone and laminated calcilutites, and (ii) the channel-fill successions comprising calcarenites and clast supported polymict conglomerates. The Basin-margin Association is characterised by massive, graded calcarenites, interbedded with chalks and marls, with local occurrences of conglomerates and slump features. The Basin-plain Association lithologies are dominated by planktonic foraminiferal, nannofossil chalk and marl. Eaton and Robertson's (1993) depositional model for the Pakhna Formation

remains valid for this study. This chapter concentrates on the sediments of the Basin-margin and Basin Plain Associations.

As a result of this study the Pakhna Formation has been further lithostratigraphically subdivided. Figure 2.2 illustrates the subdivisions of the Pakhna Formation as proposed in this study. This study splits the Pakhna Formation into four Members: Kottaphi Member (chalk/marl couplets), Spitali Member (calcarenites interbedded with chalk and marl), Agrokipia Member (marl), and Koronia Member (Reef Limestones). The lower Miocene-aged reef limestone, the Terra Member is not described further in this study. The Spitali Member is characterised by an increase in allochthonous calcrudite-calcarenite deposits, inter-bedded with the pelagic chalk/marls of the Kottaphi Formation. The base of the Spitali Member is highly gradational with the Kottaphi Member and has rapid lateral and vertical facies variations. The ages for the Pakhna Formation are derived from calcareous nannoplankton biostratigraphy and are compared to the integrated timescale of Berggren *et al.* (1995) are discussed further in section 2.3.

The evaporitic facies of the Kalavasos Formation overlies the Pakhna Formation and are penecontemporaneous with other similar facies deposited in Mediterranean region during the Messinian. A major transgression during the Pliocene restored marine conditions, though the sedimentary structures and fossils in the resulting siltstones and calcarenites of the Nicosia Formation indicate shallow water sedimentation (Avery, 1997; Givens, 1997). Due to rapid uplift of the Troodos terrain in the Pleistocene, the Nicosia Formation is overlain by coarse-grained sandstones, conglomerates and breccias (the Fanglomerate Group, Wilson, 1959).which represent major incision and erosion of the Troodos ophiolite.

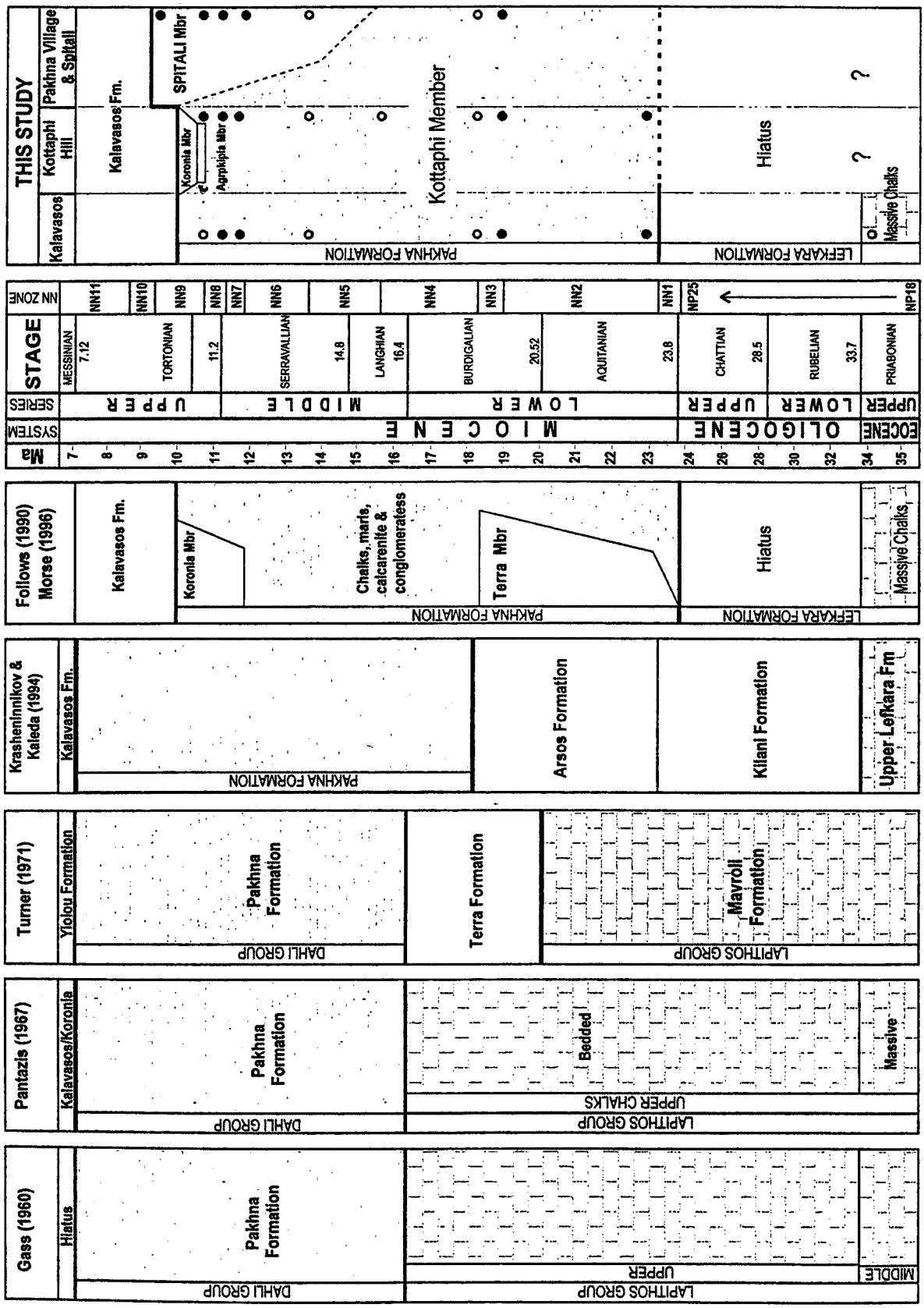

Figure 2.1 The lithostratigraphical classification of different authors for the late Eocene to late Miocene sediments of Cyprus. Redrawn from Morse (1996). ⊛ - FO biostratigraphical datum, ⊙ - LO biostratigraphical datum for this study.

2.2 Deep Marine Facies of the Pakhna Formation

Figure 2.1 illustrates the four field localities used to describe the deep-marine facies of the Pakhna Group. Kottaphi Hill (1) is situated to the north the Troodos mountains, where the Pakhna outcrop is restricted to a thin band by the overlying Nicosia and Fanglomerate series deposited in the Mesaoria sub-basin. The Pakhna village (2) , Spitali (3) and Kalavasos (4) locations are aligned west to east, south of the Troodos massif. Kalavasos and Kottaphi Hill contain similar facies, whereas Spitali and Pakhna Village host a considerable allochthonous component, making up ~15-30% of sediment thickness. These basic facies differences across Cyprus probably result from partial basin compartmentalisation, during the early-mid Miocene (Eaton and Robertson, 1993) where local tectonics and sources of terrigenous sediment differed between basins. The Spitali and Pakhna Village localities lie within the Khalassa sub-basin and Kalavasos within the Maroni sub-basin. Compartmentalisation was caused by a series of WNW-ESE trending lineaments produced by the deformation of the Limassol Forest Block in the early-mid Miocene, which was thrust south-westwards over the Lower Tertiary cover sequence (Morel, 1960). The Yerasa fold and thrust belt is the most prominent of these lineaments and separates the Khalassa sub-basin effectively detaching the Pakhna village and Spitali localities, from Kalavasos in the Maroni sub-basin (Eaton and Robertson, 1993). The early-mid Miocene timing of this uplift, centred around the Limassol Forest Block coincides with the gradual introduction of allochthonous facies of the Spitali Member in the upper sections of the Pakhna Village and Spitali sections in the Khalassa sub-basin in biozone NN5.

2.2.1 Autochthonous Sediments

The autochthonous sediments comprise pelagic carbonates that are differentiated into four facies by their relative proportion of terrigenous clay. The four facies represent a balance between two fluxes; carbonate rain produced from planktonic organisms and clay minerals from fluvial and aeolian input. The marl facies indicates periods of increased terrigenous clay

flux entering the depositional environment. Figure 2.3 shows the weight percentage of the non-carbonate material within the four facies, deduced from removal of carbonate by HCL. The amount of clay roughly halves with each step towards the purer carbonate of the chalk facies. Figure 2.4 illustrates a section of graphic log from Kottaphi Hill, the full logs are in Appendix A. The bulk of the section is composed of just four facies which are described in detail below. The four facies are stacked in couplets (Figure 2.4 and 2.5), with a relatively clay-rich bed overlain gradationally by a purer carbonate, suggesting that this was a gradual transition. The contact between the purer carbonates and the overlying relatively clay-rich beds is mostly sharp, and therefore defines the base of each couplet. Such variations in carbonate content are common in deep sea chalk successions (Fischer, 1993; Olivero, 1996) and were interpreted to represent the Earth's precessional cycles in 1895 (Gilbert, 1895).

Foraminiferal chalk facies

The foraminiferal chalk facies is prevalent throughout all exposures of the Pakhna Group. It is typically white in colour and usually contains less than 5 wt% clay. The chalk varies from a wackestone to a packstone depending upon the abundance of bioclasts, though it dominantly displays packstone characteristics as it is grain-supported (~50–70% grains), with a matrix of coccolith ooze. Bioclastic material is dominated by pelagic foraminifera, which are clearly visible in hand specimen Other bioclasts include echinoderm and bivalve fragments. Macro fauna is extremely rare but complete nautiloids have been found within this facies at Pakhna Village (*i.e.* bed number 125 and 208) and Spitali Road Cut sections (*i.e.* bed number 598 and 885). The facies is often well bioturbated the trace fossil assemblage is dominated by *Thalassinoides* and *Teichichnus* with less amounts of *Chondrites and Zoophycos.* At Kalavasos, this facies and the marly-foraminiferal chalk facies often have sub-centimetre discontinuous marly stringers, which gave rise to the Wavy-Bedded Limestone Member classification by Bagnall (1960). Bagnall (1960) suggests that they probably originate from irregular reaction to loading, and from adjustment by flowage in water laden, fine-grained

sediments. This wavy or flaser bedded chalk has also been noted in the Cretaceous-age chalks of England, and is thought to arise from the dissolution of carbonate resulting in the concentration of marl in wavy bands (Kennedy, 1975). The facies is interpreted here to represent deposition in a deep marine environment (below storm wave base) during periods of low terrigenous input.

Marly foraminiferal chalk sub-facies

Foraminiferal chalks that are an off-white to buff in colour, and contain around 10 wt% terrigenous clay, are classified as marly-foraminiferal chalks. They are slightly less resistant to weathering than the more robust foraminiferal chalks, due to their greater clay component, but do not fragment easily like the more clay-rich marl facies. These again were deposited in a deep marine environment, though the flux of terrestrial material was sufficient to reach the depositional environment in the form of weak suspension fall-out, which cause a slight dilution of the carbonate rain. Bioturbation is common within this facies and remains similar to that of the foraminiferal chalk facies.

Marl facies

The marl facies has a wackestone texture and contains pelagic forams and mollusc debris suspended in a matrix of terrigenous clay and coccolith ooze. The marl is typically light-grey in colour and preferentially weathers away due to its relative softness compared to the chalk. When wet the rock is easily fragmented. The marl facies contains ~30% clay which indicates a period of increased influx of terrigenous clay into the depositional environment. This has the effect of significantly diluting the background sedimentation of carbonate rain, as pelagic foraminifera and coccoliths are still present as grains in the matrix. *Chondrites* burrows are the dominant ichnotaxa, though towards the upper parts of the beds, minor *Thalassinoides* burrows occur along with <5 mm fragmented bivalve debris . It is in this upper part of the

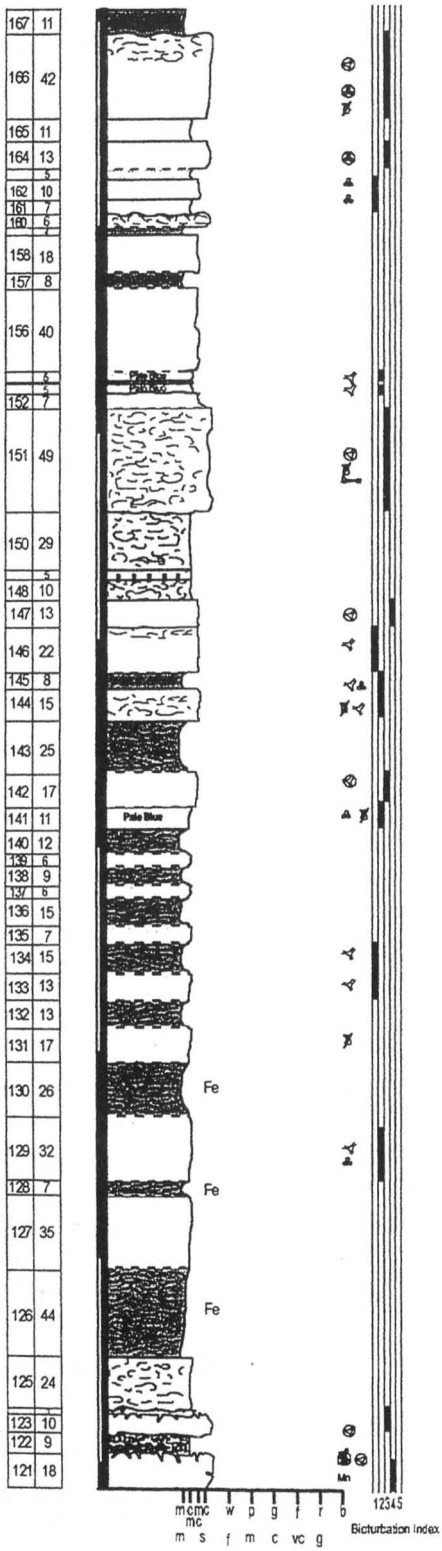

Lithology	Original Weight (g)	Remaining Weight (g)	Clay (Wt.%)
Marl	59.7	18.3	30.7
Cemented Marl	57.5	10.9	19.1
Marly-Chalk	56	5.3	9.3
Chalk	54.1	2.3	4.3

Figure 2.3 Weight percentage clay for the four facies, deduced from the dissolution of the carbonate fraction by HCL.

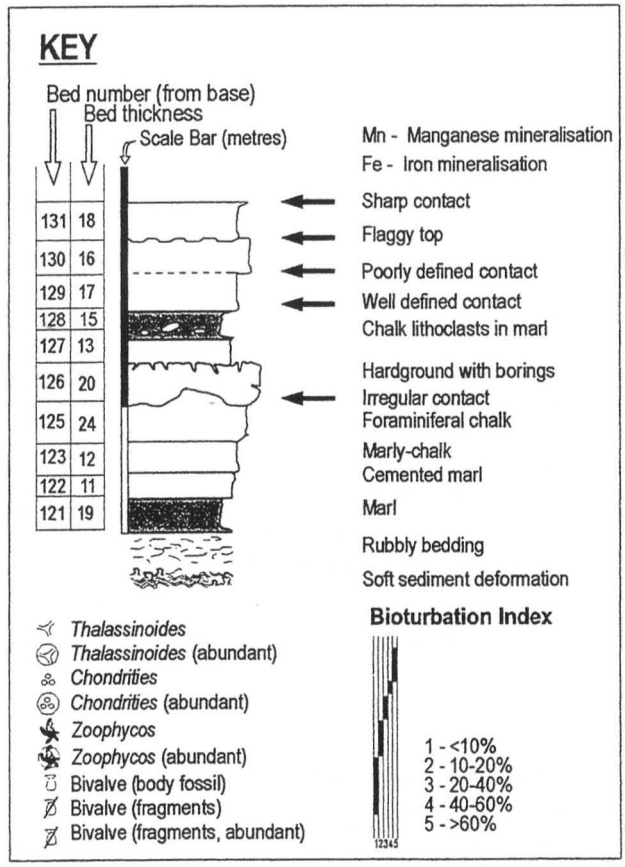

Figure 2.4 Section of a graphic log from Kottaphi Hill. Note that the couplets change from marl rich to carbonate rich between beds 141 and 142. Full logs in Appendix A

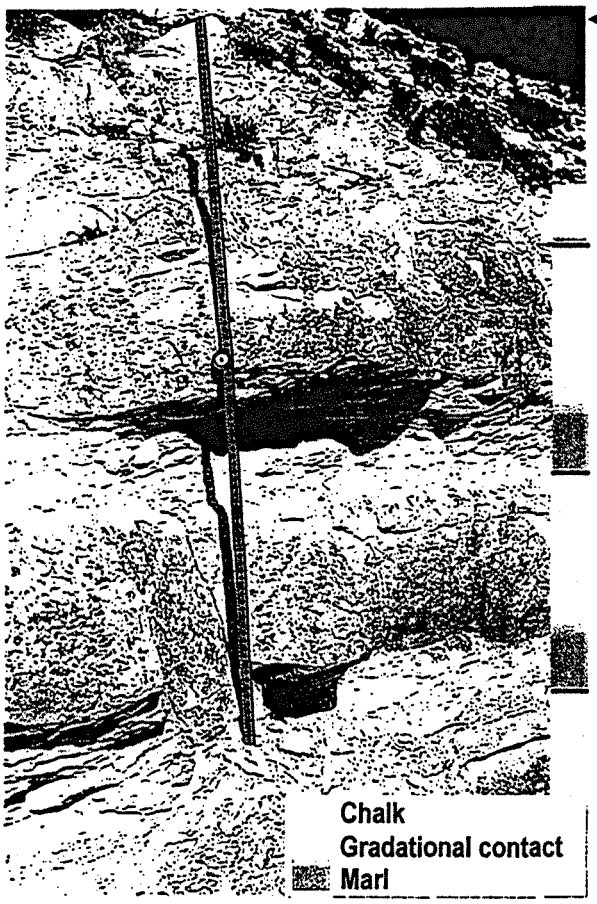

Figure 2.5 Photograph from Kottaphi Hill showing the weathering profile of three and a half marl-chalk couplets. The marls, forming the base of the couplet, are preferentially weathered compared to the overlying foraminiferal chalks. Scale bar is 1 metre.

Figure 2.6 Soft sediment deformation caused by de-watering, in a marl-rich inter-hardground bed. Scale in centimetres.

Figure 2.7. Detailed view of a hardground surface at Kottaphi Hill (bed 123). Note the abundance of pre-lithification *Zoophycos* traces, and dark Manganese mineralisation. Scale bar is in centimetres.

marl beds that the carbonate content starts to increase, as suggested by a lightening in colour and an increase in the resistance to weathering. The contact with the overlying chalk is gradational. This gradational zone often shows a slight concentration of bivalve fragments (mainly oysters) relative to the remainder of the marl bed. This suggests that environmental factors were encouraging colonisation, probably due to increased oxygenation.

Cemented marl sub-facies

The cemented-marl facies is distinguished from marl usually by its tendency to be more resistant to weathering, it does not disintegrate so easily when handled, especially when wet, and subsequently has a blockier weathering profile. Its trace fossil assemblage, like the marl facies, consists mainly of *Chondrites* with minor *Thalassinoides.* It represents a period when the terrigenous flux wanes slightly compared to the marl facies, resulting in the carbonate rain being less diluted, allowing a marl to form with a higher concentration of carbonate, but still a having ~20% clay content.

Hardgrounds, Nodular Chalks and Firmgrounds

Many hardgrounds have been identified within the study sections, the most notable of which is at Kottaphi Hill (Figures 2.4 (bed number 123), 2.6 &.2.7; Appendix A). The hardgrounds form at the top of foraminiferal-chalk and marly-foraminiferal-chalk facies beds. They tend to make the foraminiferal chalk and marly foraminiferal chalk beds harder, more resistant, and sound metallic when stuck with a hammer. This is caused by increased cementation, that occurred at, or near to, the sediment water interface during the earliest stages of diagenesis. The bedding surfaces are often irregular and occasionally nodular. The main hardground at Kottaphi Hill (bed 123, Figure 2.4) shows sporadic dark grey-black and red mineralisation, probably manganese and iron. The *Zoophycos* ichnotaxa is very abundant on the top surface of bed 123 (Figure 2.7) and must have been created prior to lithification of the bed, it also suggests that there was a significant reduction in sedimentation rate, to allow time for

successive generations of the *Zoophycos* animal to populate the surface to account for its abundance. Beneath this hardground there are thinly bedded marls which display soft sediment deformation due to de-watering (Figure 2.6). These structures are interpreted to have formed due to the increased impermeability and weight caused by the early marine cementation of the overlying hardground. Fluid migration would then be confined to conduits between the lithified blocks that coalesce to form a persistent hardground. *Thalassinoides* burrows are well defined and over print the *Zoophycos* traces. Both these ichnotaxa are, in-turn, over printed by borings. Boring organisms require a solid substrate, so they must have formed once lithification was nearly complete. Borings also indicate that the hardground surface was exposed at the sea bed as the substrate had to be available for the colonisation of boring organisms. Mineralisation of the hardground suggests a significant hiatus in deposition. The successive tiering of ichnofacies reflects changing conditions in the sediment substrate during the progressive cementation stages of the hardground. The significance of the main Kottaphi Hill hardground is discussed further in terms of sequence stratigraphy and climate in Chapters 3 and 5.

Bed number 71 at Kottaphi Hill is a good example of a nodular bed. In these cases early diagenetic cementation was only sufficient to form a semi-continuous nodular horizon instead of displaying a continuously lithified layer like true hardgrounds. This is probably a result of the nodular chalk bed not having enough time in the zone of cementation, possibly due to an increase in sedimentation rate. It was not exposed for long periods on the sea floor, as the lithified nodules lack borings and/or mineralisation.

Firmgrounds are the hardest of the early cementation beds to identify, as they only represent the first stages of diagenetic cementation, and therefore represent relatively little time when compared true hardgrounds and nodular chalks (Kennedy, 1975). Bed Number 166 at Kottaphi Hill however is a good example of a firmground. The bed is more resistant than the

foraminiferal chalk facies, and trace fossil walls are well defined with sharp edges and the spreite are well developed.

2.2.2 Allochthonous sediments

At Spitali and Pakhna Village localities many beds contain a significant allochthonous component which is not seen at Kalavasos or Kottaphi Hill. These beds occur throughout these sections, but tend to be concentrated towards the top. They appear in several forms and vary according to composition and grain size (fine- to coarse-grained calcarenites, and calcrudites).

Silty-mudstone facies

The silty-mudstone facies is only present at the Pakhna Village locality (e.g. bed number 60), and occurs in relatively thick (20-100 cm) beds. It is characterised by a dark brown colour and extremely poor cementation, it weathers recessively leading to marked undercutting of the overlying bed, and produces muddy talus. It often shows well defined planar lamination picked out by slightly coarser-grained, paler brown, fine-grained calcarenites. These calcarenite layers can attain thickness of 2 cm though none are continuous for more than a couple of metres. These sediments have the lowest carbonate content of all the facies discussed in this chapter, displayed by the distinct dearth of nannoplankton and pelagic foraminifera. Where present, foraminifera are poorly preserved and corroded. Bioturbation is rare in this facies, partly due to its tendency to crumble, though the occasional *Thalassinoides*-type burrow is preserved in the coarser-grained layers and towards the top of the beds. The primary lamination suggests a lack of any infauna during the time of deposition. Fauna may have been excluded, due to anaerobic conditions or a period of increased sedimentation rates. The deficiency of the planktonic calcareous component suggests rapid sedimentation, as the persistent carbonate rain is highly diluted. These deposits probably represent an extreme end member for carbonate dilution, where the allochthonous, terrigenous derived material dominates.

Calcarenite facies

The calcarenite facies is the most abundant of the allochthonous facies, at Pakhna Village it is interbedded with more calcareous pelagic sediments (Figure 2.8). The bases of the allochthonous beds are erosional, and plane off the underlying chalks to produce sharp contacts. Bed truncation is not observed, however, 60 cm clasts of well-bedding chalk are found lying within medium calcarenite beds, and are obviously very locally sourced (Appendix A; Pakhna Village, bed number 253). This suggests that the weaker un-lithified units were planed-off by flows down to the more resistant semi- or fully-lithified unit. There is enough density contrast between the calcarenite and any underlying semi-lithified chalk to produce load and flame structures that accounts for the wavy bedding as illustrated in Figure 2.8 & 2.9. Fine-, medium- and coarse- grained calcarenites all have a similar composition. Clasts consist mainly of bioclastic and lithoclastic material. Bioclasts include reworked pelagic forams, echinoid and mollusc fragments, with rarer coral, nautiloid and scaphopod debris. Lithoclasts are composed of foraminiferal chalk, marl and basic igneous rocks. Normal grain size grading is often observed, particularly in the coarse-grained calcarenite units, where basal clasts can reach up to 5 mm in diameter (Figure 2.9). Many of the coarser-grained allochthonous units contain rip-up clasts from the chalks and marls below. These features suggest that the deposits arise from small scale debris flows. Bioturbation within the calcarenites is not as diverse as in the more calcareous deposits, and tends to be concentrated towards the top of the bed and dominated by *Thalassinoides.*

Debrites

Coarse-grained debris flows only occur near the top of the Spitali and Pakhna Village sections, within the Spitali Member. Good examples are shown at Spitali (bed numbers 719 and 775) and at Pakhna Village at (bed number 427). Figure 2.10 illustrates bed number 775 at Spitali. This polymictic breccia is texturally and mineralogically immature. The maximum clast size observed within these flow is 170 mm (c-axis), though the mean clast size is about

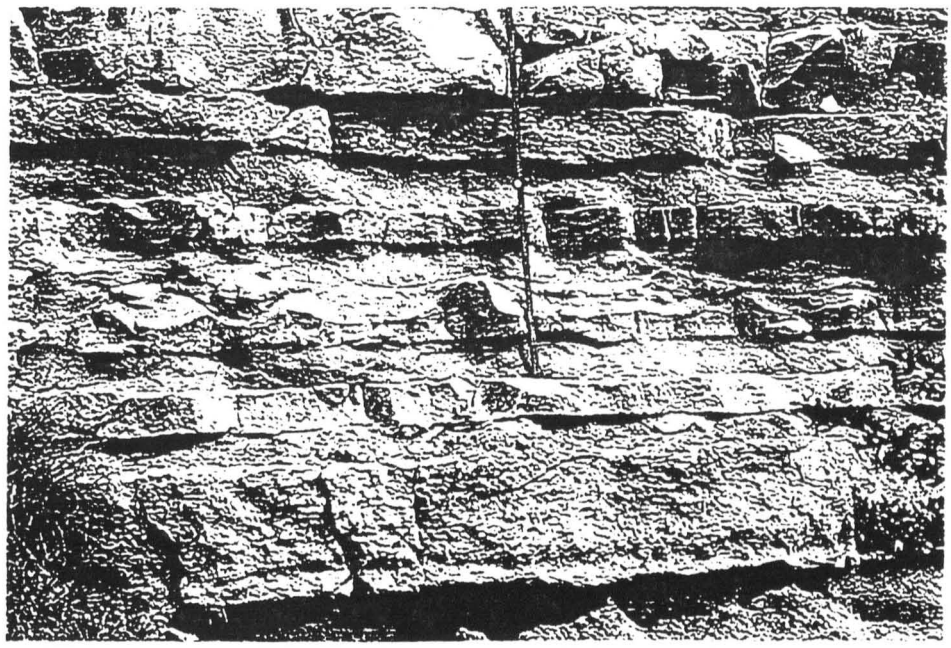

Figure 2.8. Photograph of interbedded fine- to medium-grained calcarenites at Pakhna Village. Note the wavy nature some of the bedding Pelagic carbonates are light grey, calcarenites are brown/red. Scale bar is 1 metre (25 cm sections).

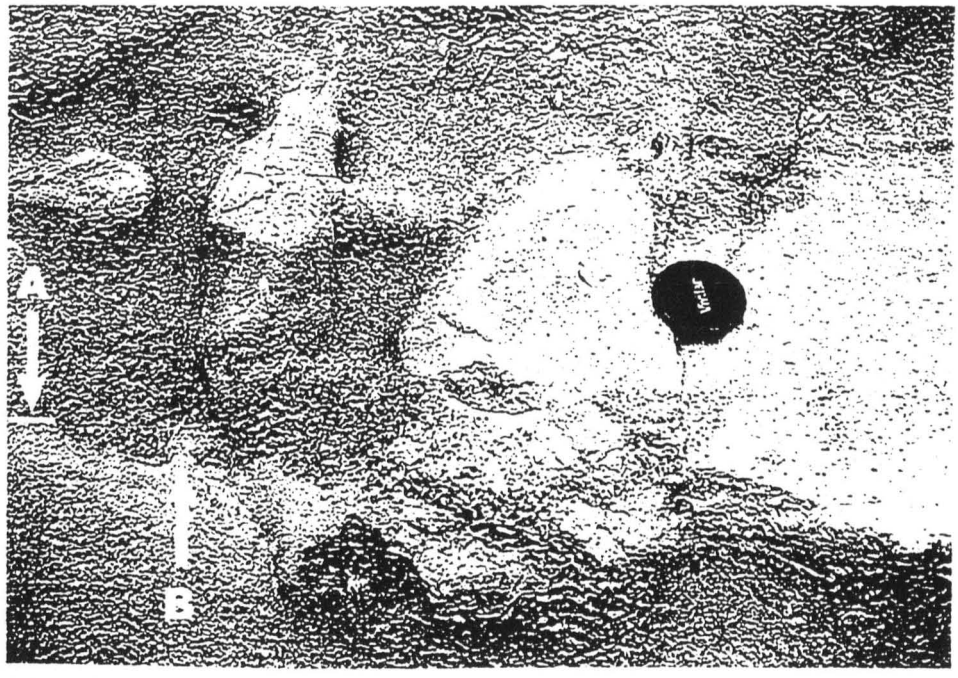

Figure 2.9. Photograph from Pakhna Village illustrating features of calcarenite beds. (A) Base of upper flow, note the coarse-grained base composed of 3-5mm basalt and chalk clasts. (B) Flame structures produced with the underlying medium grained calcarenite. The area around the lens cap (72 mm diameter) is an early diagenetic

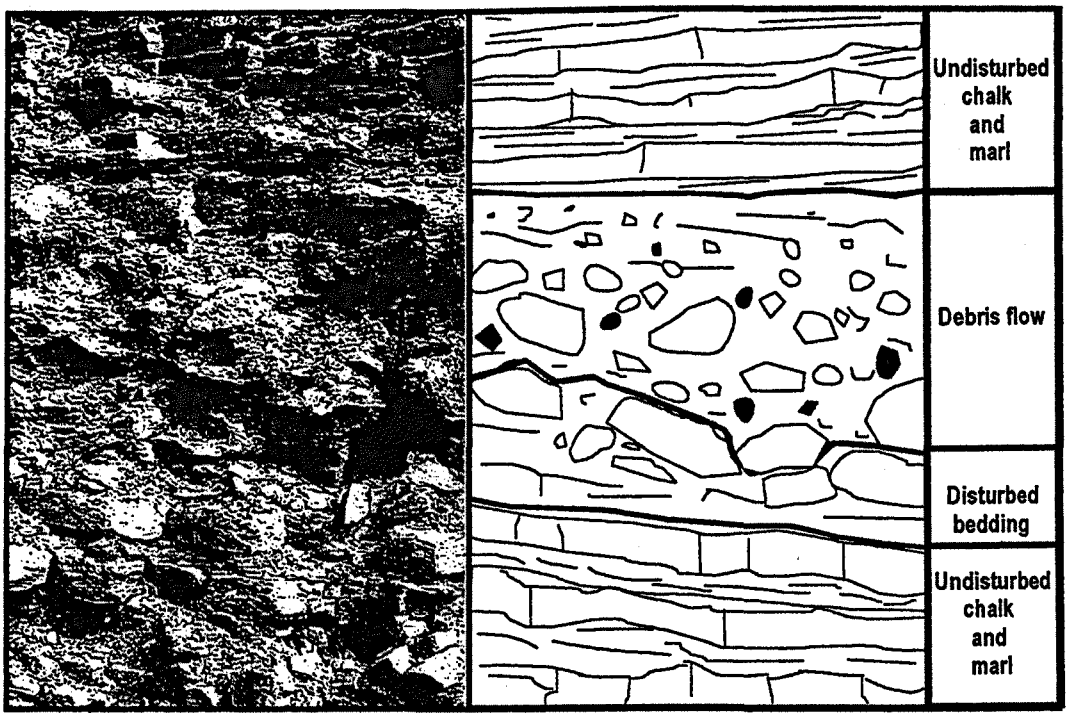

Figure 2.10. Photograph of a debrite (bed 775) at the Spitali road-cut. The flow is bounded, both above and below, by undisturbed, well-bedded chalk and marls beds. Immediately below the flow there is an area of disturbed bedding caused by the motion of the debris flow. The flow itself shows normal grainsize grading, until it becomes a bedded calcarenite before returning to undisturbed chalk and marls. Scale bar is 1 metre.

5-10mm with a finer-grained calcarenite matrix. Clast are composed of dominantly chalk and marl (larger clasts) with minor amounts of chert, reefal material (colonial coral fragments) and basalt. The debrite at Spitali (bed 775) had sufficient erosive power to disturb and fragment the underlying chalks and marls (Figure 2.10). There is evidence within these chalks and marls of soft sediment deformation due to the sudden input of clastic material. For instance, the debrite pinches out up dip, due to its broad lenticular structure (>30m). It attains a maximum thickness of about 1.8 metres, where the largest clast are concentrated. There is also significant truncation of the underlying chalks and marls, which can be seen to re-appear where the debrite pinches out. Its geometry and clast imbrication suggests a southerly flow direction.

In the Spitali Road Cut the debrites are more numerous and coarser-grained than at the Pakhna Village locality which is dominated by the calcarenite facies. This probably arises

due to Spitali's closer geographical position to the Troodos Ophiolite (5km compared to 10km from Pakhna Village) and hence the source of sediment.

2.3 Biostratigraphy of the Pakhna Formation

2.3.1 Previous biostratigraphical data on the Pakhna Formation

Figure 2.2 illustrates the ages of lithostratigraphical units defined by previous authors and compares the correlation with the lithostratigraphic units with the data gained from this study. Reconnaissance studies as part of regional mapping (e.g. Bagnall 1960; Bear, 1960; Gass 1960; Pantazis; 1967; Wilson, 1959) attributed the Pakhna Formation to be middle Miocene in age and form part of the Dahli Group (Figure 2.2). The Pakhna Formation was deposited diachronously during a transgression and in most areas has an unconformable contact with the Lefkara Formation (Pantazis, 1967). Samples of the basal Pakhna Formation collected from a borehole near Ayios Nikolaos (15 km north of Pakhna Village) suggest an Aquitanian age (Gass *et al.*, 1994; comparable to NN1-part NN2 calcareous nannofissil zonal range). Krasheninnikov and Kaleda (1994) suggest an alternative lithostratigraphical division of the Miocene-aged sedimentary cover of the Troodos Ophiolite (Figure 2.2). They date the base of the Pakhna Formation (their Kilini Formation, Member III; Morse, 1996) to the planktonic foraminiferal zone P22 (Oligocene-Miocene boundary), and date the biostratigraphical range of the entire Pakhna Formation to planktonic foraminiferal zones P22-N16 (NP25- part NN11 calcareous nannofossil equivalent). Morse (1996) conducted a detailed biostratigraphic study of the Cretaceous to late Miocene sediments in SW Cyprus. He dated the Pakhna Formation as ranging from NP25 -NN9 (latest Oligocene-early upper Miocene (Figure 2.2). Morse also identified that the entire Oligocene is absent in SW Cyprus (Figure 2.2).

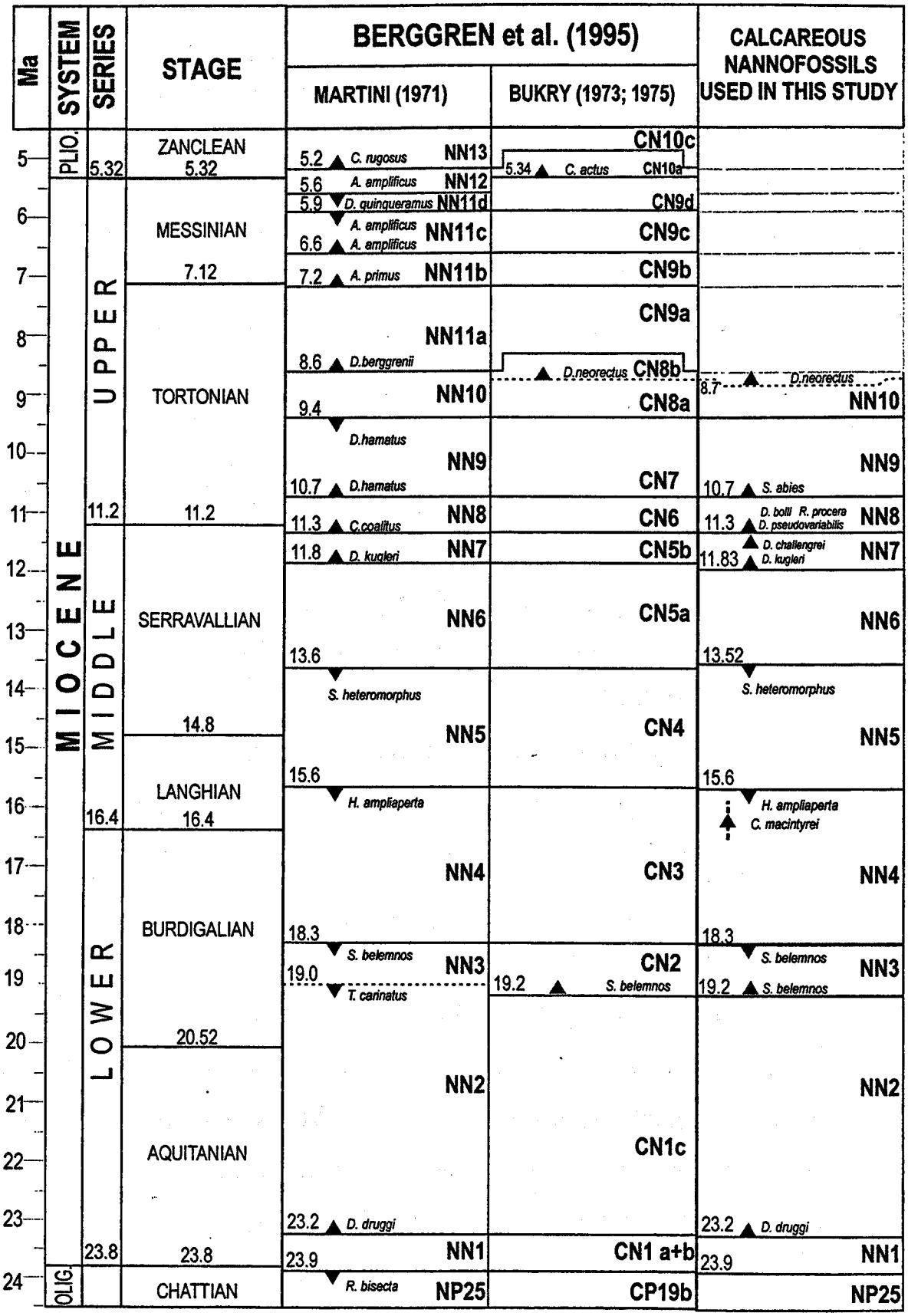

Figure 2.11. The calcareous nannofossil zonal schemes of Martini (1971) and Bukry (1973; 1975) for the Miocene. Zonal taxa from both schemes, and other age diagnostic taxa used in this study are indicated.

2.3.2 Calcareous nannoplankton as biostratigraphical markers.

182 samples were prepared using the standard smear slide technique (Appendix B) and analysed on an optical microscope (Olympus BH2). 126 samples, contained biostratigraphically useful taxa. The biostratigraphical schemes proposed by Martini (1971) and Bukry (1973; 1975) as revised by Breggren *et al.*, (1995) and Raffi (1999) have been applied with minor modification, outlined below. The scheme presented here has been calibrated to orbital cyclostratigraphy (Backman and Raffi (1997) and magnestostratigraphy (Maiorano and Monechi, 1998).

Figure 2.11 illustrates the biostratigraphical zonations of Martini (1971) and Bukry (1973; 1975), compared to the Breggren *et al.* (1995) absolute time scale, with the zonal markers from both schemes, and additional taxa implemented for biostratigraphy in this study. These zones are defined as follows:

NN1 (23.9-23.2 Ma)

The base of NN1 is defined by the last occurrence (LO) of *Rhabdolithus bisecta* to the first occurrence of *Discoaster druggii* (Martini and Worsley, 1970). The base of NN1 is not observed in the study sections.

NN2 (23.2-19.2 Ma)

The first occurrence (FO) of *D. druggii* (Figure 2.12(1)) is used to define the base of NN2 in the study sections. However, the LO of *Triquetrorhabdulus carinatus* that defines the top of NN2 (Martini and Worsley, 1970) is absent. The FO of *Sphenolithus belemnos* (Figure 2.12(2)) is used to define the top of NN2 in Cyprus (defines the base of CN2 (Figure 2.11) (Bukry, 1973; 1975)).

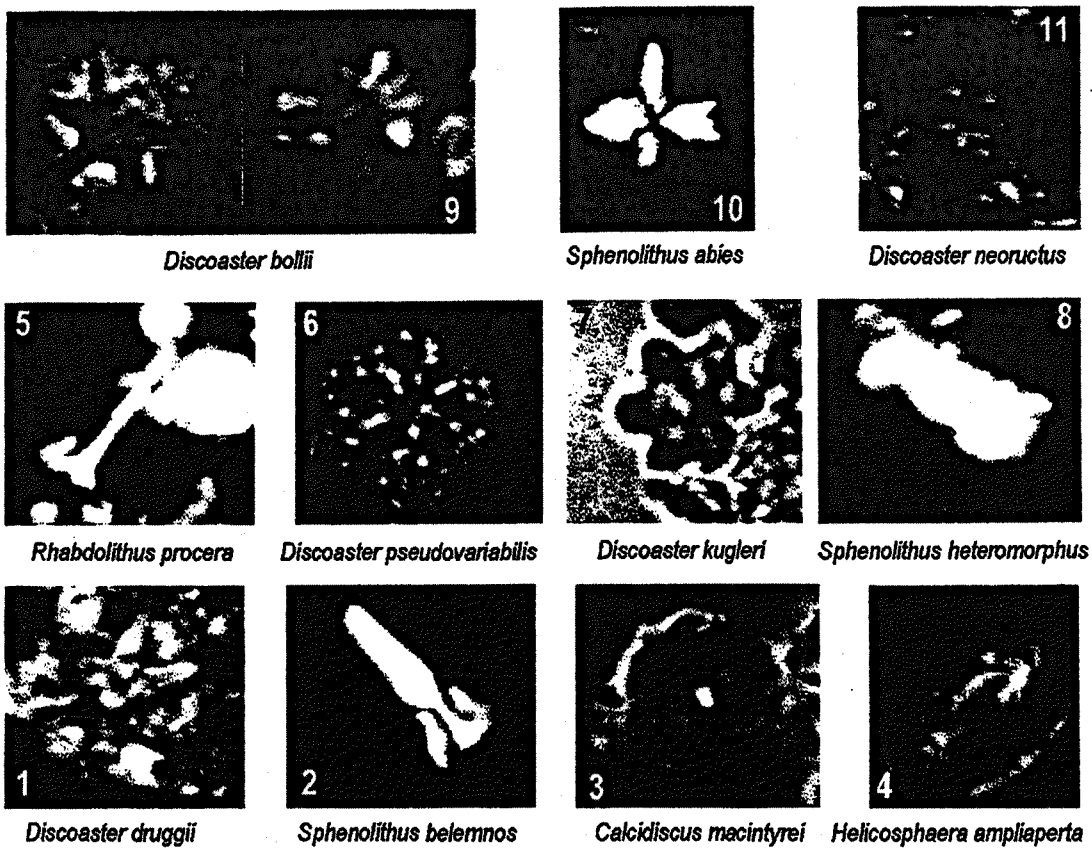

Figure 2.12 Calcareous nannoplankton used as zonal markers in this study

NN3 (19.2-18.3 Ma)

NN3 in Cyprus is defined by the phylogenetic range *S. belemnos* in Cyprus. The FO of *S. belemnos* identifies the top of NN2 successfully and the LO of *S belemnos* were used to define the top of NN3 by both the Martini (1971) and Bukry (1973; 1975).

NN4 (18.3-15.6 Ma)

NN4 is defined from the LO of *S. belemnos* to the LO of *Helicosphaera ampliaperta* (Martini, 1971; Bukry 1973). *H. ampliaperta* is very rare in the study sections and is therefore a poor marker for the top of NN4. However, the FO of *Calcidiscus macintyrei* (Figure 2.12(3)) occurs close to the LO of *H. ampliaperta* Perch-Nielsen (1985) and is used in this study to strengthen correlations. The precise position of the NN4/NN5 boundary in the study sections is often difficult to define.

NN5 (15.6-13.6 Ma)

The base of NN5 is marked by the LO of *H. ampliaperta* and or the FO of *C. macintyrei.* The top of NN5 is defined by the LO of *Sphenolithus heteromorphus* (Figure 2.12(8), Martini (1971) and Bukry (1973; 1975)).

NN6 (13.6-11.8 Ma)

The LO of *S. heteromorphus* successfully defines the base of NN6 in the study sections, the FO of *Discoaster kugleri* (Figure 2.12(7)) defines the top of NN6 (of Martini 1971; Bukry 1973; 1975), is rarely abundant.

NN7 (11.8-11.3 Ma)

The FO of *D. kugleri* defines the base of NN7 in the Cyprus. Martini (1971) defines the top of NN7 as the FO of *Calcidiscus coalitus* a species not found in the study sections. Consequently the top of NN7 in this study is defined by a FO of *Discoaster pseudovariabilis* (Figure 2.12(6)) an event likely to be synchronous with the FO of *Discoaster coalitus* (Perch-Nielson, 1985). *Discoaster challengeri* also has its FO in NN7 (Perch-Nielsen1985), and can be used to support correlations.

NN8 (11.3-10.7 Ma)

In the absence of *C. coalithus* the FO of *Discoaster pseudovariabilis* is used to define the base of NN8 in this study. *Rhabdolithus procera* (Figure 2.12(5)) appears in NN8 (Jafar 1975) after a long interval where rhabdoliths are hardly ever found (Perch-Nielsen, 1985). Morse (1996) also successfully used *Rhabdolithus procera* to constrain the base of NN8 in his biostratigraphical analysis of the Cretaceous to Miocene sediments of SW Cyprus. *Discoaster bollii* (Figure 2.12(9)) has its FO in NN8 (Perch-Nielsen, 1985) and is used as a marker for NN8 in this study. The top of NN8 is marked by the FO of *Discoaster hamatus*

(Martini, 1971), though is absent in the study sections. Morse (1996) used the FO of *Sphenolithus abies* (Figure 2.12 (10) to identify the top of NN8 in Cyprus.

NN9 (10.7-9.4 Ma)

This zone is defined by the phylogenetic range *Discoaster hamatus* in both the Martini (1971) and Bukry (1973; 1975) schemes. In its absence in the study sections the FO of *S abies* is to define the base of NN9 in this study, as it is a suitable marker for that age (Morse, 1996). No suitable species were observed in the study sections to constrain the top of NN9.

NN10 markers (8.7 Ma)

No suitable markers are found to constrain the base of NN10. Bukry (1973) subdivided NN10 in to CN8a and CN8b, with the base of CN8b (≡ NN11) marked by the first occurrence of *Discoaster neorectus*(Figure 2.11 and 2.12(11)). *D. neorectus* is present in study sections and is used as the youngest FO datum in the Pakhna Group at 8.7 Ma.

2.3.3 Kottaphi Hill

The lower ~55m of the Kottaphi Hill section is composed of rhythmically bedded chalks and marls and is the type section for the Kottaphi Member (Figure 2.14). Overlying this is a poorly exposed ~12 m marl unit, the Agrokipia Member. The top of Kottaphi Hill is capped by reefal facies of the Koronia Member.

Figure 2.13 illustrates the ranges of eponymous zonal and biostratigraphically useful taxa in this section. Details of the sampling locations at Kottaphi Hill are presented in the detailed graphic log in Appendix A.

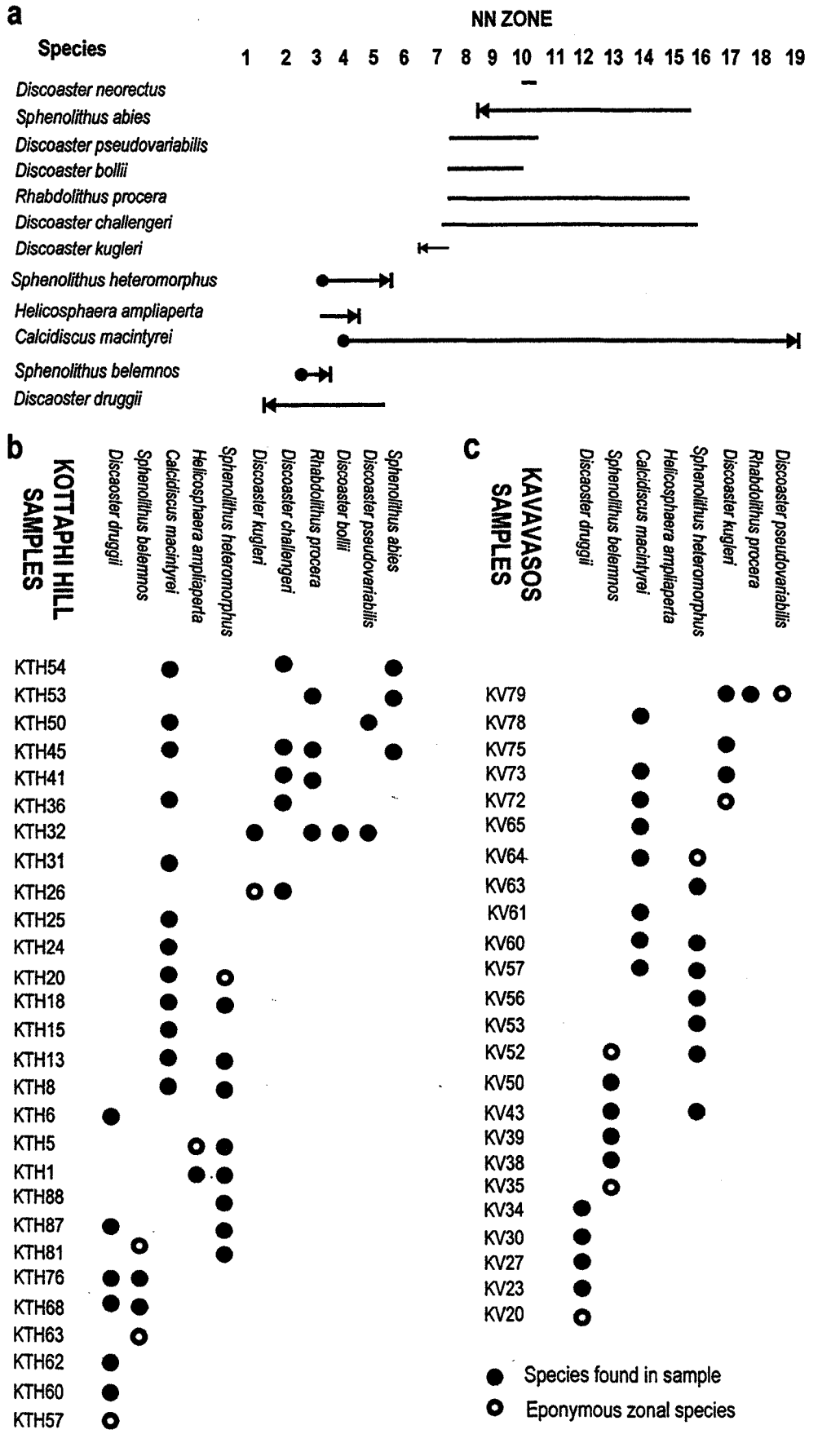

Figure 2.13 (a) Ranges of zonal taxa used in this study. Distribution of calcareous nannofossils from samples processed for biostratigraphy at (b) Kottaphi Hill and (c) Kalavasos.

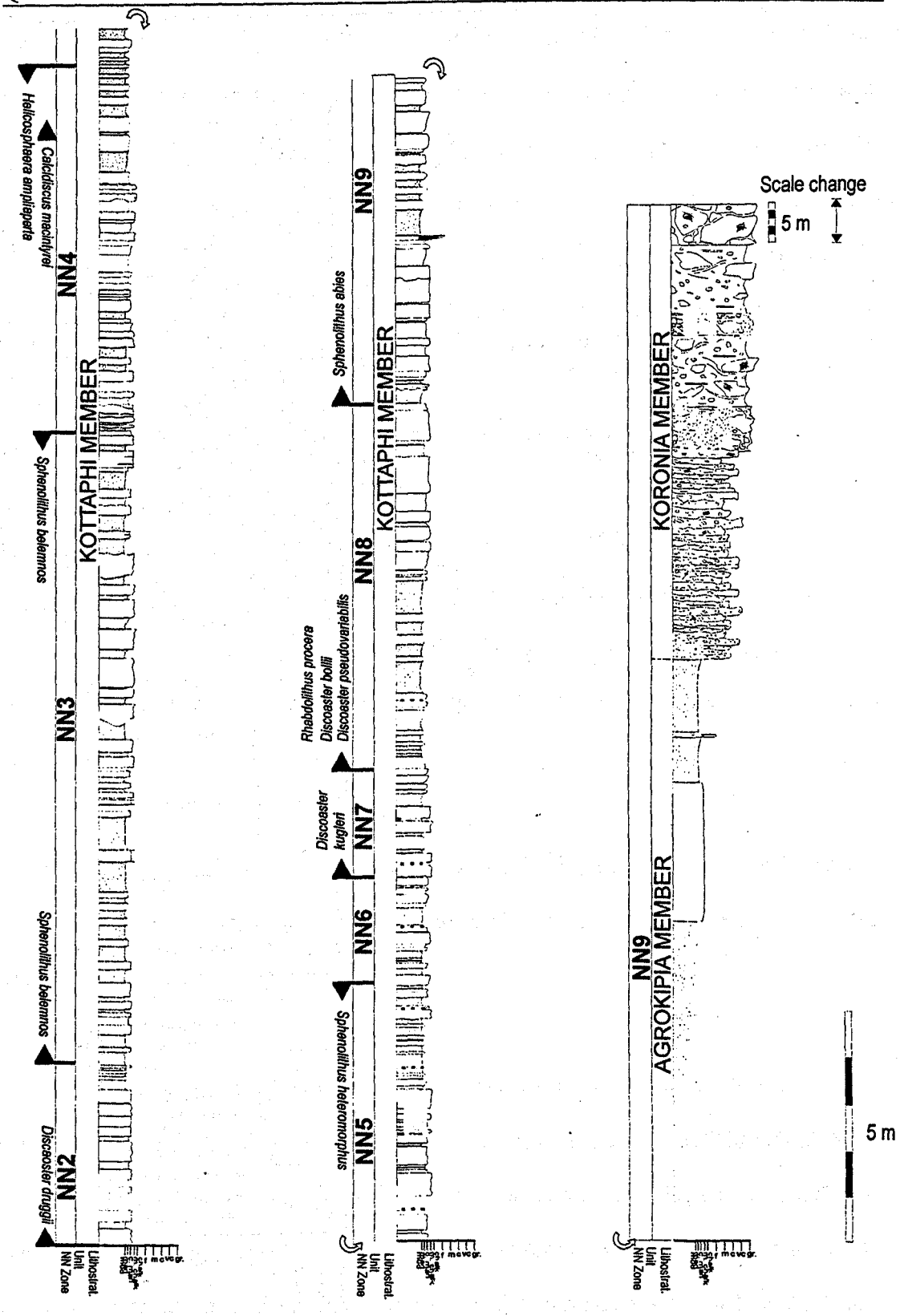

Figure 2.14. Graphic log of the Kottaphi Hill locality illustrating the locations of zonal calcareous nannoplankton FO and LO, and the division of lithostratigraphic units. Key on figure 2.15.

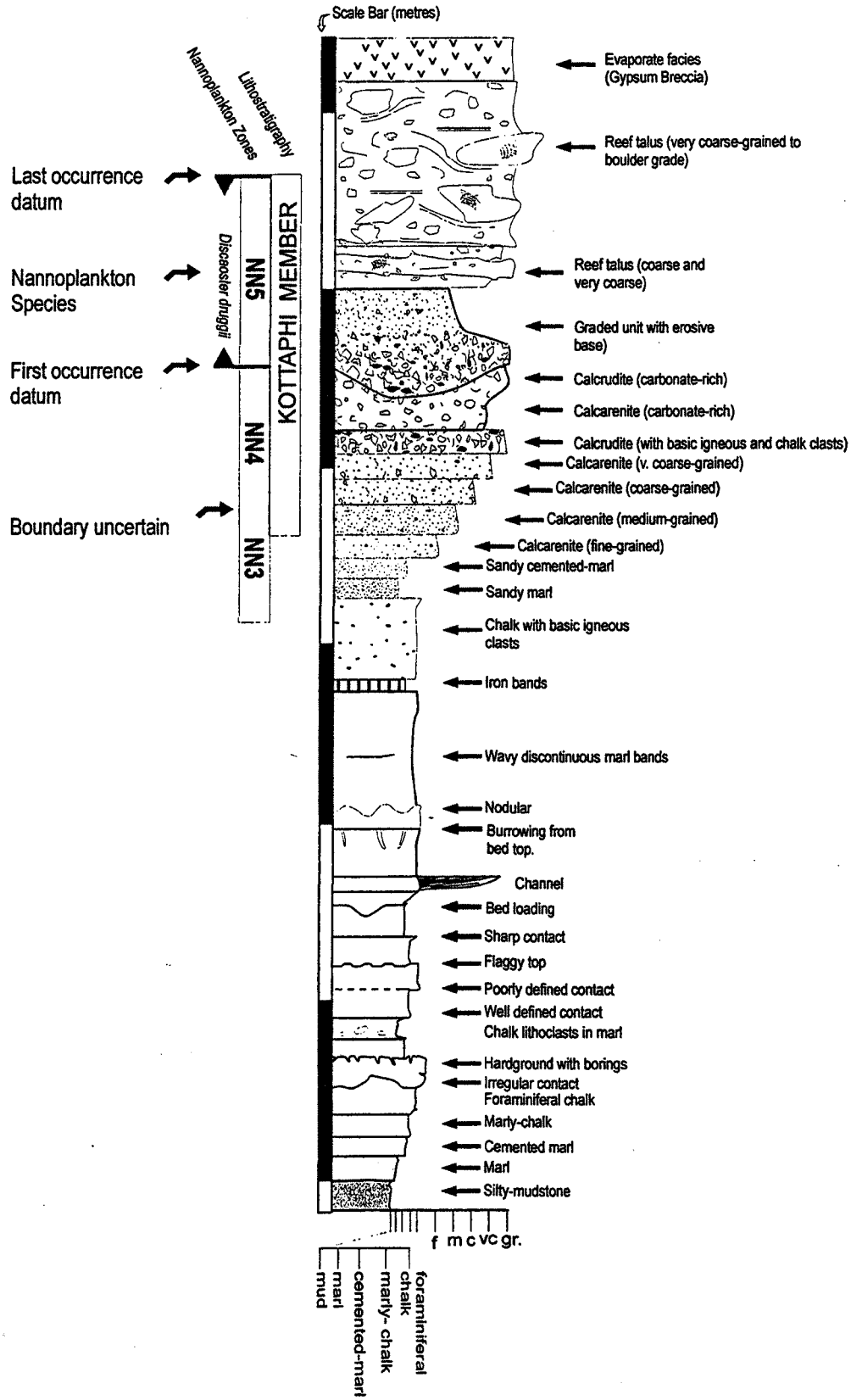

Figure 2.15 Key for graphic logs in this chapter

The base of Kottaphi Hill forms the lower part of the Kottaphi Member and lies within NN2 on the presence of *D. druggii* and the absence of *S. belemnos* (sample KH57). The chalk and marls of the Kottaphi Member, continue to NN9, suggested by the presence of *S. abies* in sample KH45. No younger taxa are found in the sampled section at the Kottaphi Hill. The base of the Agrokipia and Koronia Members also fall within NN9. This is in agreement with Morse (1996) who suggested the top of the Kottaphi Formation is no older than NN9 (Appendix A; Kottaphi Hill).

2.3.4 Kalavasos

The lower ~10 m of the Kalavasos section (Figure 2.16) is composed of thick pure chalk, with chert and forms part of the Lefkara Formation (Middle Lefkara massive chalks). Unconformably overlying this are the interbedded chalks and marls of the Kottaphi Member, which is ~45 m thick. Unconformably overlying this are brecciated evaporites of the Kalavasos Formation.

Figure 2.13 illustrates the ranges of eponymous zonal and biostratigraphically useful taxa in this section. Details of the sampling locations at Kalavasos are presented in the detailed graphic log in Appendix A.

The lower part of the section (Middle Lefkara Formation) at Kalavasos (samples KV1-KV19) contains abundant *Discoaster barbadiensis* indicating an Eocene (NP10-NP-15; 54.8-33.7 Ma) age. KV20 contains *D. druggii*, but not *S. belemnos*, suggesting that the base of the Kottaphi Member at Kalavasos is within NN2, as Kottaphi Hill. This suggests the entire Oligocene is missing from this section. Morse (1996) also found a comparable hiatus below the Pakhna Formation in sections in SW Cyprus south of the main outcrop of the Troodos Ophiolite.

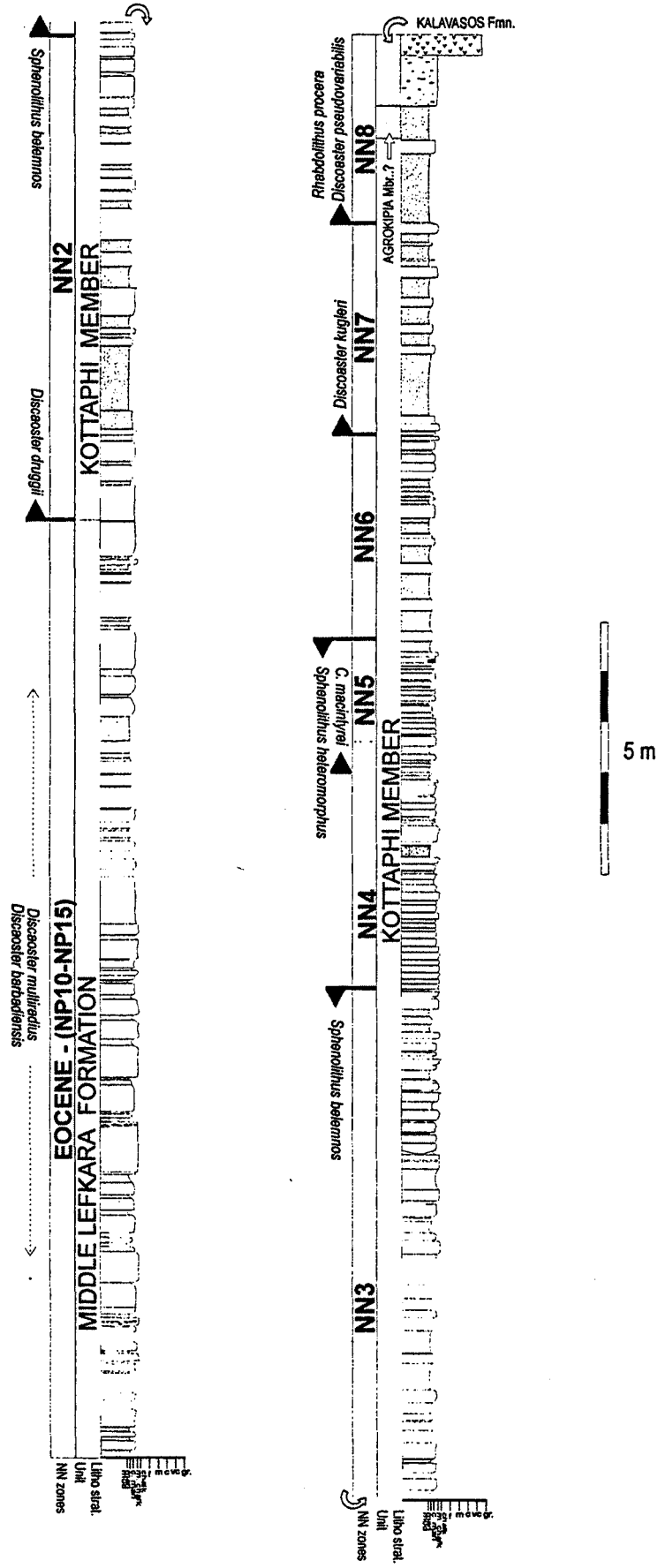

Figure 2.16. Graphic log of the Kalavasos locality illustrating the locations of zonal calcareous nannoplankton FO and LO, and the division of lithostratigraphic units. Key on figure 2.15.

Sample KV70, below the base of the Kalavasos Formation contains *Discoaster pseudovariabilis* indicative of NN8, giving a minimum age for the interbedded chalks and marls of the Kottaphi Member at Kalavasos. The Kottaphi Member is overlain unconformably by the Kalavasos Formation, as the Agrokipia Member is missing. This means that the evaporites of the Kalavasos Formation have a maximum possible age of NN8 (Appendix A; Kalavasos).

2.3.5 Pakhna Village

The Pakhna Village locality is composed of interbedded chalk and marl, with allochthonous calcarenites and calcrudites beds becoming more abundant up the section (Figure 2.18) The lower ~55 m is dominated by interbedded chalk and marl with the occasional allochthonous unit, and is assigned to the Kottaphi Member of the Pakhna Formation (Figure 2.2). The boundary with the overlying Spitali Member is hard to define at the Pakhna Village locality due to its highly gradational base, and is placed where there is an pronounced increase in the frequency of abundance beds (Figure 2.18).

Figure 2.17 illustrates the ranges of eponymous zonal and biostratigraphically useful taxa in this section. Details of the sampling locations at Pakhna Village are presented in the detailed graphic log in Appendix A.

The Pakhna village locality ranges from NN3-NN9. Sample PA2 contains *Sphenolithus belemnos* suggesting that the base of the section starts within the Kottaphi Member during NN3. The base of the Spitali Member occurs within NN6 as sample PA37 mark the LO of *Sphenolithus heteromorphus*. The Spitali Member continues until the top of the Pakhna Village section which is dated to NN9 by the FO of *Sphenolithus abies* in sample PA106 (Appendix A; Pakhna Village).

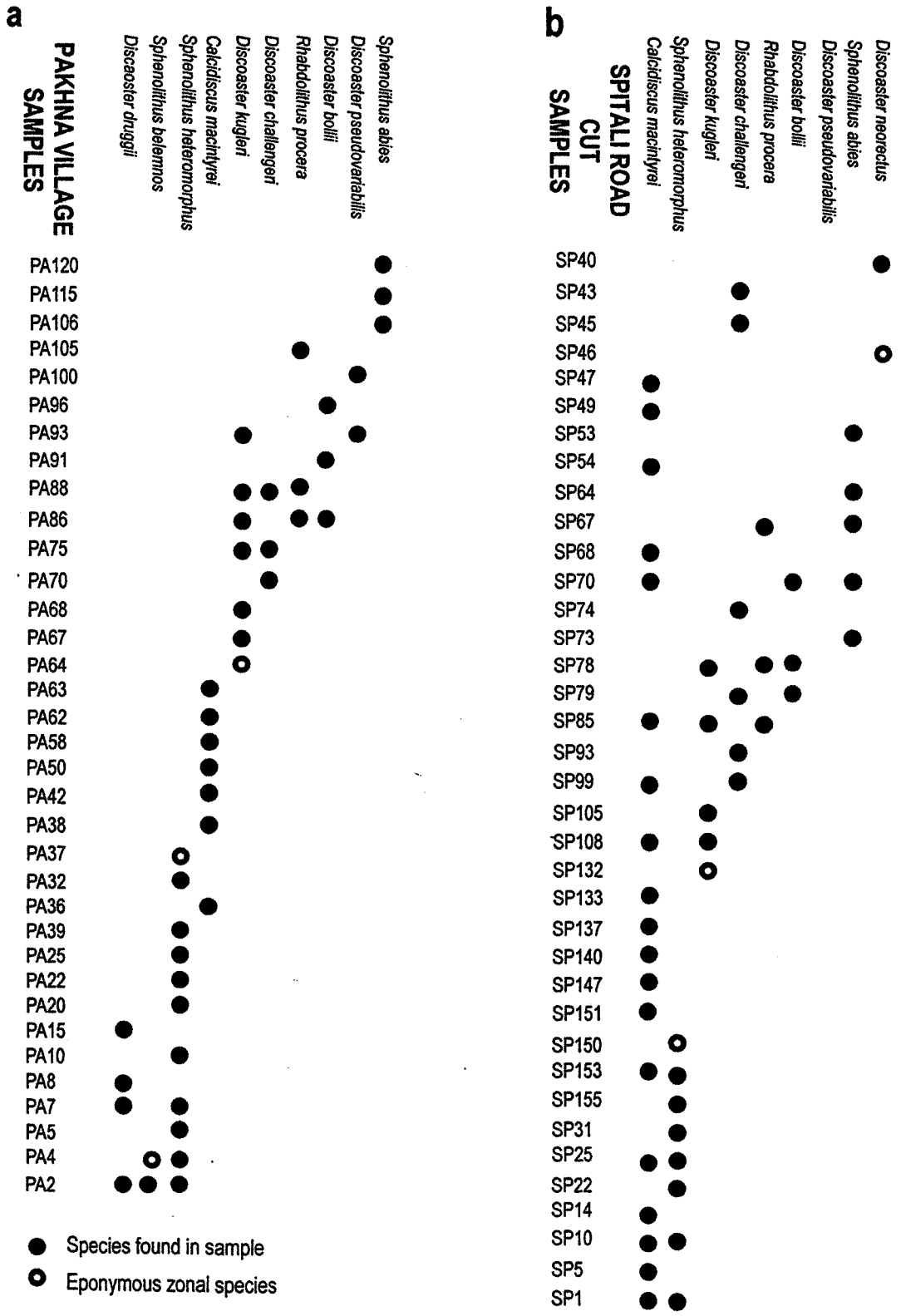

Figure 2.17 Distribution of calcareous nannofossils from samples processed for biostratigraphy collected at (a) Pakhna Village and (b) Spitali Road Cut.

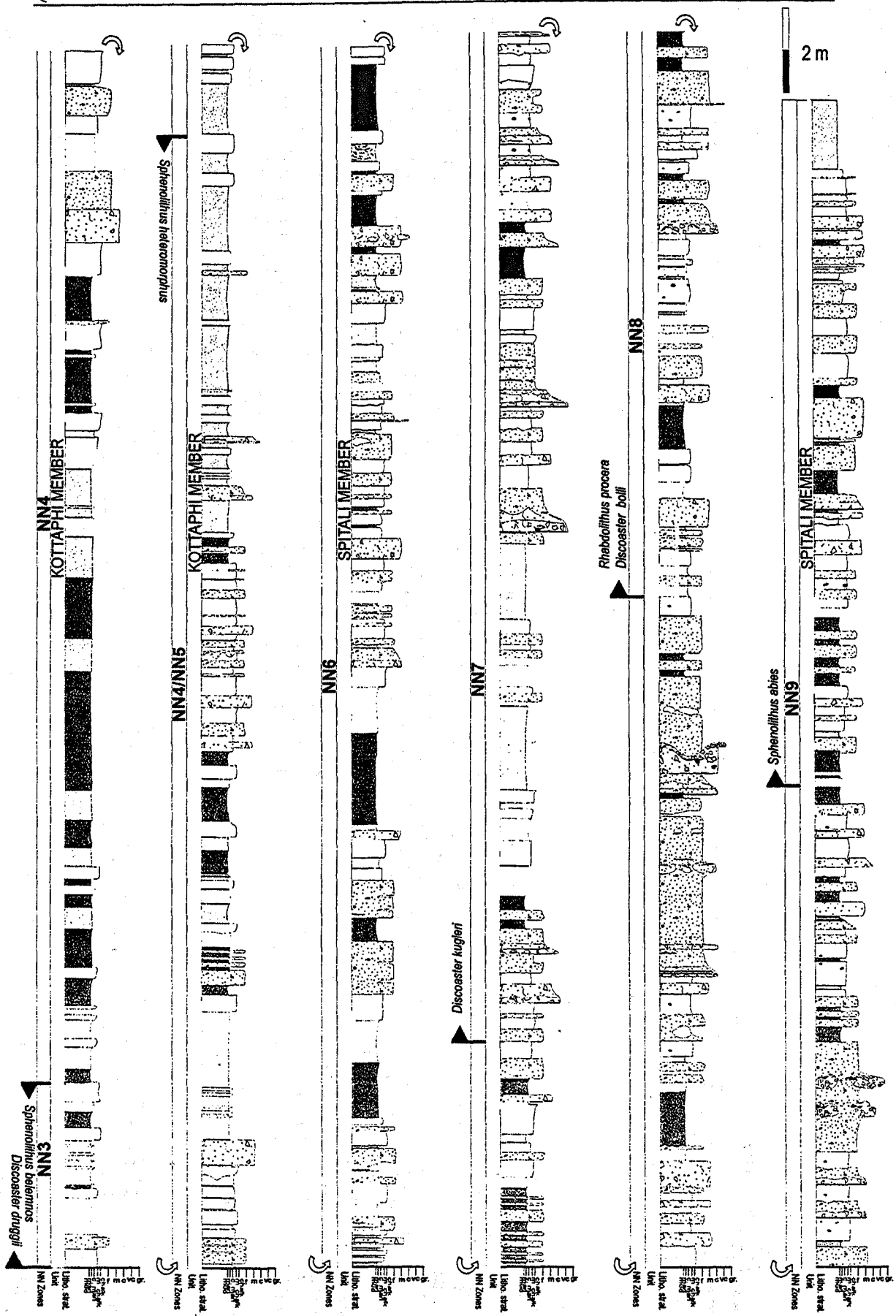

Figure 2.18. Graphic log of the Pakhna Village locality illustrating the locations of zonal calcareous nannoplankton FO and LO, and the division of lithostratigraphical units. Key on figure 2.15.

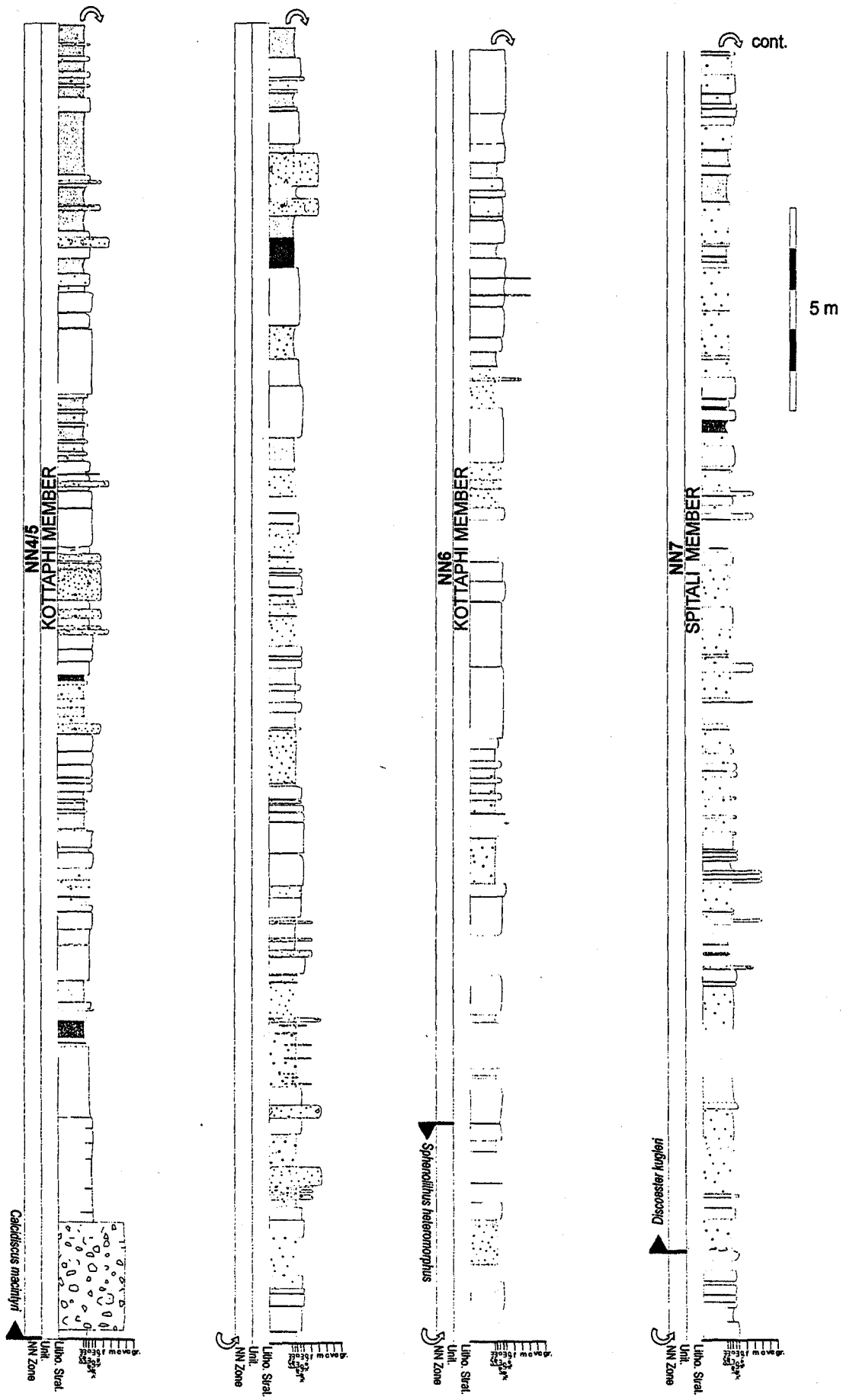

Figure 2.19. Graphic log of the Spitali Road Cut illustrating the locations of zonal calcareous nannoplankton FO and LO, and the division of lithostratigraphic units. Key on figure 2.15.

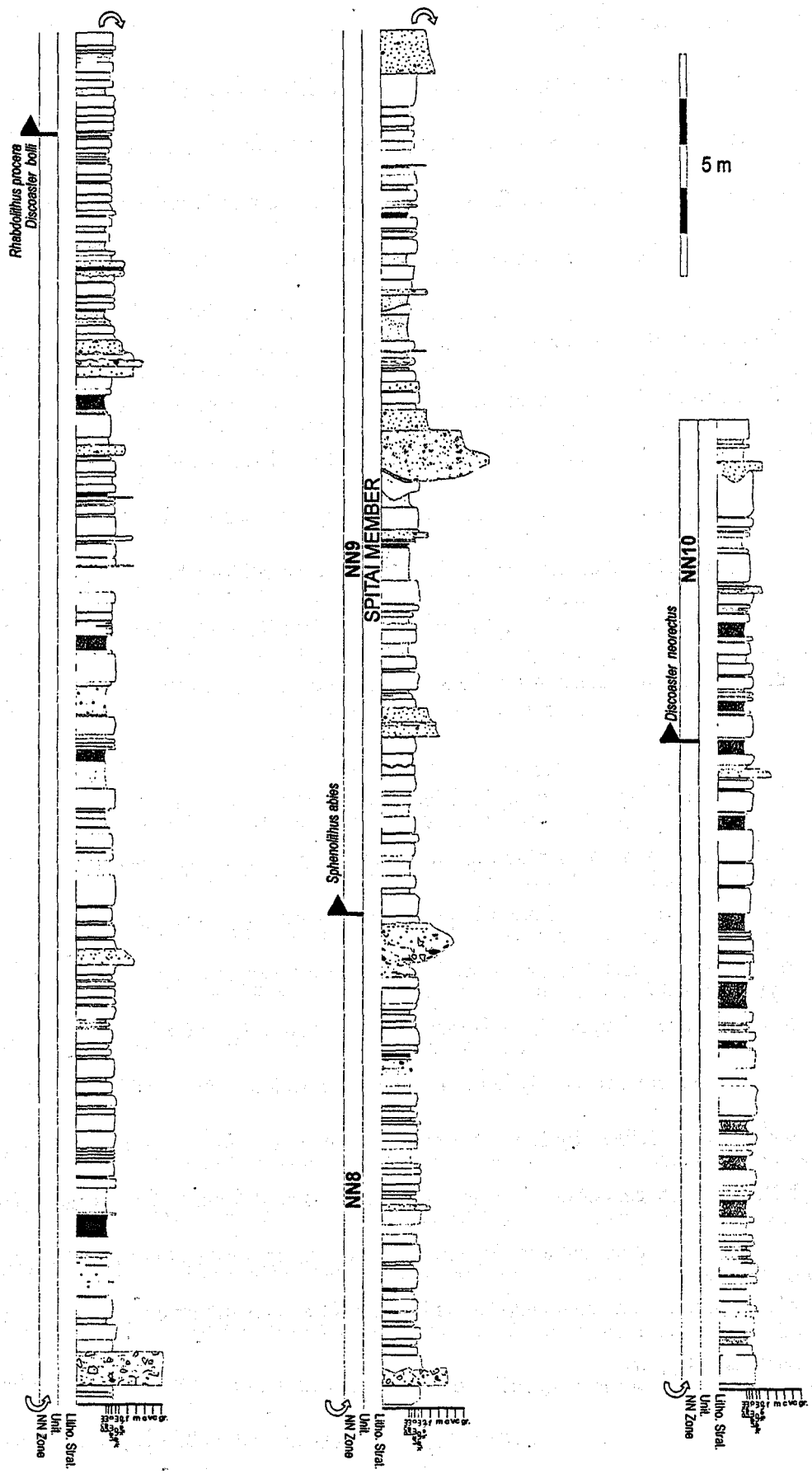

Figure 2.19. continued

2.3.6 Spitali Road Cut

At Spitali Road Cut the lower ~130 m of the section is composed of interbedded chalk and marl with scattered occurrences of calcarenites and calcirudites, this is assigned to the Kottaphi Member (Figure 2.19). The base of overlying Spitali Member is marked by an increase in allochthonous material, mainly within marl units.

Figure 2.17 illustrates the ranges of eponymous zonal and biostratigraphically useful taxa in Spitali Road Cut. Details of the sampling locations at the section are presented in the detailed graphic log in Appendix A. The base of the Spitali Road Cut lies within NN4/5 as sample SP1 contains *C. macintyrei* and *S. heteromorphus.* Sample SP 132 includes the FO of *D kugleri* (NN7) and coincides with the base of the Spitali Member, which composes the rest of the Spitali Road Cut section. The top of the Spitali Road Cuts location is dated as NN10 by the FO of *D. neorectus* in sample SP46 (Appendix A; Spitali Road cut)

2.3.7 Reliability of nannoplankton biostratigraphy in the study sections

The calcareous nannoplankton biostratigraphy of the study sections is generally good. All sections have at least three FO occurrence datums that are not potentially affected by reworking like LO datums. Reworking has been noted during analysis. *Discoaster kugleri* has its FO and LO in NN7, but is found in samples dated to NN8 in all sections. This error is hard to overcome, especially in determining the position of NN3, NN4, and NN5, the tops of which are all defined by LO. Due to the absence of *Helicosphaera ampliaperta* the NN4-NN5 boundary cannot be identified at the Kalavasos, Pakhna Village or the Spitali road Cut localities. This potential error is minimised by looking for the FO of *Calcidiscus macintyrei*, which though not a zonal taxa, has its FO in NN4 and creates an evolutionary datum between sections in Cyprus.

2.4 Summary

The Pakhna Formation dominantly comprises deep water chalk and marl deposits, which are subdivided into into four litho-facies, chalk, marly-chalk, cemented-marl and marl, defined on increasing clay content. These facies are stacked into couplets with a marl-rich base and chalk-rich top. They are interpreted to form due to fluctuations in terrigenous clay, which dilutes the background carbonate rain. This style of sedimentation that characterises the Kottaphi Member, is found at all the study sections. It ranges from NN2-NN9 (~23-9 Ma) at Kottaphi Hill and Kalavasos; from NN3-NN6 at Pakhna Village; and NN4/5-NN7 at the Spitali Road Cut.

At the Pakhna Village and Spitali Road Cut locations allochthonous units are interbedded with chalk and marl, and become more abundant up the sections. Allochthonous units are split into silty-mudstone, calcarenite or debrite facies depending on their gransize. They are interpreted to represent periodic flows of various severity interrupting the background chalk and marl sedimentation. The allochthonous units contain basic igneous material that is sourced from the Troodos Ophiolite. The onset of increased allochthonous derived material defines the base of the Spitali Member, and has a highly gradational contact with the chalk and marl of the Kottaphi Member. The Member ranges in age from NN7-NN10 (~12-9 Ma) at the Spitali Road Cut and NN6-NN9 at Pakhna Village.

The marl-rich Agrokipia Member is poorly exposed and is interpreted to represent sedimentation in shallower marine conditions due to the increase input of terrigenously derived clay. It is absent south of the Troodos and is only found at Kottaphi Hill. It is dated to lie within NN9. The reef debris of the overlying Koronia Member further reinforce the trend of marine shallowing into the upper Miocene. The base of the Koronia Member (only observed Kottaphi Hill in this study) is also dated as NN9.

Chapter 3

A Model for Pelagic Carbonate Sequence Stratigraphy from the Pakhna Formation, Cyprus

3.1 Introduction

The Miocene-aged sediments of the Pakhna Formation, Cyprus, were deposited on an uplifting section of oceanic crust, the Troodos Ophiolite (Robertson, 1977). The formation records part of an overall marine shallowing-upward succession, from the latest Cretaceous-Oligocene deepwater chalks of the Lefkara Formation, to the evaporite facies of the upper Miocene Kalavasos Formation (Robertson, 1977; Orszag-Sperber *et al.* 1989; Robertson; 1998). The Pakhna Formation comprises shallow- to deep-water carbonates and subordinate terrigenous sediments that were mainly deposited by pelagic and gravity controlled processes (Eaton and Robertson, 1993). The formation outcrops in patches around the circumference of the Troodos massif (Figure 3.1) with its largest exposure situated in the southern part of the island.

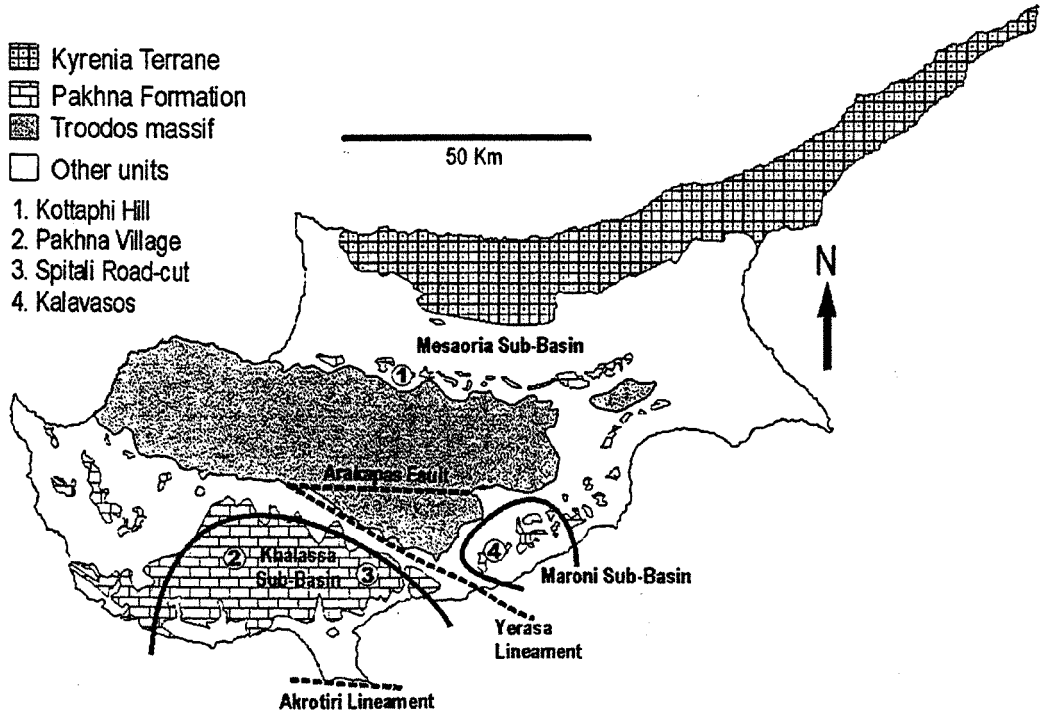

Figure 3.1 Geological map of Cyprus illustrating the outcrop pattern of the Pakhna Formation. 1-4 mark the localities discussed in this chapter.

Robertson *et al.* (1991) address the role of tectonic verses global seal-level change in the Neogene evolution of the Cyprus active margin. They state that the influence of eustatic changes on sedimentation is well established for well-dated successions in tectonically stable areas, and has allowed global sea-level curves to be proposed for Phanerozoic time (*e.g.* Hardenbol *et. al.* 1998). However, lateral facies variation, poor preservation, and limited age dating of many active margin successions makes recognising sea-level changes a difficult task. Robertson *et. al.* (1991) summarise the tectonic evolution of the Cyprus active margin, and establish that the onset of subduction in the Early Miocene led to the development of four WNW-ESE structural lineaments of which the Yerasa lineament (Figure 3.1) is the most prominent. They propose that compression along these lineaments exerted a dominant control on sedimentation during the Miocene and gave rise to a series of sub-basins with individual depocentres (Figure 3.1). By comparing the Neogene global sea-level curve with the stratigraphical record of Cyprus Robertson *et al.* (1991) establish a relative sea-level curve based on the most conformable stratigraphical contacts preserved between units for any given time interval. The study was hampered by some of the inadequacies of biostratigraphical data and the fact that marginal facies, which are sensitive environmental indicators, were largely eroded. They conclude that a global eustatic sea-level change signal can be discerned above the "noise" generated by local tectonics. However, tectonic processes dominated sedimentation overall. A later study by Eaton and Robertson (1993) also invokes a tectonic control on the deposition of the Pakhna Formation sediments, and relates it to the onset of northward subduction the south of Cyprus during the early Miocene.

This study benefits from an improved biostratigraphical data set coupled with an increased understating of the processes responsible for sequence boundary development with the Pakhna Formation. The chalk and marl couplets of the Pakhna Formation (which is termed here the Kottaphi Member (Chapter 2)) are grouped into distinct stacking patterns which were identified by graphic logging at several localities on the island. The objective here is to

interpret the distinct sedimentary cyclicity in terms of an appropriately modified sequence stratigraphical model, and to interpret couplet stacking patterns in terms of changes in relative sea-level. The timing of sequence boundaries (gauged from nannoplankton biostratigraphy (Chapter 2)), is compared to the Cenozoic sequence chronostratigraphy constructed from other European sections, particularly the North Sea (Hardenbol *et al.*, 1998) and the New Jersey Margin, USA, to assess the possible correlation of sequence boundary development in Cyprus.

3.2 Sequence stratigraphy and chalk dominated successions

Sequence stratigraphy is a technique for dividing the sedimentary record into meaningful packages of genetically related sediments resulting from relative changes in sea-level (Walker and James, 1992). The technique was developed on passive margin siliciclastic successions (Mitchum, 1977; Vail *et al.*, 1977; van Wagoner *et al.*, 1988, Vail *et al.*, 1991), where relative sea-level change is defined as variation in water depth resulting from both tectonic and eustatic changes. Research has extended the sequence stratigraphic model to carbonate successions, though these have primarily concentrated on shallow marine settings (Sarg, 1988; Kendal, 1992; Robertson-Handford and Loucks. 1993; Vecsei and Sanders, 1999). The importance of sequence stratigraphy as a correlative and interpretative tool in deep-water pelagic carbonate facies is becoming increasingly recognised (Gale, 1996; Grant, *et al.*, 1999). Gale (1996) established a set of criteria for the identification of key sequence stratigraphic surfaces in the Turonian chalks of southern England, which Grant *et al.*, (1999) built upon to produce a sequence stratigraphic model for the chalk succession of the upper Cretaceous, Anglo-Paris Basin. Chalk deposition responds differently to sea-level changes compared to near-shore sediments due to: 1) the relatively large distances from land, 2) deeper water depths and 3) the dominance of biogenic $CaCO_3$ precipitation over a terrigenous sediment supply. These issues necessitated Grant's (1999) modification of the sequence stratigraphical model. The model is based mainly on the recognition of key surfaces, where

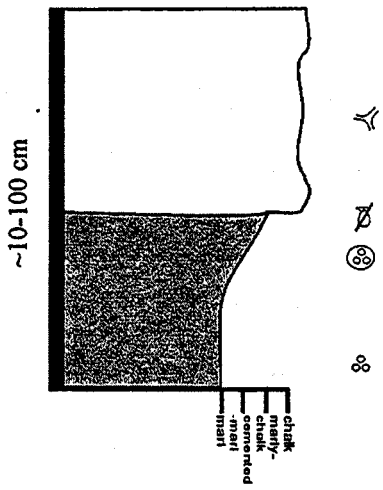

Figure 3.2. Idealised chalk-marl couplet from the Pakhna Formation. Key on Figure 3.5

hardgrounds and nodular chalks mark the sequence boundary and the transgressive surface. Lowstand chalks typically contain marl bands and often show evidence for reworking and erosion. Transgressive and highstand deposits are chalk rich with the latter containing more flint bands, and sponge beds. The position of the maximum flooding surface is variously represented by a winnowed and fossiliferous horizon, nodularity, or the onset of typical highstand systems tract deposits. The sequence stratigraphic model proposed here for the Pakhna Formation is based on the Grant (1999) model, but differs due to the greater extent in which terrigenously derived material influences deposition within all of the systems tracts.

3.3 Sequence stratigraphy of the pelagic carbonates of the Pakhna Formation

The recognition of sequence stratigraphic surfaces is based on field observations, and relies heavily on the stacking pattern, composition and relative proportions of chalk and marl within the chalk-marl couplets that dominate the sedimentary style of the Kottaphi Member.

3.3.1 Idealised chalk-marl couplet

The idealised couplet consists of two facies, foraminiferal chalk, and marl (Figure 3.2). The base of the couplet comprises a marl bed, this has a gradational contact with the overlying chalk. The marl has a planar contact with the underlying foraminiferal chalk of the previous couplet. *Chondrities* dominates the marl ichnofauna, and becomes more abundant towards the top of the bed, where it is often accompanied by bivalve fragments and minor occurrences of *Thalassinoides*. The foraminiferal chalk bed is dominated by *Thalassinoides* and contains well preserved planktonic foraminifera. The couplets vary in thickness from a few cm to ~1 m, and are interpreted to represent different degrees of dilution of the background carbonate rain by a variable flux of terrigenously supplied material. In such a

scenario marl beds are deposited during periods of increased supply of terrigenous material that significantly dilutes the carbonate rain of planktonic organisms. In contrast, a reduction in the flux of terrigenous material allows the carbonate rain to settle, relatively undiluted, to form foraminiferal chalk. Short-term climate variation is interpreted to account for the variation in the flux rate of terrigenous material (see Chapter 4). Higher levels of precipitation during humid periods account for an increase in the transport of terrestrial material which is discharged by fluvial systems, and transported to basinal areas in suspension. More arid climatic conditions will characterise foraminiferal chalk deposition where levels of precipitation and therefore fluvial discharge are dramatically reduced. Foraminiferal chalk and marl are the two end member states in a continuum of variable degrees of carbonate dilution that occur in a couplet. A four-fold classification of pelagic carbonates is adopted in this study; marl, cemented-marl, marly-chalk and foraminiferal chalk reflecting less terrigenous dilution dilution respectively (Chapter 2). Every couplet is composed of two of these lithotypes, with the relatively marl-rich lithology forming the base of the couplet.

3.3.2 Features of the depositional sequences

An ideal marl-chalk depositional sequence (Figure 3.3) has been derived from field observations on several depositional sequences. Unlike the Grant (1999) model, where identifying systems tracts relies mainly on the recognition of keys surfaces, the model proposed here assigns system tracts to the succession based mainly on the composition and variability displayed within couplets.

In the ideal depositional sequence a hardground signifies a sequence boundary (SB, Figure 3.3) which is a planar, well-defined surface that is characterised by borings and authigenic mineralisation (e.g. Fe and Mn). It represents a period of low sedimentation rate, where the hardground surface was exposed at the sea floor, allowing time for boring organisms to

colonise and mineral-rich fluids to precipitate. A well-developed, bored and mineralised hardground defines SB(f) at Kottaphi Hill (Figure 3.4 & 3.6; Appendix A, bed 123); however, SB are not always marked by hardgrounds. Nodular beds (e.g. SB(e), Figure 3.4 & 3.6 at Kottaphi Hill, Appendix A, bed 71) firmgrounds (SB(e) Figure 3.4 & 3.7; Appendix A, Kalavasos bed 256), and prominent foraminiferal chalk beds (SB(d) Figure 3.4 & 3.9; Appendix A, Spitali Road Cut, bed No.4) can also signify sequence boundaries. Sequence boundaries represent the point across which there is a sharp increase in the terrigenous material, due to relative sea-level fall. This transition is marked by a pronounced change from chalk dominated couplets of the previous HST, to marl dominated couples of the following LST (Figure 3.3). At Kottaphi Hill SB(h) (Figure 3.6 and Appendix A, bed 280) sea-level was sufficiently low to allow current activity to impinge on the sea floor to produce a broad, shallow channel. Mineralisation (limonite) is particularly conspicuous at SB(e) and SB(f) at Kalavasos (Appendix A, beds 256 and 294).

The lowstand systems tract (LST) is characterised by marl-rich couplets (Figure 3.3). True foraminiferal chalks are not generally present in LST couplets, instead the couplets are usually either marl and cemented-marl or marl and marly-chalk. Lower relative sea-levels in the LST, result in a greater exposure of land area, and cause rejuvenation in fluvial systems (incision), both of which increase the potential for dilution of the carbonate rain by the terrigenous sediments. Periods of slightly lower terrigenous flux rate were responsible for an increase in the carbonate content to produce cemented marl or marly-chalk. LST couplets are often iron stained, probably as a result of the inclusion of very fine-grained Troodos derived basic igneous material (sequence E at Kottaphi Hill and sequences E and F Kalavasos, Figure 3.6 and 3.7 and Appendix A).

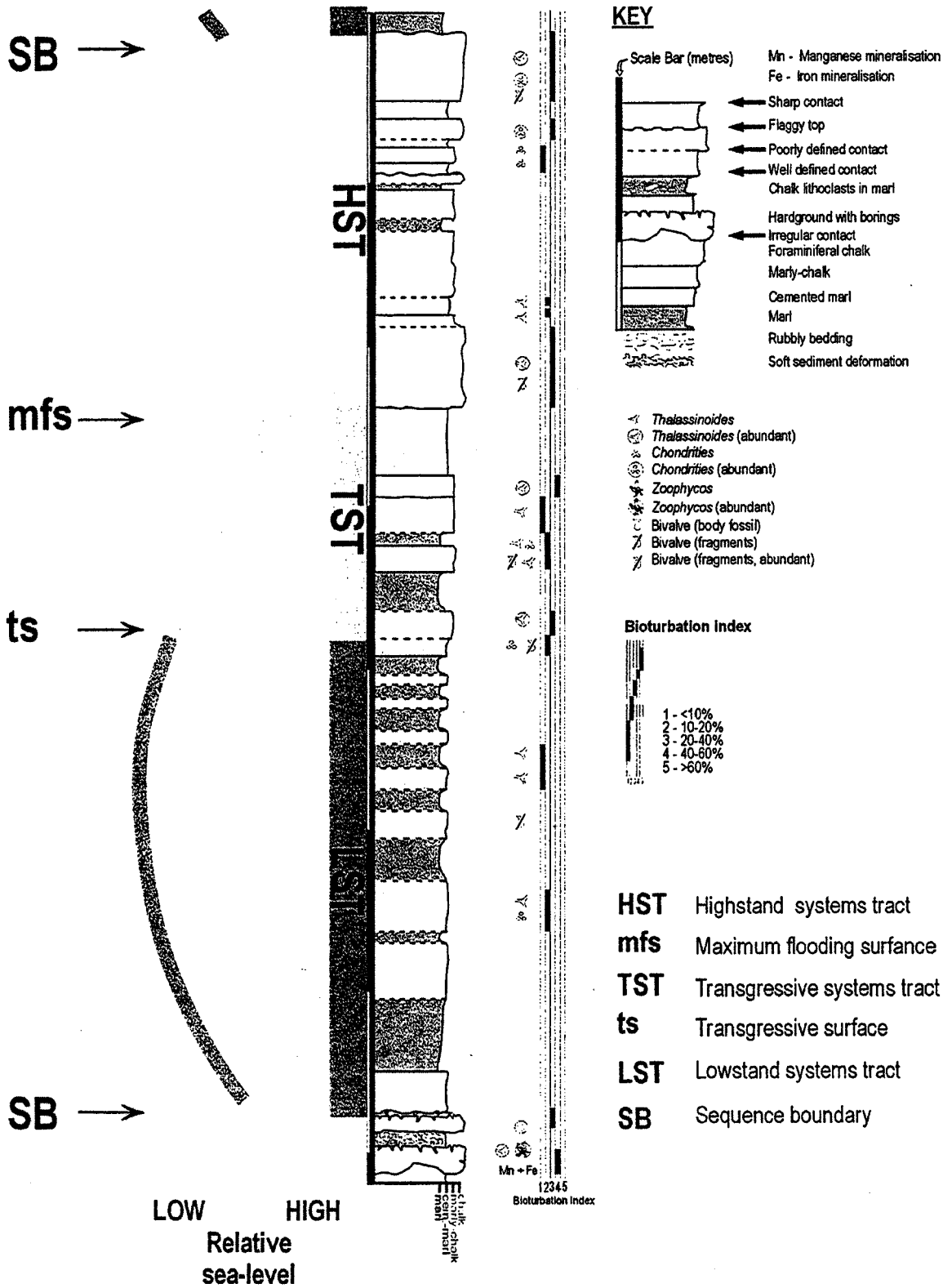

Figure 3.3 Idealised depositional sequence for the pelagic chalks of the Pakhna Formation showing typical features.

The first significant foraminiferal chalk in the section is interpreted to mark the transgressive surface (ts), and is often located where there is a notable increase in bioturbation. The ts indicates that relative sea-level was rising, and had is interpreted to indicate that it has attained a sufficiently high level to reduce the terrigenous flux sufficiently to allow the formation of foraminiferal chalk formation. Couplets within the transgressive systems tract (TST) have a roughly equal thickness of chalk-rich and marl-rich beds (Figure 3.3), and tend to be well bioturbated with *Thalassinoides* and *Chondrities*. Theoretically the ts can be viewed as a threshold above which the flux of terrigenous material and carbonate rain within each couplet equilibrate (thought still alternate), as neither chalk-rich or marl-rich deposits dominate the individual couplets.

Since the long-term relative sea-level change is continuing to rise through the TST, the smaller scale cyclicity, demonstrated by the couplets, will become increasingly dominated by relatively marl-free facies, as the terrigenous clay supply is becoming restricted. The position of the maximum flooding surface (mfs) is problematical, as the transition to chalk-rich couplets is often gradational. It is however usually taken at the base of the first thick chalk-rich couplet that characterise the HST deposits (Figure 3.3). Marl beds are present within the HST, though are thinner than in the TST, but often become more common and thicker near the top of the HST close to the overlying SB.

3.3.3 Definition and correlation of depositional sequences

Graphic logging at Kottaphi Hill (Figure 3.1), reveals nine complete depositional sequences in the Pakhna Formation (Figure 3.4). As the Kalavasos, Pakhna Village and Spitali Road Cut sections (Figure 3.1) cover different and overlapping time intervals, seven depositional sequences are correlated, within the resolution of biostratigraphy, throughout the Pakhna Formation. Figure 3.4 summarises, these correlations and sequence development in all locations. At the Pakhna Village and Spitali Road Cut locations up to 15 depositional

sequences are developed, though the sequence stratigraphic interpretation is complicated by the introduction allochthonous material from the Spitali Member. Sequence definition at Kottaphi Hill and Kalavasos is less ambiguous than at the Pakhna Village and Spitali Road Cut sections, and they are therefore used as reference sections for sequence development in Cyprus. Depositional sequences are referred to by a letter (A-J) with their corresponding sequence boundaries named SB9(a)-SB(j).

Table 3.1 summarises the character of all the depositional sequences developed within the Pakhna Formation. The stratigraphical position of each sequence is marked on graphic logs of the four localities (Figures, 3.6, 3.7, 3.8 and 3.9).

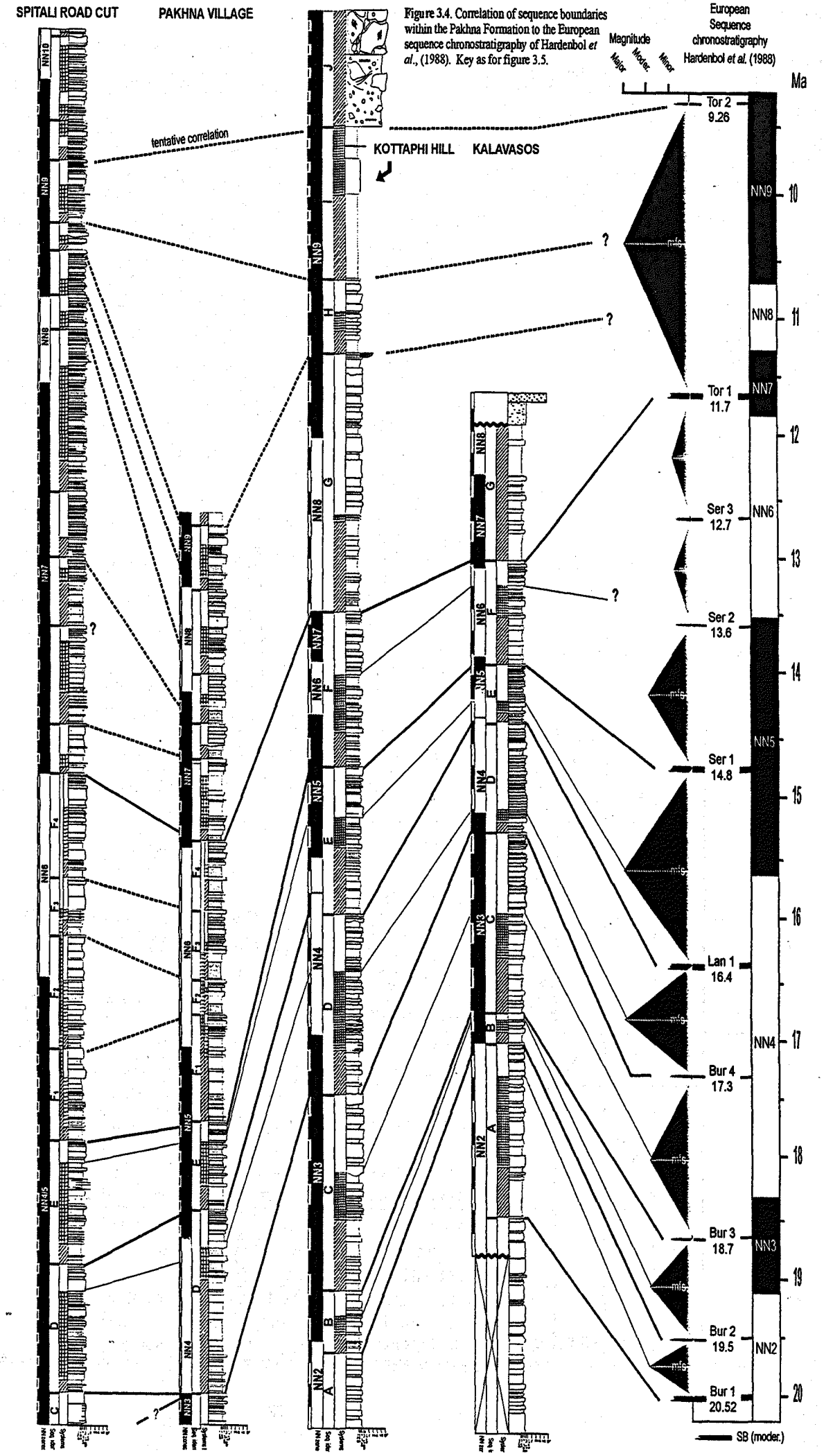

Figure 3.4. Correlation of sequence boundaries within the Pakhna Formation to the European sequence chronostratigraphy of Hardenbol *et al.*, (1988). Key as for figure 3.5.

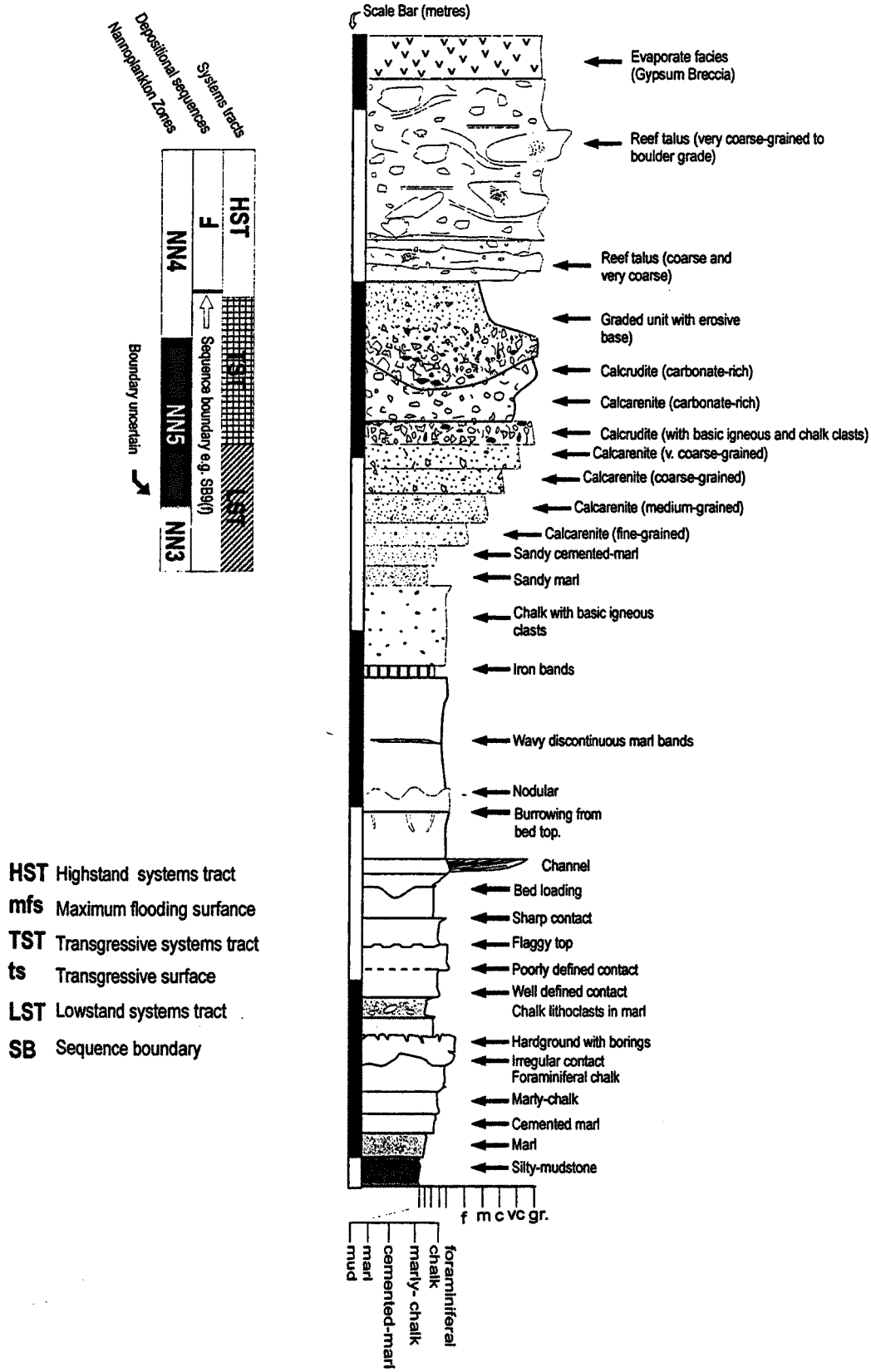

Figure 3.5 Key for graphic logs in this chapter

Table 3.1 Characteristic features of depositional sequences developed in the Pakhna Formation, Cyprus. The ages proposed for the sequence boundaries in figure 3.3, are those used for the Hardenbol et al. (1998) sequences, which are integrated into the Berggren et al., (1995) time scale using calcareous nannofossil and planktonic foraminifera biostratigraphy. ? indicates an unknown correlation, N/P = Not Preserved (no sedimentary record), N/D = Not Developed, i.e. no evidence. Shaded cells indicate where sequence boundaries are developed.

Sequence	Systems Tract	Charateristic features	Kottaphi Hill	Kalavasos	Pakhna Village	Spitali Road Cut
J <9.26 Ma	LST	Only identifiable at Kottaphi Hill this system tract is composed of reef talus from the Koronia Member	1450+ cm	N/P	?	?
	SB(j)	Marked by the transition from marl-rich deposits to coarse-grained reef talus		N/P	?	?
I <9.26 Ma	TST	Poorly exposed systems tract, composed of ~300 cm foraminiferal chalk and marl beds	575 cm	N/P	?	?
	LST	Poorly exposed and composed entirely of marl.	575 cm	N/P	?	?
	SB(i)	Marked by the transition from chalk rich couplets to marl-rich deposits		N/P	?	?
H 9.25 - ? Ma	HST	Moderately well-developed systems tract with ~30 cm thick foraminiferal chalks and subordinate ~15 cm thick marls and cemented marls.	150 cm	N/P	?	?
	TST	15-20 cm thick marl, and marly-chalk beds	150 cm	N/P	?	?
	LST	Well-developed 80 cm thick marl and cemented marl couplets	95 cm	N/P	?	?
	SB(h)	Characterised by well bioturbated foraminiferal chalk with a 13 m wide, 1 m deep erosional scours at Kottaphi Hill, overlain by marl-rich couplets.		N/P	?	?
G 11.7-9.25 Ma	HST	Well-developed thick systems tract dominantly composed of ~45 cm thick foraminiferal chalks and marly-chalks. Marl and cemented-marl bed are subordinate and generally <10 cm thick, though attain a maximum of 29 cm in thickness.	730 cm	N/P	?	?
	TST	Poorly developed systems tract, characterised by 8-10 cm thick foraminiferal chalks and marl.	25 cm	N/P	?	?
	LST	Well-developed systems tract composed dominantly of 25-150 cm thick marls, ~20 cm thick cemented-marls and ~15 cm thick marly-chalks. Thicker at Kalavasos and not fully preserved, due to an unconformity within the Kalavasos Formation.	415 cm	615 cm	?	?
	SB(g)	Well-defined at Kalavasos by a planar surface at the top of a marly-chalk, overlain by marl-rich couplets. Moderately well-defined at Kottaphi Hill and Pakhna Village by a marly-chalk with a sharp-top, and at the Spitali Road Cut by the transition from chalk-rich to marl-rich couplets.				

Sequence	Systems Tract	Charateristic features	Kottaphi Hill	Kalavasos	Pakhna Village	Spitali Road Cut
F **14.8-11.9 Ma** **also see footnote F1, F2, F3 and F4**	**HST**	Relatively marl-rich and poorly-defined systems tract at Kottaphi Hill, Pakhna Village, and Spitali Road Cut. At Kottaphi Hill foraminiferal chalks and marly-chalks are <25 cm thick and marls and cemented-marls average 15 cm in thickness. At Pakhna Village and Spitali thick (~40-100 cm) foraminiferal chalk and marly-chalks are interbedded with thick (~20-100 cm) marl and cemented-marls. At Kalavasos foraminiferal chalks and marly-chalk are ~15 cm thick and interbedded with <8 cm marls and cemented marls. Both Kottaphi Hill and Kalavasos show iron mineralisation. At Kottaphi Hill iron occurs in <6 cm bands and at Kalavasos as coating on allochems. This systems tract is highly expanded at Pakhna Village.	295 cm	110 cm	950 cm	1180 cm
	TST	A relatively marl-rich systems tract at all locations. At Kottaphi Hill and Kalavasos marl-rich beds average ~16 cm in thickness, and chalk-rich beds average ~18 cm thickness. At Pakhna Village and Spitali ~30-100 cm thick foraminiferal chalks and marly-chalks are interbedded with ~50-150 cm thick marl-rich beds. Iron mineralisation is observed at both Kottaphi Hill and Kalavasos and bands and staining. This systems tract is highly expanded at Pakhna Village and Spitali.	205 cm	120 cm	605 cm	1550 cm
	LST	Well-defined at Kalavasos and Kottaphi Hill, and composed entirely of marl dominated couplets. Marls are ~20 cm thick at Kottaphi Hill, and interbedded with ~10 cm thick cemented-marls. There are also ~3 cm thick iron bands. At Kalavasos marl beds are ~45 cm thick and interbedded with ~18 cm thick iron stained cemented-marls. At Pakhna Village and Spitali marls average ~80 cm in thickness and are interbedded with cemented marls ~20-40 cm thick and marly-chalks <30 cm thick. This systems tract is highly expanded at Pakhna Village and Spitali.	150 cm	208 cm	715 cm	528 cm
	SB(f)	At Kottaphi Hill this SB is marked by a 42 cm thick foraminiferal chalk firmground surface. At Kalavasos it is marked by the contact between a sharp-topped, iron stained foraminiferal chalk with marl-rich couplates. At Pakhna Village the SB is marked by the contact between a nodular foraminiferal chalk and marl-rich couplets. At the Spitali Road Cut it is marked by a marly-chalk bed, overlain by a 84 cm marl.				

Sequence	Systems Tract	Charateristic features	Kottaphi Hill	Kalavasos	Pakhna Village	Spitali Road Cut
E 16.4 – 14.8 Ma	HST	Well-developed at Kottaphi Hill and Spitali, where ~30-80 cm thick foraminiferal chalks are interbedded with ~10 cm thick marls and cemented-marls. At Kalavasos iron stained foraminiferal chalks and marly-chalks are ~10 cm thick, with interbeds of iron stained marls and cemented-marls that are 1-9 cm thick. At Pakhna Village the systems tact is poorly developed and marl-rich.	210 cm	120 cm	190 cm	190 cm
	TST	At Pakhna Village and Spitali the systems tract is stratigraphically expanded compared to the other locations and generally marl-rich. Marl and cemented-marl beds are ~20-130 cm thick with ~20-70 cm thick foraminiferal chalk and marly-chalk beds. At Kottaphi Hill the systems tract is represented by ~16 cm thick foraminiferal chalks and marly-chalks interbedded with ~20 cm thick marls and cemented-marls that contain iron bands. At Kalavasos the systems tract is iron stained and poorly represented and comprises ~10 cm thick foraminiferal chalks interbedded with ~7 cm marls and cemented-marls.	155 cm	390 cm	390 cm	640 cm
	LST	At Kottaphi Hill and Kalavasos the systems tract is well-developed and composed of iron stained, interbedded marls and cemented-marls. In both section marls dominate over cemented marls and are typically 12-44 cm thick where the cemented-marls are 4-36 cm thick. At Spitali and Pakhna Village iron stained marls (~50-200 cm thick) are also dominant over cemented-marls (~10-25 cm thick), but are occasionally interbedded with marly-chalks	385 cm	205 cm	205 cm	195 cm
	SB(e)	At Kottaphi Hill this SB is represented by a well-developed hardground surface with borings and iron and probably Mn mineralisation. At Kalavasos the top surface of an iron stained firmground defines this SB. At the Spitali Road Cut the SB is defined by the surface of an iron stained foraminiferal chalk underlying iron stained marl-rich beds. At Pakhna Village it is marked by an irregularly based foraminiferal chalk firmground surface.				

Sequence	Systems Tract	Charateristic features	Kottaphi Hill	Kalavasos	Pakhna Village	Spitali Road Cut
D 17.3 – 16.4 Ma	HST	At Kottaphi Hill and Kalavasos this systems tract is composed of thinly bedded (~15 cm thick) foraminiferal chalks and marly-chalks. These are generally interbedded with 1-2 cm thick marls at Kalavasos and 10-40 cm thick cemented-marls at Kottaphi Hill. At Pakhna Village the systems tract is composed of ~15-50 cm thick foraminiferal chalks and marly-chalks interbedded with ~2-35 cm thick marly-chalks. At Spitali the systems tract is composed of thick (~20-110 cm) foraminiferal chalk and marly-chalks interbedded with thin (<25 cm thick) marls.	275 cm	400 cm	320 cm	138 cm
	TST	At Kottaphi Hill and Kalavasos this systems tract is composed of 15-30 cm thick foraminiferal chalks and marly-chalks interbedded with ~15 cm thick marls and cemented-marls. At Pakhna Village the systems tract is composed of ~30 cm thick foraminiferal chalks, interbedded with thick 1 m marl-rich beds. At Spitali the systems tract is expanded and composed of groups of ~20-50 cm foraminiferal chalks and marly-chalks interbedded with groups of ~5-25 cm marls and cemented marls.	195 cm	35 cm	275 cm	765 cm
	LST	At Kottaphi Hill, Kalavasos and Spitali this systems tract is composed of ~10-30 cm thick marls and cemented-marls, with occasional ~20 cm thick marly-chalks. At Pakhna Village this systems tract is expanded where the marl-rich beds are thicker and reach 200 cm in thickness.	195 cm	45 cm	1250 cm	100 cm
	SB(d)	At Kottaphi Hill this SB is marked by a nodular foraminiferal chalk surface, and a Kalavasos by a foraminiferal chalk firmground, both underlying marl-rich couplets. At Pakhna Village it is marked by the top surface of an irregularly topped foraminiferal chalk. At Spitali the SB is developed on the top surface of a 115 cm marly chalk, underlying marl-rich couplets.				

Sequence	Systems Tract	Charateristic features	Kottaphi Hill	Kalavasos	Pakhna Village	Spitali Road Cut
C 18.7 – 17.3 Ma	HST	Well-defined and fully exposed at Kottaphi Hill and Kalavasos, where it is chalk-rich, and composed of 15-40 cm thick foraminiferal chalks and marly-chalks interbedded with thinner ~2-20 cm thick marls and cemented-marls. At Spitali it is composed of 1+ m foraminiferal and marly-chalks. At Pakhna Village it is more marl-rich with ~15-50 cm thick marls and cemented marls.	350 cm	350 cm	410+ cm	440+ cm
	TST	Well-defined and composed of thickening upwards foraminiferal chalks ranging from 10-15 cm thick, interbedded with ~10-20 cm thick marls and cemented-marls.	207 cm	195 cm	N/P	N/P
	LST	Moderately well-defined and composes of ~20-40 cm thick marls interbedded with subordinate ~15 cm thick cemented-marls and occasional marly-chalk beds.	330 cm	250 cm	N/P	N/P
	SB(c)	Poorly-developed SB, marked by the contact of a marly-chalk bed at Kottaphi Hill and Kalavasos with overlying marl-rich couplets.			N/P	N/P
B 19.5 - 18.7 Ma	HST	Poorly-defined and composed dominantly of ~15-30 cm thick foraminiferal chalk and marly-chalk beds, with subordinate ~20 cm thick cemented marls.	78 cm	31 cm	N/P	N/P
	TST	Poorly-defined and composed of ~10-15 cm thick marly-chalks interbedded with 10-15 cm thick marls and cemented marls.	80 cm	60 cm	N/P	N/P
	LST	Poorly-developed and comprises 20-30 cm thick marls with subordinate ~5 cm thick cemented-marls.	75 cm	50 cm	N/P	N/P
	SB(b)	Defined at Kottaphi Hill and Kalavasos by the contact of a marly-chalk bed underlying marl-rich couplets.			N/P	N/P
A 20.52-19.	HST	Well-developed and only fully exposed at Kalavasos, it comprises ~15-40 cm thick marly-chalks interbedded with 10-30 cm thick cemented-marls.	220+ cm	90 cm	N/P	N/P
	TST	Marl-rich systems tract dominated by ~10-30 cm thick cemented-marls interbedded with ~10-20 cm thick marls, and infrequent ~15-35 cm thick foraminiferal and marly-chalks.	N/P	290 cm	N/P	N/P
	LST	Well-defined and composed dominantly of thick (20-170 cm) marls, interbedded with ~ 10 cm thick cemented-marls and marly-chalks	N/P	150 cm	N/P	N/P
	SB(a)	Defined by the contact between a 40 cm foraminiferal chalk, with overlying marl-rich couplets.	N/P		N/P	N/P

Alternative depositional sequences identified at the Pakhna Village and the Spitali Raod Cut localities, within sequence F

Sequence	Systems Tract	Charateristic features	Kottaphi Hill	Kalavasos	Pakhna Village	Spitali Road Cut
F4 Between 14.8-11.7 Ma	HST	Chalk-rich systems tract at Pakhna Village and Spitali, composed of ~20-80 cm thick foraminiferal chalks and marly-chalk interbedded with ~10-20 cm thick marl-rich beds.	N/D	N/D	210 cm	295 cm
	TST	Marl-rich at Pakhna Village with ~100 cm thick marls interbedded with ~25 cm thick marly-chalks. At Spitali the systems tract is stratigraphically expanded and chalk-rich with ~40-90 cm thick foraminiferal chalk and marly-chalks interbedded with ~~20-80 cm thick marl-rich beds.	N/D	N/D	120 cm	450 cm
	LST	Composed of ~30-120 cm thick marl-rich beds interbedded with subordinate ~20 cm thick cemented-marls and marly-chalks.	N/D	N/D	250 cm	160 cm
	SB (f4)	Marked by the contact between a sharp-topped foraminiferal chalk at Pakhna and a marly-chalk at Spitali, with overlying marl-rich couplets	N/D	N/D		
F3 Between 14.8-11.7 Ma	HST	Comprises thickly bedded (~30-120 cm) foraminiferal-chalks and marly-chalks at Spitali, interbedded with 1 cm tick marls. At Pakhna the systems tract is more marl-rich with ~20-40 cm thick chalk-rich beds interbedded with ~5-35 cm thick marls and cemented-marls.	N/D	N/D	280 cm	270 cm
	TST	Stratigraphically thin systems tract composed of ~20 cm thick marls and ~10 cm thick marly-chalks at Spitali, and ~30 cm thick foraminiferal chalks interbedded with ~5~25 cm thick marls and cemented-marls at Pakhna Village.	N/D	N/D	90 cm	95 cm
	LST	Composed of ~ 40-130 cm thick marl-rich sediments at Spitali and Pakhna Village.	N/D	N/D	230 cm	220 cm
	SB (f3)	Marked by the contact between a prominent foraminiferal chalk at Spitali and Pakhna Village, with overlying marl-rich couplets.	N/D	N/D		

Sequence	Systems Tract	Charateristic features	Kottaphi Hill	Kalavasos	Pakhna Village	Spitali Road Cut
F2 Between 14.8-11.7 Ma	HST	Stratigraphically expanded at Spitali this systems tract comprises ~20-90 cm thick foraminiferal chalks and marly-chalks. At Pakhna Village it is composed of ~15-30 cm thick foraminiferal chalks and marly-chalks interbedded with ~20 cm cemented-marls.	N/D	N/D	90 cm	390 cm
	TST	Stratigraphically expanded at Spitali this systems tract is marl-rich with ~10~60 thick cm marls and cemented-marls interbedded with ~25-40 cm thick chalk rich-beds. At Pakhna Village the systems tract is composed of interbedded ~35 cm thick marly-chalk and marl-rich beds.	N/D	N/D	70 cm	380 cm
	LST	Composed of ~40-100 cm thick interbedded marl-rich beds.	N/D	N/D	160 cm	120 cm
	SB (f2)	Marked by the contact of a prominent 100 cm thick foraminiferal chalk at Spitali, and a 10 cm thick marly-chalk at Pakhna Village with marl-rich couplets.	N/D	N/D		
F1 Between 14.8-11.7 Ma	HST	Only developed at Pakhna Village and Spitali this systems tract is composed of ~20-100 cm thick foraminiferal chalks ~20-50 cm thick marl-rich beds.	N/D	N/D	85 cm	255 cm
	TST	A marl-rich systems tract, expanded at Spitali with ~50 cm thick cemented-marls and marls interbeded with relatively thin (~15-20 cm) chalk-rich beds. At Pakhna Village it comprises 10-100 cm thick marls interbedded with ~10-30 cm thick chalk-rich beds.	N/D	N/D	280 cm	415 cm
	LST	Marl-rich systems tract at both Pakhna Village and Spitali, is comprises ~100 cm thick marls, with occasional ~15 cm hick cemented marls. Expanded at Pakhna Village	N/D	N/D	545 cm	120 cm
	SB(F)	Same SB as SB(f), depositional sequence F.	N/D	N/D		

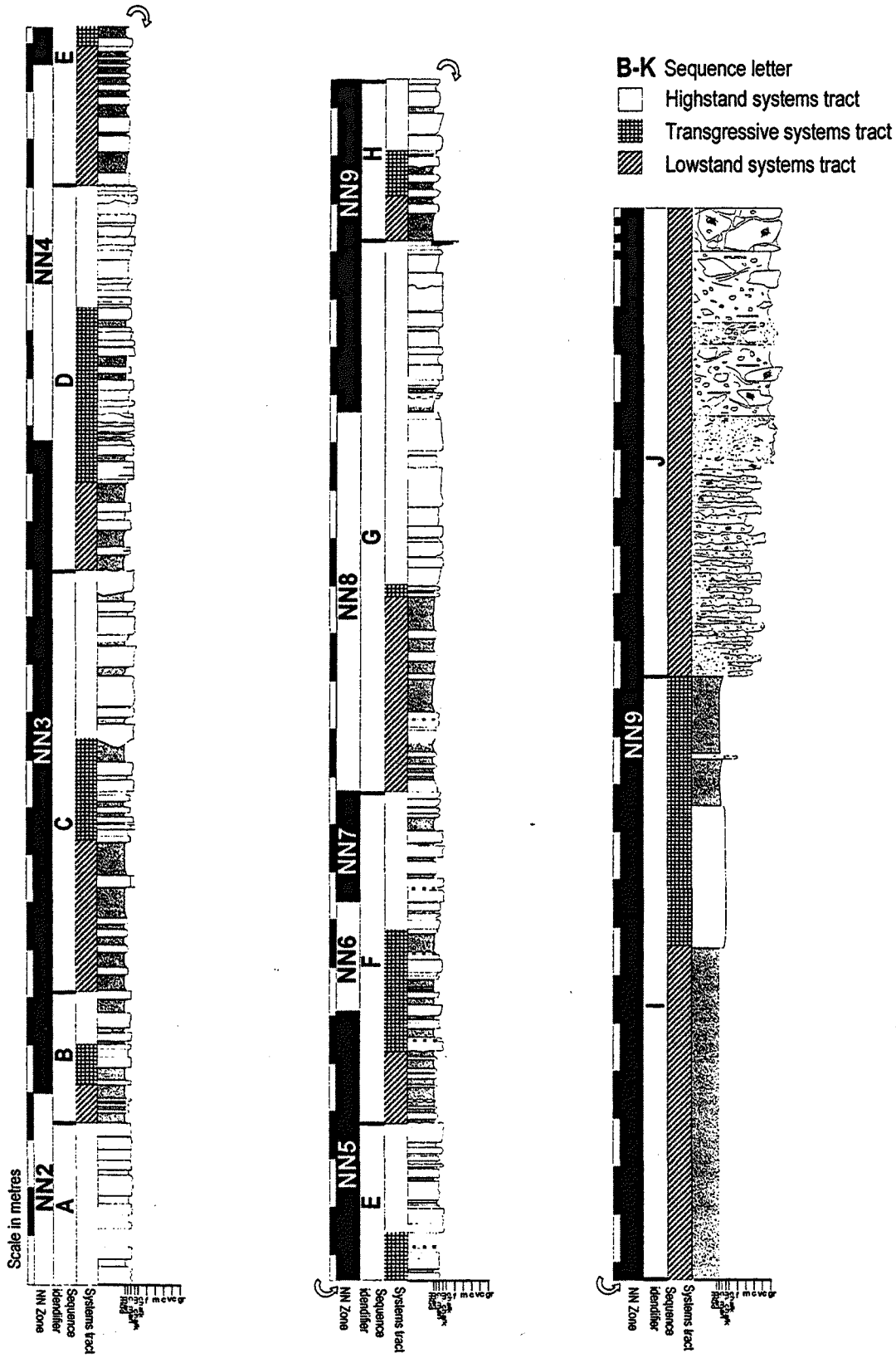

Figure 3.6 Graphic log illustrating the sequence stratigraphic interpretation of Pakhna Formation at Kottaphi Hill. Key for graphic log figure 3.5. Scale bar in metres.

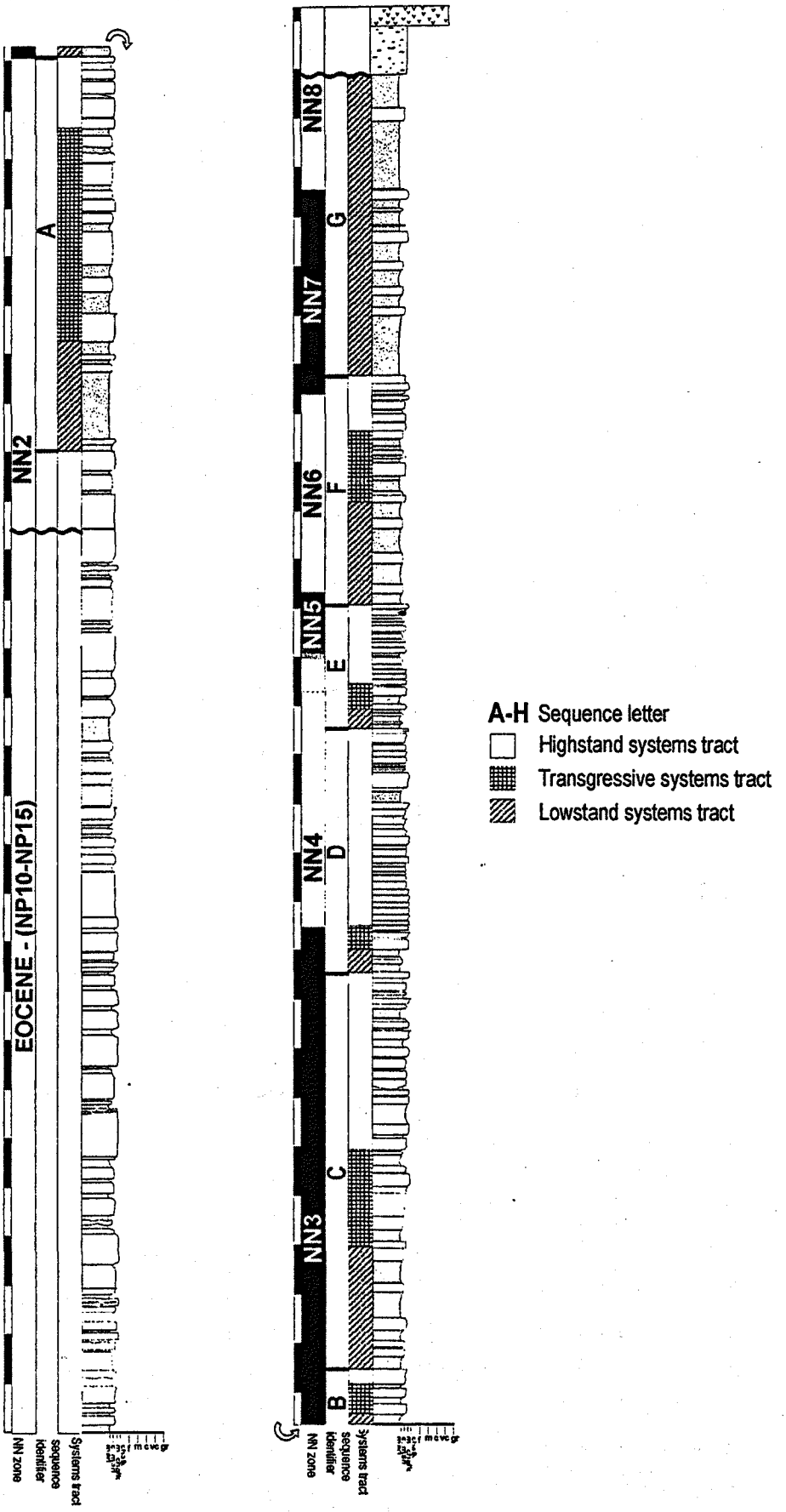

Figure 3.7 Graphic log illustrating the sequence stratigraphic interpretation of the Pakhna Formation at Kalavasos. Scale bar in metres. Key on figure 3.5

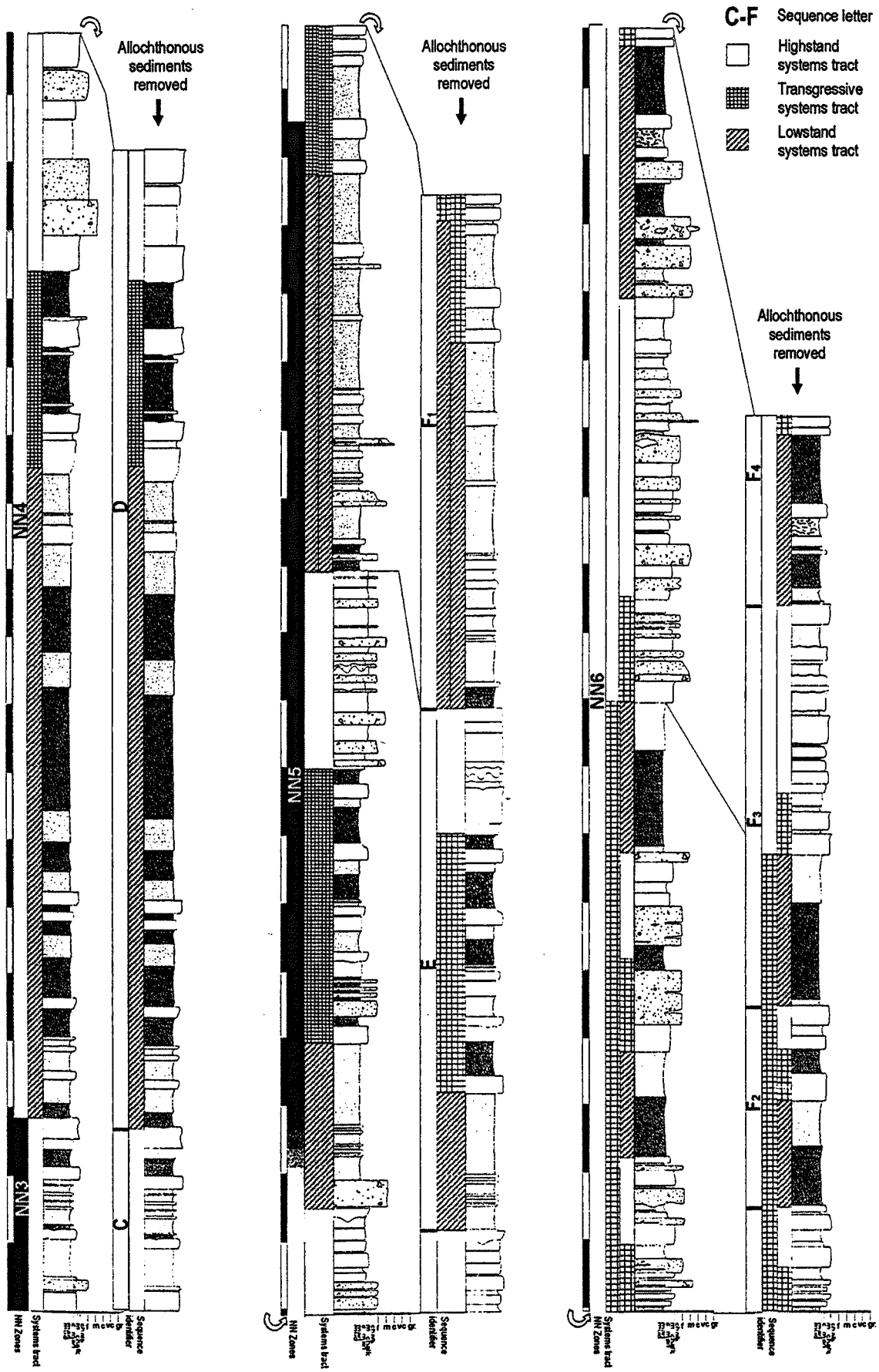

Figure 3.8 Graphic log illustrating the sequence stratigraphic interpretation of the Pakhna Formation at Pakhna Village. Scale bar is in metres. Key on figure 3.5. See section 3.3.4 for explanation.

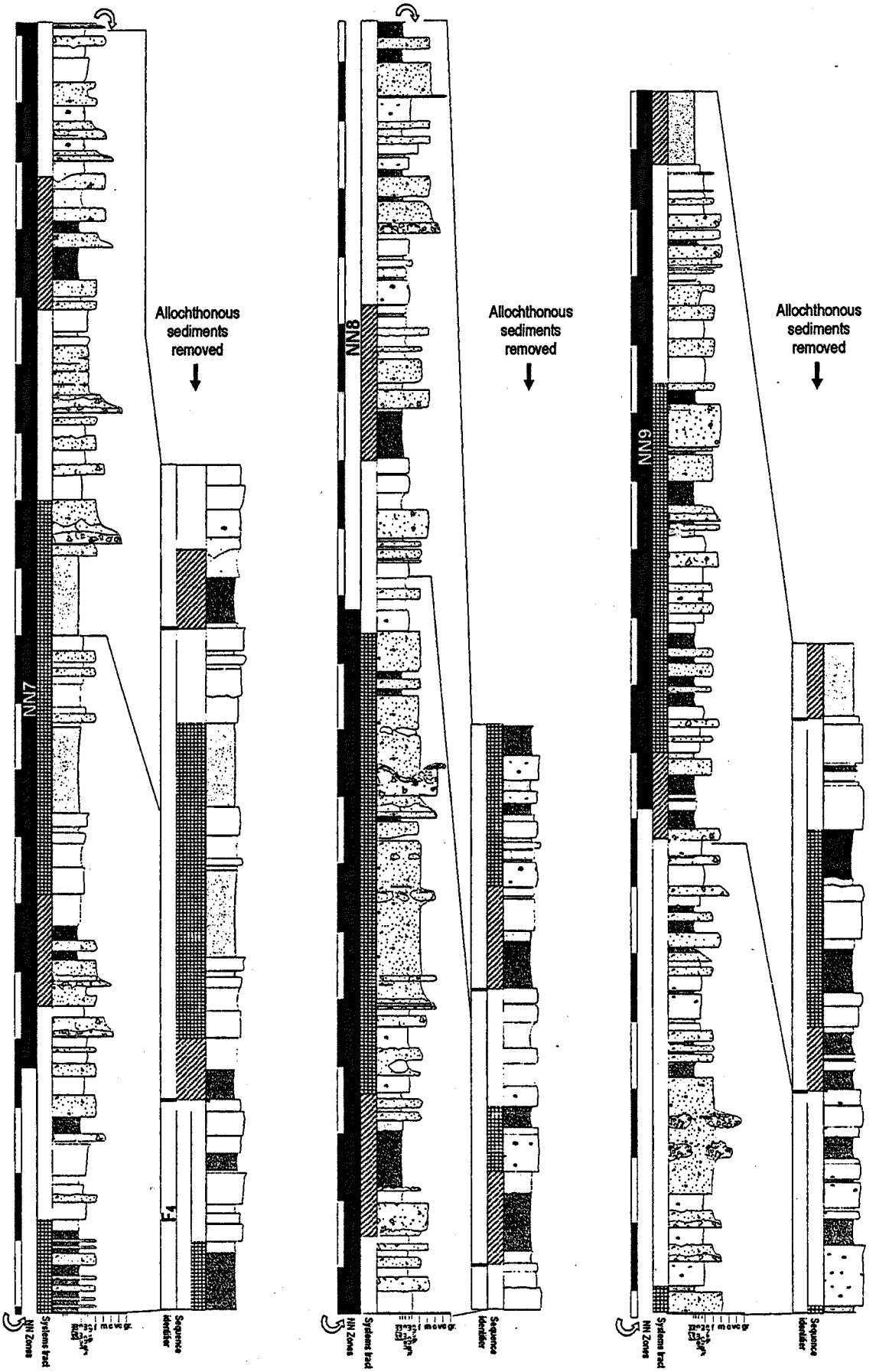

Figure 3.8 continued

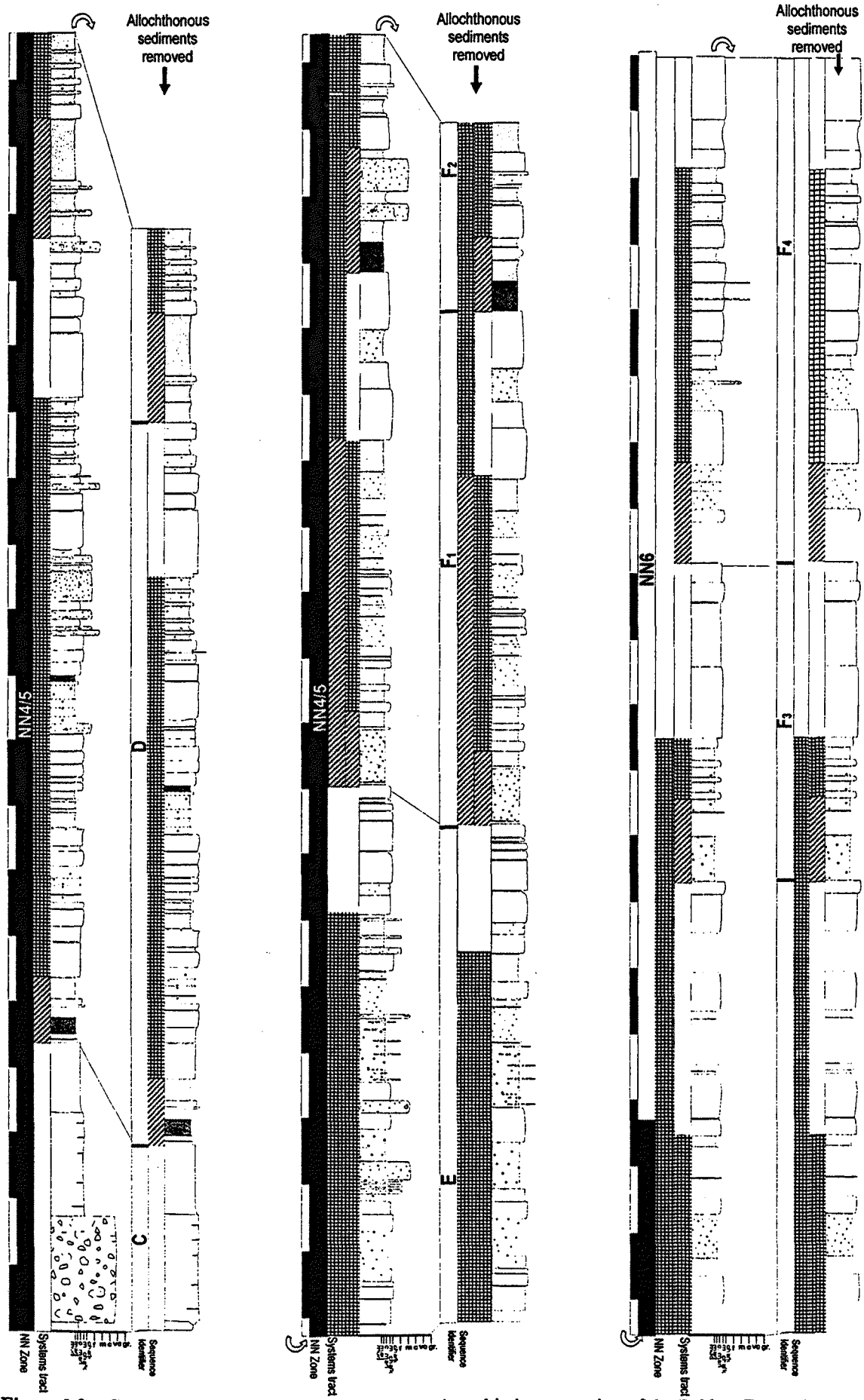

Figure 3.9 Graphic log illustrating the sequence stratigraphic interpretation of the Pakhna Formation at the Spitali Road Cut locality. Scale bar is in metres. Key on figure 3.5. See section 3.3.4 for explanation.

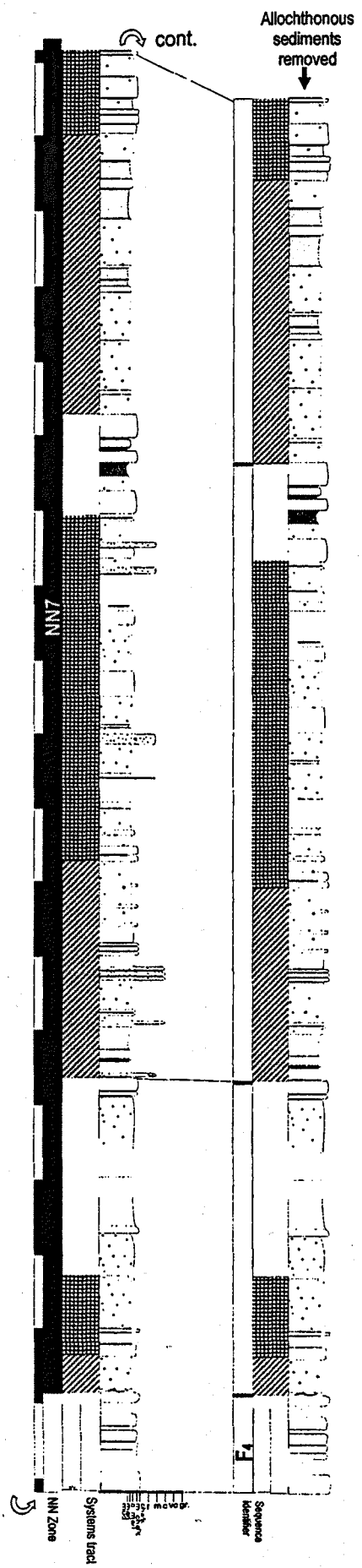

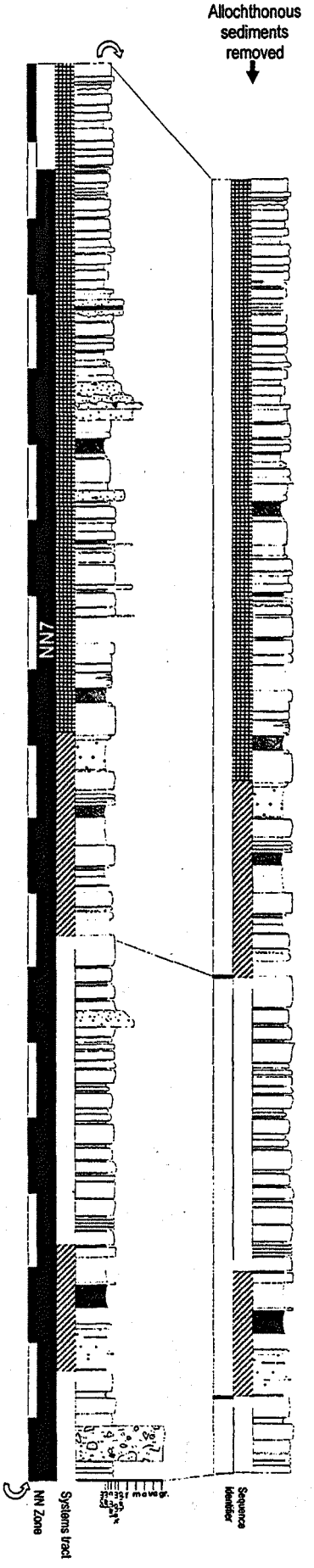

Figure 3.9 continued.

Figure 3.9 continued.

3.4 Problems applying the sequence stratigraphical model

The sequence stratigraphic model proposed here works well for depositional sequences at Kottaphi Hill and Kalavasos, but it breaks-down above NN7 at the Pakhna Village and Spitali Road Cut sections. Figures 3.8 and 3.9 are graphic logs of the Pakhna Village and Spitali Road Cut. The data is shown in two ways, firstly as a full log and secondly, in order to facilitate the sequence stratigraphic interpretation, with the allochthonous units removed. All calcarenite and calcrudite beds were considered allochthonous and in the right hand columns of Figures 3.8 and 3.9 have been removed. This considerably aids the identification of the chalk-marl couplets, and hence the sequence stratigraphic interpretation. The silty-mudstone facies has not been removed as it is interpreted to represent an extension to the continuum of carbonate dilution by terrigenous derived material during lowstand deposition. The coarser-grained allochthonous beds are clearly transported and have erosional bases with the background chalk-marl couplets. Unlike the silty-mudstone facies they represent total dilution by terrigenous and reworked material. These event beds are not interpreted, in this circumstance, to strongly relate to relative sea-level fluctuation, but to near constant tectonic activity associated with the uplifting Troodos massif, because for depositional sequences that are well-defined at Pakhna Village and Spitali (C-E), allochthonous material is not confined to any one systems tract.

During the deposition of sequences C-F at Pakhna Village and Spitali, the input of allochthonous material appears to have been sufficiently low not to totally disrupt the background pelagic carbonate deposition. The increasing influence of erosional allochthonous sedimentation (the Spitali Member) in interpreted to have had the effect of removing large parts of the background carbonate-rich deposits, hindering the sequence stratigraphic interpretation above NN7 (sequence F). Due to this, only a tentative attempt has been made to identify deposition sequences within the Spitali Member at Pakhna Village and the Spitali Road Cut above NN7 (Figures 3.8 and 3.9).

It is possible to interpret the sequence stratigraphy of sequence F at Pakhna Village and the Spitali Road Cut two ways, either as one whole depositional sequence (F) or as four smaller sequences (F1 to F4) Sequence F, at both localities, generally shows chalk rich couplets becoming more frequent up the section, with more marl-rich beds at its base (Table 3.1; Figures 3.8 and 3.9). Sequences F1, F2, F3 and F4 are developed on a smaller scale (5-10 m), within the couplets in sequence F, which can be interpreted to represent four additional, less well-defined, depositional sequences (Table 3.1; Figures, 3.8 and 3.9). It is thought that at least three of these sequences relate to regional sea-level change, as, within the constrains of biostratigraphy they correlate to minor depositional sequence developed in European Basins (Hardenbol *et al.*, 1998). Sequences F1, F2, F3 and F4 are not developed in the Kottaphi Hill and Kalavasos successions.

3.3.5 Regional and local significance of the Pakhna Formation depositional sequences

Figure 3.4 summarises the sequence stratigraphic interpretation of all locations investigated in Cyprus and shows the possible correlation to the European Basin sequence chronostratigraphy (Hardenbol *et al.*, 1998).

Within the resolution of biostratigraphy all depositional sequences developed at Kottaphi Hill and Kalavasos correlate well with each other. The depositional character of the individual sequences is also remarkably similar between the two sections (Figure 3.4). This is particularly true for sequences B, C and D. Sequences boundaries d-g correlate within the resolution of biostratigraphy throughout all the study sections, and SB(b)-SB(g) at Kottaphi Hill and Kalavasos. The most plausible correlation within the Spitali Member at the Pakhna Village and Spitali Road Cut sections is shown in Figure 3.4.

In order to establish if sequence development within the Pakhna Formation is a result of regional relative sea-level changes, the sequence stratigraphic framework established here is compared to the sequence chronostratigraphic record gained from European Basins (Figure 3.4). This record is derived from seismic, geophysical and outcrop data (Hardenbol *et al.*, 1998). The sequences developed in Cyprus correlate, within the constraints of biostratigraphy (Chapter 2), to the sequences defined by Hardenbol *et al.*, (1998) with one the possible exception, SB(d). SB(d) lies stratigraphically below the last occurrence datum (LO) of *Sphenolithus belemnos* (NN3) and is suggested to correlate to the Bur 4 sequence boundary of Hardenbol *et al.*, (1998). If this is the case then the LO of *Sphenolithus belemnos* must be reworked. The base of NN3 and NN7 are certain and constrain the time interval over which sequence boundaries are developed at Kottaphi Hill and Kalavasos as they are FO datums, and are not susceptible to reworking.

The ages proposed for the sequence boundaries in Table 3.1, are those used for the Hardenbol *et al.* (1998) sequences, which are integrated into the Berggren *et al.*, (1995) time scale using calcareous nannofossil and planktonic foraminifera biostratigraphy.

Sequence boundaries Ser 2 and Ser 3 (13.6 and 12.7 Ma respectively) defined by Hardenbol *et al.*, (1998) are not represented in the Kottaphi Hill or Kalavasos sections (Figure 3.4). However, within sequence F at the Pakhna Village and Spitali Road Cut sections there are three additional sequence boundaries developed (SB(f2), SB(f3),SB(f4), Figures 3.4, 3.8 and 5.9), that are likely, in part, to correlate to Ser 2 and Ser 3. Ser 2 and Se 3 are interpreted to be minor sequence boundaries (Hardenbol *et al.*, 1998), and are indeed the most minor over the time interval considered. It is interpreted that the control on relative sea-level for these three sequences was insufficient to effect these pelagic sections or possibly that the evidence for them has been removed by the overlying major sequence boundary, SB(g). At both Kottaphi Hill and Kalavasos there is evidence for the possibility of missing strata; at

Kalavasos depositional sequence E is condensed, and iron stained, and it is possible that there is a hiatus at SB(f) that occluded the development of subsequent depositional sequences. At Kottaphi Hill sequence F is characterised by several 2-8 cm iron bands that may represent hiatuses, accounting for the absence of sequences Ser 2 and Ser 3.

Miller and Sugarman (1995) have correlated Miocene depositional sequences developed in the Kirkwood Formation (New Jersey; ODP Leg 150X) with global $\delta^{18}O$ and Maryland outcrops. Miller *et al.* (1996) correlate these with sequences (slope reflectors) on the New Jersey shelf (ODP Leg 150). Sequences developed on the shelf are constrained by Sr isotope stratigraphy, magnetostratigraphy and with planktonic foraminiferal, nannofossil, dinocycst and diatom biostratigraphy. Figure 3.10 shows a correlation of sequence boundaries developed in the New Jersey, both on- and off-shore, with those developed over the same interval in the Miocene of Cyprus. A good correlation exists between SB(d), SB(e), SB(f) and SB(g) and the slope reflectors M5.2, M5, M4, and with the correlative sequences in the Kirkwood Formation (Figure 3.10). The additional depositional sequences developed at Pakhna Village and the Spitali Road Cut, also have

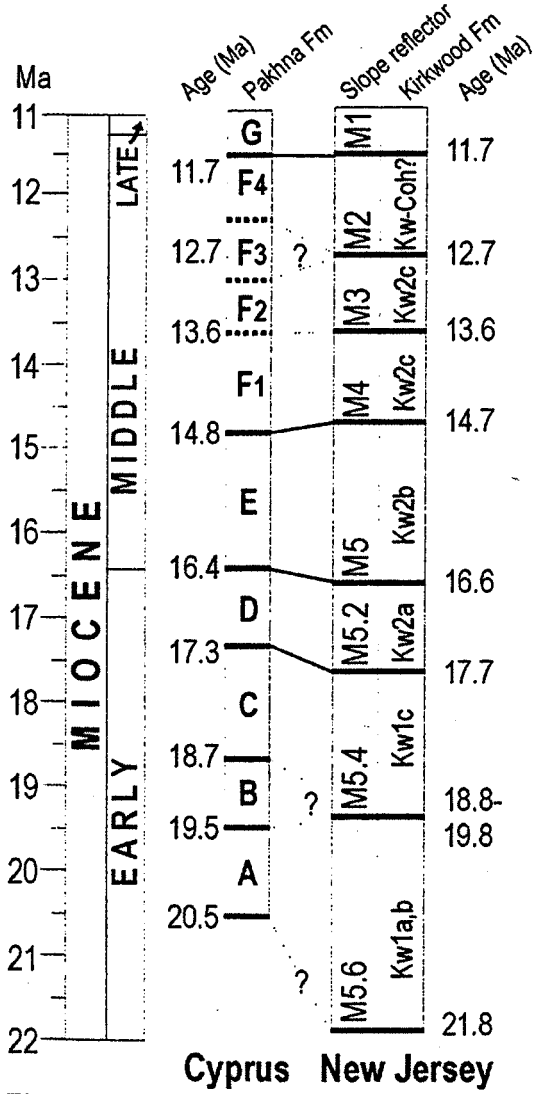

Figure 3.10 Ages of sequence boundaries developed in the Pakhna Formation, compared to those developed on the New Jersey margin (on-shore, Kirkwood Formation, and off-shore slope reflectors). Dates from (Miller *et al.*, 1996). Timescale from Berggren *et al.*,(1995).

correlative sequences boundaries on the New Jersey Margin. F2 correlates to M3 and either, or both, F3/F4, correlate to the M4 slope reflectors (Figure 3.10).

The positive correlation between sequences developed during the tectonically active Miocene of Cyprus and those of European sequence chronostratigraphy and the New Jersey Margin, suggests that they resulted from at least regional and possibly global, variation in relative sea-level, and not localised tectonic events. The influence of tectonics on the Pakhna Formation appears therefore to be restricted to providing allochthonous material, and possibly modifying depositional sequences, via erosional processes.

3.4 Summary

The packages of chalk and marl couplets of the Kottaphi Member are interpreted using sequence stratigraphic nomenclature, and reveal at least 9 depositional sequences from the Lower to Upper Miocene.

Lowstand systems tracts are characterised by marl-rich couplets. The transgressive surface is marked by the first prominent foraminiferal chalk and by the change to couplets with ~equal thickness chalk and marl, typical of the transgressive systems tract. The maximum flooding surface separates ~equal thickness chalk and marl couplates, of the TST, from chalk dominated couplets of the highstand systems tract. Sequence boundaries are expressed as either a hardground or firmground or cessation of typical chalk dominated HST deposits in favour of marl-rich couplets which mark the LST.

At the Pakhna Village and Spitali Road Cut locations the sequence stratigraphic interpretation is hampered by the introduction of large amounts of allochthonous calcarenite and calcrudite units in the upper part of the Spitali Member. These units are interpreted to mainly derive

from tectonic activity and therefore removing them from the graphic logs helps to elucidate the sequence stratigraphical model defined by the pelagic chalk and marl couplets. These allochthonous units are also interpreted to have partially removed pelagic carbonate units.

Within the constraints of biostratigraphy the sequence boundaries developed correlate across Cyprus, and to sequences defined by European sequence chronostratigraphy and the New Jersey Margin, which indicates that sequence development in the Pakhna Formation was a result of at least pan-European-American relative sea-level change.

Chapter 4

Orbital Cyclicity in Miocene Pelagic Carbonate Successions of the Pakhna Formation

4.1 Introduction

The Miocene-aged Pakhna Formation forms part of the late Cretaceous-Recent sedimentary cover sequence of the Troodos Ophiolite (Robertson, 1977). The formation was deposited during a tectonically active regime, dominated by the uplift of the Troodos Ophiolite, which has been situated above a northward dipping subduction zone since the early Miocene (Morse, 1996; Robertson 1998; Lagroix and Borradaile, 2000). The Kottaphi Member forms part of the Pakhna Formation and is dominantly composed of interbedded chalk, marly-chalk, cemented-marl and marl beds. These facies are grouped into couplets. The lower, marl-rich bed of each couplet, is interpreted to represent the increased dilution of background carbonate rain by an influx of terrigenous material (Chapter 2). The couplets vary in thickness and grouping to reveal a larger scale cyclicity that is interpreted to relate to relative sea-level change (Chapter 3). This chapter utilises the spectral analysis of stratigraphic time series, based on bed thickness and facies data, to detect regular cyclicity developed in the Pakhna Formation (Kottaphi Member). Regular cyclicity is often indicative of climatic variation that alters due to the intensity and distribution of incoming solar insolation (Schwarzacher, 2000) that is primarily determined by the periodic orbital parameters (or Milankovitch cycles). If multiple cyclicity (with different wavelengths) is detected, with ratios similar to those of the eccentricity (~100 and 410 kyr), obliquity (41 kyr) and precessional (~21 kyr) Milankovitch cycles then orbital parameters are strong candidates for cycle development in Cyprus, and not localised tectonic activity.

4.2 Stratigraphic time series and spectral analysis

An introduction to spectral analysis and its geological significance is discussed in Chapter 1 and by (Weedon, 1991). Spectral analysis is an objective, statistical method for detecting regular cyclicity in data called stratigraphic time series (Weedon, 1991). It cannot explain why there is a connection between climatic variability and sedimentation, but can provide supporting evidence that such a connection existed (Weedon, 1991). A detailed mathematical explanation of the spectral analysis of stratigraphic time series is provided by Priestly (1981). A stratigraphic time series consists of observation of some parameter obtained at a constant interval of time or space (Weedon, 1991), and often takes the form of geochemical or bed thickness data. In this context the term stratigraphic time series is used to describe bed thickness or "length series" data which can be equated to time using sedimentation rates based on known age tie points. Weedon (1991) stresses the importance of relating stratigraphic time series data to the geological parameter that is linked to orbital-climate variability. The technique is based on Fourier analysis of stratigraphic time series in terms of component sine and cosine waves. The power spectrum plots the squared average amplitude (power) of each regular component sine and cosine wave against frequency (Weedon, 1993). The significance of peaks on the power spectrum is tested against a "red noise" time series generated by an independent random process (Weedon, 1991). This process produces limits (e.g. 5 and 95% limits) that form bands or confidence intervals of constant height above and below the theoretical noise level (Weedon, 1991). Peaks that emerge from this band are then distinguishable from the red noise model at a certain level of confidence and might then be attributed to a regular cyclicity in the stratigraphic time series (Weedon, 1991).

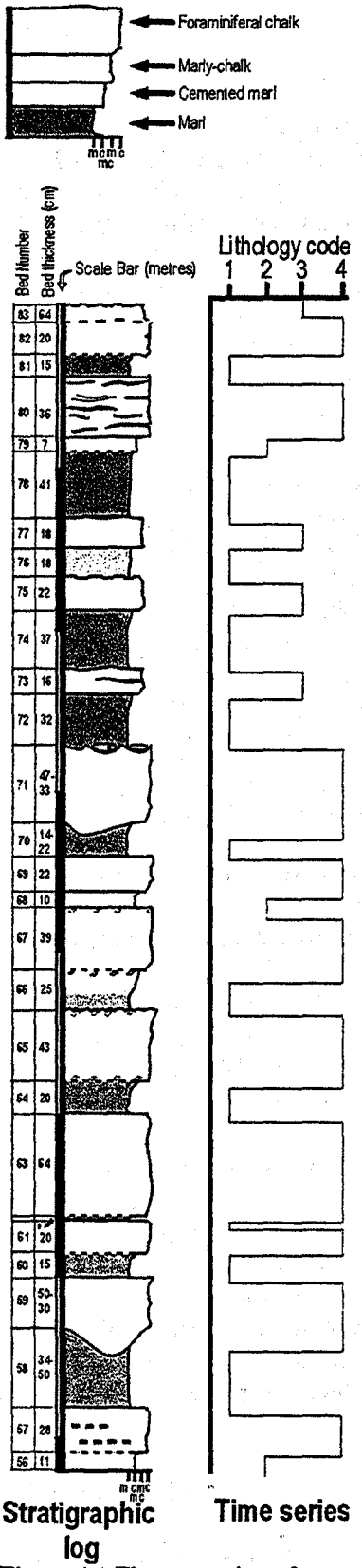

Figure 4.1 The generation of stratigraphic time series at Kottaphi Hill. Bed thickness data is combined with the lithology code 1 = marl, 2 = cemented-marl, 3 = marly-chalk and 4 = foraminiferal chalk

4.3 Methodology – stratigraphic time series generation of the Kottaphi Member

Stratigraphic time series were generated for Kottaphi Hill by digitising stratigraphic logs. Kottaphi Hill was selected for stratigraphic time series analysis as it is well-exposed, shows a clear cyclicity, and lacks allochthonous beds. Figure 4.1 illustrates a section of stratigraphic time series compared to the stratigraphic log of the same interval. Bed thickness data are combined with a code for lithology, (1 = foraminiferal chalk (<5 wt.% clay), 2 = marly-chalk (~10 wt.% clay), 3 = cemented-marl (~20 wt.% clay) and 4 = marl (~30 wt.% clay)) to produce a stratigraphic time series with a the square–wave (Figure 4.1). Analysing a two-fold (*i.e.* chalk-rich and marl-rich) division of facies in a stratigraphic time series, yielded poor results, with few significant peaks, as thinner, less contrasting cycles will be omitted. A four-fold division of lithology is interpreted to be more sensitive to climate change, as it divides the degree of carbonate dilution further, and will therefore pick out smaller variations in the supply of terrigenous material, that are interpreted to reflect climate. The stratigraphic time series for the Kottaphi Hill is split into eight separate data files, with limits defined by obvious changes in sedimentation rate (sections of expanded or condensed beds) and hiatuses (hardgrounds and

sequence boundaries).

The limits of each stratigraphic time series data file is illustrated on Figure 4.2 and raw data files are included in Appendix B. KOT SEC 1 starts at the base of the Kottaphi Hill section and incorporates depositional sequences A, B, and the LST the TST (lower part) of sequence C, and is characterised by beds of ~10-30 cm thick. KOT SEC 2 spans the TST (upper part) and HST of sequence C, and the LST and TST (lower part) of sequence D. It marks an interval of increased sedimentation rate, inferred by a notable increase in bed thickness (~20-65 cm thick). KOT SEC 3 spans the TST (upper part) and HST of sequence D. It marks a return to lower sedimentation rates (<25 cm bed thickness) and ends at the prominent hardground of SB(f). KOT SEC 4 spans the LST of sequence F and is characterised mainly by ~10-25 cm thick beds. KOT SEC 5 comprises the TST an HST of sequence F, and the LST, TST and HST (lower part) of sequence G, and is composed mainly of ~10-35 cm beds. KOT SEC 6 spans the HST (upper part) of sequence F, and most of the LST of sequence G. It is composed of mainly of 10-20 cm beds, suggesting lower sedimentation rates. KOT SEC 7 spans the LST (upper part), TST and HST of sequence G, and is characterised by ~20-60 cm thick beds. KOT SEC 8 starts at SB(h) and spans sequence H, and is composed of ~20-40 cm beds.

Hiatuses in the sections will only be important at times of changing sedimentation rate or if particularly long, such as a hardground (Weedon, pers. comm.). Periods of approximately equal sedimentation rate are therefore joined together to maintain continuity of the stratigraphic time series.

4.4 Results

Figure 4.2 illustrates the power spectra produced for stratigraphic time series KOT SEC 1-8, matched to their corresponding intervals of the graphic log of Kottaphi Hill. Power spectra in Figure 4.2, with peaks above the 90 % C.L., are labelled with the cycle thickness in metres, and are also shown in Table 4.1.

Table 4.1 Confidence levels and thickness (m) of significant peaks in KOT SEC 1-8

Stratigraphic time series	99 % C.L.	98 % C.L.	95 % C.L.	90 % C.L
KOT SEC 8		0.342		
KOT SEC 7	1.383		0.519	
KOT SEC 6	1.61			0.439
KOT SEC 5	0.899	2.247		0.349
KOT SEC 4			0.400	
KOT SEC 3	0.359		0.898	
KOT SEC 2	0.561	0.810	0.317	
KOT SEC 1	0.447		0.215	0.996

A clear hierarchy of regular cyclicity is evident in the data. Three scales of cyclicity are noted in KOT SEC 1, 2 and 5. The smallest cycle varies between 0.215-0.349 m, the intermediate cycle varies between 0.447-0.899 m, and the largest cycle varies between 0.810-2.247 m. This variability between cycle thickness is interpreted to occur due to different sedimentation rates between the stratigraphic time-series data. The remaining power spectra (KOT SEC 3, 4, 6 and 7, show either one or two significant peaks that fall into one of the previous defined hierarchical cycles. The intermediate cycle appears to be the most prevalent throughout the section and has an overall average thickness of 0.499 m.

4.5 Interpretation

In order to interpret the results each stratigraphic time series needs to be considered separately, as its the ratio between the significant peaks that is important and not the actual cycle wavelengths. The orbital parameters of eccentricity (~100 kyr), obliquity (41 kyr) and

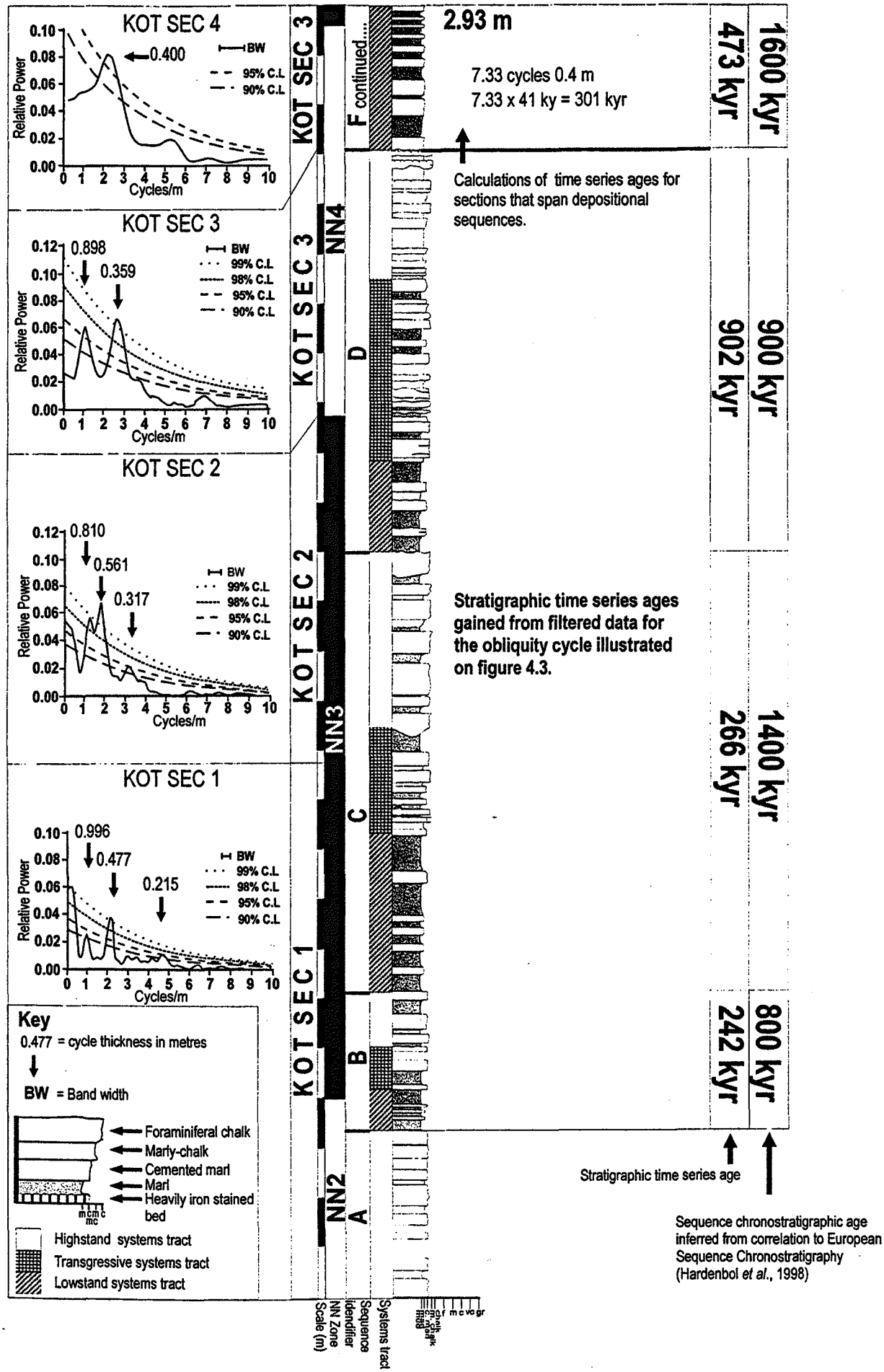

Figure 4.2 Graphic log illustrating power spectra gained from stratigraphic time series generated from Kottaphi Hill bed thickness and lithology data. Significant peaks on the spectra are labeled in metres. Ages based on time series data (this figure and figure 4.3), for depositional sequences are compared with those gained from sequence chronostratigraphy. Scale bar in metres.

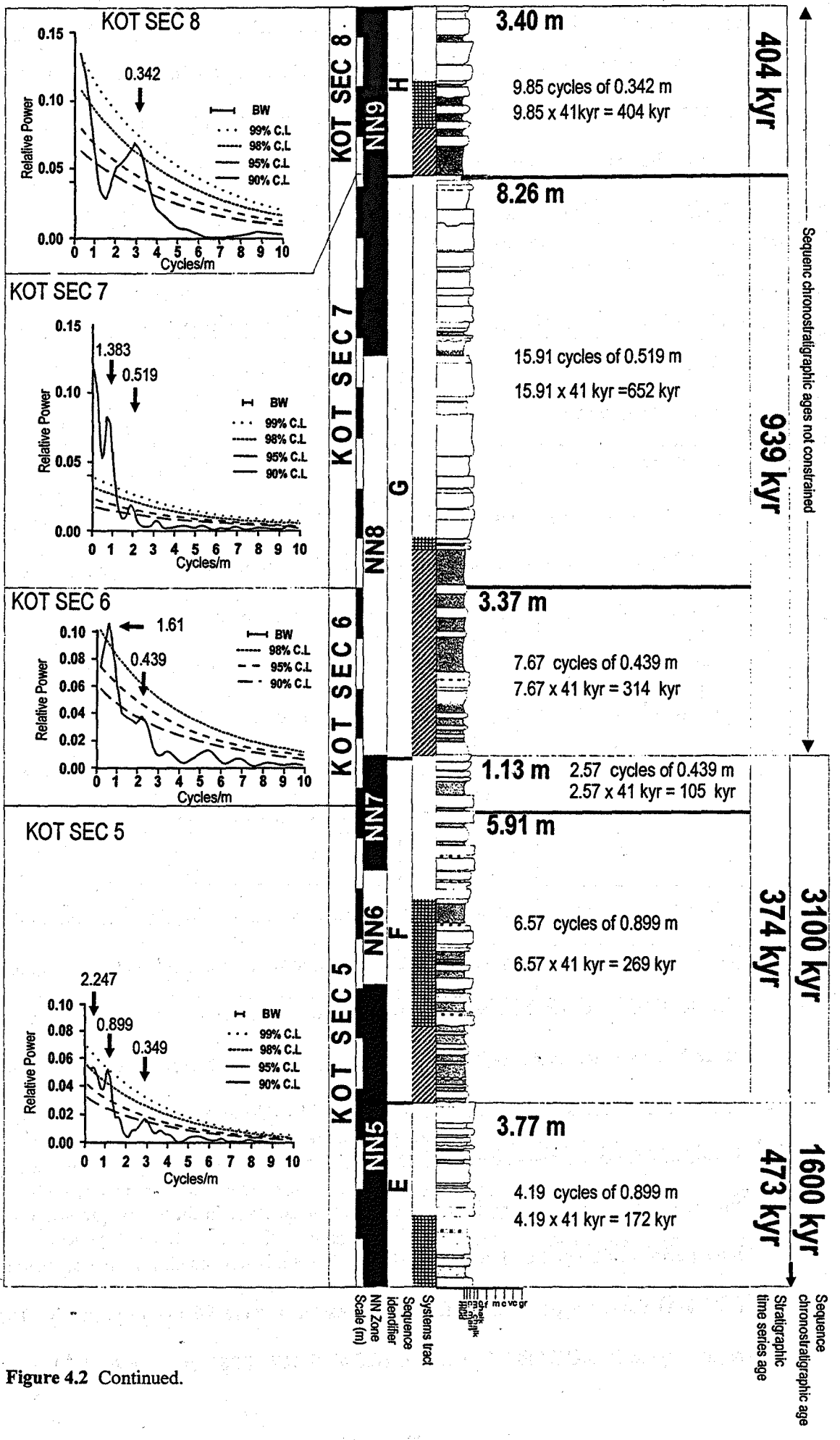

Figure 4.2 Continued.

precession (~21 kyr) identified by Milankovitch (discussed in Chapter 1) have a characteristic ratios, approximately 1:2.5:2 (~100/41/~21 kyr). It should be noted that the eccentricity cycle has its most important cycle at period of ~400 kyr with other significant cycles between 128 and 94 kyr (Schwarzacher, 2000). The obliquity cycle has a period of 53 to 41 kyr, though is termed the 41 kyr cycle (Weedon, 1993). The main precessional cycle periods are at 23 and 19 kyr, thought the precessional cycle is generally referred to a as the 21 kyr cycle (Schwarzacher, 2000). To test if the cycles are in the ratio of the Milankovitch orbital parameters, the intermediate peak of the three cycles identified is taken to be the 41 kyr cycle. As three scales of cyclicity are identified in KOT SEC 1, 2 and 5 (Figure 4.2), this assumption allows periods (in kyr) to be deduced, by calculating the wavelength ratios for other significant peaks. If the ratios and periods of the significant peaks match those of previously defined Milankovitch cycles, then a good case can be made for orbital cycles, particularly if the stratigraphic time series is constrained by a biostratigraphical or sequence stratigraphical framework. Table 4.2 contains the periods of significant peaks gained when assuming the intermediate peak as the 41 kyr obliquity cycle. This process is not suitable for KOT SEC 4 and 8 as they only have one significant peak.

The ratio of the cycles suggests that the small, intermediate and large scale cycles developed at Kottaphi Hill are likely to relate to the eccentricity, obliquity and processional cycles (Table 4.2). A match between the ratios of three significant peaks and the periods of the three Milankovitch cycles will strongly support a lithological response to orbital parameters. KOT SEC 1, 2 and 5 have three significant peaks (Table 4.1 and 4.2; Figure 4.2). The periods of the small scale cycles in KOT SEC 1 and 2, (20 and 23 kyr) match well with the precessional cycle (~21 kyr), though the largest scale cycle in these stratigraphic time series have periods of 86 and 60 kyr. KOT SEC 5 shows a better match for the eccentricity cycle (102 kyr) though a poor match for the precessional cycle 16 kyr respectively. The large regular cycle in KOT SEC 3, 5 and 7, (0.898, 2.247, 1.383 m respectively) have periods

close to the ~100 kyr eccentricity cycle, at 103, 102, and 109 kyr. The good match between peak ratios and Milankovitch cycles strongly supports the argument for the intermediate cycle representing the 41 kyr obliquity cycle.

Table 4.2. The periods (to the nearest kyr) of significant spectral peaks, based on the assumption of the intermediate peak representing the 41 kyr obliquity cycles. X = no small scale cyclicity identified in the power spectra above 90 % C.L.

Stratigraphic time series		Eccentricity (400, 128-94 kyr)	Obliquity (41 Kyr)	Precession (23 & 19 Kyr)	Ratio (~1:2.5:2)
KOT SEC 7	Frequency (m)	1.383	0.519	X	
	Period (kyr)	**109**	**41**	X	1:2.6:N/A
KOT SEC 6	Frequency (m)	1.61	0.439	X	
	Period (kyr)	**150**	**41**	X	1:3.6:N/A
KOT SEC 5	Frequency (m)	2.247	0.899	0.349	
	Period (kyr)	**102**	**41**	**16**	1:2.4:2.5
KOT SEC 3	Frequency (m)	0.898	0.359	X	
	Period (kyr)	**103**	**41**	X	1:2.5:N/A
KOT SEC 2	Frequency (m)	0.810	0.561	0.317	
	Period (kyr)	**60**	**41**	**23**	1:1.4:1.7
KOT SEC 1	Frequency (m)	0.996	0.477	0.215	
	Period (kyr)	**86**	**41**	**20**	1:2.1:2

4.5.1 Lithological response to orbital parameters

The three scales of regular cyclicity were identified by stratigraphic time series analysis of lithology and bed thickness data, and therefore must have a lithological expression in the sedimentary record. As orbital parameters operate synchronously, the pattern of cyclicity observed in the rock record will be a combination of these three cycles and will not be

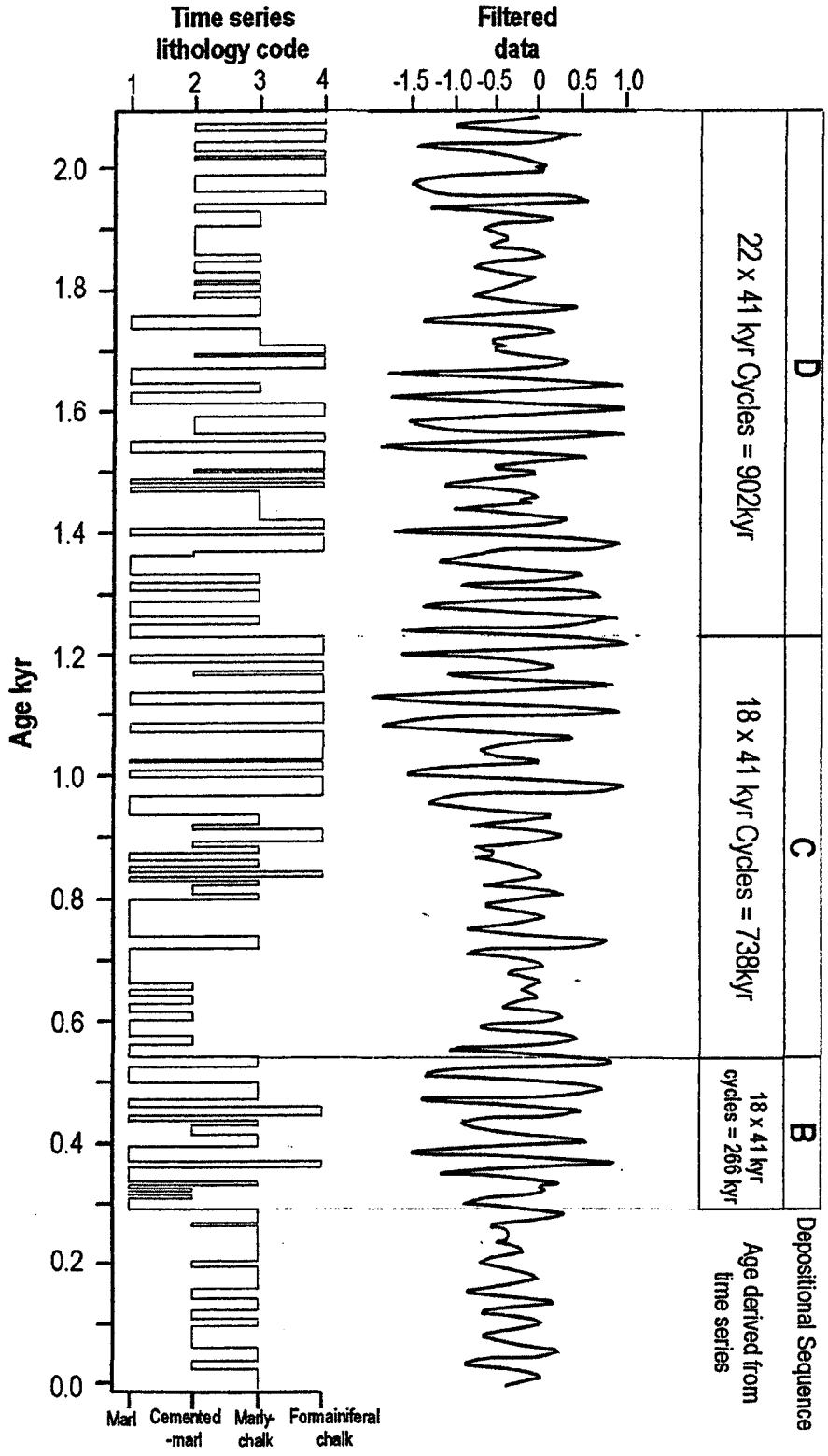

Figure 4.3 Results of band pass filtering the bed thickness stratigraphic time series (KOT SEC 1-3). Band pass filtering isolates the strong intermediate peak, interpreted as the 41 kyr obliquity developed on the individual power spectra for KOT SEC 1-3 (Figure 4.2) and plots the cycle using a time axis. This allows the position of the interpreted obliquity cycle to be seen in the stratigraphic time series data. The filtered data suggests the interpreted obliquity cycle, is represented by couplets. The minimum age estimates for depositional sequences B-D is deduced by counting the number of obliquity cycles developed in that sequence.

pervasive throughout the section. It is stressed therefore, that the lithological response to the three orbital parameters are unlikely to be clearly seen in isolation in the rock record, due to in-phase and out-of-phase relationships between these cycles. It is this combined signal that stratigraphic time series analysis separates into component frequencies. The thickness of the significant power spectra peaks give an estimate of the cycle thickness as recorded in the rock record. Bandpass filtering is used to effectively isolate certain frequencies developed in the power spectra (Weedon, 1999). Bandpass data (Figure 4.3) is produced from the combined stratigraphic time series of KOT SEC 1-3 only, as they show a strong intermediate cyclicity (interpreted as the 41 kyr obliquity cycle), constrained by other significant peaks, with relatively little variation in sedimentation rate (Figure 4.2). The process isolates the intermediate (obliquity) peak and plots it as a function of time. This is shown against the original lithology coded stratigraphic time series data in Figure 4.3. The data shows the position of successive obliquity cycles, through the stratigraphic time series. The thickness of these cycles vary according to differing sedimentation rates in KOT SEC 1-3. Each obliquity cycle (peak-peak) on Figure 4.3 correlates to medium-large scale couplets developed at ~30-70 cm thickness. The thickness of this obliquity cycle determined by the power spectra (Figure 4.2) varies between 0.359 m and 0.899m, depending on sedimentation rate. Though this thickness relates to average cycle thickness, it clearly encompasses stratigraphic thickness of medium-large scale couplets at Kottaphi Hill. In KOT SEC 2, for example, the obliquity cycle is particularly strong (table 4.1 and Figure 4.2) and has a 0.561 m cyclicity that is probably represented by the couplets of the HST of sequence C (Figure 4.2; Appendix A, Kottaphi Hill, bed nos. 59-71). The smallest scale regular cycle, interpreted as the precessional cycle, is represented by a cyclicity developed between 0.215 m and 0.349 m, depending on sedimentation rate. This is likely to be picked out as the smallest scale couplets, which are well preserved in KOT SEC 1, for example, in the LST of sequence B (Figure 4.2; Appendix A, Kottaphi Hill, bed nos. 16-21). The largest scale regular cycle, interpreted as the ~100 kyr eccentricity cycle, is represented by a cyclicity developed between

0.898 m and 2.247 m, depending on sedimentation rate. Its representation in the rock record is more enigmatic as the eccentricity cycle mainly modifies the intensity of the precession effect. It may therefore represent the balance between the smaller scale couplets (precessional) and the larger couplets (obliquity), but it is by no means clear. An example of this occurs in KOT SEC 5 where all three cycles are present. The eccentricity cycle is developed here are 2.247 m is may be depicted by the transition between thin couplets in the LST of sequence F and the thicker couplets of the TST, also in sequence F (Figure 4.2).

4.5.2 Age implication of the stratigraphic time-series data

The data gained from spectral analysis can be used to further estimate the relative age of the section. Relative ages gained from this method are not expected to match those of the biostratigraphical (Chapter 2) and sequence chronostratigraphical (Chapter 3) frameworks, as the sedimentary record is never complete. In this scenario stratigraphic time series age estimates will always be either accurate or underestimates of the ages gained from biostratigraphy or sequence chronostratigraphy, as the latter rely on assuming that events are approximately synchronous through time, and not a near continuous record of deposition. There are two methods of determining ages from stratigraphic time series analysis, bandpass filtering and cycle thickness. The former is more accurate, as cycle thicknesses on power spectra peaks only show the average thickness of the regular cyclicity, which varies between, and within, stratigraphic time series data due to variable sedimentation rates. By counting the number of 41 kyr cycles developed in the bandpass data (Figure 4.3) an age can be gained for depositional sequences. Figures 4.2 and 4.3 show ages gained via this process for depositional sequences B, C and D. Stratigraphic time series ages for sequences B and C, (266 and 738 kyr) are significantly lower (66 % and 47 %) lower than the ages gained from sequence chronostratigraphy (800 and 1400 kyr; Figure 4.2). The stratigraphic time series age for sequence C, (902 kyr) shows an excellent match to the age gained from sequence chronostratigraphy (900 kyr). For sections of Kottaphi Hill that do not have bandpass data,

stratigraphic time series ages are calculated from the number of 41 Kyr cycles developed per metre, as identified in the power spectra (Figure 4.2).

Figure 4.2 illustrates the ages gained from this method for sequences F-H, and compares them to the ages gained from sequence chronostratigraphy. As the stratigraphic time series cover different intervals than the depositional sequences, the age estimates for each depositional sequence is gained from combining ages gained from different sections of the stratigraphic time series (Figure 4.2). The intermediate significant peak, interpreted to represent the 41 kyr obliquity cycle, forms the basis for the dating the stratigraphic time series as is often dominant and present in all spectra. The stratigraphic time series age for sequence E, is 30% lower than that of the sequence chronostratigraphical date (473 verses 1600 kyr) and the stratigraphic time series date for sequence F only 12 % (374 verses 3100 kyr). Sequences F, G and H do not clearly correlate with sequences developed on the Hardenbol *et al.*, (1998) sequence chronostratigraphy chart, and therefore do not have comparative sequence chronostratigraphic ages (see Chapter 3) to compare with orbitally calculated dates.

Ages of depositional sequences gained from sequence chronostratigraphy are generally much larger that the minimum ages gained from stratigraphic times series analysis. These time differences are more than likely the result of hiatuses and or erosion at sequence boundaries, transgressive surfaces, maximum flooding surfaces and other less identifiable, minor, though probably more numerous, hiatuses between individual couplets. At sequence F for example where the strongest mismatch occurs between the two ages, there are many iron bands that, that are likely to represent minor hiatuses. Hiatuses in this depositional sequence are also probable as further depositional sequences are developed in this interval in the Pakhna Formation at the Pakhna Village and Spitali Road Cut localities in southern Cyprus (see Chapter 3).

4.6 The geological context of orbital forcing at Kottaphi Hill

The effects of orbital parameters on climate is poorly understood (Valdes and Glover, 1999), as climate is governed by a complex interaction between the atmosphere, hydrosphere, cryosphere, biosphere, and insolation. The latter is only dictated by orbital parameters and is the main forcing mechanism that influences climate (Valdes and Glover, 1999). Climatic variation is then preserved in the sedimentary record, via changes in sea-level and other aspects of the environment (Valdes and Glover, 1999). Orbital parameters have little effect on insolation on the global mean, annual basis. Obliquity influences the degree of seasonality, precession governs the degree of seasonal heating, and eccentricity modulates the precessional signal (Valdes and Glover, 1999; Chapter 1). The influence of the orbital parameters also varies with latitude. At low latitudes the precessional signal dominates, whereas at high latitudes the obliquity cycles dominates, however, at no latitude does the eccentricity dominate (Berger and Pestiaux, 1984; Berger *et al.*, 1993). This suggests that at the mid-latitude (Cyprus), neither the precessional or obliquity will dominate, and that the effects of both are likely to be observed. The beds within the couplets at Kottaphi Hill are interpreted to result from alternating periods of relative humidity and relative aridity, effecting the supply of terrigenous material (Chapter 2). Valdes and Glover (1999) review the current status of climate modelling and its response to orbital forcing. They note the importance of the precessional cycle in affecting the strength of monsoons at low latitudes. They further show that marginal monsoonal areas (mid-latitude) will be affected by small shifts in the monsoon, leading to changes between arid and humid climates in these areas. This is in agreement with the hypothesis suggested for couplet formation at Kottaphi Hill, as Cyprus is at mid-latitude, though the couplets probably represented by the obliquity, as well as the precessional cycle. This model requires the development of monsoons that are related to the uplift of the Himalayas (Frakes, *et al.*, 1992). The Sr isotope ratio of sea-water shows a sudden increase starting at ~20 Ma, and is interpreted to represent an increase chemical

weathering rates associated with the uplift of the Himalayas (Hodell and Woodruff, 1994). It is a possibility, therefore, that monsoon-type weather patterns existing during the early Miocene. As the eccentricity cycle effects the strength of the precessional cycles it is therefore feasible that this will be recorded in the pelagic carbonates of Cyprus as regular variation in the couplet size. The obliquity cycle controls the degree of seasonality (Weedon, 1993), and also provides a suitable mechanism for controlling run-off. Periods of highly contrasting seasons (i.e. cold winters and warm summers) will be characterised by increased run-off over those periods of low seasonal contrast. Weedon (1985) has identified obliquity and precessional cycles in the Jurassic-aged Blue Lias of southern Britain, and attributed cyclic sedimentation to variations in precipitation. In this model, periods of reduced precipitation resulted in the coccolithophore-derived carbonate dominating the sediment. Periods of increased run-off resulted in the relative increase in clay supply resulting in muddier facies. A similar mechanism in suggested for couplet formation in the Pakhna Formation.

4.7 Summary

Spectral analysis of stratigraphic time series data generated from bed thickness and lithology, reveals three scales of regular cyclicity developed at Kottaphi Hill. The frequency of these three scales of cyclicity, are at similar ratios to the eccentricity, obliquity and precessional orbital cycles. The smallest scale regular cyclicity is interpreted to represent the precessional (~21 kyr) cycle, which is probably represented by ~30 cm couplets in the Kottaphi Hill section. They are interpreted to result from climate variability, at least regionally, oscillating between humid and arid; controlling run-off, and terrigenous supply. The intermediate, obliquity cycle is dominant through the section, and is likely be represented in the rock record by the ~40-50 cm couplet scale. The supply of terrigenous material, in this instance is controlled by the obliquity cycle that governs the contrast between the seasons; where cooler mid-latitude winters will be wetter. The eccentricity cycle is suggested to alter the magnitude

of the precessional cycle, and therefore is difficult to observe in the rock record, though it may influence the dominance of relatively thin or thick couplets.

Chapter 5

Miocene Oxygen and Carbon Stable Isotope Events in the Mediterranean: a record from the Kottaphi Member of the Pakhna Formation

5.1 Introduction

This study documents the presence of the Monterey stable carbon isotope excursion and stable oxygen isotope events in Miocene-age pelagic carbonates (Kottaphi Member) from Cyprus in the Eastern Mediterranean. Globally recognised stable oxygen isotope events correlate with deposits interpreted to represent relative-sea level fall within the Kottaphi Member. This suggests that sedimentation was controlled by globally synchronous climatic events rather than localised tectonics related to the uplift of the Troodos ophiolite.

The Monterey Excursion is a well-recognised perturbation in the stable carbon isotope record that is interpreted to relate to the deposition of organic-rich sediments, that, via a series of positive feedback mechanisms, resulted in global cooling during the mid-Miocene. It is identified in all the main oceans by the stable isotope analysis of marine, calcite precipitating organisms.

The Kottaphi Member comprises rhythmically bedded chalk and marl beds that form part of the late–Cretaceous to Recent sedimentary cover succession of the Troodos ophiolite, Cyprus. The Member displays cyclicity developed at two scales. Firstly, chalk and marl couplets, that are interpreted to represent changes in runoff, related to climate change caused by the 41 kyr obliquity cycle (Chapter 4). Periods of higher runoff supply more terrigenous material to basin areas, and therefore dilute the pelagic carbonate rain significantly to form marl (Chapter 2). Secondly, depositional sequences that are defined by the variation in couplet composition (chalk-rich or marl-rich) and are interpreted to relate to eustatic sea-level

variation (Chapter 3). The Pakhna Formation was deposited during a tectonically active regime, dominated by the uplift of the Troodos ophiolite, which has been situated above a northward dipping subduction zone since the early Miocene (Morse, 1996; Robertson 1998; Lagroix and Borradaile, 2000).

The Kottaphi Member ranges from calcareous nannoplankton zone NN2 to NN9 (~23-9 Ma, Chapter 2). This time interval spans a period of rapid oceanographic, climatic and cryospheric changes (Chapter 1) that effectively divide the Miocene into a relatively warm early-Miocene and a cooler mid- to late- Miocene (Flower and Kennet, 1993).

The stable oxygen and carbon isotope records for the Kottaphi Member are compared to other isotopic records for the Miocene to further assess the extent of well-recognised stable isotope events. The systematic behaviour of oxygen and carbon stable isotopes in natural systems is now widely accepted, and is reviewed in Chapter 1.

5.2 Stable isotope records of the Miocene

Various stable isotope, palaeontological, sedimentological studies (Frakes *at al.*, 1992) have shown that the cool climates of the early Oligocene warmed during the late Oligocene, reaching an optimum during the late early Miocene (warmest since the late Eocene) and then underwent rapid cooling during the middle Miocene (Shackelton and Kennett, 1975; Savin *et al.*, 1975; Miller *et al.*, 1987; Hornibrook, 1992; Flower and Kennet, 1994). This later cooling trend is widely identified in the $\delta^{18}O$ records of the Miocene (e.g. Miller *et al.*, 1991, Flower and Kennet, 1993; Hodell and Woodruff, 1994, Chapter 1). Two of these stable oxygen isotope records, derived from benthic foraminifera, together with the associated stable carbon isotope records are shown in Figure 5.1, these are from ODP Site 747 (Miller *et al.*, 1991), south Indian Ocean, and DSDP 588A (Flower and Kennet, 1993), south Pacific. These are well-constrained high-resolution isotopic signatures and have been used to erect a

series of globally recognised stable oxygen carbon isotope events (Miller *et al.*, 1991; Wright and Miller 1992; Flower and Kennet, 1993; Abreu and Haddad, 1998). These two records are used in this study for comparison and correlation purposes. The stable isotope record from Malta (Jacobs *et al*, 1996), and the Petrobás Well A site (Brazilian continental shelf; Abreu and Haddad, 1998) are also presented in Figure 5.1. The Malta record provides an intra-basinal comparison to the Cyprus isotopic data. The Petrobás Well A data is used by Abreu and Haddad (1998) to refine and add to the series of oxygen isotope events ($\delta^{18}O$ maxima) identified by Miller *et al.* (1991) and Wright and Miller (1992), for the Oligocene and Miocene (MBi-1 to MSi3).

Two pronounced increases in the Miocene $\delta^{18}O$ record are associated with cooling and growth of the East Antarctic Ice Sheet (EAIS) during the middle Miocene (Figure 5.1 (~14.5-12.5 Ma) ODP Site 747 and DSPD Site 588A) and are recorded in every ocean (Vincent *et al.*, 1985; Miller and Fairbanks 1985, 1983; Savin *et al.*, 1981). These two $\delta^{18}O$ events (MSi-2 and MSi-3) form part of a series of stable oxygen isotope events identified in the Miocene $\delta^{18}O$ records (Figure 5.1, Miller *et al.*, 1991; Wright and Miller, 1992; Abreu and Haddad 1998). The events are constrained by biostratigraphy and magnetostratigraphy from DSDP Sites 529, 563 and 608 (Miller *et al.*, 1991), ODP Site 747 and the Petrobás Well A (Abreu and Haddad, 1998). These events are considered globally significant as they correlate between sites within the resolution of biostratigraphy and magnetostratigraphy (Miller *et al.*, 1991). The revised Abreu and Haddad (1998) events identified over the interval considered in this study are illustrated on the ODP Site 747 $\delta^{18}O$ record and the Petrobás Well A record (Figure 5.1).

Woodruff and Savin (1991) established a second set of positive and negative stable oxygen isotope events that characterise the mid-Miocene cooling event. The events are identified on the high-resolution $\delta^{18}O$ record from DSDP Site 588A (Figure 5.1; Flower and Kennet,

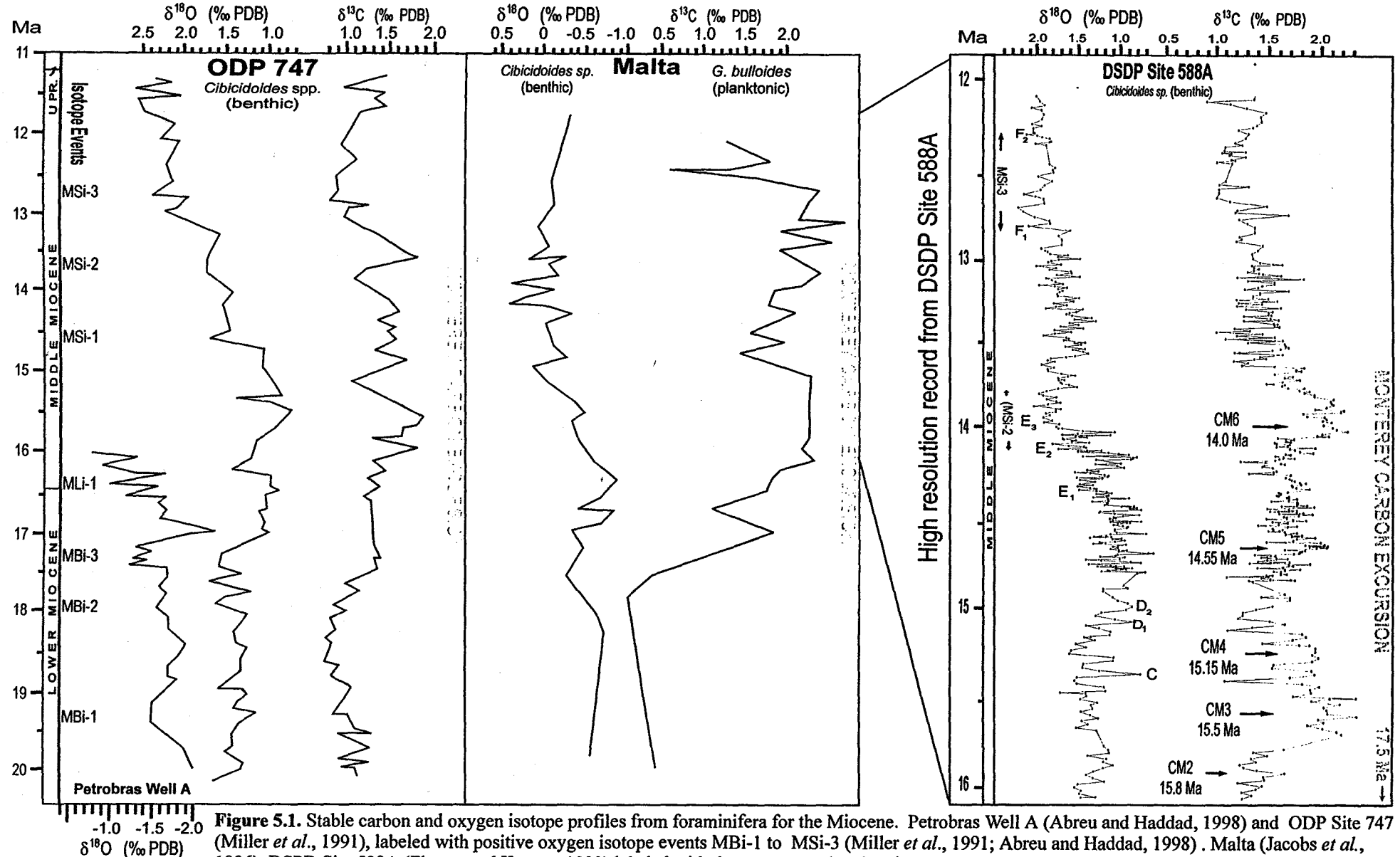

Figure 5.1. Stable carbon and oxygen isotope profiles from foraminifera for the Miocene. Petrobras Well A (Abreu and Haddad, 1998) and ODP Site 747 (Miller *et al.*, 1991), labeled with positive oxygen isotope events MBi-1 to MSi-3 (Miller *et al.*, 1991; Abreu and Haddad, 1998) . Malta (Jacobs *et al.*, 1996). DSPD Site 588A (Flower and Kennet, 1993) labeled with the oxygen and carbon isotope events of Woodruff and Savin (1991). Shaded areas

1993) and labelled using the nomenclature of Woodruff and Savin (1991). E_1 (14.3 Ma), E_2 (14.2 Ma), and E_3,(14.1 Ma) are three smaller separate $\delta^{18}O$ increases preceding the major $\delta^{18}O$ maxima MSi-2 (Figure 5.1; Flower and Kennet, 1993). F_1 (12.9 Ma) and F_2 (12.5 Ma) are two smaller $\delta^{18}O$ increases that are interpreted to comprise the MSi-3 $\delta^{18}O$ event. (Figure 5.1; Flower and Kennet, 1993). The three older $\delta^{18}O$ minima established by Woodruff and Savin, (1991); C (15.3 Ma), D_1 (15.0 Ma), and D_2 (14.9 Ma), are also recognised by Flower and Kennet (1993) in DSDP site 588A. These $\delta^{18}O$ minima events are interpreted as representing short-lived warming within a longer period of low mean $\delta^{18}O$ values (Figure 5.1).

A negative shift occurs in the $\delta^{18}O$ record of Malta between 13-11.8 Ma, based on planktonic and calcareous nannoplankton biostratigraphy, that is not observed in the other deep-sea records (Figure 5.1). Jacobs *et al.* (1996) suggested this Mediterranean trend to be an expression of the isolation of the Mediterranean Sea from the Indo-Pacific Ocean at ~14 Ma. Decreasing $\delta^{18}O$ values would result from an increased influx of fresh water and changes in temperature and/or salinity (Jacobs *et al.*, 1996).

Woodruff and Savin (1991) erected a series of $\delta^{13}C$ maxima within the stable carbon isotope record of the Monterey Excursion, five of which are identified in the DSPD Site 588A (southwest Pacific) $\delta^{13}C$ record (Figure 5.1; Flower and Kennet, 1993). These $\delta^{13}C$ maxima (CM2, CM3, CM4, CM5, and CM6), are now considered useful for global correlation with other $\delta^{13}C$ profiles representing the middle Miocene Monterey Excursion (Flower and Kennet 1993; Hodell and Woodruff, 1994).

5.3 Monterey carbon isotope excursion and global cooling

Previous studies (Vincent and Berger, 1985; Vincent *et al.*, 1985; Flower and Kennet, 1994) have identified a ~1.0 ‰ positive excursion in the $\delta^{13}C$ record which lasts for 4.5 myr) during the middle Miocene (17.5-13 Ma; Figure 5.1). Vincent and Berger (1985) associated this global $\delta^{13}C$ excursion with large-scale burial of organic-rich sediments and increases in bioproductivity, due to upwelling in coastal areas, as recorded in the Monterey Formation, California. They link this increase in organic carbon burial to middle Miocene global cooling, and the growth of the East Antarctic Ices Sheet (EAIS), by the drawdown of atmospheric pCO_2, and a series of positive feedback mechanisms. In their "Monterey Hypothesis" the development the circum-polar current in the early-Miocene (Kennet, 1995), thermally isolated Antarctica from the other oceans. The model proposes that the resulting polar cooling invigorated oceanic thermohaline circulation and lead to increased upwelling on continental margins. As the supply of nutrient rich upwelling water increases, bioproductivity intensifies, which leads to the removal of more carbon from the oceanic reservoir as organic-rich sediments are deposited. The resulting drawdown of atmospheric CO_2 leads to global cooling via a reversed greenhouse effect. These series of mechanisms create a positive feedback; cooling intensifies the global temperature gradient and increases oceanic circulation, producing more vigorous upwelling on continental margins and increased bioproductivity. This global perturbation in the carbon cycle has mainly been identified in OPD and DSDP stable isotope data, which is obtaind from deep-water settings (Flower and Kennet 1993a; Wright and Miller, 1992). Jacobs *et al.*, (1996) have identified the Monterey Excursion in shallow water carbonates in Malta, central Mediterranean (Figure 5.1). They date the Monterey Excursion as starting at 18 Ma, attaining its most positive values at around 17 Ma and ending at 12.5 Ma, based on correlating planktonic foraminifera and calcareous nannoplankton biostratigraphy to the Berggren *et al.* (1995) radiometric timescale. Major episodes of phosphate deposition occur before and during the Monterey Excursion (24-16

Ma) on the Malta shelf, and are interpreted to result from a period of accelerated weathering, erosion and transfer of nutrient to the oceans.

The $\delta^{18}O$ record of the Miocene shows features that are recognised globally. The mid-Miocene is marked by a total increase of 1.5 ‰ in benthic foraminifera $\delta^{18}O$ values that is generally interpreted to represent major growth of the East Antarctic Ice Sheet (EAIS) and cooling of bottom waters (Figure 5.1; Shackleton and Kennet, 1975; Savin *et al.*, 1975; Kennet, 1995). The increase is largely incorporated in two distinct steps, an initial increase of 0.8 ‰ from 14.5 to 14 Ma and a second of 0.7 ‰ from 13.5 to 12.4 Ma (Figure 5.1; Kennet, 1995). The first $\delta^{18}O$ increase occurs ~3 myr after the inception of the Monterey Excursion at 17.5 Ma (Figure 5.1; Vincent and Berger, 1985). This suggests a lag time between organic carbon burial and major global cooling, and has been a point of much discussion (Vincent and Berger, 1985; Flower and Kennet, 1993; Flower and Kennet, 1994). To explain this lag time Vincent and Berger (1985) modelled the response time of atmospheric pCO_2 drawdawn to carbon burial, and suggest that 2-3 myr is required to reach a threshold where pCO_2 levels are lowered sufficiently to cause global cooling. An alternative explanation for the lag time is provided by Hoddell and Woodruff (1994) who recognise the importance of a globally identified, mid-Miocene $\delta^{18}O$ minima (*eg.* OPD Site 747 (Figure 5.1) shows a prominent decrease in $\delta^{18}O$ values between ~17 Ma and ~14 Ma). Hodell and Woodruff (1994) attribute this global decrease to reflect the climatic optimum of the middle Miocene (17-14.5 Ma), which occurred during the Monterey Excursion. They suggest that the eruption of the Colombia River Flood Basalts in the northwestern United States provided a significant source of carbon dioxide to the atmosphere that, via the greenhouse effect accounted for this warming event. The Colombia River Flood Basalts erupted rapidly over a period of 2 Ma (Hooper, 1990), with the main volume erupting at 15.1 ±0.3 Ma (Carlson and Hart, 1988), which correlates in time with very low $\delta^{18}O$ values in the ODP Site 747 and

DSPD Site 588A $\delta^{18}O$ records. Hodell and Woodruff (1994) suggest that the rapid output of volcanically sourced CO_2 had the effect of stalling global cooling, as the organic carbon burial in the Monterey deposits acted as a sink for CO_2. After removal of atmospheric CO_2 contributed by the eruption of the Colombia River Flood Basalts, organic carbon burial eventually led to cooling via further drawdown of atmospheric CO_2..

5.4 Methodology for stable isotope analysis in the Cyprus sections.

Two sections, Kottaphi Hill and Kalavasos, in Cyprus, were selected for isotopic analysis due to good exposure and clearly definable depositional sequences. The absence of benthic foraminifera in this study restricts analysis to the planktonic species *Globoquadrina altispira* (Cushman and Jarvis, 1936) that is recognised as a suitable species for oxygen isotope analysis (Vincent and Berger 1985; Corfield and Cartlidge 1993). The Kottaphi Hill and Kalavasos sections were sampled every 20 cm. The exact sampling positions are indicated on the detailed graphic log of these localities in Appendix A. Electron microscope examination confirmed that foraminifera retained their primary calcite, and were suitable for isotope analysis, though there was some evidence for minor secondary cements.

Rock samples were roughly fragmented, soaked in water and placed into an ultrasound bath for anything up 30 hours to separate the foraminifera and partially remove any secondary calcite cement. The residue was then sieved to retrieve the 125-1000 μm fraction for picking. Approximately 20 individuals were picked for each stable isotopic analysis using a binocular microscope. While picking, foraminifera that were degraded or showed evidence for secondary mineralisation were not selected. The samples were analysis with Micromass Optima dual inlet gas source mass spectometer at NIGL, Keyworth using the standard technique (Appendix B) outlined by Corfield (1995) and Hudson and Anderson (1989). The raw isotope data and ages gained from sequence stratigraphy and biostratigraphy are tabulated in Appendix B. All isotopic data are expressed using the standard δ notation in per

mil relative to the Pee Dee belemnite carbonate standard (Appendix B). The instrumental error is 0.1 ‰.

5.4.1 Dating the records

Figure 5.2 and 5.3 illustrate the Kottaphi Hill and Kalavasos $\delta^{13}C$ records dated to the sequence stratigraphical and biostratigraphical frameworks established in Chapters 2 and 3. This provides an independent age constraint on the isotope data. Nannoplankton zonation schemes during the lower to middle Miocene are mainly based on the last occurrence datums (LO) of zonal index species, and in this context, are considered unreliable due to evidence of reworking. The first occurrence datum (FO) of *Sphenolithus belemnos* (base of NN3 at 19.2 Ma) and the FOD of *Discoaster druggii* (base of NN7 11.8 Ma) effectively bracket the isotope data. Within these two datum planes the isotope data is further constrained by sequence boundaries developed in Kottaphi Member, and their correlation with the sequence chronostratigraphy of Hardenbol *et al.* (1998). The seven datums used for dating the isotope data are illustrated on the $\delta^{18}O$ and $\delta^{13}C$ records for Kottaphi Hill and Kalavasos (Figures 5.2 and 5.3), and are reviewed in Table 5.1. Figure 5.4 shows the $\delta^{18}O$ and $\delta^{13}C$ records on the graphic logs for Kottaphi Hill and Kalavasos sections.

Table 5.1 Biostratigraphical and sequence chronostratigraphical datums use to constrain stable isotope data at Kottaphi Hill and Kalavasos. Y = Datum present, N = datum not present. Datums also illustrated on the isotope records of the study sections (Figures. 5.2-5.4).

Datum	Age (Ma)	Kottaphi Hill	Kalavasos
FOD *Discoaster kugleri*	11.8	Y	N
SB(f)	14.8	Y	N
SB(e)	16.4	Y	Y
SB(d)	17.3	Y	Y
SB(c)	18.7	Y	Y
FOD *Sphenolithus belemnos*	19.2	Y	Y
SB(b)	19.5	Y	Y

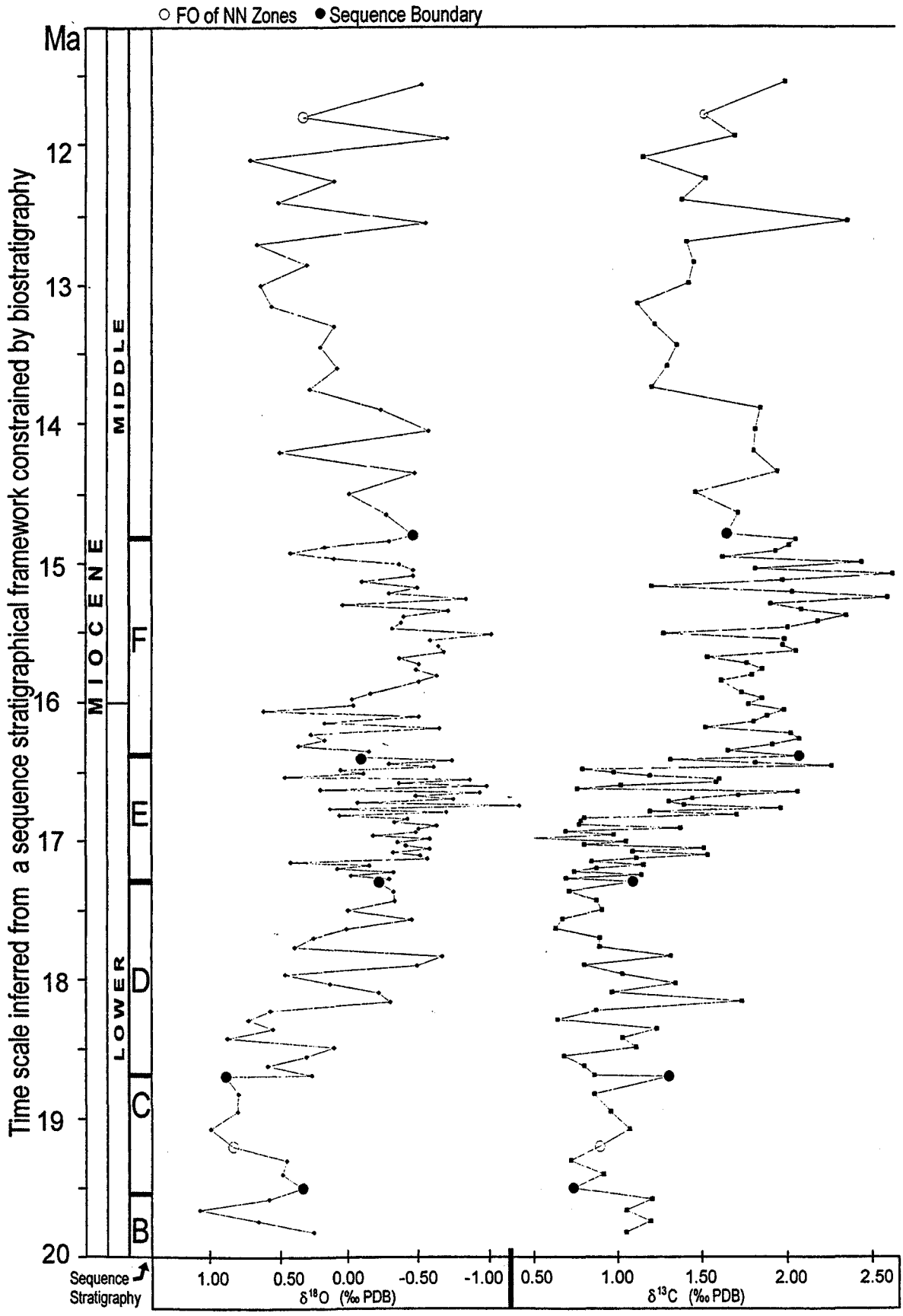

Figure 5.2 Oxygen and carbon isotope records of *G. altispira* at Kottaphi Hill to the time scale of Breggren *et al.* (1995). Time scale derived from correlation of sequence boundaries identified at Kottaphi Hill and constrained by calcareous nannoplankton biostratigraphy to European Sequence Chronostratigraphy (Hardenbol *et al.*, 1998),

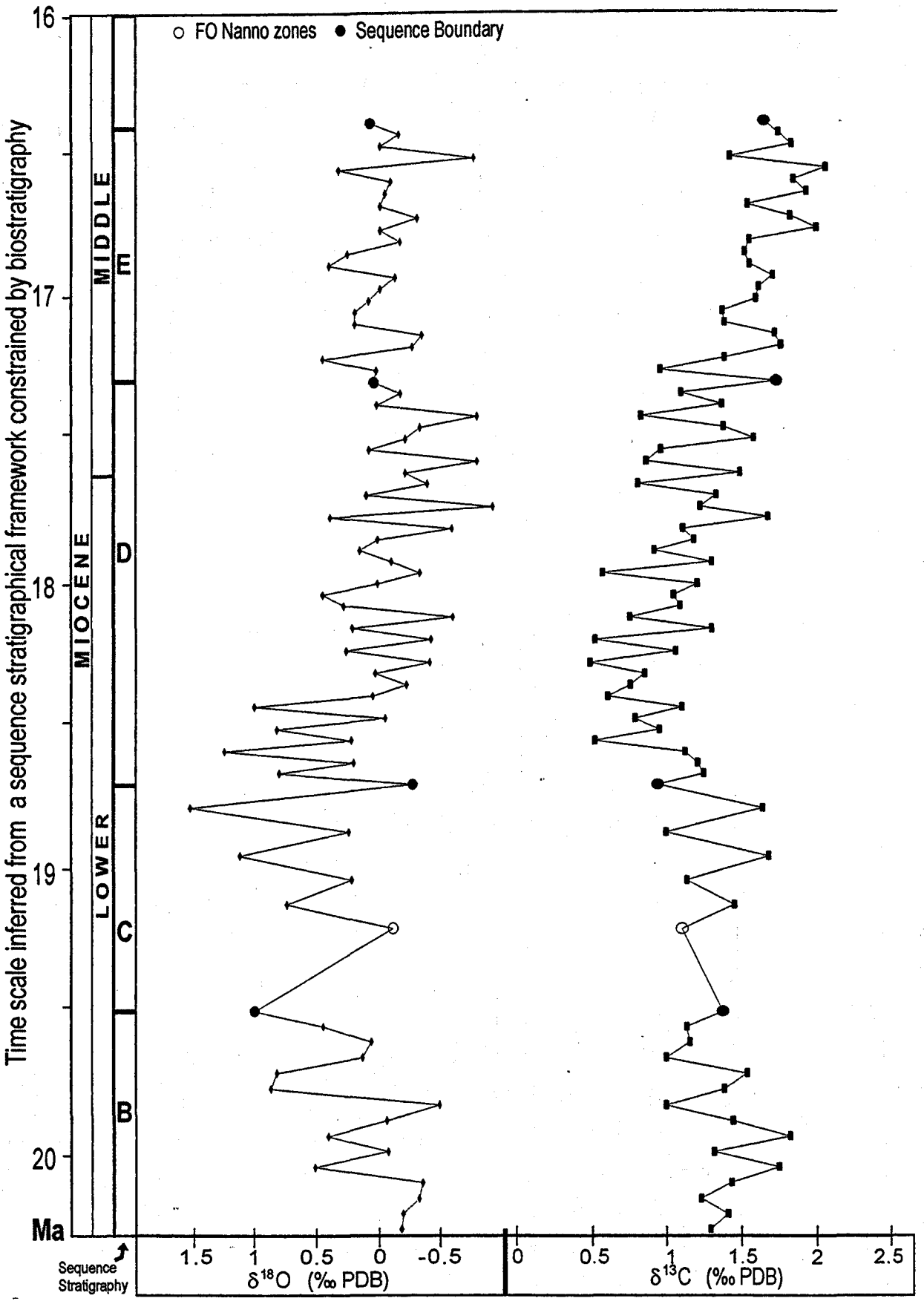

Figure 5.3 Oxygen and carbon isotope records of *G. altispira* at Kalavasos plotted on the time scale of Breggren *et al.* (1995). Time scale derived from the correlation of sequence boundaries and constrained by calcareous nannoplankton biostratigraphy to European Sequence Chronostratigraphy (Hardenbol *et al.*, 1998),

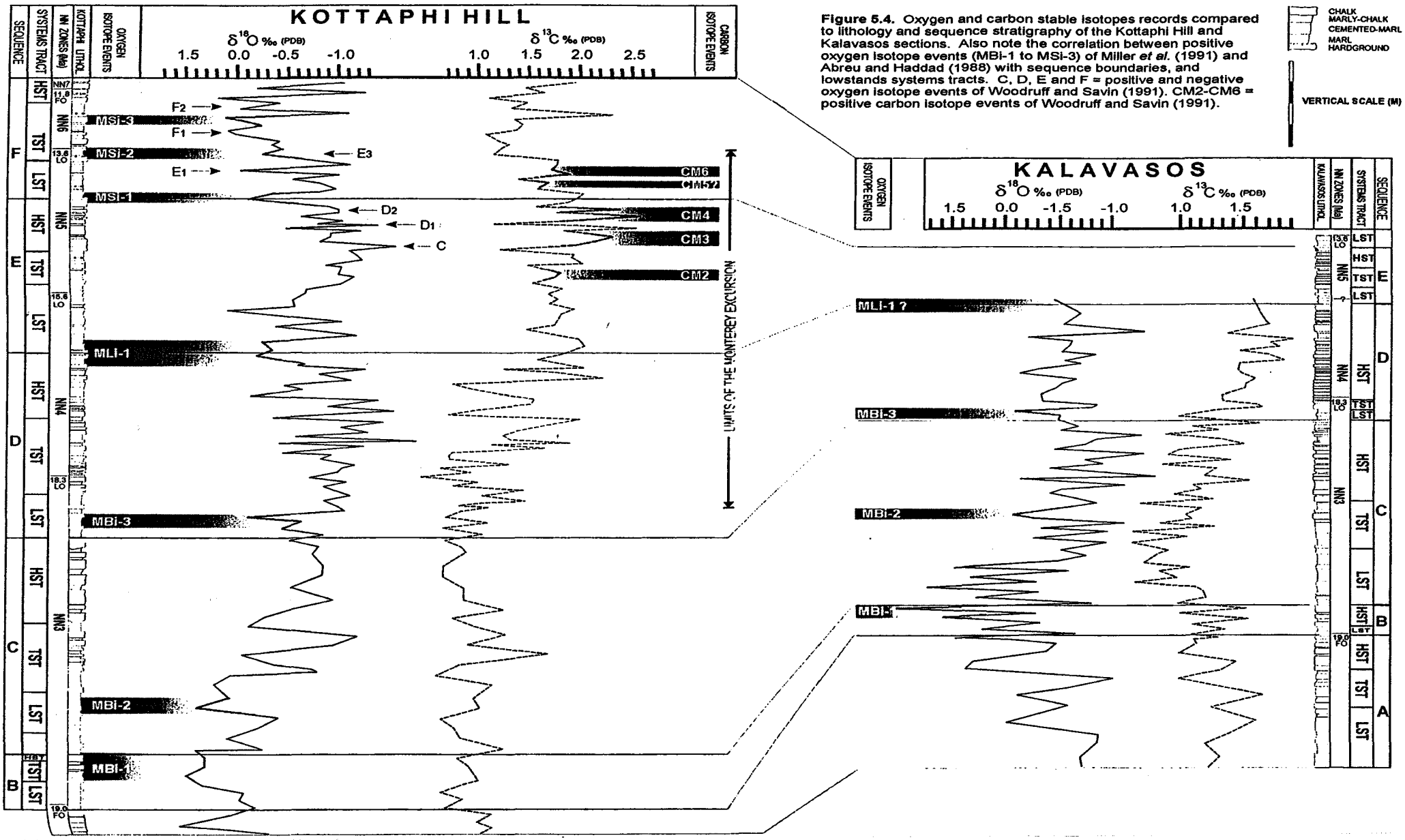

Figure 5.4. Oxygen and carbon stable isotopes records compared to lithology and sequence stratigraphy of the Kottaphi Hill and Kalavasos sections. Also note the correlation between positive oxygen isotope events (MBi-1 to MSi-3) of Miller *et al.* (1991) and Abreu and Haddad (1988) with sequence boundaries, and lowstands systems tracts. C, D, E and F = positive and negative oxygen isotope events of Woodruff and Savin (1991). CM2-CM6 = positive carbon isotope events of Woodruff and Savin (1991).

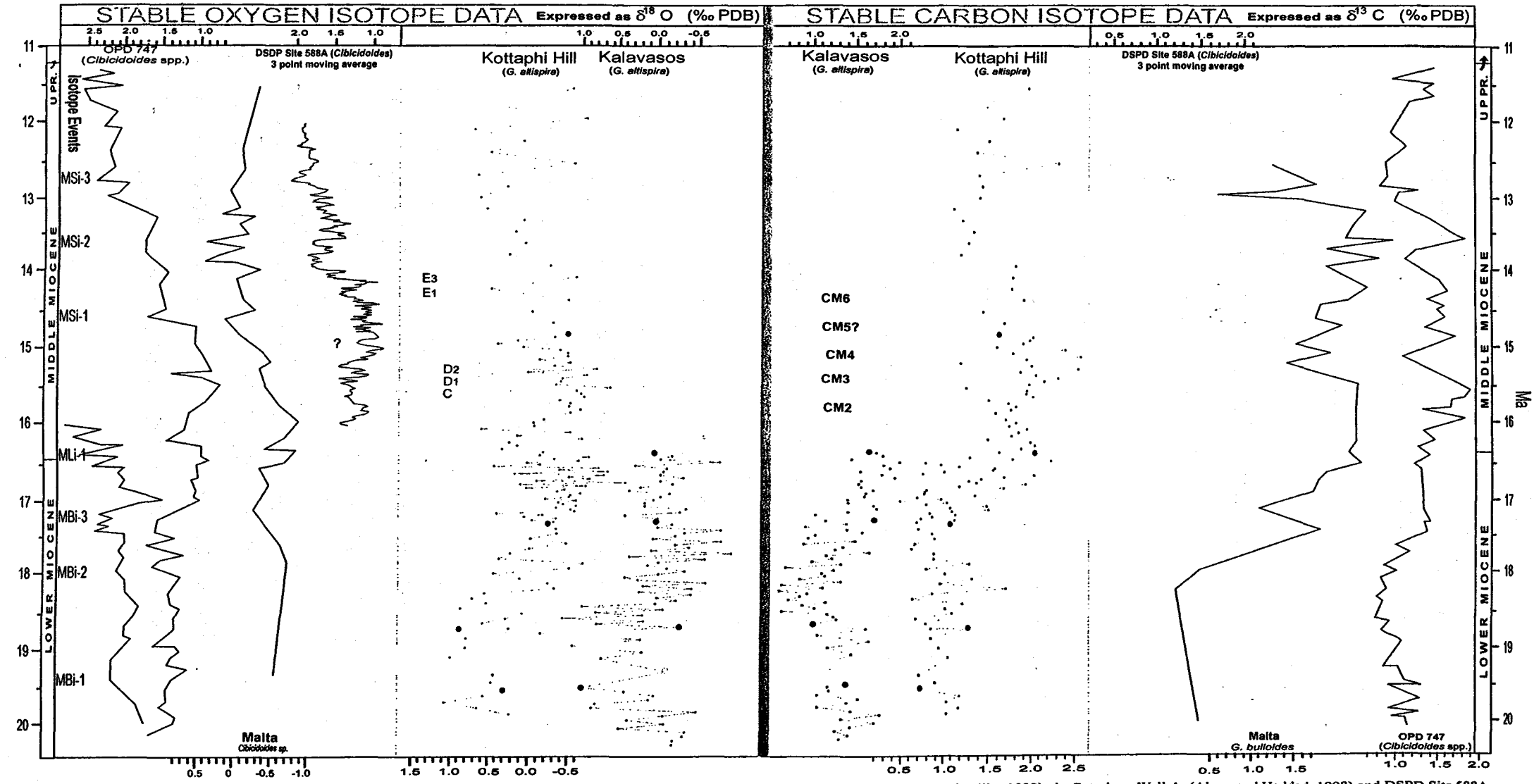

Figure 5.5 Stable oxygen and carbon isotopes from Kottaphi Hill and Kalavasos matched with the Malta (Jacobs *et al.*, 1996), ODP Site 747 (Wright and Miller 1992), the Petrobras Well A, (Abreu and Haddad, 1998) and DSPD Site 588A Flower and Kennet, 1993) records. Shaded area on the carbon isotope data denotes the limits of the "Monterey Excursion" (Vincent and Berger, 1985). See text for detailed explanation.
:M2-CM6 Positive oarbon isotope events (Woodruff and Savin, 1991). Positive oxygen isotope events MBi1to- MSi-3 (Abreu and Haddad, 1998; Miller et al. (1991), C, D, E and F oxygen isotope events(Woodruff and Savin, 1991)
Sequence chronostratigraphical datum. ‹, Biostratigraphical datum

5.5 Carbon isotope records of the Kottaphi Member, Cyprus

The Monterey Excursion can be clearly identified in the $\delta^{13}C$ record of Kottaphi Hill (Figures 5.2, 5.3, 5.4 and 5.5). The $\delta^{13}C$ record shows a ~1.5 ‰ increase from ~17 to 16.5 Ma where values reach ~2.0 ‰. $\delta^{13}C$ remains high and increases further to a 2.5 ‰ maximum at ~15 Ma, from where $\delta^{13}C$ values decrease by 1.25 ‰ and return to pre-excursion levels of ~1.2 ‰ at 13.5 Ma.

At Kalavasos the $\delta^{13}C$ record obtained covers a shorter span than that from the Kottaphi Hill record (Figure 5.3), and as a consequence, only the start of the Monterey Excursion is identified beginning at ~18 Ma (Figure 5.5). This 1.0 ‰ increase is more gradual than the Kottaphi Hill record and attains maximum values of ~2.0 ‰ at 16.5 Ma.

Within the resolution of biostratigraphy and sequence chronostratigraphy, the $\delta^{13}C$ excursion identified in the Kottaphi Hill section correlates to previously published dates (17.5-13 Ma) that define the Monterey Excursion (Vincent and Killingley, 1985; Vincent and Berger, 1985). Global synchroneity of the Kottaphi Hill and Kalavasos $\delta^{13}C$ records is illustrated by the positive correlation with the ODP Site 747 (Wright and Miller 1992), DSDP Site 588A (Abreu and Haddad, 1998), and Malta (Jacobs *et al.*, 1996) $\delta^{13}C$ records, where the Monterey Excursion starts at ~17.5 Ma and ends at ~13 Ma (Figure 5.5).

Figure 5.5 shows a comparison between the $\delta^{13}C$ record of Kottaphi Hill with the $\delta^{13}C$ record of *Cibicidoides* at DSDP Site 588A (Flower and Kennet, 1993). The carbon isotope maxima are labelled using the nomenclature of Woodruff and Savin (1991). The five $\delta^{13}C$ maxima (CM2-CM6) correlate within the resolution of biostratigraphy and sequence chronostratigraphy to five $\delta^{13}C$ maxima recorded in the Kottaphi Hill record. The stratigraphic positions of these maxima are illustrated on Figure 5.4 and listed in Table 5.2.

The Kottaphi Hill $\delta^{13}C$ data provides a detailed record of the Monterey Excursion in the Mediterranean. It builds on the Malta $\delta^{13}C$ record of Jacobs *et al.* (1996) by extending the recognition of the event to the eastern Mediterranean, and identifying globally recognised carbon maxima.

5.6 Oxygen isotope records from the Kottaphi Member, Cyprus

The $\delta^{18}O$ record from Kottaphi Hill (Figure 5.2) correlates well with the stable oxygen isotope trends observed in other $\delta^{18}O$ records from the Miocene (Figure 5.5). Relatively high $\delta^{18}O$ values (~0.75 ‰) between 20-18.5 Ma are followed by a ~1.5 ‰ decrease to -0.75 ‰ at 16.5 Ma. Relatively low values are maintained until ~14 Ma, where the $\delta^{18}O$ record shows a stepped ~1.0 ‰, increase to 0.6 ‰ $\delta^{18}O$ at ~13 Ma. From 13.0-11.5 Ma the $\delta^{18}O$ record shows a gradually decreasing trend.

At Kalavasos the $\delta^{18}O$ record (Figure 5.3) shows a general increase of ~1.0 ‰ between 20-19 Ma. This is followed by a decreasing trend to 17.5 Ma of 1.2 ‰, where values remain low at -0.25 ‰ to the end of the record at 16.4 Ma.

Figure 5.5 compares the $\delta^{18}O$ records of Kottaphi Hill and Kalavasos to the $\delta^{18}O$ records of ODP site 747 (Wright and Miller 1992), the Petrobrás Well A, (Abreu and Haddad, 1998), and Malta (Jacobs *et al.*, 1996). The $\delta^{18}O$ record of planktonic forams from Kottaphi Hill show a strong correlation with the ODP Site 747 benthic foram record. Both Cyprus records show especially low $\delta^{18}O$ values between ~17 and ~15.5 Ma, with a characteristic positive peak at ~16.5 Ma, that represents the Miocene climatic optimum (Hodell and Woodruff, 1994). From ~14.5 to 12.5 Ma both records show a trend of increasing $\delta^{18}O$ values.

A similar overall trend is observed in the Malta $\delta^{18}O$ record, though the correlation is less clear. Both the Kottaphi Hill and Malta records share the negative $\delta^{18}O$ trend from ~13 Ma, which is interpreted (Jacobs *et al.*, 1996) to relate to the closure of the Mediterranean at 12 Ma, when an increasing influx of fresh water and changes in temperature and/or salinity may have produced a decrease in $\delta^{18}O$. The TST and HST of sequence F at Kottaphi Hill (Figure 5.4) cover this time interval, though there is no obvious lithological response in the section to increasing oceanographic isolation. The start of the negative $\delta^{18}O$ trend occurs stratigraphically below the initiation of long-term shallowing related features at Kottaphi Hill, the eldest of which is the channel (SB(h)), and the youngest late-Miocene aged gypsum deposits of the Kalavasos Formation.

Table 5.2. Ages of the Abreu and Haddad (1998) and Flower and Kennet (1993) stable oxygen and carbon isotope events using the Breggren *et al.* (1995) time scale, with the stratigraphic positions of correlative events at Kottaphi Hill and Kalavasos, Cyprus (Figure 5.4). Detailed graphic logs of the Kottaphi Hill and Kalavasos sections are provided in Appendix A. Shaded boxes indicate stable oxygen and carbon isotope events that are developed beyond the time frame of the Cyprus isotope data.

Oxygen Isotope Events. (Miller *et al.* 1991; Abreu and Haddad, 1998)	Oxygen isotope events (Flower and Kennet, 1993)	Age (Ma)	Kottaphi Hill		Kalavasos	
			Bed Nos.	Height above base of section (m)	Bed Nos.	Height above base of section (m)
	F2	12.5	201	33.6-33.95		
MSi-3		12.7	197-199	33.2-33.5		
	F1	12.9	192-194	32.8-33.1		
MSi-2		13.6	182-186	31.5-32.1		
	E3	14.1	185	32.8-4.0		
	E1	14.3	179	32.1-32.3		
MSi-1		14.6	166-168	29.5-30.2		
$\delta^{18}O$ mini	D2	14.9	162-166	29.1-29.6		
	D1	15.0	157-158	28.8-28.95		
	C	15.3	151	27.75-28.0		
Mli-1		16.4	117-125	22.5-23.5	249-255	42.9-42-7-
MBi-3		17.2	73-76	15.6-16.5	195-199	38.2-34.9
MBi-2		18.0	39-42	7.4-8.4	160-163	34.2-34.9
MBi-1		19.4	25-32	5.6-6.1	142-144	29.9-30.4
Carbon Isotope Events	CM6	14.0	181-179	31.2-31.4		
	CM5	14.65	173-175	30.45-		
	CM4	15.15	158-165	28.8-29.5		
	CM3	15.5	151-156	27.8-28.5		
	CM2	15.8	143-145	26.3-26.7		

Oxygen isotope events MBi-1, MBi-2, MBi-3, MLi-1, MSi-1, MSi-2 and MSi-3 are present in the Kottaphi Hill record (Figure 5.5). Oxygen isotope events MBi-1, MBi-2, and MBi-3, are present in the Kalavasos $\delta^{18}O$ record (Figure 5.5). The stratigraphic positions of these maxima in the Kottaphi Hill and Kalavasos records are illustrated on Figure 5.4 and listed in Table 5.2.

Figure 5.6 shows the record $\delta^{18}O$ of *Cibicidoides* at DSDP Site 588A (Flower and Kennet, 1993), with the oxygen minima and maxima labelled using the nomenclature of Woodruff and Savin (1991). The three $\delta^{18}O$ minima, C, D_1 and D_2, in the DSDP Site 588A record are correlated with $\delta^{18}O$ minima in the Kottaphi Hill record (Figure 5.6). The E_1, and E_3 maxima in the DSDP Site 588A $\delta^{18}O$ record correlate with two positive steps in the Kottaphi Hill $\delta^{18}O$ record. Sample resolution is insufficient to identify the E_2 maxima in the Kottaphi Hill record. The F_1 $\delta^{18}O$ maxima in the DSDP Site 588A record, is represented by a further step in the $\delta^{18}O$ record of Kottaphi Hill. The F_2 maxima in the DSPD Site 588A is tentatively correlated to positive peak in the Kottaphi Hill record (Figure 5.6). As this interval has a low sample density, and few stratigraphical constraints, the correlations are mainly based on the shape of the $\delta^{18}O$ record at Kottaphi Hill. Correlations over part of this interval (sequence F, Figure 5.4) are particularly tenuous as the section due to the succession being incomplete, containing numerous iron stained horizon interpreted as hiatuses. The stratigraphical incompleteness is highlighted by stratigraphic time series analysis (Chapters 4) and sequence stratigraphy (Chapter 3).

5.7 Global significance of the Cyprus $\delta^{18}O$ records

As the $\delta^{18}O$ and $\delta^{13}C$ signatures of Kottaphi Hill and Kalavasos clearly contain the well documented isotopic events of the Miocene (the Monterey Excursion, mid Miocene global cooling and previously identified individual stable isotope minima and maxima). The

biostratigraphical and sequence chronostratigraphical frameworks suggest that these events are synchronous with other sites around the world.

5.8 Stable oxygen and carbon isotope trends in couplets

The couplets of the Kottaphi Member are interpreted to portray changes in climate (Chapters 2 and 3). The relatively marl-rich bed represents deposition in a more humid, wetter climate, compared to the overlying chalk-rich bed. Time series analysis on bed thickness/coded lithology data at Kottaphi Hill (Chapter 4) suggests that couplets mainly relate to the 41 kyr obliquity cycle caused by variation in the angle of the Earth's axis. The obliquity cycle, determines the magnitude of seasonality (Weedon, 1993; Valdes and Glover, 1999) on the Earth. Greater seasonal contrast will result in wetter winters and increased runoff, which is interpreted to account for the marl-rich beds. Figure 5.6 shows the stable isotope records of two individual couplets within sequence D at Kottaphi Hill. Ten samples were collected over a lowstand systems tract couplet (Bed nos. 130 and 131, Appendix A; Kottaphi Hill), and six samples collected over a highstand systems tract couplet (Bed nos. 157 and 158, Appendix A; Kottaphi Hill). Both the LST and HST couplets show an overall slight increase of about 0.2 ‰ in $\delta^{18}O$ into the upper more calcareous bed, though this is less significant in the LST couplet. The $\delta^{13}C$ record of the HST couplet shows significantly decreased (~0.4 ‰) values in the upper more calcareous bed. The LST couplet shows a <0.2 ‰ $\delta^{13}C$ increase in the chalk bed, though this trend is barely above instrumental error. Clay wt.% values for both couplets show significant decreases into the upper calcareous bed. The LST couplet shows a decrease of ~10 % wt.% clay and the HST shows a 15 % wt.% clay decrease, in the upper calcareous bed.

The interpreted climatic conditions prevalent during deposition of each part of the couplet also explain the trends observed in the isotope data. The slightly lower $\delta^{18}O$ values result

from increased dilution of oceanic surface water by isotopically light meteoric water, that is also responsible for supplying terrigenous material, as recorded by the clay-rich marl. The $\delta^{13}C$ of the HST couplet shows higher values during marl deposition, which possibly result from increased runoff supplying nutrients from surrounding landmasses. The data for the HST shows a greater contrast, in absolute values, between the two couplet beds, than the LST, reflecting the greater contrast in lithologies displayed in the HST couplet.

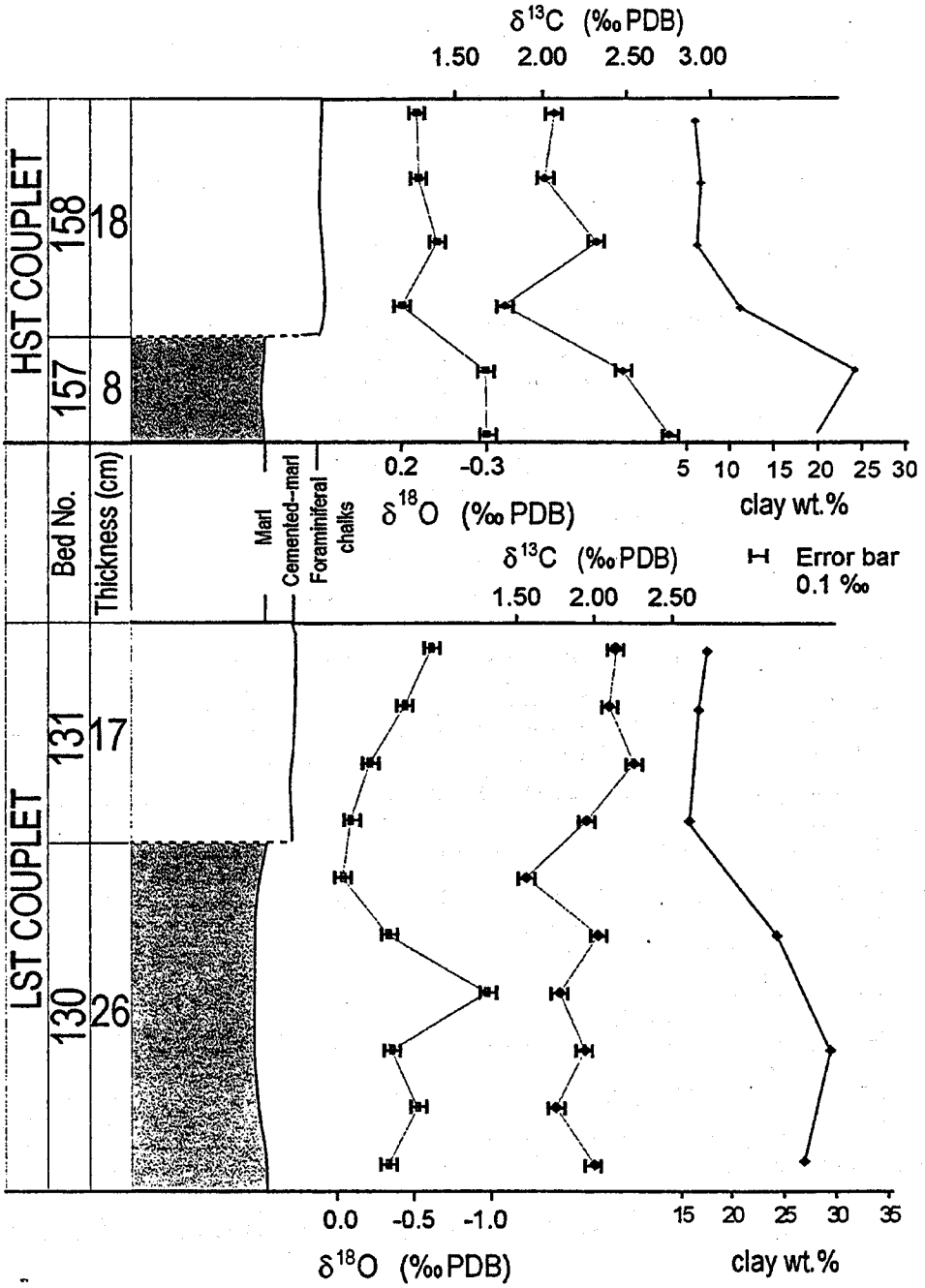

Figure 5.6 The stable oxygen and carbon isotope records of *G. altispira*, with clay wt.% for a highstand and lowstand systems tract couplet at Kottaphi Hill. The relatively negative $\delta^{18}O$ values of the lower bed are interpreted to reflect increased input of meteoric water, which is responsible supplying more terrigenous material to the basin.

5.9 Stable oxygen isotopic trends in relation to sequence stratigraphy

If there is a causal relationship between increased ice volume and relative sea-level falls, then sequence boundaries should correlate with the inflection points of $\delta^{18}O$ increases in benthic and low-latitude planktonic foraminifera (Miller *et al.*, 1991). Abreu and Haddad (1998) demonstrate a good correlation with oxygen isotope events and sequence boundaries on the sequence chronostratigraphical cycle chart of Hardenbol *et al.*, (1998). Figure 5.4 illustrates the $\delta^{18}O$ records of Kottaphi Hill and Kalavasos compared to the sequence stratigraphical interpretation. There is a good correlation between $\delta^{18}O$ maxima and deposits interpreted to represent relative sea-level fall (sequence boundaries and LST; Figure 5.4, Table 5.3). Oxygen isotope events MLi-1 and MSi-1 are particularly well developed and coincide precisely with SB(e) and SB(f) at Kottaphi Hill (Figure 5.4 and Table 5.3). The match is less convincing during Sequence F (MSi-2 and MSi-3), though this period has previously been identified as stratigraphically incomplete (Chapters 2 and 3). The $\delta^{18}O$ record of this interval, represents the first major $\delta^{18}O$ increase associated with the development of the EAIS, and may, therefore in-part be responsible for the development of significant hiatuses caused by stronger bottom currents, and hence more erosion.

Table 5.3. The Abreu and Haddad (1998) oxygen isotope events: sequence stratigraphical positions at Kottaphi Hill and Kalavasos. Shaded area indicates stable oxygen isotope events developed beyond the time frame of the isotope data.

Oxygen Isotope Event (Abreu and Haddad)	Kottaphi Hill	Kalavasos
MSi-3	TST of Sequence F	
MSi-2	ts of Sequence F	
MSi-1	SB(f)	
MLi-1	SB(e)	HST Sequence D
MBi-3	LST Sequence D	LST Sequence D and SB(d)
MBi-2	LST/TST Sequence C	TST Sequence C
MBi-1	HST Sequence B	HST Sequence B

5.10 Summary

- The Kottaphi Member of the Pakhna Formation comprises interbedded, chalk, marly-chalk, cemented-marl and marl, reflecting increasing dilution of the carbonate rain by terrigenously derived material. Couplets are interpreted to represent short-term variability between humid and more arid climates. $\delta^{18}O$ analysis over two couplets reveals more negative $\delta^{18}O$ values in the lower, more marl-rich bed, that is likely to result from increased meteoric input. The $\delta^{13}C$ record of a HST couplet supports this; higher values are present in the lower, marl-rich bed, that is interpreted to result from increased runoff supplying nutrient sourced from surrounding landmasses.

- The stable carbon and oxygen isotope records of Cyprus show synchroneity with the globally defined mid-Miocene Monterey carbon excursion, the early Miocene climatic optimum and the cooling steps associated with the build up of the East Antarctic Ice Sheet. This correlation effectively de-couples the depositional sequences developed at Kottaphi Hill and Kalavasos from the localised affects of relative sea-level change associated with Troodos tectonics, as $\delta^{18}O$ is recording globally identified events that can be identified in the rock record.

- The Kottaphi Hill $\delta^{13}C$ data provides a detailed record of the Monterey Excursion in the Mediterranean. It builds on the Malta $\delta^{13}C$ record of Jacobs *et al.* (1996) by extending the recognition of the event to the eastern Mediterranean, and identifying globally recognised carbon maxima.

- The identification and good correlation between the oxygen isotope events defined by Abreu and Haddad (1998) with sediments deposited during interpreted relative sea-level fall suggest a eustatic (climatic) control on sedimentation for the Kottaphi Member.

Chapter 6

Plio-Pleistocene Submarine-fan Sedimentation, Southern Cyprus

6.1 Introduction

This Chapter documents the exposure in a ~14 km^2 area in the vicinity of the villages Khirokitia, Tokhni and Psematismenos (Figure 6.1). The area was first mapped by Bagnall, (1960) during his work for the Geological Survey Department of Cyprus. The report noted the excellent cliff exposures of extremely coarse-grained conglomerates and breccias on the eastern bank of the Maroni River valley, 500m north of Khirokitia village. They were attributed to be part of the Fragmental Limestone Member of the Miocene-aged Pakhna Formation on the basis of their topographically lower position compared to the *Discospirina* Band, a biostratigraphical marker for the upper Miocene within the Pakhna Formation. Houghton *et al.*, (1990) investigated these sediments further and with the aid of biostratigraphical dating (calcareous nannoplankton and foraminifera) showed them to be uppermost Pliocene in age and not Miocene. To account for their topographically lower relationship with the Pakhna sediments, they were attributed to be part of a

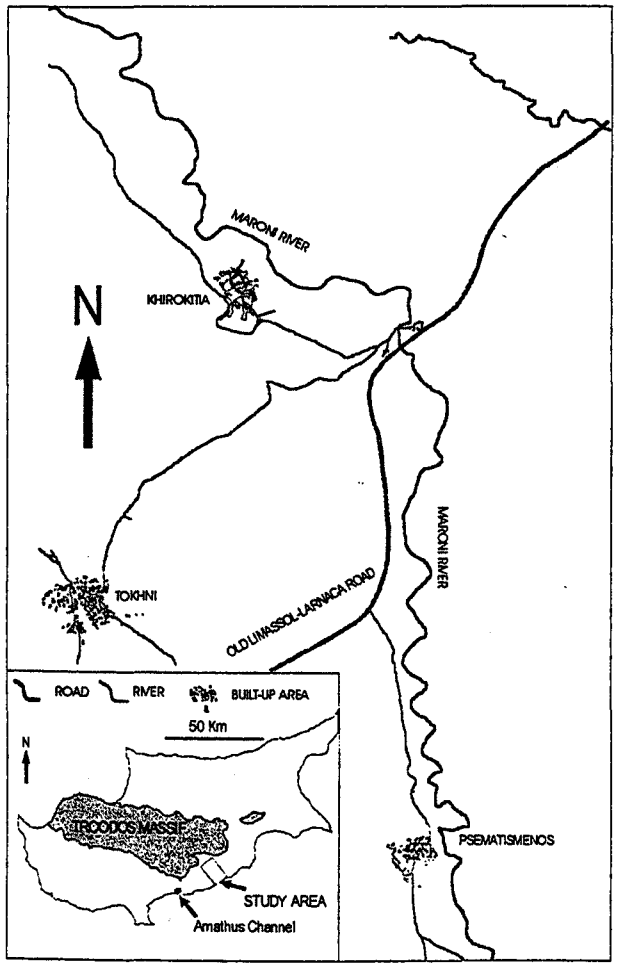

Figure 6.1. Geographical map for the study area

canyon fill that was cut into the Palaeocene-aged Lefkara Formation and Miocene-aged Pakhna Formation. Schirmer (2000) identified, within the Maroni River valley, a succession of 10 individual channels embedded into a monotonous, sequence of basinal silty marlstones. Each channel ranges from 0.7-10m in thickness and contains poorly sorted chalk, reworked coralline material and Troodos derived basic igneous clasts. Channels 1-6 are discrete and separated by a relatively thin fine-grained clastic top, while channels 7-10 are more amalgamated and have a higher carbonate content. Schirmer (2000) interprets the succession as a linear debris supply onto the basin margin, which scooped out flat channels and filled them with material supplied by erosion from a steep sided exposed hinterland. Schirmer suggests a smooth uplift history of the Troodos ophiolite during deposition of the fan complex due to the small amount of erosion (0.7-10m) displayed the channels. He suggests that all three facies associations (channel fill sands and conglomerates, basinal marlstones and marly-carbonates of the surrounding Pakhna Formation) are stratigraphically within he Pakhna Formation. This contrasts with the repeated incision and deposition of a Pliocene canyon proposed by Houghton *et al.*, (1990). Schirmer (2000) dates the succession to Miocene in age due to the presence of the topographically higher Messinian-aged gypsum of the Kalavasos Formation and the *Discospirina* band, however, no explanation is given for the Pliocene date provided by Houghton *et al.*, (1990).

This study builds on this work, through detailed mapping and graphic logging, concentrating particularly on the area to the north and east of Khirokitia and Tokhni.

6.2. Summary of the tectonic uplift history of the Troodos Massif

Since the formation of the Troodos Ophiolite in the Late Cretaceous (Cenomanian-Turonian, 91.6±1.4Ma (Mukasa and Ismail, 1987)) the massif has experienced dramatic uplift. The peak of Mount Olympus, at 2000m above sea-level, forms the highest point on the island and is composed of mantle derived ultramafic tectonites and peridotites (Dilek *et al.*, 1990;

Pantazis, 1980) that formed ~3-4 km beneath the ocean floor. The subsequent ~8-9 km of uplift (accounting for the oceanic water depth) was not always gradational and occurred in pulses (Payne and Robertson, 1995; Robertson, 1977; Robertson, 1998). Gradual uplift occurred from the late-Cretacoeus to the end-Oligocene during the deposition of pelagic chalks and chert of the Lefkara Formation, at estimated water depths of 2000-3000m (Kahler, 1994; Kahler and Stow, 1998). The initiation of the present day, northward dipping, subduction zone to the south of Cyprus, during the early to mid-Miocene (Eaton and Robertson, 1993; Stow *et al.*, 1995) marked the first phase of rapid uplift and deformation, resulting in the basin compartmentalisation discussed in Chapter 2.. The loci of this uplift was concentrated in south-western Cyprus, on the Limassol Forest Block which was thought to have been emergent (Robertson, 1998), and resulted in partial slumping of the chalks and marls of the Pakhna Group in the area (Farrell and Eaton, 1988). The Upper Miocene to Early Pliocene was relatively tectonically quiescent until the Late Pliocene-Pleistocene when major, rapid uplift, centred on the Mount Olympus, occurred resulting in the massif's present day domal shape. Serpentinisation of mantle derived ultramafic rocks is considered the causal mechanism for this uplift and to have resulted in the deposition of the coarse-grained Fanglomerate Group (McCallum and Robertson, 1995; Poole and Robertson, 1991; Robertson, 1977).

6.3 Composition and facies

The Pliocene-Pleistocene sediments of the Khirokitia-Psematismenos-Tokhni area can be characterised at three hierarchical scales with the whole canyon fill being the largest. This canyon fill can be sub-divided into six mappable debris flow units, each of which is characterised by periods of high debris flow activity and are separated from the overlying event by finer-grained marls and calcarenites representing the background sedimentation of carbonate rain and minor debris flows. Within each of these six periods of debris flow activity, there are individual debrites that are not laterally continuous or independently

Figure 6.2 Geological map of the Khirokitia-Psematismenos fan complex

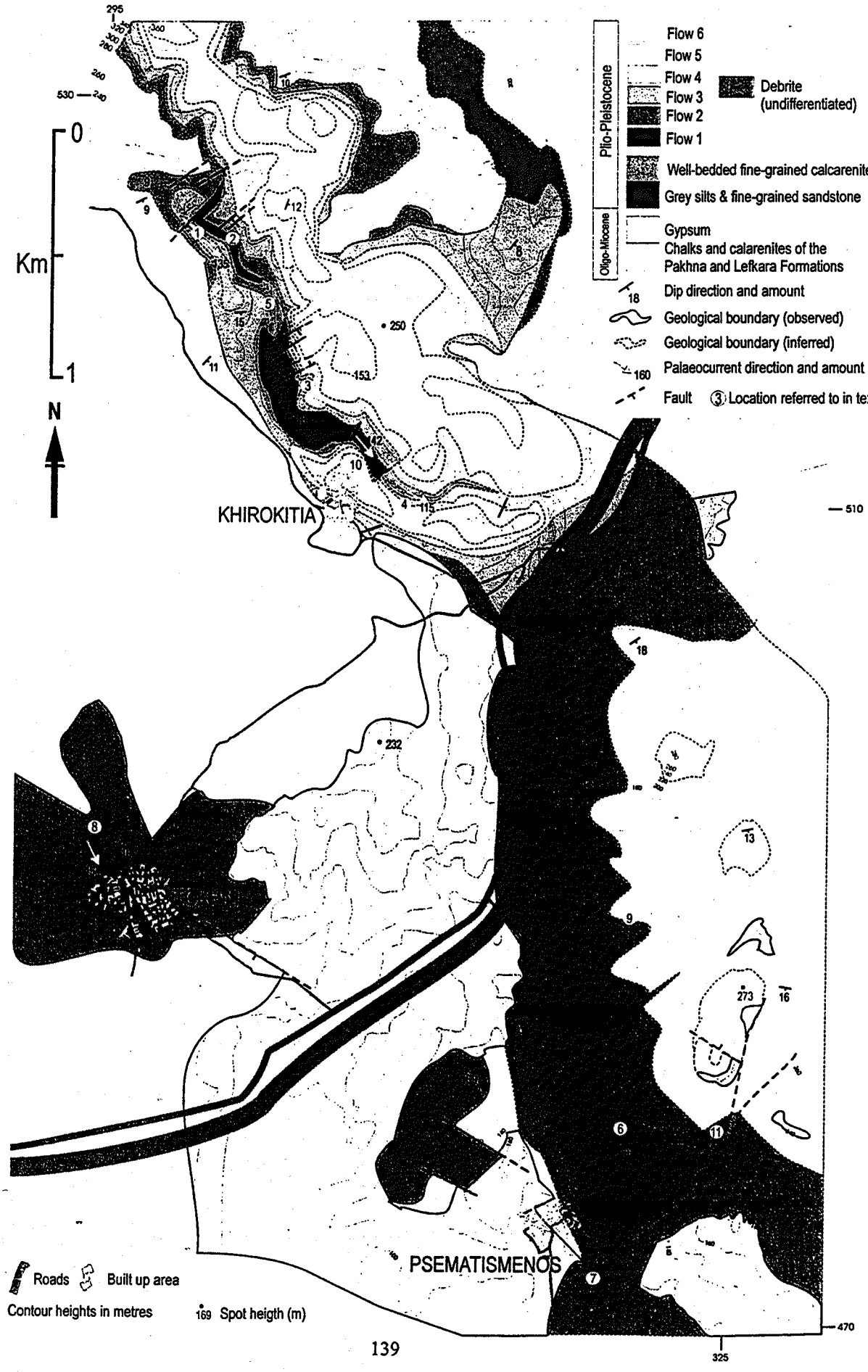

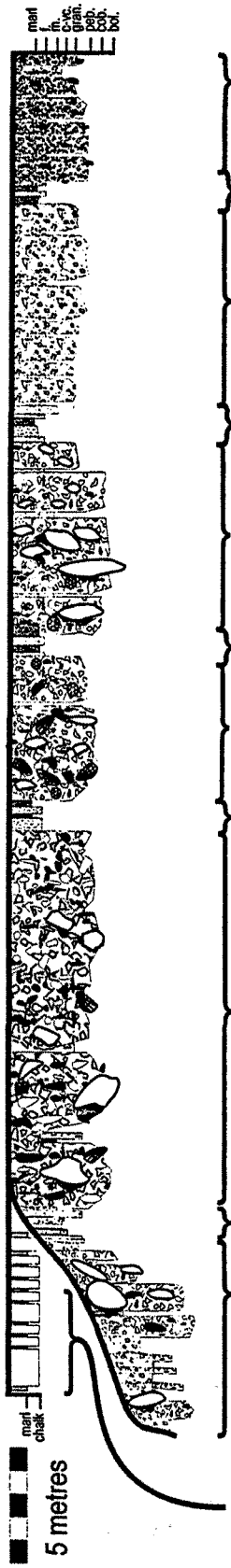

Flow 6: >8 m thick (full flow not exposed)
Top flow unit capping gorge sides, Troodos clasts dominant
Largest clast size ~20 cm
Average clast size ~2 cm.
Clast lithologies: Basalt/Dolerite (40%), Chalk/Chert (25%), Micro-gabbro (15%), Ultramafics (10%), Corals (5%), Other (5%)
Mainly matrix supported.

Interflow Sediments

Flow 5: ~10 m thick
Poorly exposed calcarenite dominated flow, recessive weathering
Largest clast size ~25 cm
Average clast size ~2 cm
Clast lithologies: Chalk/Chert (40%), Basalt/Dolerite (40%), Coral (5%), Micro-gabbro (5%), Ultramafics (5%), Other (5%)
All matrix supported

Interflow Sediments

Flow 4: ~8 m thick
Well exposed chalk clast dominated flow.
Largest clast size ~5 m
Average clast size ~15 cm
Clast lithologies: Chalk/Chert (80%), Basalt/Dolerite (10%), Coral (10%).
Mostly clast supported

Interflow Sediments

Flow 3: ~7 m thick
Well exposed coral/chalk clast dominated flow
Largest clast size ~60 cm
Average clast size ~3 cm
Clast lithologies: Chalk/Chert (40%), Coral (40%), Basalt/Dolerite (15%) other (5%)
Mostly clast supported

Interflow Sediments

Flow 2: >17 m thick
Well exposed flow
Largest clast size ~2 m
Average clast size ~7 cm.
Clast lithologies: Chalk/Chert (80%), Basalt/Dolerite (15%), Corals (5%)
Clast and matrix supported

Interflow Sediments (<0.5 m thick). Well-bedded medium-grained calcarenites and marls. Show no erosional bases and often truncated by Flow 2

Flow 1: >8 m thick
Stratigraphically lowest flow and most poorly exposed flow due burial by successive flows.
Largest clast size ~1.5 m
Average clast size ~4 cm
Clasts lithologies: Chalk/Chert (85%) and Basalt/Dolerite (15%)
Mainly matrix supported

Pakhna Group: Kottaphi Formation
Interbedded chalks and marls. Faulted/incised contact with debrites (figure 6.4).

Figure 6.3. Idealised log of the proximal facies compiled from logged sections to the north of Khirokitia Village (locations 1-5 & 10 on figure 6.2). Note the differing clast compositions and inter-flow sediments that distinguish events. The stratigraphically lowest unit (Flow 1) rests unconformably on the mid-Miocene aged Kottaphi Formation.. The relationship is erosional (channel incision) and/or faulted.

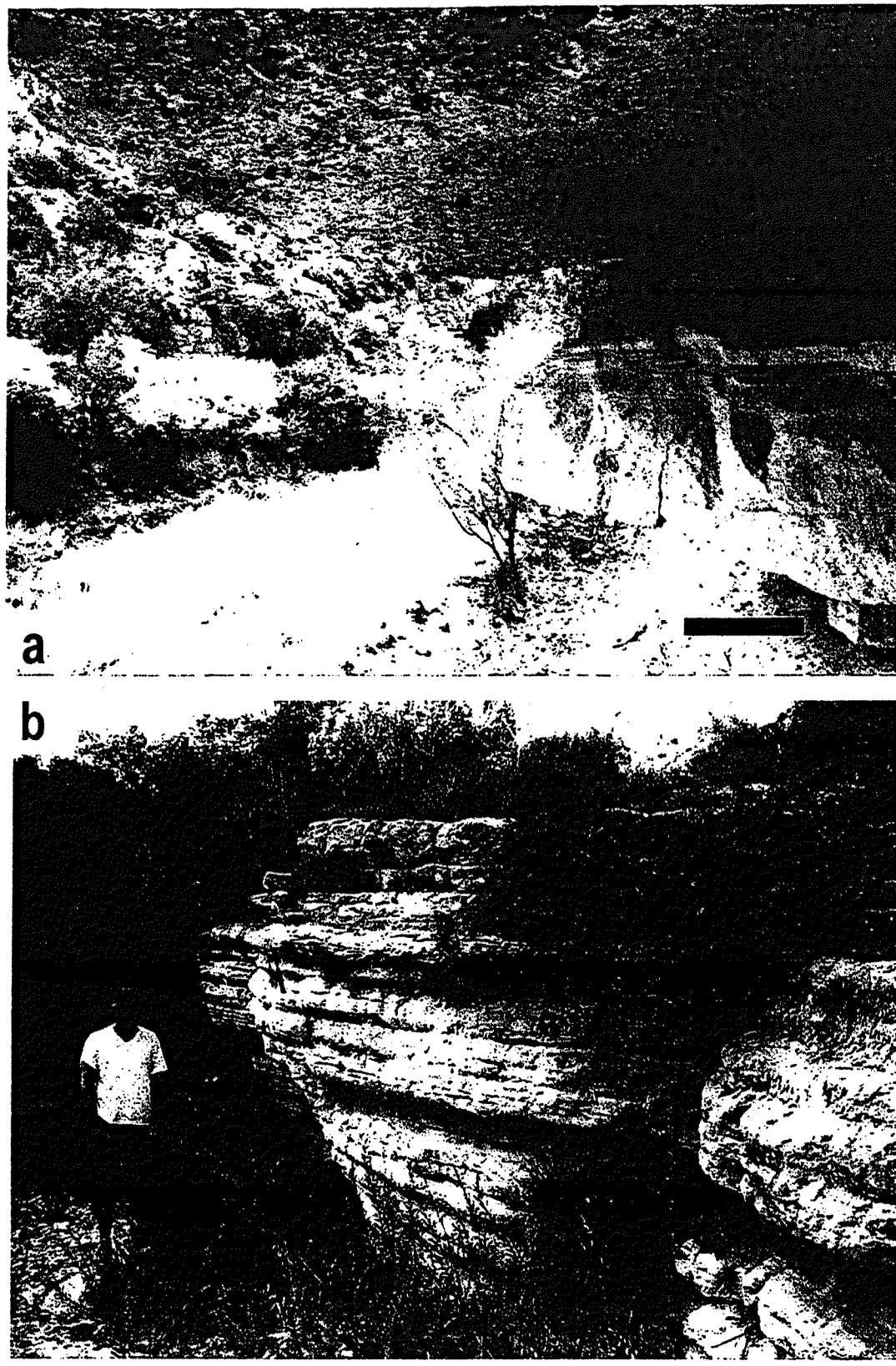

Figure 6.4. (a) View from locality 2 (figure 6.2) looking back at locality 1. Well-bedded marls and fine-grained calcarenites form a semi-continuous marker horizon between Flow 1 and Flow 2. Note the finer-grained base of Flow 2. Scale bar is 25 cm. **(b)** The chalky calcarenite and grit facies at location 5 (figure 6.2). Edward is 2 m tall.

identifiable through lithological variation. The six periods of debris flow activity (termed Flows 1-6 herein) form the foundation to ascertaining the internal structure of the fan, as they have sufficient lithological contrast to distinguish them in the field. The six mapped flow units are illustrated on Figure 6.2, where the fan-shaped geometry can clearly be seen. Initially, the stratigraphy of the fan complex was established at three key cliff localities (localities 1, 3 and 5) where the Maroni river has cut a gorge through the fan complex, mirroring the trend of the Pliocene canyon. Once established, this stratigraphy could then be adopted at the other less well-exposed localities. Figure 6.3 outlines the features of the six flows.

This section first characterises the proximal to distal facies changes associated with the deposition of Flow 1, and then the features of successive flows.

Interflow sediments

The semi-continuous bands that denote periods of drastically reduced debrite activity are composed of unbioturbated fine- to medium-grained chalk-rich calcarenites and marls (Figure 6.4a). The calcarenites contain no clasts over 5 mm and do not truncate any underlying beds. These sediments are interpreted to represent the accumulation of the background carbonate rain, which is periodically interrupted by weak, low density turbidites. The interflow sediments are often not laterally continuous due to erosional truncation by successively younger flow events, though their occurrence is frequent enough for them to provide a useful marker horizon between flow events.

6.3.1 Flow 1

Flow 1 is stratigraphically the oldest period of debrite activity encountered, and as such its outcrop is restricted to a few cliff sections at the base of the gorge. The individual debrites that constitute Flow 1 are numerous and have well-developed bedding (20-30 cm thickness)

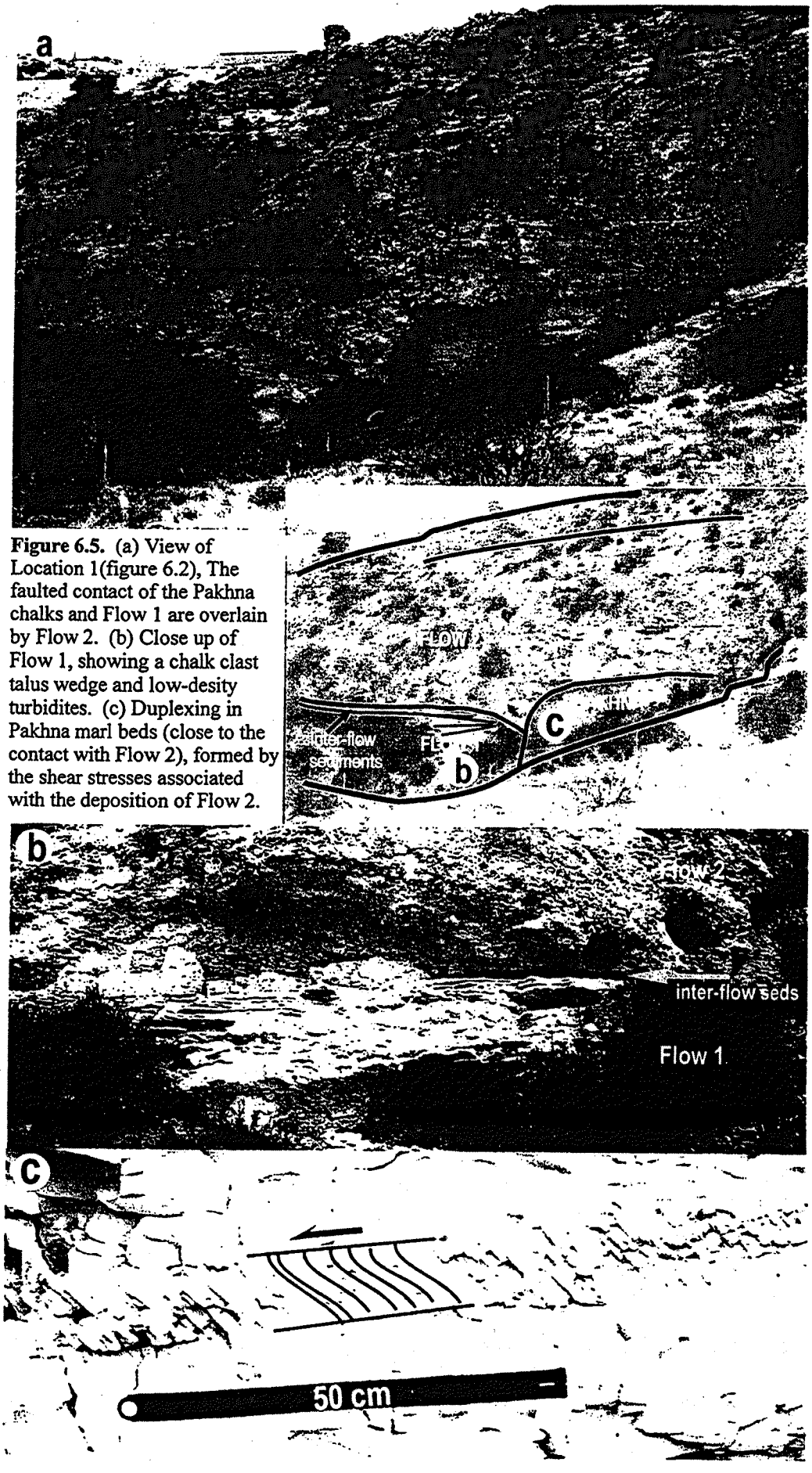

Figure 6.5. (a) View of Location 1(figure 6.2), The faulted contact of the Pakhna chalks and Flow 1 are overlain by Flow 2. (b) Close up of Flow 1, showing a chalk clast talus wedge and low-desity turbidites. (c) Duplexing in Pakhna marl beds (close to the contact with Flow 2), formed by the shear stresses associated with the deposition of Flow 2.

which is accentuated by its high matrix content (~50%). These buff brown rocks have an average grain size of about 5 mm, and are composed dominantly of chalk with minor occurrences of basalt. Interbedded with these relatively well-bedded units are coarser-grained beds (1.5 m maximum clast size), of clast supported conglomerate with clasts dominated by chalk and chert (85%) with minor occurrences of basalt and dolerite (15%). The largest chalk clasts are observed near to outcrops of either the Pakhna Group (Kottaphi Formation) or Lefkara Formation from which they were derived, especially where the Lefkara and Kottaphi Formations are faulted. The basalt and dolerite clasts must have originated from the Troodos Ophiolite (from the extrusive volcanic sequence) as it is the only source of basic igneous material in south-east Cyprus. At locality 1 (Figure 6.2, 6.5, & 6.13) these coarser-grained units have a wedge shaped geometry and rest on the tilted hangingwall block of a fault in the Kottaphi Formation. Towards the top of Flow 1, bedding becomes more pronounced, marking a cessation in the frequency and vigour of debrites. Relatively soft marls and fine-grained calcarenites that produce a recessively weathering unit (indicated by an arrow on Figure 6.5c) mark the boundary between Flow 1 and Flow 2. These fine-grained sediments (Figure 6.4a & 6.6) show well-developed lamination and are unbioturbated. They are sometimes erosionally truncated by Flow 2 but still provide a useful marker band between the flows. The debrites of Flow 1 grade laterally into progressivly finer-grained facies to the south of the locality 1. The distal facies of fan-complex are well developed and can be grouped into three facies (1) chalk-rich calcarenites and grits, (2) grey siltstones and fine-grained sandstones, and (3) well-bedded calcarenites. Though only the chalk-rich calcarenites and the grey siltstones and fine-grained sandstones facies are observed to grade from Flow 1. The well-bedded calcarenite facies is a distal facies of Flows 2-6, and is discussed in section 6.3.7. These distal facies have in intimate relationship with the proximal facies and are observed to grade and inter-digitate with them. Figure 6.7 outlines the charateristic features of the chalk-rich calcarenites and grits, and the well-bedded calcarenite facies.

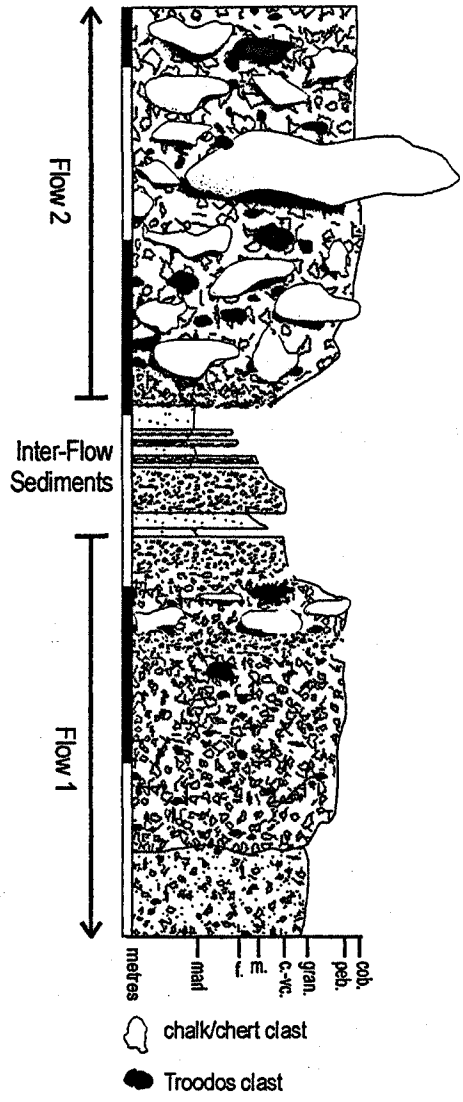

Figure 6.6. Graphic log of locality 2 (Figure 6.2), showing the relationship between the upper debrites in Flow 1 and the interflow marls and calcarenites underlying the lower debrite of Flow 2.

Chalk-rich calcarenites and grits

The chalky calcarenites represent the distal equivalents to the extremely coarse-grained debrites of Flow 1 (Figure 6.12 & 6.13). The reduced flow velocity only permitted the finer-grained fraction to be transported and deposited. The chalk-rich calcarenite and grit facies are best developed at location 5 (Figure 6.2, 6.4b & 6.7). The facies is composed of <25 cm thick, interbedded fine-, medium- and coarse-grained calcarenites, with the occasional marl bed. The white-weathering calcarenites contain a high abundance of chalk, both as clasts and matrix. Troodos derived clasts exist, but comprise <10%, resulting in a speckled appearance on a fresh surface. Bed bases are often erosional, though scouring is restricted only to the underlying bed. The fine- to medium-grained calcarenites often have parallel-wavy lamination, defined by weakly developed discontinuous mud laminae. Bioturbation is poorly developed, but *Thalassinoides* burrows are found in the occasional marl bed. Towards the lower part of the section at locality 5 (Figure 6.7), coarser-grained breccias increase in abundance. These matrix-supported breccias have a maximum clast size of 30 cm with an average of ~3 cm, and are composed of chalk (~85%) and basalt (~15%). They are interpreted to represent debrites of Flow 1 that inter-digitate with the chalk-rich calcarenite facies. They become finer-grained and pinch out completely towards the southeast, along the palaeoflow direction, and have a havea similar clast composition to Flow 1. Towards the top of location 5 a

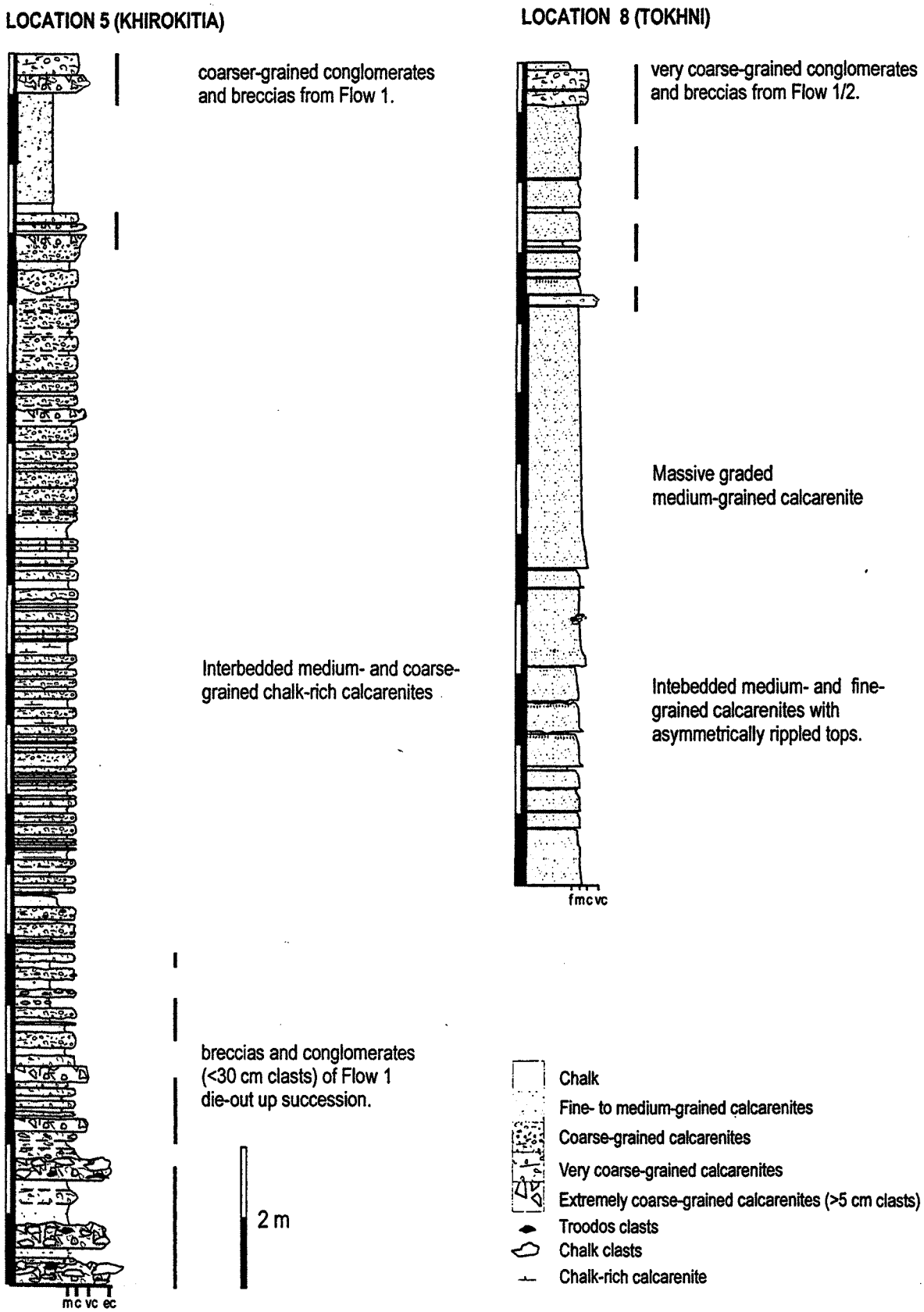

Figure 6.7. Graphic logs illustrating the distal facies of the fan complex. Log of locality 5 (figure 6.2) represents the distal equivalent to Flow 1 and its inter-digitation with the finer-grained calcarenites. Log of locality 8 (figure 6.2), represents calcturbidite deposition away from the main canyon. Scale bar in metres.

gradual coarsening-upward trend is observed within the chalk-rich calcarenites facies, by the inclusion of breccias and coarse-grained grits. The breccias are similar to those found lower down the succession. The grits have a higher content of Troodos derived material (~30%) with clast sizes no larger than 7 mm. They are relatively well-sorted and poorly cemented.

Grey siltstones and fine-grained sandstones

This facies comprises interbedded grey siltstones and fine-grained sandstones, and is in excess of 30 m thick. It is clearly observed at locations 5 and 10 (Figure 6.2 & 6.13). The deposits owe their grey colour to Troodos derived material. Bedding is typically less than 10 cm thick, with no evidence for erosional surfaces. Neither bioturbation nor sedimentary structures are developed. These sediments represent dilute turbidite flows of silt grade material. Periodically slightly higher velocity flows transported sand-grade material producing the fine-grained sandstone beds. The lack of bioturbation is probably the result of high sedimentation rates restricting colonisation by infauna. This facies interdigitates with, and grades down the palaeo-slope, from the chalky calcarenite facies, and reflects the continuation of the progressive decrease in the influence of current energies associated the debrites of Flow 1. Location 6 (Figure 6.2), which is a more distal exposure of this facies there is a reduction in the number and thickness of fine-grained sandstone beds.

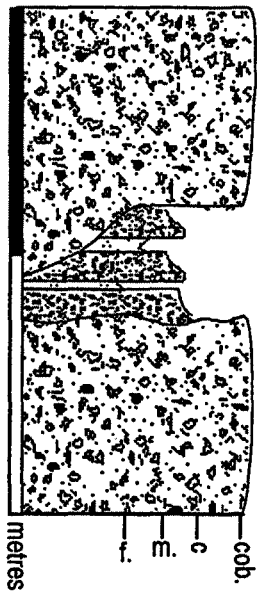

Figure 6.8. Graphic log of a debrite truncating coarse-medium-grained calcarenites (minor/distal debrites) at the top of the cliff at locality 1.

6.3.2 Flow 2

Flow 2 forms the majority of the cliff face at location 1 (Figures 6.2, & 6.5a), and is a least 17 m thick. The flow is well exposed along the length of the Maroni river gorge, north of

Khirokitia. Clast lithologies are similar to Flow 1 (Figure 6.3), though there is also evidence for the erosion and transportation of the Koronia Limestone due to the presence of colonial coral clasts. Basalt and dolerite clasts are larger and often preserved as whole pillow lavas. Figure 6.4c illustrates the loading effect of debrite deposition on the underlying chalks and marls of the Kottaphi Formation. The less competent marl beds have absorbed the shear stresses associated with the rapid deposition of the debrite by forming imbricate duplex structures (Figure 6.5c). The individual flow events that make up Flow 2 are substantially thicker than those of Flow 1, measuring up to 7 m. The transition between individual debrite events are marked by ½ -2 m small-scale scours and in places recessively weathering ~10 cm thick coarse-grained calcarenite beds (Figure 6.8). The lower 20 cm of the first debrite in Flow 2 is a finer-grained, matrix supported conglomerate, with clasts no larger than 8 cm (Figure 6.4a & 6.9). Where this unit is mainly matrix-supported, and its underside is exposed, flute marks are visible which give palaeocurrent directions towards the southeast (Figure 6.2). The debrites towards the top of Flow 2 are finer-grained (<35 cm clasts) with bedding on a metre-scale, which becomes progressively more pronounced. These are interbedded with coarse-grained and medium-grained calcarenites, which are eroded into by the base of each of the overlying coarse-grained debrites (Figure 6.8). Directly above Flow 2 lies another semi-continuous unit of marl and calcarenite about 50 cm in thickness. Unlike Flow 1 the transition to finer-grained, distal sedimentation is less pronounced, though Flow 2 sediments become thinner and finer-grained towards the south. At locality 3 (Figure 6.2) Flow 2 loses most of its coarse-grained fraction and the flow is dominated by calcarenites, with the occasional large clast up to 3 m long (Figure 6.9).

6.3.3 Flow 3

Flow 3 is the thinnest flow and probably only attains a maximum thickness of ~ 10m. It is characterised by its high content of coralline clasts, which can be up to 80 cm in length. At locality 4 (Figure 6.2) the flow is near to ground level which allow close examination (Figure

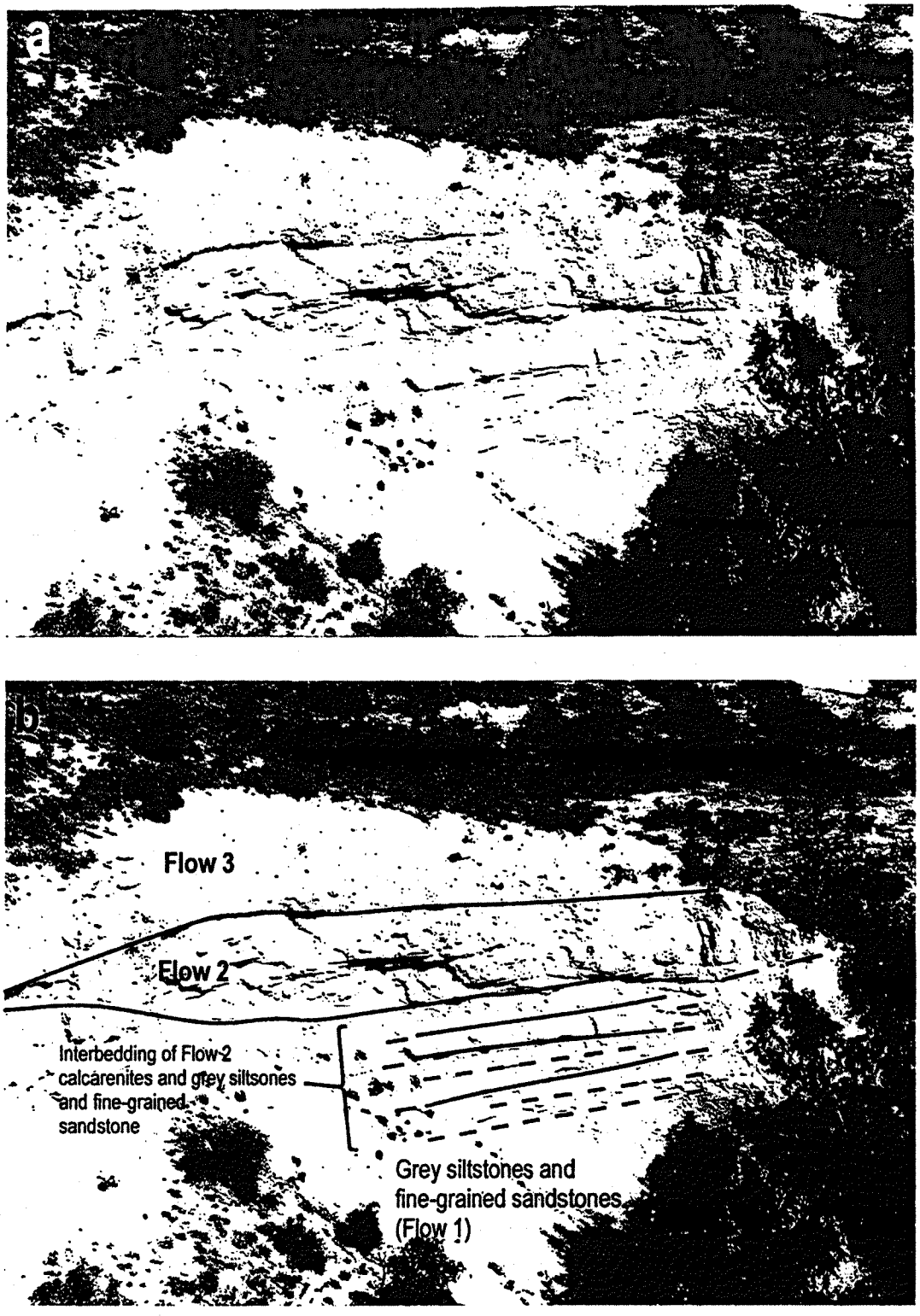

Figure 6.9. (a) Photograph of location 3. (b) Interpretation showing the passive, interbedded nature of the contact between Flow 2 and the grey siltstone and fine-grained sandstone facies, which form the base of the cliff. Flow 3 forms the top of the cliff section. Note that calcarenites dominate Flow 2 in this area. Height of cliff is approximately 25 metres.

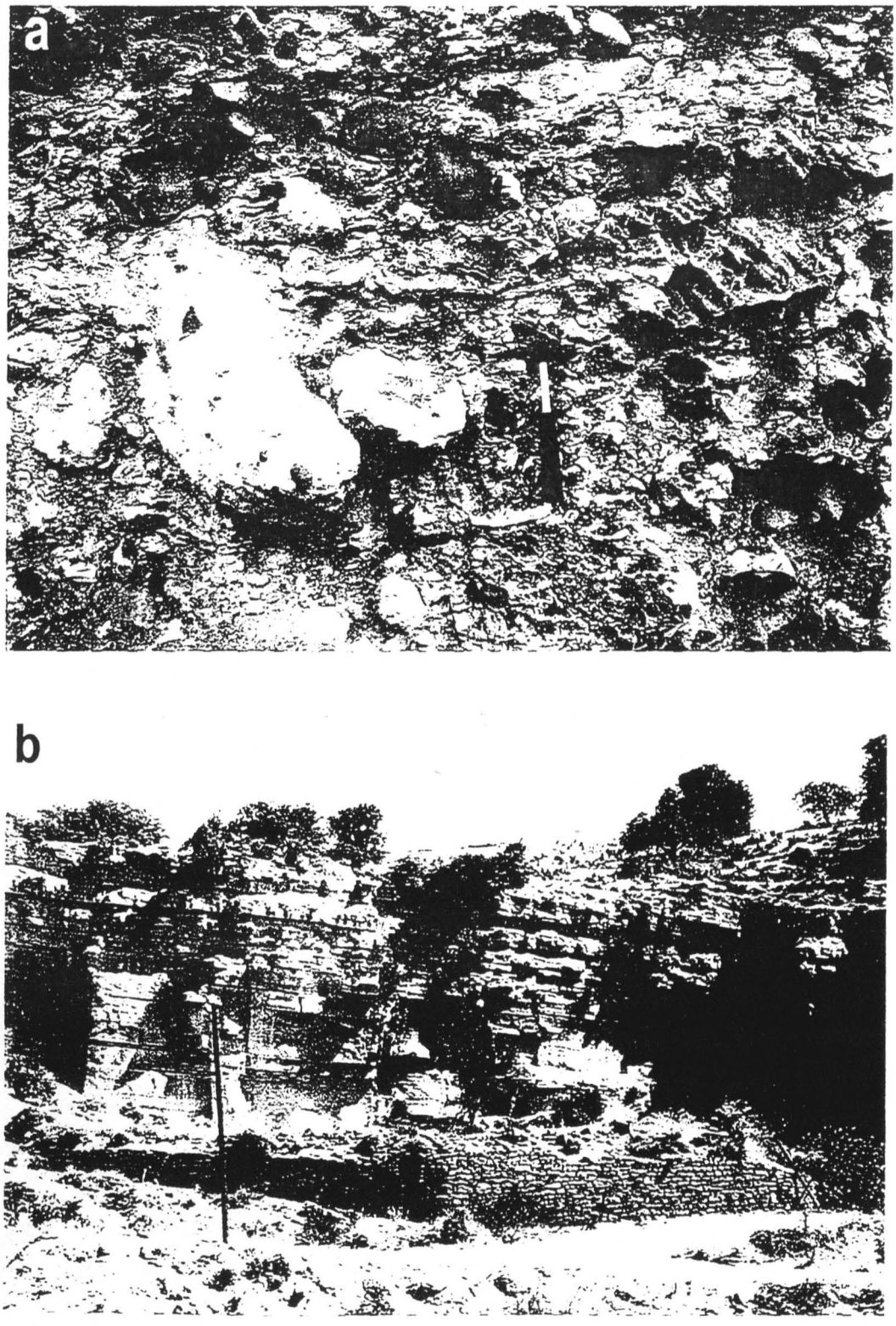

Figure 6.10. (a) Clast compositions of Flow 3. Note large colonial coral clasts to the right of the hammer, and a reworked conglomerate clast to the left. Hammer is 30 cm long.. (b) Well-bedded calcarenite facies at location 8 (Tokhni Quarry). Thick calcarenites at the base of the cliff are ~2m thick.

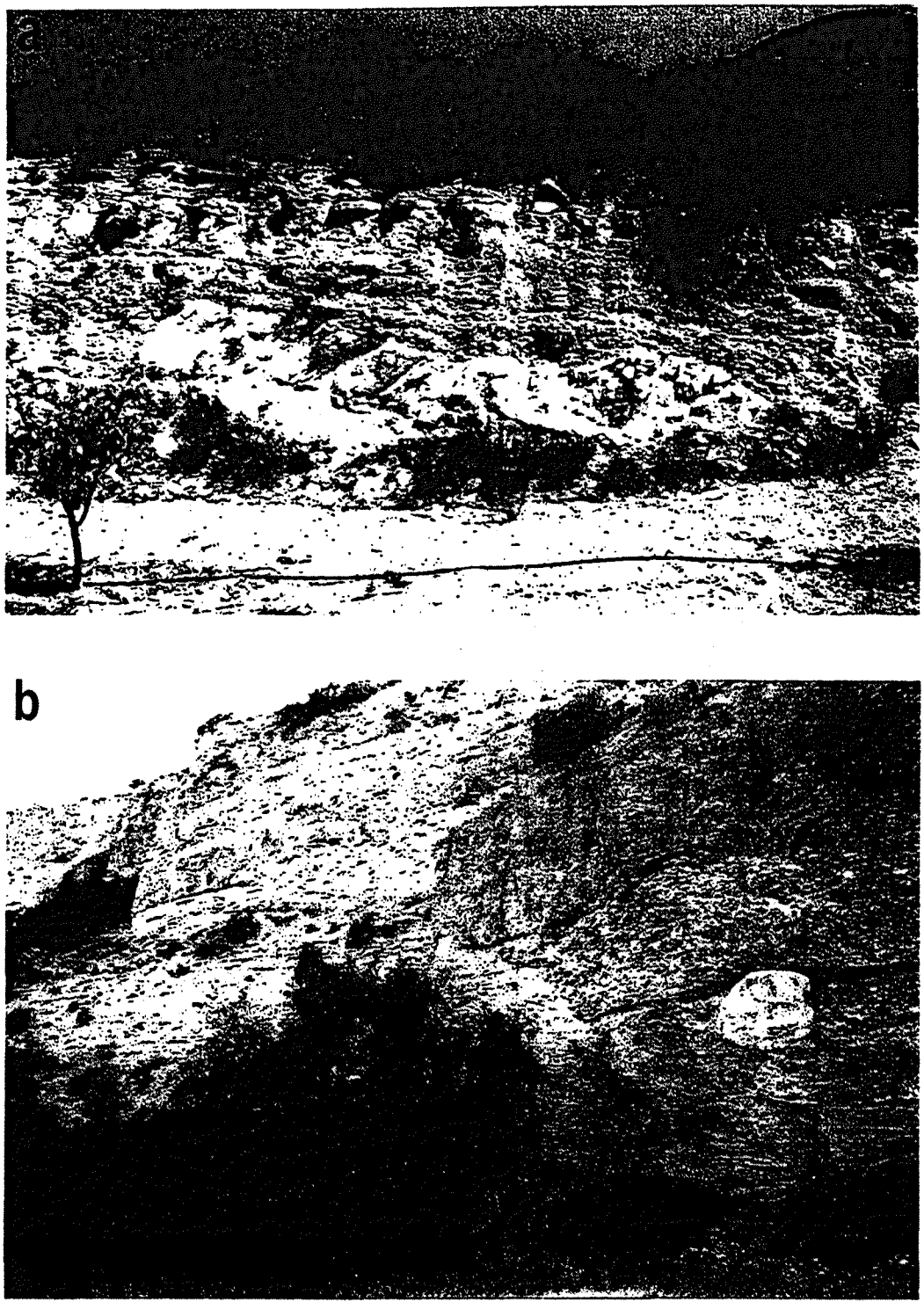

Figure 6.11. (a) Two large clasts of interbedded chalk and marl in the chalk dominated Flow 4 at location 2 (figure 6.2). The left-hand clast is 5 m in length with bedding visible dipping to the left at about 35 . The right-hand clast is 3 m in length and has bedding dipping to the left at about 20 m. (b) Large scale channel incision into the grey siltstones and fine-grained sandstone facies, which represents the distal facies of Flow 1, at location 10 (Figure 6.2). Grey silts form the base of the cliff and underlie the channel fill to the right of the photograph. The base of the channel in-fill is marked by Flow 2 (with the large 2 m chalk clast), with Flow 6, capping the cliff.

6.10a). As well as chalk and chert (45%), coral (40%), basalt and dolerite (15%) clasts there are rarer clasts of matrix-rich conglomerate that must have been reworked from one of the previous flows. This conglomerate (indicated in Figure 6.10a) has clasts composed of basalt, chert and chalk. Many of the corals in Flow 3 have bored surfaces, suggesting exposure and/or reworking of the Koronia Limestone in a marine environment. The reworking of the Koronia Limestone reached its zenith during the deposition of Flow 3, as successive and previous flows have significantly lower abundances of coralline material. This suggests that the Koronia Limestone was either exposed very locally or had an extensive outcrop in the source area.

6.3.4 Flow 4

Flow 4 is best exposed at locality 3 (Figure 6.2) and is dominated by chalk and chert clasts (80%) with subordinate amounts of basalt and dolerite (10%), and coralline material (10%; Figure 6.3). In the logged section (locality 3) it is ~8 m in thickness, though can attain thicknesses of 20+ m indicated by its field relationships with the Flows 3 and 5. The character of Flow 4 varies considerably; it is sometimes dominantly clast supported, with generally small chalk clasts (<3 m, average ~15cm), but elsewhere it is composed of matrix-supported, well-bedded calcarenites (Figure 6.11a). Floating within these calcarenites there are extremely large clasts of chalk, up to 5m in length. Figure 6.11a illustrates two such clasts that are resting next to each other. Both clasts show clear interbedding of chalk and marl. They are interpreted to arise from the collapse of the canyon wall, with little or no transport, as any significant transportation would result in the clast fragmenting along its bedding planes. The two sub-facies (calcarenite dominant and conglomerate dominant) probably result from channelisation of the individual debrites in Flow 4. The coarser-grained facies represents the main flow itself, while the calcarenites depict sedimentation marginal to the debrite, near to an unstable canyon wall. The calcarenites are well-bedded on a sub-metre scale (typically 10-20 cm) and can show cross cutting accretion surfaces, suggesting that in

these marginal areas debrites deposits were subtly channelised, and had enough energy to erode and truncate previous deposits.

6.3.5 Flow 5

Flow 5, is well exposed at location 3 (Figure 6.2) where it is ~10 m thick and dominated by coarse-grained calcarenites and matrix-supported conglomerates (Figure 6.3). Clasts are generally smaller with an average size of ~2 cm (largest 25 cm). They are composed in roughly equal proportions of chalk/chert (45%) and basalt/dolerite (40%) with contributions of coralline material (5%) and micro-gabbro (5%). The flow weathers recessively and complete sections are poorly exposed. Bedding is generally developed on a metre scale, with only minor evidence for erosional truncation. The presence of micro-gabbro is significant, as it indicates that the plutonic sequence of the Troodos was exposed and acting as a minor source of material during the deposition of Flow 5.

6.3.6 Flow 6

Flow 6 is the youngest flow exposed and forms the "cap" to most of the hills in the immediate area (Figure 6.2 & 6.3). It is well exposed at locations 3 where it is a least 8 m thick, and is matrix-supported, with clasts mainly of basalt/dolerite (40%) chalk/chert (25%), micro-gabbro (15%) ultramafics (10%) and coralline material (5%). As well as containing the most diverse clast assemblage, it is the finest grained flow overall, with an average clast size of ~2 cm and a rare maximum size of ~20 cm. The individual debrite events that make up this flow are numerous, as bedding is generally on a sub-metre scale with erosional truncation commonplace. The presence of ultramafic clasts shows that the plutonic sequence of the Troodos was exposed at this time, however, basalt and dolerite still dominate the igneous assemblage of this deposit.

6.3.7 Well-bedded calcarenites

The well-bedded calcarenite facies represent the distal equivalent of Flows 2-6 and is best developed to the south of Psematismenos and at Tokhni, where it is still quarried for building stone and masonry (locations 7 and 8, Figures 6.2, & 6.10b). Due to a lack of exposure of this facies, and restricted access to parts of the field area, the transition between Flows 2-6 and the well-bedded calcarenite facies is not observed, but deduced from field mapping. At location 11 (Figure 6.2) restricted exposures of the well-bedded calcarenite facies outcrop below debrites 5 and 6, indicating that deposition occurred prior to these flow events during the deposition of Flows 2-4. The characteristic features of this facies are outlined in the graphic log on Figure 6.7. These medium- to coarse-grained buff-brown calcarenites have well-developed bedding (20-470 cm thick) and display normal grainsize grading, with parallel lamination towards the top. The tops of these graded units occasionally have a current rippled surface, giving palaeocurrent directions to the southeast. Sole marks (load casts) on the bases of these units testifies to rapid deposition onto unconsolidated deposits. These coarser-grained calcarenites are interbedded with thinner (<5cm) finer-grained, sandstones, siltstones and mudstones. All lithologies within this facies contain a significant sub-millimetre grade Troodos derived fraction (~10-30%). The association of normal graded bedding, planer lamination and current ripples suggest turbidite deposition, with Bouma units (Bouma, 1962) Ta (structureless), Tb (parallel laminated), Tc (ripples) and Te (hemipelagic) are all represented here within different flows. However, Bouma units Ta and Tb (separated by Te) are dominant, and best characterise the style of deposition within the well-bedded calcarenite facies.

6.4 Fan geometry and internal structure

6.4.1 Fan geometry

Mapping the boundary between the fan facies and the Lefkara and Pakhna Group, reveals that the fan complex to the north of Khirokitia Village has a confined canyon geometry, with an

east-west lateral extent of ~500-900 m (Figure 6.2). In this area, most parts of the canyon fill are infilling topographical lows in the surrounding older rocks of the Lefkara and Kottaphi formations. This restriction is mainly due to debrite deposition being confined to a Pliocene canyon, which is mimicked today by the gorge cut by the Maroni River. The area further south, towards Psematismenos, is highly disrupted by neo-tectonic faulting, making flow mapping impracticable, though the fan margins are still traceable. The fan-complex here, broadens-out to over a kilometre wide, and appears to still be semi-confined to a topographical depression bounded to the east by Kalavasos Formation (gypsum). The western margin of the fan could not be deduced due to restricted access, though appears to widen further to over 2 km adjacent to Psematismenos. The overall geometry of the fan-complex is that of a confined canyon widening out to a submarine-fan to the south. It has a NNW-SSE orientation, which is concurrent with palaeocurrent data, suggesting that the outcrop is not a function of erosion or topography. The fan complex tapers out to the northwest, about 2 km south east of the present-day outcrop of the Troodos ophiolite, suggesting the fan was fed by a point source.

The outcrop of the well-bedded calcarenite facies at Tokhni (location 8, Figure 6.2), does not lie within the confines of the main fan complex outcrop. This suggests that either these sediments originate from a different fan complex to the west, or more likely that the area between these two outcrops has been eroded, isolating the Tokhni locality as there is a topographically low-lying region between Khirokitia Village and Tokhni (Figure 6.2). There is no physical evidence for a second fan complex and the similarity between the Tokhni lithologies and those to the south east of Psematismenos implies that both deposits result from the same flow.

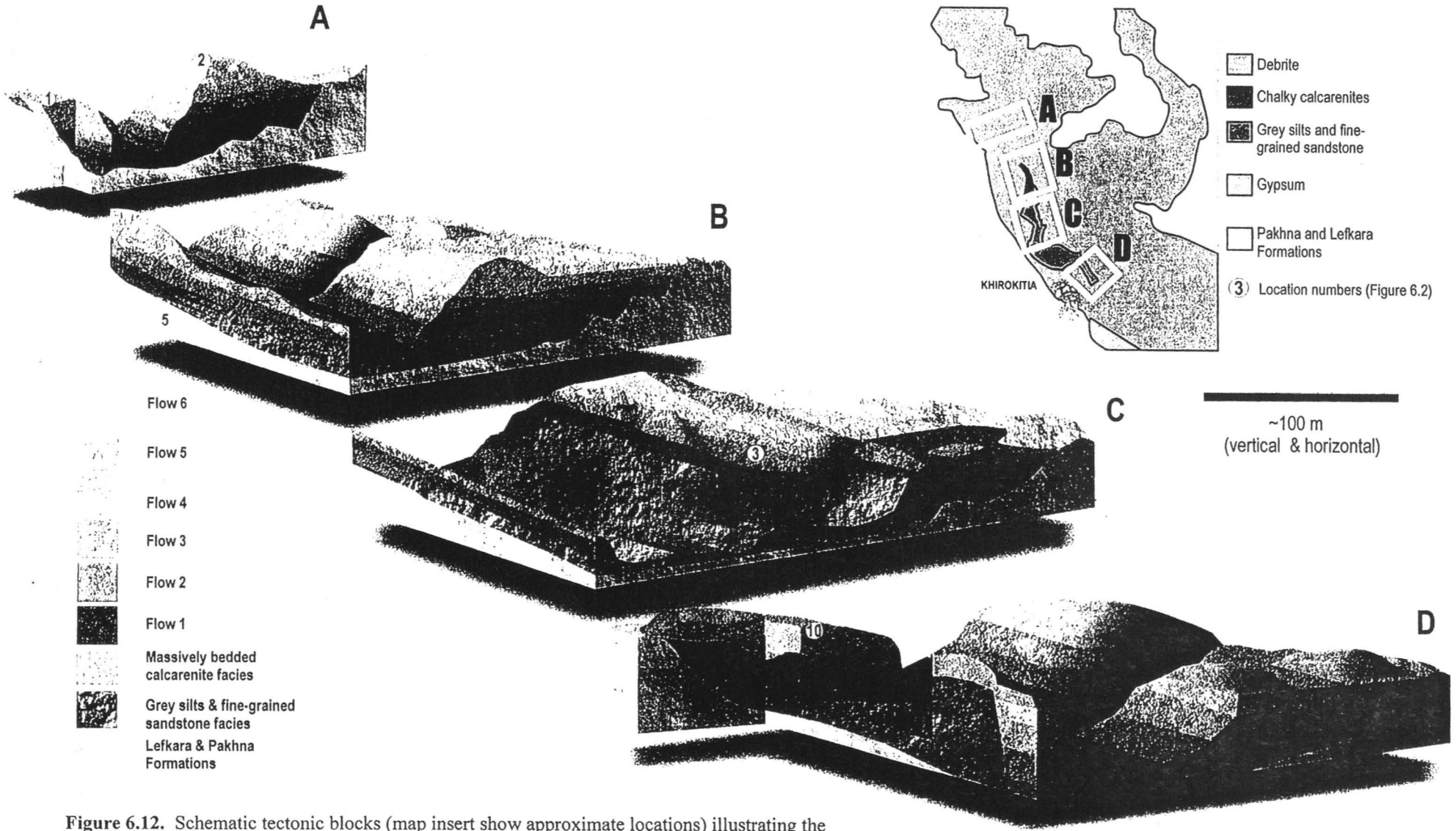

Figure 6.12. Schematic tectonic blocks (map insert show approximate locations) illustrating the facies relationships between Flow1-6, chalky calcarenites and grey silts & fine-grained sandstone facies. See text for details.

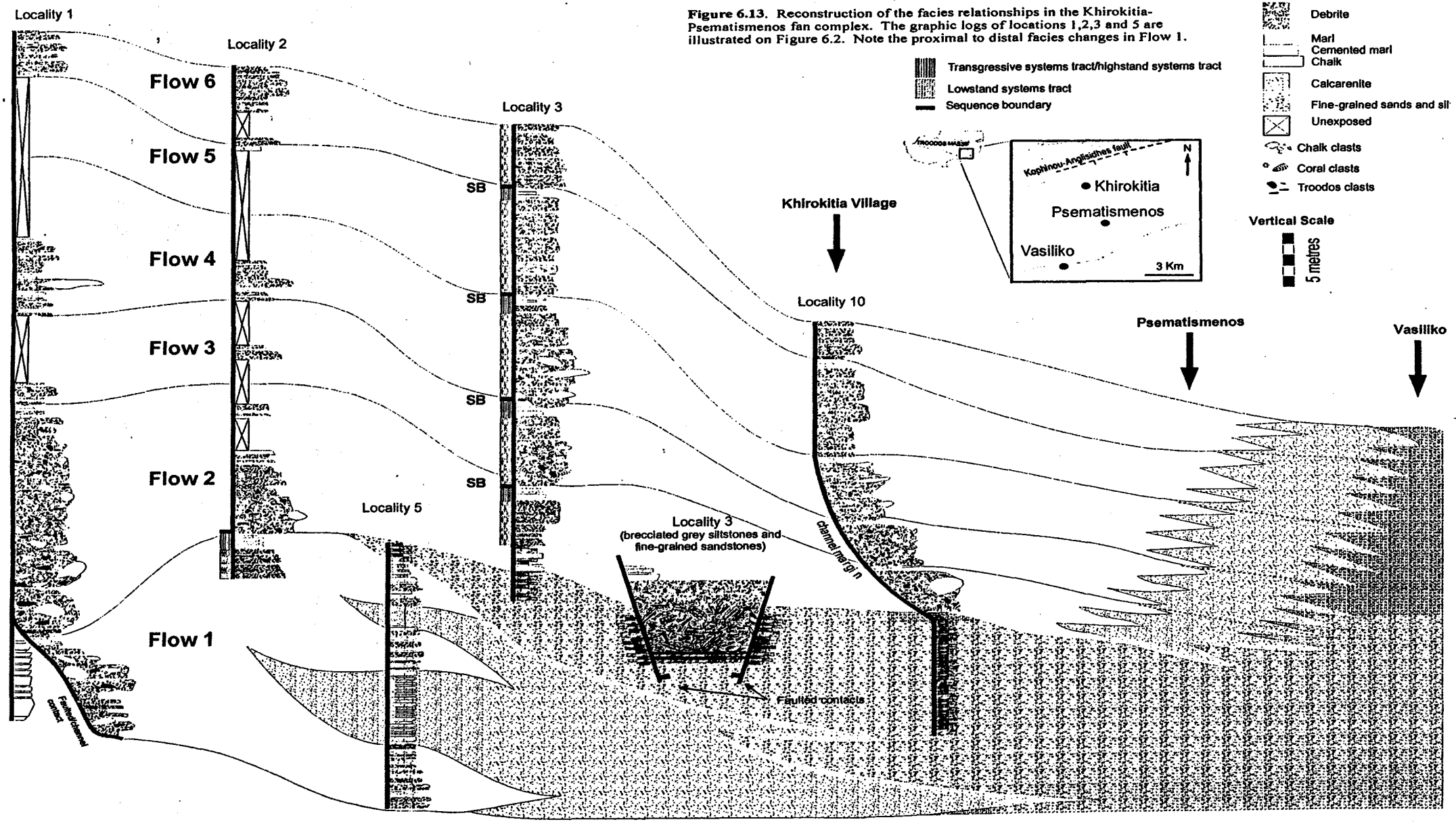

Figure 6.13. Reconstruction of the facies relationships in the Khirokitia-Psematismenos fan complex. The graphic logs of locations 1,2,3 and 5 are illustrated on Figure 6.2. Note the proximal to distal facies changes in Flow 1.

6.4.2 Internal Structure

The inter-relationships between the six flows and their associated distal facies give some insight into the scale and evolution of submarine fan complexes. The area occupied by the fan complex is dissected by a series of WSW-ENE trending normal faults (Bagnall, 1960) that originated due to the uplift of the Troodos mainly during the Pliocene (Figure 6.2). There is good evidence to suggest that these faults were responsible for positioning, concentrating and maintaining palaeoslope gradients for ensuing debrite sedimentation in this area. At location 1 (Figures 6.2, 6.5c & 6.13) an early SW-NE syn-sedimentary fault exists along the canyon margin within the Pakhna chalks. It ceased activity before the deposition of Flow 2 and has a talus cone developed on its footwall *within* Flow 1. At location 3 (Figure 6.2 & 6.13) a ENE-WSW syn-sedimentary faulting has caused dramatic disturbance of the grey siltstone and fine-grained sandstone facies. Brecciated metre scale blocks of the grey siltstone and fine-grained sandstone are housed in a downthrown graben, which is overlain by undisturbed calcarenites of Flow 2. The upthrown sides of the graben (horst blocks) contain undisturbed well-bedded grey siltstones and fine-grained sandstone. It is suggested that the faulting occurred while the grey silts and fine-grained sandstones were semi-lithified, as some of the blocks show ductile deformation.

The contact between the fan complex and the underlying Lefkara and Pakhna Formations is diachronous. At location 9 (Figure 6.2) the beds of Flow 5 are observed to onlap onto the chalks and marls of the Kottaphi Formation. This implies that Flow 1 was not ubiquitously deposited on the Pakhna Group, and that successive flows have a greater lateral extent, building out to the south east over the Pakhna Group and the distal facies of previous flows.

The proximal-distal transition between facies belts is best observed in Flow 1, where three facies grade laterally into each other over a distance 1 km. The 3D block diagrams (Figure

6.12) and graphic logs (Figure 6.13) illustrate this facies change. The coarse-grained debrites of Flow 1 become finer-grained and grade into the chalky calcarenite facies, which in turn grades into the grey silt and sandstone facies. This facies succession repeatedly prograded and retrograded through time (depending on the frequency and severity of debrites), to produce the observed inter-digitation of these three facies belts (Figure 6.13 & 6.17).

The grey siltstone and fine-grained sandstone facies is laterally extensive, and is interpreted to be the distal part of all flows. As well as outcropping near Psematismenos it is exposed at Vasiliko some 5 km to the south (Figure 6.13), where it is more clay rich and contains an infaunal bi-valve assemblage and a significant foraminiferal component. This is probably a reflection of reduced sedimentation rates in distal settings, allowing colonisation of fauna and less dilution of the background carbonate rain.

The coarse-grained facies of Flow 2 has a greater distal extent than that of Flow 1. The proximal facies of Flow 2 also extends further towards the Troodos ophiolite. This suggests that the submarine canyon was back stepping in much the same way as a nich point would react to rejuvenation on a fluvial profile. The base of Flow 2 becomes rich in calcarenites at location 3 (Figure 6.2) and is interbedded with the grey silt and fine-grained sandstone facies (location 3, Figure 6.9 & 6.13). This passive relationship with the grey siltstones is not exhibited at location 10 (Figure 6.2) where a ~17 m deep channel is cut into the grey siltstones (location 10, Figure 6.11b 6.12, & 6.13). The channel fill is comprised of four debrite events (Flows 2-4), which are separated by prominent finer-grained sediments that are not erosionally truncated by the overlying debrites. This indicates that successive flows were passively in-filling a pre-existing channel that formed prior to, or during the deposition of Flow 2. The orientation of the channel axis and sole marks on the bases of the debrite units indicate palaeoflow to the south east, which implies that channel formation was a result of debrite erosion. Flows 5 and 6 at location 10 are not affected by the channel depression and

overly the fill of Flows 2-4. The interbedding between Flow 2 and the grey siltstones occurs within 500 m of the channel (locations 3 and 10, Figure 6.2), and probably represents deposition marginal to the channel. The sediments marginal to the channel are finer-grained (calcarenites) where as the channel deposits of Flow 2 have an average clast of ~3 cm (2 m max.). Channelling was probably initiated by a lowering of base level, and heightened by current energies becoming funnelled by surrounding upthrown blocks of contemporaneous syn-sedimentary faults.

The proximal facies of Flow 2-4 grades into the distal well-bedded calcarenite facies exposed Psematismenos and Tokhni. These calcarenites are similar to the chalk-rich calcarenite facies of Flow 1, accept for their lower chalk content and thicker bedding. These difference maybe a function of confinement by the canyon walls on the chalk-rich calcarenite, or the sediment supply. To the south of the area investigated, towards Vasiliko on the coast (Figure 6.13), it is predicted that the well-bedded calcarenites grade into the grey siltstone and fine-grained sandstone facies. This effectively defines the lowest energy end member of the fan complex, where distinction between the flows could only be made on lithological differences.

6.5 Fan classification and analogies with other ancient examples

Considerable recent research has been conducted on ancient submarine fan complexes (e.g. Seidler, 2000; Taylor *et al.*, 2000; Wonham *et al.*, 2000; Cronin and Kidd, 1998; Ito, 1998) due to their economic importance, as they contain 15% of the world current hydrocarbon reserves (Richards *et al.*, 1998). Many attempts have been made to classify the variability of submarine-fans over the last 20 years, with predictive models based on grain size and source (Normark, 1974; 1978), efficiency (Mutti and Johns, 1978) and an all encompassing model by Walker (1978). A review of such models is provided by Reading and Richards (1994). The classification scheme adopted in this study is that of Richards *et al.* (1998), whose classification embraces all deep-water clastic depositional systems and is based on grain size,

nature of sediment supply and the number of entry points feeding the system. One of their models is that of a gravel-rich submarine fan which generally forms on an active margin. These types of fan are associated with high slope gradients and develop locally on a small scale (<50 km radius). They have an abrupt proximal-distal grain size grading from conglomerates and talus to more sandy lithofacies at the margins. Proximal conglomerates have wedge a shaped geometry which often taper towards footwall scarps, while distal areas are sheet like with turbidite facies Ta, Tb and Tf. The Khirokitia-Psematismenos fan complex fits the gravel-rich submarine fan description defined by Richards *et al.* (1998), as it is developed on an active margin and on a small scale. It also has abrupt proximal to distal facies variation, from coarse-grained conglomerates and breccias to turbidite units Ta and Tb.

Many similarities exist between the Khirokitia-Psematismenos fan complex and other ancient examples of fan complexes. These are discussed in terms of canyon geometry, facies, facies distribution, and the evolution of the canyon fill.

6.5.1 Canyon geometry

To the north of Khirokitia Village the canyon is ~500 m wide and ~100 m deep, broadening out to a semi-confined fan ~1500 m wide and 180 m deep around Psematismenos. The fan complex varies in length from ~600m (Flow 1) to 7-8 km in the case of the younger flows.

Lower Triassic submarine canyons in eastern Greenland that are interpreted to have been deposited during a period of active rifting (Seidler, 2000), are developed on a similar scale (250-2000 m width and 60 m depth) to the Khirokitia-Psematismenos fan complex, suggesting that this scale of canyon necessitates tectonic activity to maintain suitably high gradients. The Greenland canyons, like the Khirokitia-Psematismenos canyon, shows a transition from confined, high-density turbidites which have low amounts of lateral bed

continuity to less-confined low density turbidites, with much more widespread lateral bed continuity.

Taylor *et al.* (2000) examined a series of late Quaternary submarine canyon on the north Norwegian margin where canyon development is on a much larger scale (10.6 km width, 420 m depth) than that observed in Cyprus. Like the Khirokitia-Psematismenos canyon the Norwegian canyons have a coarse-grained proximal facies which often contain large blocks of material derived from the canyon wall. The discrepancy in scale is probably a function of the reduced sediment supply; the Cypriot landmass during Plio-Pleistocene must have been at least half the size of today (<4500 km^2 for the present day Troodos outcrop) considering that the marine proximal facies of the fan is only a few kilometres from the contact with the Troodos ophiolite.

The Lower Miocene-age Baliste-Crécerelle canyon of the Gabon coast is considered to be a typical example of a large submarine canyon and extents for 120 km basinwards from the palaeo-shelf, with a width of up to 10 km and a thickness of 500 m (Wonham *et al.* 2000). The Baliste-Crécerelle and the Norwegian canyons developed on the shelf break of mature passive margins. This differs from the Cyprus margin, which is active and extremely narrow, with water depths attaining 1000 m about 15 km off shore. The Khirokitia-Psematismenos fan complex is developed within the shelf, and not on the shelf-break. It is interpreted that the necessary gradient and the break in slope for the Khirokitia-Psematismenos fan are provided by the Kophinou-Anglisidhes fault system (Figure 6.13), a major fault zone that is suggested to be the southern boundary fault of the Troodos massif (Bagnall, 1960).

6.5.2 Facies and facies distribution

The composition of submarine fans and canyons is largely dependent on the character of the source material, gradient, basin morphology and climate.

Facies within Flow 1 of the Khirokitia-Psematismenos fan complex grade from very coarse-grained conglomerates to fine-grained sandstone and siltstone over 1 km. Successive flows grade to the finer-grained well-bedded calcarenites facies over 4-5 km and the grey siltstone and fine-grained sandstone facies at 7-8 km. The coarser-grained deposits are mainly confined towards the fan centre, and the marginal areas are typified by calcarenites.

The similar sized canyons in east Greenland (Seidler, 2000) have lithofacies (and distribution) similar to the Khirokitia-Psematismenos canyon. Seidler (2000) noted the lateral discontinuity (tens of metres) of individual debrites in proximal areas, which graded basinwards into finer-grained turbidites with far greater lateral continuity. This transition of facies in the east Greenland canyons occurs over 4-5 km, comparable in scale to the proximal facies grading of the debrites at Khirokitia to the laterally continuous well-bedded calcarenites developed at Psematismenos (*i.e.* proximal-distal facies transitions are occurring at similar distances from the source in both fans). The overall upward coarsening observed in the grey siltstones and fine-grained sandstone facies is interpreted to represent the basinward progradation of a coarser-grained wedge of proximal debrites. This relationship also occurs in the east Greenland canyons, where distal clean shales grade into silty mudstones which host an increasing frequency of interbedded turbidites, reflecting progradation (Seidler 2000).

At Point Lobos, California, a Palaeocene-aged canyon-fill has inter-canyon conglomeratic facies concentrated towards the canyon margins, suggesting lateral flow (Cronin and Kidd, 1998). This contrasts to the confinement of the coarse-grained facies, to the centre of the Cypriot canyon, which probably results from the morphology of the canyon floor. The Point

Lobos canyon has a flat base, allowing lateral flow, whereas the Khirokitia-Psematismenos canyon is probably v-shaped, focusing the coarse-grained facies towards the centre. Individual debrites within the Point Lobos canyon are thin and not laterally continuous, (Cronin and Kidd, 1998) akin the Khirokitia-Psematismenos debrites, but more extensive flows are also observed in the Point Lobos canyon which define the bases of five major fining-up sequences.

6.5.3 Evolution of the canyon fill

The canyon fill of the Khirokitia-Psematismenos is divided into six discrete fining-upwards packages (Figure 6.13). The base is defined by the introduction of coarse-grained conglomerates and breccias, which grade upward into finer-grained conglomerates and calcarenites and are each overlain by interbedded marl, chalk and calcarenites.

Walker (1992) reviews the relationship between relative sea-level and the development of submarine-fans. He suggests that during periods of relative sea-level fall and lowstand the fan experiences a phase of growth as coastal depocentres prograde and cause sediment instability near fan canyon head. During relative sea-level rise and periods of highstand the fan becomes abandoned and a condensed layer of hemipelagic sediments are blanketed over the previous lowstand's deposits. The Khirokitia-Psematismenos canyon fill can be interpreted in this way (Figure 6.13). The bulk of sedimentation, characterised by the debrite deposition in proximal areas is interpreted to have occurred during relative sea-level fall, when a larger area of the Troodos massif and cover sequence was exposed and acting as a sediment source. During relative sea-level rise, the reduced area of land mass available for erosion effectively resulted in the canyon becoming abandoned; allowing the background carbonate rain and other fine-grained material (terrigenous clays) to accumulate undiluted. The well-bedded fine- to medium-grained calcarenites that are also interbedded with the background marl sedimentation indicates that low density turbidites were occurring

periodically during sea-level rise/highstand. This then repeats in response to a further lowering of sea-level rejuvenating debrite sedimentation.

Cyclicity is also observed on other submarine canyon-fills. The Palaeocene-aged Point Lobos canyon-fill, California, has five cycles developed, each of which is subdivided into three separate units (Cronin and Kidd 1998). A coarse-grained conglomoratic unit that can be mapped over large distances marks the base of the sequence. This is overlain by thick channel-fill turbidite sandstones, interbedded with coarser-grained debrite deposits. The final phase of sedimentation is marked by the deposition of shale. This cycle represents the successive progradation of the canyon fill and has similar lithotypes as the Khirokitia-Psematismenos fan. The Khirokitia-Psematismenos fan does not have such large proximal-distal facies shifts (migration of facies) as the Point Lobos fan, because the grey siltstones and fine-grained sandstone facies is not repeated in vertical succession. The cyclicity is only produced by the repeated abandonment of the fan complex during relative sea-level rise.

The notion that highstand deposits within submarine fan environments consists of blankets of pelagic/hemipelagic sediments (Weimer, 1990; Kolla and Coumes, 1987) is based on study of mud-rich, elongate submarine fans like the Mississippi, Indus and Amazon (Ito 1998), all of which are developed on passive margins. This interpretation is similar to that proposed here for the Khirokitia-Psematismenos fan complex. However, Ito's (1998) study of a Plio-Pleistocene-aged submarine fan (lower Kazusa Group, Japan) deposited in a forearc setting revealed that there was an active supply of coarse-grained clastic sediments due to progradation of shallow marine depositional systems even during sea-level highstands. Ito's (1998) sequence stratigraphic interpretation of the lower Kazusa Group, is constrained by correlating fan sedimentation to near-shore sediments (which are more sensitive to sea-level change) with the use volcanic ash marker beds. His interpretation has coarse-grained sandstone-dominated beds marking lowstand deposition. His transgressive and highstand

sediments are however, stratigraphically thicker and are silt dominated. High sedimentation rates and well developed transgressive and highstand deposits are not observed in the Khirokitia-Psematismenos fan complex despite its active margin setting. This is probably due to the reduced area of landmass available for erosion during the transgressive and highstand times.

6.6 Biostratigraphy and its implications for sedimentary cyclicity in the Khirokitia-Psematismenos fan complex

Dating of the Khirokitia-Psematismenos fan complex is problematical for two reasons. Firstly, there is a lack of foraminiferas and age-diagnostic *Discoaster* species within these sediments, which was also noted by Houghton *et al.* (1990). Secondly, nannoplankton stratigraphy for the Pliocene-Pleistocene is mostly based on last occurrence datums (Bolli *et al.*, 1985) and the Khirokitia-Psematismenos sediments contain many reworked taxa from the Palaeogene and Neogene.

Houghton *et al.* (1990) dated the marls and siltstones immediately below Flow 2, east of Khirokitia Village (locality 10, Figure 6.2), and attributed the lack of Pliocene-Pleistocene *Discoaster* species and foraminiferas to an ecological-control (near-shore environment). Their study did find, however, the same nannoplankton (coccolith) assemblage at Khirokitia, as that of the Amathus Channel section further to the south (Figure 6.1). The Amathus section contains the age diagnostic *Discoaster* species *D. triradiatus* (NN17-NN18) suggesting a date of uppermost Pliocene-age (1.95-2.55 Ma). The Amathus Channel's lithostratigraphical position and its similar coccolith assemblage led Houghton *et al.* (1990) to say "the faunal and floral data just presented leaves little doubt that the channel deposits and fine-grained sediments below (*i.e.* at Khirokitia), are of upper most Pliocene-age".

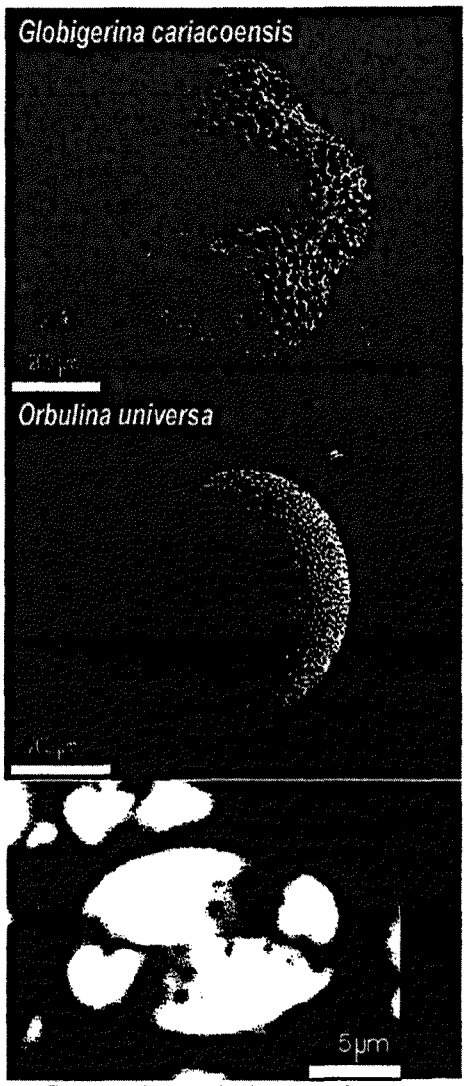

Figure 6.14. SEM pictures of *Globigerina cariacoensis* and *Orbulina universa.* XPL image of the late Pleistocene calcareous nannofossil *Pontosphaera indooceanica*

This study sampled the lateral equivalent of the grey siltstone and fine-grained sandstone facies at Vasiliko (Figure 6.13) and revealed a greater diversity of foraminifera, probably as a result of its more offshore depositional setting. The presence of *Orbulina universa* (Figure 6.14) in one sample indicates a maximum age of Lower Pliocene (PL1, 5.6 Ma), however, occurrences of *Globigerina cariacoensis* (Figure 6.14) which originated at the Pliocene-Pleistocene boundary suggests a minimum age of (PT1 1.77 Ma - lower Pleistocene)). The Vasiliko sediments are interpreted as the basinal equivalent of the Khirokitia-Psematismenos fan complex as Flows 1-6 grade into this distal facies. Distinguishing between the flows in this distal setting was not possible. Since the biostratigraphical sampling level could not be established at Vasiliko, the younger age of lower Pleistocene (compared with the upper Pliocene date provided by Houghton *et al.* (1990) is interpreted to result from sampling stratigraphically higher within this lateral equivalent deposit than the Houghton *et al.* study. The Houghton *et al.* (1990) date relates to the base of Flow 2, and the younger date gained from the sediments sampled at Vasiliko, in this study, suggests that the Vasiliko sample represent the distal equivalents of flows sratigraphically younger Flow 2.

A younger, of Late Pleistocene (NN20-NN21, 460 kyr to Recent), age constraint for the Khirokitia-Psematismenos fan complex is provided by the nannoplankton *Pontosphaera*

indooceanica (Figure 6.14), which was found in the chalky fine-grained matrix of Flow 6, at the top of the fan complex at location 3 (Figure 6.2). This suggests that the Flows 5 and 6 are contemporaneous with the Fanglomerate deposition, when dramatic uplift of the Troodos occurred centred on Mount Olympos.

Figure 6.15 shows the position of the stratigraphical tie points within the context of European sequence chronostratigraphy. In the 2.09 Ma timeframe suggested (Late Pliocene-Late Pleistocene) there are six sequences developed in European Basins (Hardenbol *et al.*, 1998), which within the resolution of biostratigraphy, can be correlated with the sequence boundaries defined at the bases of Flow 1 and Flow 6 in the Khirokitia-Psematismenos fan complex. It is likely that the sequence boundaries developed at the base of Flows 2-5 are correlatable to the remaining sequence boundaries proposed by Hardenbol *et al.* (1998). Unfortunately there is little biostratigraphic control on the Flow 2-5 to further substantiate this. Out of the 18 samples prepared for analysis only one (above) proved to have any age diagnostic fauna. The fact that there are the same number of cycles over this period of time in Cyprus and Europe is suggestive that even during times of intense tectonic activity the

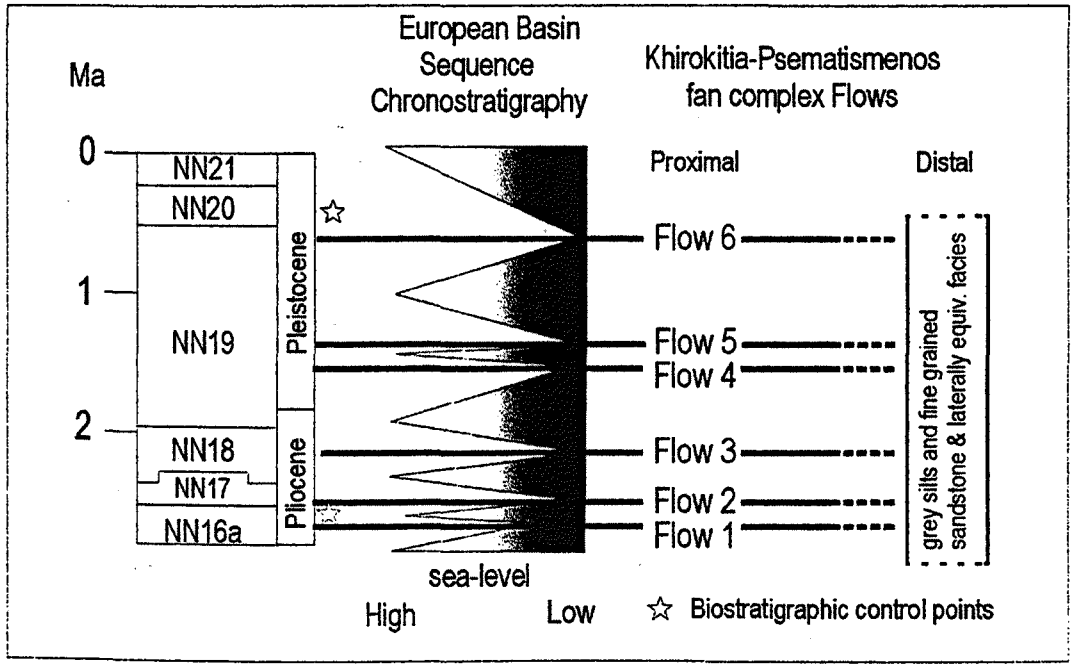

Figure 6.15. Biostratigraphy of the Khirokitia-Psematismenos fan complex in the context of European sequence chronostratigraphy. Chronostratigraphy redrawn from Hardenbol *et al.* (1998).

influence of global eustatic relative sea-level has a strong effect in defining the stacking geometry of marine sediments. In contrast, tectonics appears to provide a constant supply of sediment, define the style of sedimentation (i.e. shallow–deep marine), and some of the internal architecture, such as the amount of incision and source material.

6.7 Clast provenance of the Khirokitia-Psematismenos fan complex, and its relation to the uplift history of the Troodos Massif

The timing, erosion and subsequent incorporation of clasts into sedimentary rocks has important implications when revealing denudation and uplift rates of surrounding source areas. Geochemical analysis of Troodos derived clasts (Houghton *et al.*,1990) suggests that they originate from the Troodos ophiolite and not the Limassol Forest Transform Fault Zone. Figure 6.16 incorporates percentage based clast provenance data with biostratigraphy to infer the major phases of uplift of the Troodos massif. The general trend of clast provenance suggests a gradual increase in the amount of Troodos derived material from 10% in the Late Pliocene to 70% in the Late Pleistocene. Clasts derived from the sedimentary cover (mainly chalk and chert) display the opposite trend, from 85% in the Later Pliocene to 25% in the Pleistocene. This trend is interrupted during the deposition of Flow 4 (Lower Pleistocene) where Troodos derived clasts only constitute 10% of the debrite whereas 80% comprises chalk and 10% coralline material. The earliest evidence for the erosion of the Upper Miocene reefs (Koronia Formation) is in the Late Pliocene where is comprises 5% of the total clasts (Flow 2). Erosion of the Koronia Limestone reaches a 40% maximum during the deposition of Flow 3 in the latest Pliocene, but remains active as a sediment source until Flow 6 though at a much-reduced rate (5%). The volcanic sequence of the Troodos ophiolite was acting as a source from at least the Late Pliocene, as basalt and dolerite clasts are found in Flow1. Basalt and dolerite erosion continued to increase (especially from Flow 5) until it reached a maximum in Flow 6 (40%). The lowest occurrence of Gabbro and ultramafic

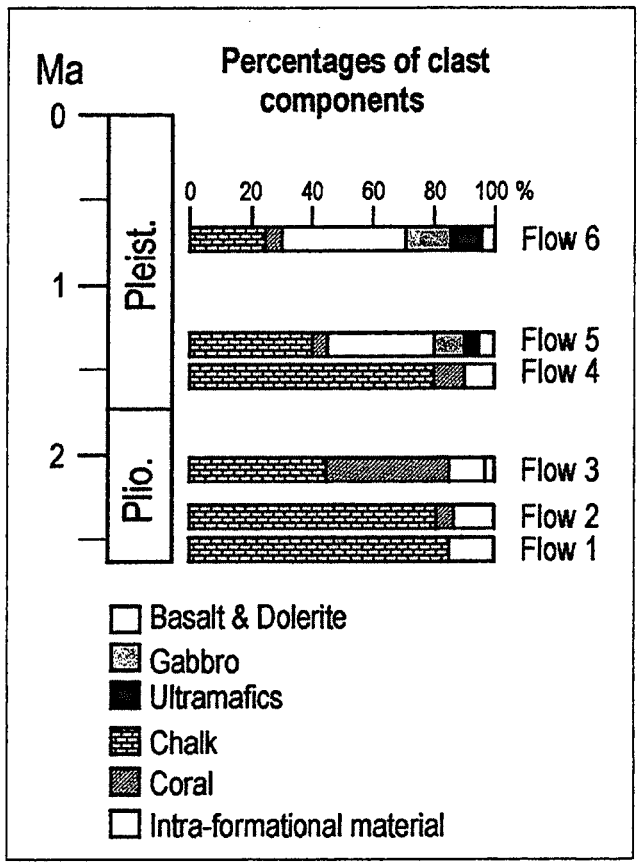

Figure 6.16. Clast provenance trends for Flows 1-6 in the Khirokitia-Psematismenos fan complex. Dates of Flows 2-4 assume correlation with the European sequence chronostratigraphy of Hardenbol *et al.* (1998)

clasts is in Flow 5 (10% and 5% respectively). These clasts increase in abundance in Flow 6 (15% and 10% respectively).

The data suggests a scenario of pulsed uplift during the Pliocene and Pleistocene. Figure 6.17 summarises the evolution of the Khirokitia-Psematismenos fan complex in the context of Troodos uplift in southern Cyprus.

The first pulse of accelerated uplift probably occurred before the initiation of fan sedimentation and was responsible for the development of Flow 1 during the mid-late Pliocene (Figure 6.17a). The extrusive volcanic sequence of the Troodos ophiolite, the Pakhna and Lefkara lithologies were all exposed and acting as a sediment source. Sustained uplift characterises the tectonic regime during the deposition of Flows 2, 3 and 4. Flow 2 saw the erosion of similar source lithologies as Flow 1 (Figure 6.17b), though the appearance of coral clasts suggests that the Koronia Limestone (locally developed within the Pakhna group) had recently become exposed to the north, probably as a result of scarp recession into the Troodos cover sediments. Flow 3 (latest Pliocene), which records the largest percentage of coral clasts records the extensive erosion of this locally exposed Koronia Formation (Figure 6.17c). Flow 4 (early Pleistocene) is characterised by a dominance of clasts of Lefkara and Pakhna lithologies (Figure 6.17d) which is interpreted as

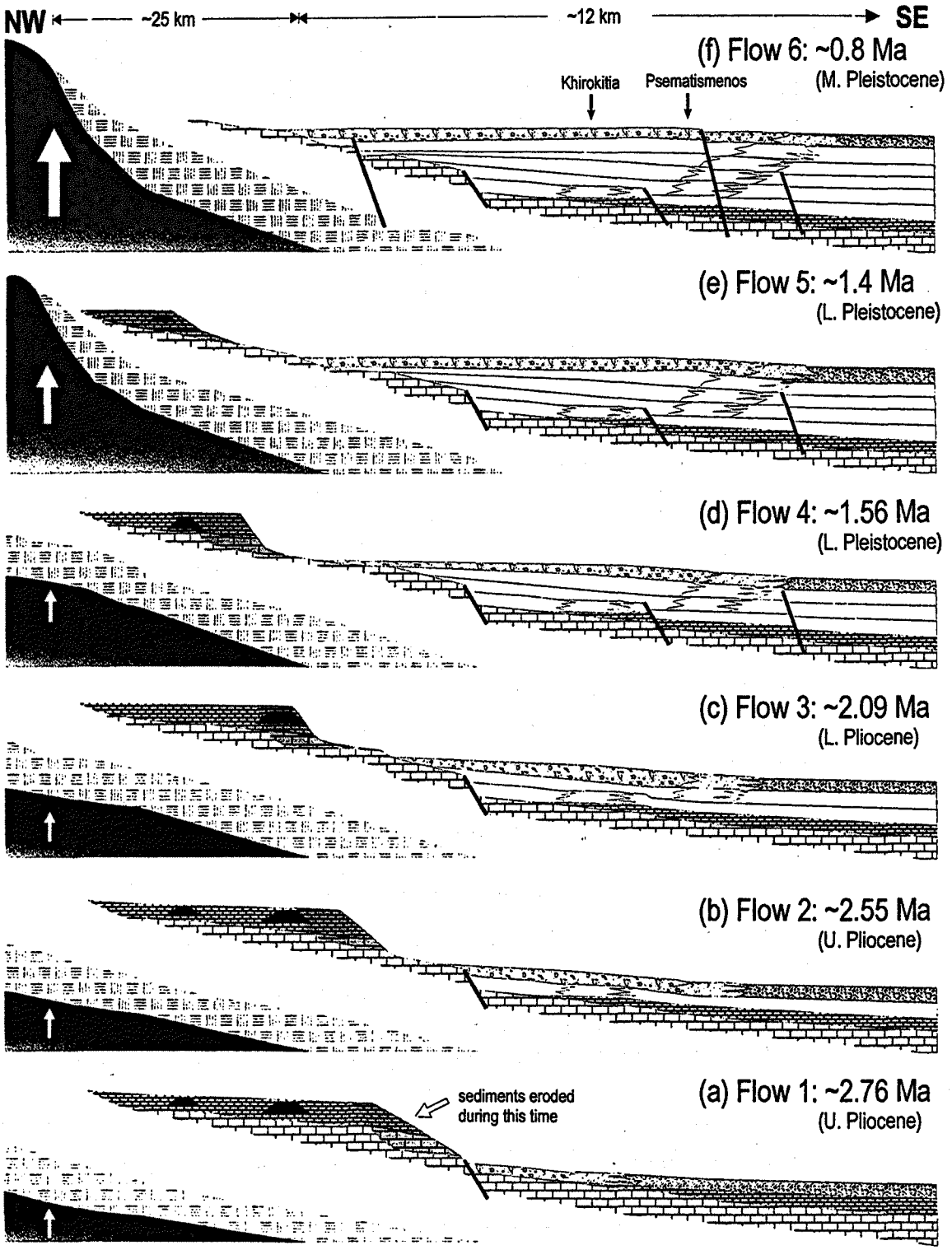

Figure 6.17. Six cartoons illustrating the development of the Khirokitia-Psematismenos fan-complex with the uplift of the Troodos Ophiolite. (a) faulting, fan initiation and the erosion of Lefkara, Pakhna and extrusive volcanic lithologies. (b) continued gradual uplift of the Troodos and further erosion of extrusive volcanics and circum-Troodos sediments. Koronia Limestone starts to become exposed. (c) Major erosion of the Koronia Limestone and continued erosion of the Lefkara, Pakhna and extrusive volcanics. (d) Faulting and continued erosion of extrusive volcanics and the Lefkara and Pakhna. (e) Major uplift exposes plutonic and ultramafics sequences. (f) Faulting and continued rapid uplift maintains supply of plutonic and ultramafic clasts; erosion removes Pakhna and Koronia lithologies from the proximal end of the fan.

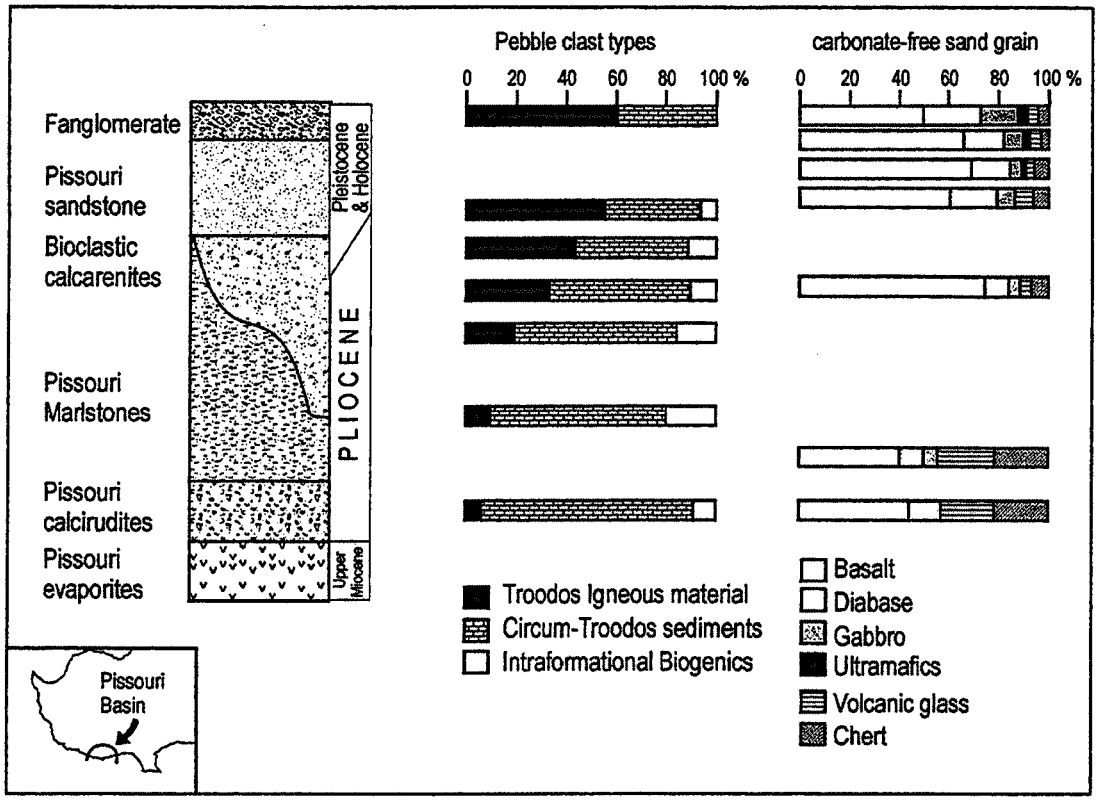

Figure 6.18. Lithostratigraphic units and clast provenance trends observed in the Pliocene-Pleistocene of the Pissouri Basin. Redrawn from Stow *et al.* (1995)

representing increased outcrop (and hence supply) of chalk due to the removal of the Koronia Limestone revealing further chalk lithologies.

The deposition of Flow 5 (lower Pleistocene) marks the initiation of another phase of highly accelerated uplift, as Troodos clasts triple in abundance and the ophiolite has its plutonic and mantle sequences exposed (Figure 6.17e). This period of uplift is maintained into the mid-late Pleistocene (Figure 6.17f), as Troodos derived clasts, as a whole, become more abundant, in Flow 6. Erosion of plutonic and mantle sequences probably doubled during this time as gabbros and ultramafics constitute nearly a half of the total incorporated Troodos clasts. Poole and Robertson (1991) identified an island-wide erosion surface and the development of large-scale alluvial fans, to the northern margin of the Troodos massif and inferred a phase of rapid uplift between 1.5-1 Ma. This period of uplift is though to be associated with the emplacement of a low-density serpentinite diaper under the summit region of Mount Olympus (Gass & Manson-Smith, 1964; Robertson 1977; Gass *et al.* 1994).

Poole and Robertson's (1991) 1.5-1 Ma date for uplift is identical to that suggested in this study (shown by the sudden increase of Troodos clasts and lithologies (Figure 6.16) which is dated by correlating with European sequence chronostratigraphy.

6.7.1 Pliocene-Pleistocene sedimentation in southwest Cyprus

Stow *et at.* (1995) investigated the Miocene to Recent sedimentological fill of the Pissouri Basin in south west Cyprus (Figure 6.13) and related it to the uplift of the Troodos ophiolite. They describe a Pliocene-Pleistocene fan-delta complex which was sub-divided into four lithostratigraphic units; Pissouri calcirudites, Pissouri marlstones, bioclastic calcarenites and the Pissouri sandstones (Figure 6.18). This succession is overlain by Holocene drift deposits and the Fanglomerates. Figure 6.18 illustrates the relationship between these lithostratigraphic units and the results of clast provenance studies that they established. The Pissouri marlstone is widespread, up to 120 m thick and shows and evolution from white micrites and marls at the base to brownish marls and terrigenous siltstones towards the top. Stow *et al.* (1995) interpreted this lithostratigraphic unit overall to represent a basinal section through the bottomset and foreset portion of a large fan delta prograding into the area from the north and west.

The bioclastic calcarenite unit, which is up to 110 m thick, is partly coeval and partly deeply incised into the Pissouri marlstone. It is composed of coarse-grained pebbly bioclastic sandstones and calcarenites. This lithofacies occurs in tongue-like bodies and are interpreted by Stow *et al.* (1995) to represent localised channelling and progradation of the fan complex into the underlying Pissouri marlstone unit. The Pissouri sandstone unit generally overlies, and is broadly conformable with the Pissouri marlstones and, more locally overlies the Bioclastic calcarenites (Stow *et al.* 1995). The facies is composed of sandstones and conglomerates and is interpreted to represent a well-supplied fan delta that rapidly prograded over the margin of the Pissouri Basin (Stow *et al.* 1995).

The provenance trends observed by Stow *et al.* (1995) are illustrated in Figure 6.18. They noted the following: (1) in pebble-grade clasts there is a decreasing trend of circum-Troodos sediment derived clasts, with a corresponding increase in Troodos igneous material. (2) They note the first occurrence of Troodos derived material to be within the Pissouri calcirudites (Early Pliocene) and Troodos derived clasts becoming more dominant within the Bioclastic calcarenites (Late Pliocene). (3) in carbonate-free sand grade material the most common lithic component was basalt and diabase, which occurred in all samples. (4) Gabbro clasts first occur in the upper Pissouri marls (Late Pliocene) and increase in number through the succession. (5) The ultramafic component is first noted at the base of the Pissouri sandstone unit and increases in frequency, into the Fanglomerates.

6.7.2 Comparisons of the Pissouri fan-delta with the Khirokitia-Psematismenos fan complex

The above lithofacies and provenance data of the Pliocene-Pleistocene Pissouri fan-delta complex obtained by Stow *et al.* (1995) has important similarities with the Khirokitia-Psematismenos fan complex, and further substantiates the depositional character of Pliocene-Pleistocene sedimentation along the southern margin of the Troodos massif during this period of tectonic uplift.

The Khirokitia-Psematismenos fan complex is generally coarser-grained than the Pissouri fan delta complex, which is interpreted to be partly due to its closer proximity to the Troodos massif and partly due to the basin geometry. The Pissouri Basin is interpreted as a line source (or series of point sources) during the Pliocene-Pleistocene (Stow *et al.* 1995), and is developed on a larger scale than the point-sourced, confined fill of the Khirokitia-Psematismenos fan complex. This confinement has the effect of concentrating sedimentation into the canyon where steep gradients provide high-energy, gravity driven flows that limit the

depositional potential of finer-grained material. The pattern of coarser-grained facies (Bioclastic calcarenites) incising a finer-grained facies (Pissouri marlstones) is mirrored in the Khirokitia-Psematismenos fan complex by the incision of the Flow 2 into the grey silt and fine-grained sandstone facies of Flow 1. There is no major change in the clast provenance between Flows 1 and 2, and a significant phase of uplift is not inferred to be associated with it, suggesting that the causal mechanism may be eustatic.

The Khirokitia-Psematismenos fan complex shares a similar provenance history as the Pissouri fan-delta complex, in that there is increasing evidence for the erosion of the Troodos ophiolite; and a reversed pattern of ophiolite stratigraphy is observed in both complexes as lithic fragments (compare Figures 6.17 & 6.19). The pre-serpentinisation Pliocene gradual uplift is marked by the increase in Troodos derived clasts in the Pissouri Basin, though gabbroic clasts from the plutonic sequence are evident during mid Pliocene. This discrepancy may arise due to the poor biostratigraphical constraints on the Pliocene-Pleistocene sediments in both the Pissouri Basin and at the Khirokitia-Psematismenos fan complex. The lower Pissouri marlstone (Figure 6.18) is the only biostratigraphical marker, in the Stow *et al.*, (1995) study and is dated to the PL1 zone (Lower Pliocene). Stow (pers. comm.) agrees that the age constraints on the gabbro bearing Pissouri marlstone is very poor and that it could potentially be deposited around the Pliocene-Pleistocene boundary. The occurrence of ultramafic clasts in the Pissouri Basin during the Lower Pleistocene is consistent with the Khirokitia-Psematismenos fan complex and the onset of serpentinisation.

6.8 Summary

The Pliocene-Pleistocene Khirokitia-Psematismenos fan complex has confined canyon morphology at is head, and grades into a semi-confined submarine fan over a distance of 4 km. The canyon fill is composed of six cycles, the bulk of which are characterised by coarse-grained conglomerates and breccias, representing periods of intense debrite activity. These

are separated by relatively condensed beds of fine- to medium-grained calcarenites and marls, representing low-density turbidites and the accumulation of background carbonate rain and fine-grained terrigenous material, during of relative debrite quiescence. The cycles have been interpreted in terms of relative sea-level, where periods of debrite activity occur during relative sea-level lowstands, and marls during relative sea-level highstands. Proximal to distal facies variation is rapid; Flow 1 grades from cobble grade conglomerates and breccias, through well-bedded calcarenites, to siltstones and fine-grained sandstones over 1 km. Successive flows also grade distally into siltstones and fine-grained sandstones over 4-6 km, but due to poorer exposure distinction between flows is not possible.

The succession of six cycles span an age of Lower Pliocene to mid-upper Pleistocene and can be correlated to sequences developed in European sequence chronostratigraphy.

Variation of clast lithologies in the different flows, plot the progressive unroofing of the Troodos ophiolite during the Pliocene, culminating in rapid, serpentinisation related, uplift during the early Pleistocene, which is marked by the erosion and deposition of ultramafic clasts. This date for rapid uplift is consistent with other, studies based on clast provenance studies (Stow *et al.* 1994) in the Pissouri Basin and erosional surfaces to the North of the Troodos (Poole and Robertson, 1991).

The possible correlation of sequence boundaries developed in the Khirokitia-Psematismenos fan complex, with those defined in European sequence chronostratigraphy, indicates that the mechanism responsible for the development of the fan complex's internal structure is most likely eustatic in origin, and that the timing of the flows is not controlled by the active tectonics of the time.

Chapter 7

Conclusions

7.1 Introduction

A major objective of this thesis has been to investigate the relative importance of tectonic and climatic controls on sedimentation. Chapters 2-5 concentrated on the deep marine sedimentation of the Miocene, and investigated the facies, biostratigraphy, cyclicity and stable isotopic records of the Pakhna Formation. Chapter 6 has investigated a Pliocene-Pleistocene-aged fan-complex deposited on the southern margin of the Troodos ophiolite. The discussion here reflects this division and summarises the tectonic and climatic controls on sedimentation firstly in the Miocene-aged Pakhna Formation and secondly, in the Plio-Pleistocene Khirokitia-Psematismenos fan complex. As both these depositional environments show a strong sedimentary cyclicity, the changing influence of these tectonic and climatic controls is discussed in the context of uplift of the Troodos ophiolite.

7.2 The Miocene Pakhna Formation: tectonic and climatic responses

This study divides the Pakhna Formation into four lithostratigraphical units; the Kottaphi Member; the Spitali Member, the Agrokipia Member, and the Koronia Member (Figure 7.1).

The Kottaphi Member is identified in all study sections and ranges from calcareous nannoplankton zone NN2 to NN9. It comprises deep water chalk and marl deposits, which are subdivided into four litho-facies, chalk, marly-chalk, cemented-marl and marl, defined on increasing clay content. These facies are stacked into couplets with a marl-rich base and chalk-rich top. They are interpreted to form due to fluctuations in runoff that supplies terrigenous material to basinal areas. The degree to which the background carbonate rain, of nannoplankton and foraminifera, is diluted by terrigenous material dictates the facies

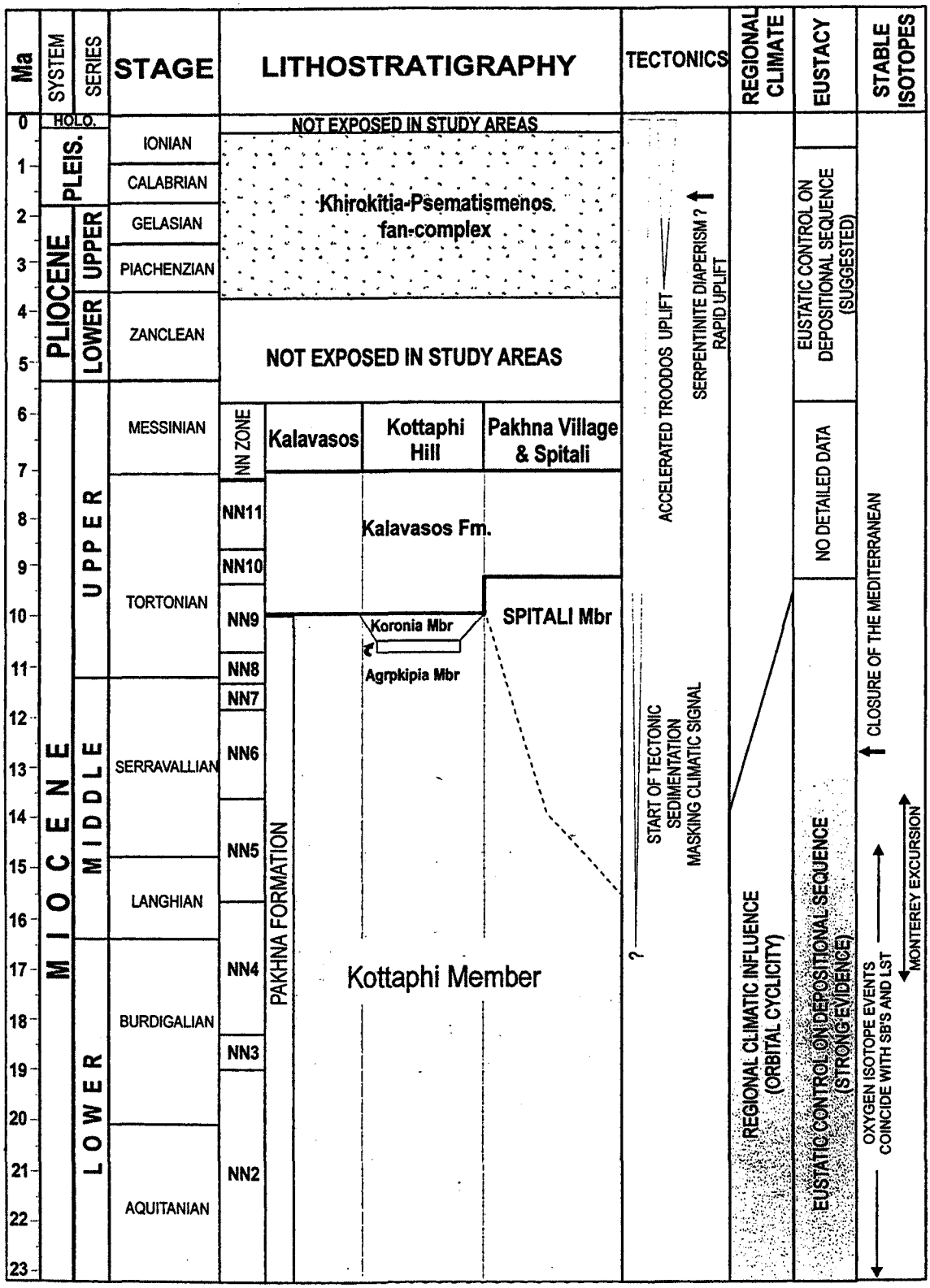

Figure 7.1 Summary of the climatic and tectonic controls on sedimentation on the Miocene - Pleistocene sedimentary cover succession of the Troodos ophiolite, Cyprus. Both regional climate and eustatic sea-level influence deposition of the Pakhna Formation. Tectonics are restricted to supplying periodic allochthonous beds. Accelerated uplift of the Troodos ophiolite during the Pliocene partly masks the climatic signal where eustatic sea-level in interpreted to control depositional sequences.

deposited. Typically foraminiferal chalks have <5 wt.% clay and marls have 25-30 wt.% clay. This interpretation is supported by stable isotopic and stratigraphic time series data. Isotopically lighter $\delta^{18}O$ values in marl-rich beds support dilution by a meteorically derived runoff source. Heavier $\delta^{13}C$ values in the marl-rich beds suggest that runoff supplied not only terrigenous material, but nutrients, derived from surrounding landmasses. Stratigraphic time series analysis of bed thickness and lithology data reveal three scales of regular cyclicity in the Kottaphi Member, that are interpreted to provide a mechanism for varying runoff. The three cycles have a wavelength ratios that match the periodicity of three Milankovitch orbital parameters, precessional, obliquity and eccentricity. The ~21kyr precessional and ~41 kyr obliquity cycles are developed at a marl-chalk couplet scale (15-100 cm) and are interpreted to represent variations in regional climate. The precessional cycle alters the path of the Monsoon (Valdes and Glover, 1999), and causes mid-latitude regions to vary between humid and dryer arid climates. The obliquity cycle controls the magnitude of seasonality (Weedon, 1991), where periods of colder winters are interpreted to provide greater annual precipitation. As the obliquity and precessional cycles operate synchronously, they both provide suitable mechanisms for controlling runoff and therefore carbonate rain dilution in basinal areas. The eccentricity cycle alters the influence of the precessional cycle with a periodicity of ~100 kyr in the Kottaphi Member. It therefore does not have a direct influence on climate itself, but influences the degree in which the precessional cycles affects climate, and hence carbonate rain dilution.

The marl-rich Agrokipia Member is poorly exposed and is interpreted to represent sedimentation in shallower marine conditions due to the increase input of terrigenously derived clay. It is absent south of the Troodos and is only found at Kottaphi Hill. It is dated to lie within NN9. The reef debris of the Koronia Member further reinforce the trend of marine shallowing in to the upper Miocene. The base of the Koronia Member (only observed Kottaphi Hill in this study) is also dated to NN9.

The Spitali Member is partially equivalent to the Kottaphi Member and ranges from NN6-NN9 (13.6-10.7 Ma) and is exposed at Pakhna Village and the Spitali Road Cut locations (Figure 7.1). It comprises allochthonous units that are divided into silty-mudstone, calcarenite or debrite facies depending on their gransize. They are interpreted to represent periodic flows of various severity interrupting the background chalk and marl sedimentation. The allochthonous units contain basic igneous material that is sourced from the Troodos Ophiolite. The onset of increased allochthonous derived material defines the base of the Spitali Member, and has a highly gradational contact with the chalk and marl of the Kottaphi Member. Allochthonous units are interbedded with chalk and marl couplets and become increasingly more abundant within the Spitali Member.

7.3 Cyclicity in the Kottaphi Member

The stacking patterns and composition (marl-rich verses chalk-rich) of couplets varies throughout the Kottaphi Member. These patterns have been interpreted using sequence stratigraphic nomenclature to reveal at least nine depositional sequences spanning from the Lower to Upper Miocene. Lowstand systems tracts are characterised by marl-rich couplets. The transgressive surface is marked by the first prominent foraminiferal chalk and by the change to couplets with approximately equal thickness chalk and marl, typical of the transgressive systems tract. The maximum flooding surface separates approximately equal thickness chalk and marl couplets, of the TST, from chalk dominated couplets of the highstand systems tract. Sequence boundaries are expressed as either a hardground or firmground or cessation of typical chalk dominated HST deposits in favour of marl-rich couplets which mark the LST. Within the constraints of biostratigraphy the sequence boundaries developed correlate across Cyprus, and to sequences defined by European sequence chronostratigraphy and developed at the New Jersey Margin, which suggests that sequence development in the Pakhna Formation was a result of at least regional relative sea-level change. A climatic control on depositional sequence development is indicated by the

$\delta^{18}O$ records of the Kottaphi Member. The major Miocene stable oxygen isotope events MBi-1 to MSi-3 (Miller *et al.*, 1991; Wright and Miller, 1992; Abreu and Haddad, 1998) are recognised in the deepwater facies of the Kottaphi Member. These positive $\delta^{18}O$ events relate to periods of global cooling and/or the build up of continental ice, both of which are accompanied by a eustatic sea-level fall. The presence of these $\delta^{18}O$ maxima at sequence boundaries and lowstand deposits in the Kottaphi Member (at Kottaphi Hill), show sea-level falls in Cyprus were synchronous with eustatic sea-level falls. This means that the sequence scale cyclicity on Cyprus is not controlled by local or regional tectonics.

The Pakhna Formation as a whole does show some evidence for local sediment supply being controlled by tectonics. At the Pakhna Village and Spitali Road Cut locations the sequence stratigraphic interpretation is hampered by the introduction of large amounts of allochthonous calcarenite and calcrudite units in the upper part of the Spitali Member. These units are interpreted to be mainly deriven from tectonic activity as they are not preferentially deposited in any particular systems tract. Removing them from the graphic logs helps to elucidate the sequence stratigraphical model defined by the pelagic chalk and marl couplets. These allochthonous units are also interpreted to have partially removed pelagic carbonate units.

In summary, the couplet cyclicity in the deepwater facies of the Pakhna Formation appears to be controlled by changes in regional climate that alter the amount of terrigenous runoff, and thus, the degree of dilution of carbonate rain in basinal areas. The larger scale depositional sequences are interpreted to be controlled by at least regional if not eustatic sea-level variations, that in turn, governs the overall supply of terrigenous material by altering the amount of river incision and runoff. A subordinate tectonic control, related to the uplift of the Troodos ophiolite, is expressed as allochthonous event beds that interrupt the background sedimentation.

7.4 Isotopic records of the Kottaphi Member

The $\delta^{18}O$ and $\delta^{13}C$ records of the Kottaphi Member show synchroneity previously identified isotope events. The $\delta^{13}C$ record builds on the research of Jacobs *et al,*. (1996) by confirming the identification of the positive carbon Monterey Excursion and extending its recognition to the eastern Mediterranean. This study benefits from a higher resolution $\delta^{13}C$ record and identifies the $\delta^{13}C$ maxima established by Woodruff and Savin, (1991) for the Monterey Excursion.

The $\delta^{18}O$ record of the Kottaphi Member is consistent with a positive $\delta^{18}O$ Mediterranean trend identified by Jacobs *et al.* (1969) from ~13 Ma. Jacobs *et al.* (1996) interpreted this tend to relate to the closure of the Mediterranean at ~14 Ma, where an increasing influx of fresh water and temperature decreased $\delta^{18}O$. That the change is so early in the Miocene is somewhat surprising as there is no sedimentological expression of the Mediterranean closure in the deep water deposits of the Pakhna Formation other than increased evidence for marine shallowing, that culminates in the overlying reefs of the Koronia Member and evaporites of the Kalavasos Formation.

7.5 Plio-Pleistocene submarine fan sedimentation: tectonic and climatic responses

The Pliocene-Pleistocene Khirokitia-Psematismenos fan complex, on the southern margin of the Troodos, has confined canyon morphology at is head, and grades into a semi-confined submarine fan over a distance of 4 km. The canyon fill is composed of six cycles, the bulk of which are characterised by coarse-grained conglomerates and breccias, representing periods of intense debrite activity. These are separated by relatively condensed beds of fine- to medium-grained calcarenites and marls, representing low-density turbidites and the accumulation of background carbonate rain and fine-grained terrigenous material, during of relative debrite quiescence. The cycles are interpreted in terms of relative sea-level, where

periods of debrite activity occur during relative sea-level lowstands, and marls during relative sea-level highstands. The succession of six cycles span an age of Lower Pliocene to mid-upper Pleistocene and can be correlated to sequences developed in European sequence chronostratigraphy.

Variation of clast lithologies in the different flows, plot the progressive unroofing of the Troodos ophiolite during the Pliocene, culminating in rapid, serpentinisation related, uplift during the early Pleistocene, which is marked by the erosion and deposition of ultramafic clasts. This date for rapid uplift is consistent with other studies based on clast provenance studies (Stow *et al.* 1994) in the Pissouri Basin and erosional surfaces to the north of the Troodos ophiolite (Poole and Robertson, 1991).

The possible correlation of sequence boundaries developed in the Khirokitia-Psematismenos fan complex, with those defined in European sequence chronostratigraphy, indicates that the mechanism responsible for the development of the fan complex's internal structure is most likely regional in origin, and that although the tectonic uplift is responsible for the overall sediment supply the *timing* of the flows is not controlled by the active tectonic.

7.6 Sedimentary style: the uplift of the Troodos ophiolite verses climate change.

Climate dominantly controls sedimentation during the Miocene of Cyprus. Tectonic activity was responsible for providing an uplifted source area, and acted as triggering mechanism for allochthonous sedimentation. The deepwater facies of the Pakhna Formation are sensitive to <100 kyr, regional climate changes, and longer term, ~1-2 myr, global climate changes, that control eustatic sea-level. The Khirokitia-Psematismenos fan complex is less sensitive to short-term climate changes. Here, large scale sedimentary cyclicity is marked by periods of coarse-grained debrites separated by periods of dominantly pelagic sedimentation. These

cycles are interpreted to be controlled by at lest regional relative sea-level changes of <1myr, where eustatic sea-level falls increase the potential for allochthonous deposition by lowering base level and increasing the subaerial exposure of the Troodos ophiolite. Eustatic sea-level rises are interpreted to sufficiently shift coarse-grained, proximal fan-facies land-ward, in the Khirokitia-Psematismenos fan complex to allow "Kottaphi Member-like" pelagic sedimentation to dominate during highstand deposition. The regional (<100 kyr) climate changes are not apparent in the fan-complex, due to a shift from dominantly pelagic sedimentation in the Pakhna Formation to dominantly allochthonous sedimentation in the fan complex, which does not have a genetically linked mechanism to alter due to humid-arid climate variation. Syn-sedimentary faulting, and the high abundance of clasts, derived from successively deeper levels of ophiolite stratigraphy testify to a period of near tectonic activity associated with the uplift of the Troodos ophiolite Pliocene (Figure 7.1), which climaxed with rapid uplift associated with serpentinite diaperism in the early Pleistocene. It is suggested that the influence of climate on sedimentation is increasingly masked by tectonic activity which is initially evidenced by the gradual introduction of allochthonous units in the Spitali Member and culminates in a near tectonic overprint in the Khirokitia-Psematismenos fan-complex.

7.7 Future work

- This project provides some answers to relative importance of climate and tectonics during the Miocene to Pleistocene evolution of the sedimentary cover of the Troodos ophiolite. A greater understanding of these influences, in Cyprus, could be gauged by Increasing the resolution of stable isotope data at Kottaphi Hill and extending the record at Kalavasos will increase the definition of the stable oxygen and carbon isotope events, and their relation to the sedimentary record. It would also allow the relationship between

$\delta^{18}O$, $\delta^{13}C$, and sea-level to be tested during the to Monterey Excursion and associated global cooling.

References

Abell, P. I. & Plug, I. (2000) The Pleistocene/Holocene transition in South Africa: evidence for the Younger Dryas event. *Global and Planetary Change*, **26**(1-3), 173-179.

Abreu, V. S. & Anderson, J. B. (1998) Glacial eustacy during the Cenozoic: sequence stratigraphic implications. *AAPG Bulletin*, **82**(7), 1385-1400.

Abreu, V. S. & Haddad, G. A. (1998) Glacioeustatic fluctuations: the mechanism linking stable isotope events and sequence stratigraphy from the early Oligocene to the middle Miocene. In: *Mesozoic and Cenozoic Sequence Stratigraphy of European Basins, Vol. 60* (Ed. by P.-C. De Graciansky, J. Hardenbol, T. Jacquin and P. R. Vail), pp. 246-259. SEPM Special Publication.

Abreu, V. S., Hardenbol, J., Haddad, G. A., Baum, G. R., Droxler, A. W. & Vail, P. R. (1998) Oxygen isotope synthesis: a Cretaceous ice-house? In: *Mesozoic and Cenozoic Sequence Stratigraphy of European Basins, Vol. 60* (Ed. by P.-C. De Graciansky, J. Hardenbol, T. Jacquin and P. R. Vail), pp. 75-80. Mesozoic and Cenozoic Sequence Stratigraphy of European Basins.

Alley, R. B. (2000) The Younger Dryas cold interval as viewed from central Greenland. *Quaternary Science Reviews, Volume*, **19**(1-5), 213-226.

Antunes, M. T., Civis, J., Gonzalez-Delgado, J. A., Legoinha, P., Nascimento, A. & Pais, J. (1997) Miocene stable isotopes ($\delta^{13}C$, $\delta^{18}O$), biostratigraphy and environments in the southern limb of the Albufeira syncline (Setubal Peninsula, Portugal). *Geogaceta*, **21**, 21-24.

Avery, E. (1997) Relationship between Pliocene marine invertebrate palaeocomunities and water depth in the Nicosia Formation, Cyprus. In: *Tenth Keck Research Symposium in Geology Proceedings*, pp. 81-88, The College of Wooster, Ohio.

Backman, J. & Raffi, I. (1997) Calibration of Miocene nannofossil events to orbitally tuned cyclostratgraphies from ceara rise. In: *Proceedings of the Ocean Drilling Program, Scientific Results* (Ed. by N. J. Shackleton, W. B. Curry, C. Richter and T. J. Bralower).

Bagnall, P. S. (1960) The Geology and Mineral Resources of the Pano Lefkara-Larnaca Area. *Geological Survey Department Cyprus*, Memoir No. **5**, 116.

Barron, J. A. (1986) Paleoceanographic and tectonic controls on deposition of the Monterey Formation and related siliceous rocks in California. *Palaeogeography, Palaeoclimatology, Palaeoecology*, **53**, 27-45.

Bear, L. M. (1960) The Geology and Mineral Resources of the Akaki-Lythrodondha Area. *Geological Survey Department Cyprus*, Memoir No. 3, 122.

Ben-Avraham, Z., Shoham, Y. & Ginzburg, A. (1976) Magnetic anomalies in the eastern Mediterranean and the tectonic settin of the Eratosthenes Seamount. *Geophys. J. R. Astron. Soc.*, **45**, 105-123.

Berger, A. (1984) Astronomical theory of paleoclimates; insolation signatures for the last glacial cycle and accuracy of long-term variations over the Quaternary. *Professional Paper - Ministere des Affaires Economiques. Administration des Mines. Service Geologique de Belgique*, **207**, 19-22.

Berger, A., Loutre, M. F. & Tricot, C. (1993) Insolation of the Earth orbital periods. *Journal of Geophysical Research*, **98**, 10341-10362.

Berger, A. & Pestiaux, P. (1984) Accuracy and stability of the Quaternary terrestrial insolation. In: *Milankovitch and climate* (Ed. by A. Berger, J. Imbrie, G. Hays, G. Kukla and B. Saltzman), pp. 83-111. D Reidel, Dordrecht, The Netherlands.

Berggren, W. A., Kent, D. V. & Flynn, J. J. (1985) Neogene goechronology and chronostratigraphy. In: *The Chronology of the Geological Record, Vol. 10* (Ed. by N. J. Snelling), pp. 211-260. Memoir of the Geological Society of London.

Berggren, W. A., Kent, D. V., Swisher, C. C. & Aubry, M. P. (1995) Cenozoic geochronology and chronostratigraphy. In: *Geochronology, Time Scales and Global Stratigraphic Correlations: A Unified Temporal Framework for an Historical Geology, Vol. 54* (Ed. by W. A. Berggren, D. V. Kent and J. Hardenbol). Society of Economic Palaeontologists and Mineralogists Special.

Bolli, H. M., Saunders, J. B. & Perch-Nielson, K. (1985) *Plankton Stratigraphy*. Cambridge University Press, 572 pp.

Bramlette, M., N. (1954) Stratigraphic value of discoasters and some other microfossils related to Recent coccolithophores. *Journal of Palaeontology*, **28**(4), 385-403.

Bramlette, M. N. & Sullivan, F. R. (1961a) Coccilithophorids and related nannoplankton of the early Tertiary in California. *Micropaleontology*, **7**, 129-188.

Bramlette, M. N. & Sullivan, F. R. (1961b) Coccilithophorids and related nannoplankton of the early Tertiary in California. *Micropaleontology*, **7**(2), 129-188.

Bramlette, M. N. & Wilcoxon, J. A. (1967) Middle Tertiary calcareous nannoplankton of the Cipero section. *Tulane Studies in Geology*, **5**(3), 93-131.

Brasier, M. D. (1980) *Microfossils*. George Allen & Unwin, London, 193 pp.

Brass, G. W., Sotham, J. R. & Peterson, W. H. (1982) Warm saline bottom water in the ancient ocean. *Nature*, **296**, 620-623.

Bukry, D. (1973) Low-latitude coccolith biostratigraphical zonation. *Initial Reports of the Deep Sea Drilling Project*, **15**, 685-703.

Bukry, D. (1975) Coccolith and silicoflagilate stratigraphy, northwestern Pacific Ocean. *Initial Reports of the Deep Sea Drilling Project*, **32**, 677-701.

Bullard, E. L., Everett, J. E. & Smith, A. G. (1965) The fit of the continents around the Atlantic. *Philosophical transactions of the Royal Society of London*, **A-258**, 41-51.

Carlson, R. W. & Hart, W. K. (1998) Flood basalt volcanism in the northwestern United States. In: *Continental Flood Basalts* (Ed. by J. D. Macdougall), pp. 65-61. Kluwer Academic, Norwell.

Clemens, S. C. (1999) An astronomical tuning strategy for Pliocene sections: implications for global-scale correlation and phase relationships. *Philosophical Transactions of the Roylal Society of London*, **357**(1757), 1949-1973.

Clube, T. M. M. & Robertson, A. H. F. (1986) The palaeorotation of the Troodos microplate Cyprus, in the late Mesozoic-early Cenozoic plate tectonic framework of the eastern Mediterranean. *Surveys in Geophysics*, **8**, 357-437.

Corfield, R. M. (1995) An introduction to the techniques, limitations and landmarks of carbonate oxygen isotope palaeothermometry. In: *Marine Palaeoenvironmental Analysis from Fossils, Vol. 83* (Ed. by D. W. J. Bosence and P. A. Allison), pp. 27-42. Geological Society Special Publication.

Corfield, R. M. & Cartlidge, J. E. (1993) Oxygen and Carbon Isotope stratigraphy of the middle Miocene, Holes 805B and 806B. *Proceedings of the Ocean Drilling Program, Scientific Results*, **130**, 307-313.

Craig, H. (1953) The geochemistry of the stable isotopes of carbon. *Geochemical at Cosmochimica Acta*, **3**, 53-72.

Cronin, B. T. & Kidd, R. B. (1998) Heterogeneity and lithotype distribution in ancient deep-sea canyons: Point Lobos deep-sea canyon as a reservoir analogue. *Sedimentary Geology*, **115**, 315-349.

Crowley, T. J. & North, G. R. (1991) *Palaeoclimatology*. Oxford University Press.

Cushman, J. A. & Jarvis, P. W. (1936) Three new foraminifera from the Miocene Bowden Marl, of Jamaca. *Contrib. Cushman Lab. foramin. Res.*, **12**, 3-5.

Dansgaard, W. & Henrik, T. (1969) Glacier oxygen-18 content and Pleistocene ocean temperatures. *Science*, **3904**, 499-502.

Diester-Hass, L. (1991) Rhythmic carbonate content variations in Neogene sediment above the oceanic lysocline. In: *Cycles and Events in Stratigraphy* (Ed. by E. e. al.), pp. 94-109. Springer-Verlag, Berlin Heidelberg.

Dilek, Y., Thy, P., Moores, E. M. & Ramsden, T. W. (1990) Tectonic evolution of the Troodos Ophiolite within the Tethyan framework. *tectonics*, **9**(4), 811-823.

Donovan, D. T. & Jones, E. J. W. (1979) Causes of world-wide changes is sea-level. *Journal of Geological Society*, **136**, 187-192.

Eaton, S. & Robertson, A. H. F. (1993) The Miocene Pakhna Formation, southern Cyprus and its relation to the Neogene tectonic evolution of the Eastern Mediterranean. *Sedimentary Geology*, **86**, 273-296.

Eicher, D. L. & Diner, R. (1991) Environmental factors controlling Cretaceous limestone-marlstone Rhythms. In: *Cycles and Events in Stratigraphy* (Ed. by E. *et. al.*), pp. 79-93. Springer-Verlag, Berlin Heidelberg.

Einsele, G. & Ricken, W. (1991) Limestone-marl alternation - an overview. In: *Cycles and Events in Stratigraphy* (Ed. by E. e. al.), pp. 23-47. Springer-Varlag, Berlin Heidelberg.

Einsele, G., Ricken, W. & Seilacher, A. (1991) Cycles and Events in Stratigraphy - Basic concepts and terms. In: *Cycles and Events in Stratigraphy* (Ed. by E. e. al.), pp. 1-19. Springer-Verlag, Berlin Heidelberg.

Emiliani, C. (1955) Pleistocene temperatures. *Journal of Geology*, **66**, 538-578.

Farrell, S. G. & Eaton, S. (1988) Foliations developed during slump deformation of Miocene sediments, Cyprus. *Journal of Structural Geology*, **10**(6), 567-576.

Faure, G. (1986) *Principles of Isotope Geology*. John Wiley and Sons, 589 pp.

Fischer, A. G. (1991) Orbital Cyclicity in Mesozoic Strata. In: *Cycles and Events in Stratigraphy* (Ed. by E. *et. al.*), pp. 49-62. Springer-Verlag, Berlin Heidlberg.

Fischer, A. G. (1993) Cyclostratigraphy of Cretaceous Chalk-Marl Sequences. In: *Evolution of the Western Interior Basin, Vol. 39* (Ed. by W. G. E. Caldwell and E. G. Kauffman), pp. 283-295. Geological Association of Canada, Special Paper.

Fisher, A. G. (1991) Orbital cyclicity in Mesozoic strata. In: *Cycles and Events in Stratigraphy* (Ed. by E. e. al.). Springer-Verlag, Berlin Heidelberg.

Flower, B. (1995) Middle Miocene deepwater palaeoceanography in the southwest Pacific: relations with East Antarctic Ices Sheet development. *Palaeoceanography*, **10**(6), 1095-1112.

Flower, B. P. & Kennet, J. P. (1993a) Middle Miocene ocean-climate transition: high-resolution oxygen and carbon isotopic records from Deep Sea Drilling project site 588A, southwest Pacific. *Palaeoceanography*, **8**(6), 811-843.

Flower, B. P. & Kennett, J. P. (1993b) Relations between Monterey Formation deposition and middle Miocene global cooling: Napels Beach section, California. *Geology*, **21**, 887-880.

Flower, B. P. & Kennett, J. P. (1994a) The middle Miocene climatic transition: East Antarctic ice sheet development, deep ocean circulation and global carbon cycling. *Palaeogeography, Palaeoclimatology, Palaeoecology*, **108**, 537-555.

Flower, B. P. & Kennett, J. P. (1994b) Oxygen and carbon isotopic stratigraphy of the Monterey Formation at Naples Beach, California. In: *Field Guide to the Monterey formation Between Santa Barbra and Gaviota, California, Vol. GB72* (Ed. by J. S. Hornafius), pp. 59-66. AAPG.

Follows, E. J. (1990) Sedimentology and tectonic setting of Miocene reef and related sediments in Cyprus, University of Edinburgh.

Follows, E. J. (1992) Patterns of reef sedimentation and diagenesis in the Miocene of Cyprus. *Sedimentary Geology*, **79**, 225-253.

Frakes, L. A., Francis, J. E. & Syktus, J. L. (1992) *Climate Modes of the Phanerozoic.* Cambridge University Press.

Gale, A. S. (1996) Turonian correlation and sequence stratigraphy of the Chalk in southern England. In: *Sequence Stratigraphy in British Geology, Vol. 103* (Ed. by S. P. Hesslebo and D. N. Parkinson), pp. 177-195. Geological Society Special Publication.

Gass, I. (1960) The geology and mineral resources of the Dhali area. *Geological Survey Department Cyprus*, Memoir No. **4**, 116.

Gass, I. G. & Manson-Smith, D. (1963) The geology and gravity anomalies of the Troodos massif, Cyprus. *Philosophical Transaction of the Royal Society of London*, **A255**, 417-467.

Gass, I. G. (1968) Is the Troodos Massif of Cyprus a Fragment of Mesozoic Ocean Floor? *Nature*, **220**, 39-42.

Gass, I. G., MacLeod, C. J., Murton, B. J., Panayiotou, A., Simonian, K. O. & Xenophontos, C. (1994) *The geology of the Southern Troodos Transform Fault Zone*, 218 pp.

Gilbert, G. R. (1895) Sedimentary measurement of geologic time. *Journal of Geology*, **3**, 121-127.

Givens, L. E. (1997) Substrate controls in the development of the Molluscan communities of the Nicosia Formation (Pliocene) of Central Cyprus. In: *Tenth Keck Research Symposium in Geology Proceedings*, pp. 89-92, College of Wooster, Ohio.

Gold, L W. Shneider, S H. and Macqueen A D. (eds) *Annals of Glaciology, Vol. 5*, pp. 203. International Glaciological Society, Cambridge,.

Gorden, A. L. (1975) general oceanic circulation. In: *Numerical Models of Oceanic Circulation, Vol. 39-53*. National Academic Science, Washington D.C.

Grant, S. (1998) Sequence stratigraphy of a pelagic chalk succession: the Coniacian - Lower Campanian of the Anglo-Paris Basin, University of Durham.

Grant, S. F., Coe, A. L. & Armstrong, H. A. (1999) Sequence stratigraphy of the Coniacian succession of the Anglo-Paris basin. *Geological Magazine*, **136**(1), 17-38.

Hallam, A. (1963) Major epirogenic and eustatic changes since the Cretaceous and their possible relationship to crustal structure. *American Journal of Science*, **261**, 164-177.

Handford, C. R. & Loucks, R. G. (1993) Carbonate depositional sequences and systems tracts - responses of carbonate platforms to relative sea-level. In: *Carbonate sequence stratigraphy* (Ed. by R. G. Loucks and J. F. Sarg). American Association of Petroleum Geologists, Tulsa.

Haq, B. U., Hardenbol, J. & Vail, P. (1987) Chronology of fluctuating sea levels since the Triassic. *Science*, **235**, 1156-1167.

Haq, B. U., Hardenbol, J. & Vail, P. R. (1988) Mesozoic and Cenozoic chronostratigraphy and cycles of sea level change. In: *Sea level changes: an integrated approach, Vol. 42* (Ed. by C. K. e. a. Wigus), pp. 71-108. Society of Economic Palaeontologists and Mineralogists Special Publication.

Hardenbol, J., Thierry, J., Farley, M. B., Jacquin, T., De Graciansky, P.-C. & Vail, P. R. (1998) Mesozoic and Cenozoic Sequence Chronostratigraphic Framework of European Basins. In: *Mesozoic and Cenozoic Sequence Chronostratigraphy of European Basins, Vol. 60* (Ed. by P.-C. De Graciansky, J. Hardenbol, T. Jacquin and P. R. Vail). SEMP Special Publication.

Hay, W. W. & Mohler, H. P. (1967) Calcareous nannoplankton from early Tertiary rocks at Pont Labau, France, and Palaeocene-early Eocene correlations. *Journal of Palaeontology*, **41**(6), 1505-1541.

Hay, W. W., Mohler, H. P., Roth, P. H., Schmidt, R. R. & Boudreaux, J. E. (1967) Calcareous nannoplankton zonation of the Cenozoic of the Gulf Coast and Caribbean-Antillean area, and transoceanic correlation. In: *Symposium on the geological history of the Gulf of Mexico, Antillean-Caribbean region*

Henson, F. R. S., Browne, R. V. & McGinty, J. (1949) A synopsis of the stratigraphy and geological history of Cyprus. *Quarterly Journal of the Geological Society of London*, **105**(1-41).

Higgs, N. C., Thomson, J., Wilson, T. R. S. & Croudace, I. W. (1994) Modification and complete removal of eastern Mediterranean sapropels by post depositional oxidation. *Geology*, **22**, 426-426.

Hilgen, F. J., Krijgsman, W., Langeresis, C. G., Lourens, L. J., Santarelli, A. & Zachariasse, W. J. (1995) Extending the astronomical (polarity) time scale onto the Miocene. *Earth and Planetary Science Letters*, **136**, 495-510.

Hinnov, L. A. (2000) New perspectives on orbitally forced stratigraphy. *Annu. Rev. Earth Planet. Sci.*, **28**, 419-475.

Hodell, D. A. & Woodruff, F. (1994) Variations in the strontium isotopic ratio of seawater during the Miocene: Stratigraphic and geochemical implications. P*alaeoceanography*, **9**(3), 405-426.

Hooper, P. R. (1990) The timing of crustal extension and the eruption of continental flood basalts. *Nature*, **345**, 246-249.

Hornafius, J. S. (1991) Facies analysis of the Monterey Formation in the Northern Santa Barbara Channel. *AAPG Bulletin*, **75**(5), 894-909.

Hornibrook, N. D. B. (1992) New Zealand Cenozoic marine paleoclimates: a review based on the distribution of some shallow water and terrestrial biota. In: *Pacific Neogene Environments, Evolution and Events* (Ed. by R. Tsuchi and J. Ingle), pp. 83-106. University of Tokyo Press.

Houghton, S. D., Jenkins, D. G., Xenophontos, C. & Gass, I. G. (1990) Microfossil evidence for a latest Pliocene age for the Amathus and Khirokitia channel deposits, southern Cyprus and thereby the unroofing of the Troodos Massif. In: *Ophiolites; oceanic crustal analogues; proceedings of the symposium "Troodos 1987"* (Ed. by J. Malpas, E. M. Moores, A. Panayiotou and C. Xenophontos). Ministry of Agriculture and Natural Resources, Nicosia, Cyprus.

Hudson, J. D. & Anderson, T. F. (1989) Ocean temperatures and isotopic composition through time. *Transactions of the Royal Society of Edinburgh*, **80**, 183-192.

Imbrie, J. (1984) Proxy records of Quaternary climate. In: *Proceedings of the Symposium on ice and climate modelling*

Isaacs, C. M. (1998) In Press: Depositional Framework of the Monterey Formation, California. In: *The Monterey Formation: from Rocks to Molecules* (Ed. by C. M. Isaacs and J. Rullkotter). Columbia University Press.

Isaacs, C. M., Pisciotto, K. A. & Garrison, R. E. (1983) Facies and diagenesis of the Monterey Formation, California: a summary. In: *Developments in Sedimentology, Vol. 36* (Ed. by I. e. al.), pp. 247-282.

Ito, M. (1998) Submarine fan sequences of the lower Kazusa Group, a Plio-Pleistocene forarc fill in the Boso Peninsula, Japan. *Sedimentary Geology*, **122**, 69-93.

Itoigawa, J. & Yamanoi, T. (1990) Climatic optimum in the mid-Neogene of the Japanese Islands. In: *Pacific Neogene Events: Their Timing, Nature and Interrelationship* (Ed. by R. Tsuchi), pp. 3-14. University of Tokyo Press, Tokyo.

Jacobs, E., Weissert, H. & Shields, G. (1996) The Monterey event in the Mediterranean: A record from shelf sediments of Malta. *Palaoceanography*, **11**(6), 717-728.

Jacobs, S. S., Ardai, J. & Bruchhausen, P. (1978) Thermohaline stratification and the sea floor below the Ross Ice Shelf. *Eos, Transactions, American Geophysical Union*, **59**(4), 308.

Jafar, S. A. (1975) Calcareous nannoplankton from the Miocene of Rotti, Indonesia. *Verh. Kon. Ned. Akad. Wetensch. afd. Nat.*, **28**, 1-99.

Jenkyns, H. C., Gale, A. S. & Corfield, R. M. (1994) Carbon- and oxygen-isotope stratigraphy of the English Chalk and Italian Scaglia and its palaeoclimatic significance. *Geological Magazine*, **131**(1), 1-34.

Kahler, G. (1994) Stratigraphy and sedimentology of the Paleogene Lefkara Formation, Cyprus, University of Southampton.

Kahler, G. & Stow, D. A. V. (1998) Turbidites and contourites of the Palaeogene Lefkara Formation southern Cyprus. *Sedimentary Geology*, **115**, 215-231.

Keller, G. & Barron, J. A. (1983) Palaeoceanographic implications of the Miocene deep sea hiatuses. *Geological Society of America Bulletin*, **94**, 590-613.

Kempler, D. (1998) Eratosthenes Seamount; the possible spearhead of incipient continental collision in the eastern Mediterranean. In: *Proceedings of the Ocean Drilling Program, Scientific Results, Vol. 160* (Ed. by A. H. F. Robertson, K. C. Emeis, C. Richter and A. Camerlenghi), pp. 709-721.

Kendal, J. (1992) Carbonate and evaporite models. In: *Facies Models, Response to Seal Level Change* (Ed. by R. G. Walker and N. P. James), pp. 265-275. Geological Association of Canada.

Kennedy, W. J. & Garrison, R. E. (1975) Morphology and genesis of nodular chalks and hardgrounds in the upper Cretaceous of southern England. *Sedimentology*, **22**, 311-386.

Kennet, J. P. (1995) A Review of Polar Climatic Evolution during the Neogene, Based on the Marine Sediment Record. In: *Palaeoclimate and Evolution With Emphasis on Human Origins.* (Ed. by E. D. Vrbs, G. Partridge, T. Burckle, L.), pp. 49-64. Yale University Press.

Kennet, J. P. & Barker, P. F. (1990) Latest Cretaceous to Cenozoic climate and oceanographic developments in the Weddell Sea, Antarctic: an ocean drilling perspective. In: *Proceedings of the Ocean Drilling Program, Scientific Results, Vol. 113* (Ed. by J. P. Kennet and P. F. Barker), pp. 937-960.

Kennet, J. P. & Stott, L. D. (1990) Proteus and Proto-Oceanus: Ancestral Palaeogene oceans as revealed from Antarctic stable isotopic results; ODP Leg 113. *Proceedings of the Ocean Drilling Program, Scientific Results*, **113**.

Kent, D. V. (1999) Orbital tuning of geomagnetic polarity time-scales. *Philosophical Transactions of the Royal Society of London*, **357**(1757), 1995-2007.

Kershaw, A. P. (1997) A bioclimatic analysis of early to Middle Miocene brown coal floras, Latrobe Valley, south-eastern Australia. *Australian Journal of Botany*, **45**(3), 373-387.

Kolla, V. & Coumes, F. (1987) Morphology, internal structure, seismic stratigraphy, and sedimentation of the Indus Fan. *American Association of Petroleum Geologists Bulletin*, **71**, 650-677.

Krasheninnikov, V. A. & Kaleda, K. G. (1994) Stratigraphy and lithology of the upper Cretaceous and Cenozoic deposits of the key Perapedhi section (Southern Cyprus) by means of radiolarians and correlation with foraminiferal zones. In: *Geological structure of the Northeastern Mediterranean (Cruise 5 of the Research Vessel Akademik Nokolaj Strakhov* (Ed. by V. A. Krasheninnikov and J. K. Hall). Historical Productions-Hall Ltd., Jerusalem.

Lagroix, F. & Borradaile, G. J. (2000) Tectonics of the circum-Troodos sedimentary cover of Cyprus, from rock magnetic and structural observations. *Journal of Structural Geology*, **22**, 453-469.

Lohmann, G. P. (1978) Response of the deep sea to ice ages. *Oceanus (Woods Hole)*, **21**(4), 58-64.

Loutit, T. S. & Keigwin, L. D. (1982) Stable isotopic evidence for the latest Miocene sea-level fall in the Mediterranean region. *Nature*, **300**, 163-166.

Maiorano, P. & Monechi, S. (1998) 1998. *Marine Micropalaeontology*, **35**, 253-255.

Margolis, S. V. (1975) Paleoglacial history of Antarctica inferred from analysis of Leg 29 sediments by scanning electron microscopy. In: *Initial reports of the Deep Sea Drilling Program, Vol. 29* (Ed. by J. P. Kennet and R. E. Houtz), pp. 1039-1048.

Martini, E. (1971) Standard Tertiary and Quaternary calcareous nannoplankton zonation. In: *Proceeding II Planktonic Conference, Vol. 2* (Ed. by A. Farinacci), pp. 739-785, Roma.

Martini, E. & Worsley, T. (1970) Standard Neogene calcareous nannoplankton zonation. *Nature (London)*, **225**(5229), 289-290.

Maslin, M. A., Li, X. S., Loutre, M.-F. & Berger, A. (1998) The contribution of orbital forcing to the progressive intensification of northern hemisphere glaciations. *Quaternary Science Reviews*, **17**(411-426).

McCallum, J. E. & Robertson, A. H. F. (1995) Sedimentology of two fan-delta systems in the Pliocene-Pleistocene of the Mesaoria Basin, Cyprus. *Sedimentary Geology*, **98**, 215-224.

Milankovitch, M. (1941) Kanon der Erdbestrahlung und seine Anwendung auf das Eiszeitenproblem. In: *Acad. Roy. Serbe, Ed. spec., Sec. Sci. mat. et nat., Vol. 133*, pp. 633.

Miller, G. M., Mountain, G. S. & al., e. (1996) Drilling and dating New Jersey Oligocene-Miocene sequences: Ice volume, global sea level, and Exxon records. *Science*, **271**, 1092-1095.

Miller, K. G. & Fairbanks, R. G. (1983) Evidence for Oligocene-Middle Miocene abyssal circulation changes in the western North Atlantic. *Nature*, **306**, 250-253.

Miller, K. G. & Fairbanks, R. G. (1985) Oligocene to Miocene carbon isotope cycles and abyssal circulation changes. In: *The Carbon Cycle and Atmospheric CO2: Natural Variations Archean to Present., Vol. 32* (Ed. by E. Sundquist and W. S. Broecker). Geophys. Monogr. Ser.

Miller, K. G., Fairbanks, R. G. & Mountain, G. S. (1987) Tertiary oxygen isotope synthesis, sea level history, and continental margin erosion. P*alaeoceanography*, **2**, 1-19.

Miller, K. G. & Sugarman, P. J. (1995) Correlation Miocene sequences in onshore New Jersey boreholes (ODP Leg 150X) with global d18O and Maryland outcrops. *Geology*, **23**(8), 747-750.

Miller, K. G., Wright, J. D. & Fairbanks, R. G. (1991) Unlocking the Ice House: Oligocene-Miocene oxygen isotopes, eustacy, and margin erosion. *Journal of Geophysical Research*, **96**(B4), 6829-6848.

Mitchum, R. M. (1977) Seismic stratigraphy and global changes of sea-level. Part 1: glossary of terms used in seismic stratigraphy. In: *Seismic stratigraphy - Applications to Hydrocarbon exploration* (Ed. by C. E. Payton), pp. 205-212. American Association of Petroleum Geologists' Memoir 26.

Mitchum, R. M. J., Vail, P. R. & Thompson, S. I. (1977) Seismic stratigraphy and global changes in sea level, Part 2: the depositional sequence as a basic unit for stratigraphic analysis. In: *Seismic Stratigraphy - applications to hydrocarbon exploration, Memoir 26* (Ed. by C. E. Payton), pp. 53-62. American Association of Petroleum Geologists.

Morel, S. W. (1960) The geology and mineral resources of the Apsiou-Akrotiri area. *Memoir of the Geological Survey Department, Cyprus*, **7**, 51-88.

Morse, T. J. (1996) Biostratigraphical constraints (calcareous nannofossils) on the late Cretaceous to late Miocene evolution of south west Cyprus. Unpublished PhD Thesis., University of Durham.

Mukasa, S. A. F. & Ismail, I. A. H. (1987) Uranium-lead ages of plagiogranite from the Troodos ophiolite, Cyprus, and their tectonic significance. *Geology*, **15**, 825-828.

Mutti, E. & Johns, D. R. (1978) the role of sedimentary bypassing in the genesis of fan fringe and basin plain turbidites in the Hecho group system (south-central Pyrenees). *Memorie Societa geologica Italiana*, **18**, 15-22.

Normark, W. R. (1974) Submarine canyons and fan valleys affecting growth patterns of deep sea fans. In: *modern and ancient geosynclinal sedimentation, Vol. 19* (Ed. by R. H. Dott and Shaver), pp. 56-68. Soc. Econ. Paleon, Mineral Spec.

Normark, W. R. (1978) Fan Valleys, Channels & Depositional Lobes on Modern Submarine Fans: Characters for the recognition of Sandy Turbidite Environments. *American Association of Petroleum Geologist*, **62**, 912-931.

Okada, H. & Bukry, D. (1980) Supplementary modification and introduction of code numbers to the low-latitude coccolith biostratigraphic zonation (Bukry, 1973; 1975). *Marine Micropaleontology*, **5**(3), 321-325.

Olivero, D. (1996) Zoophycos distribution and sequence stratigraphy. Examples from the Jurassic and Cretaceous deposits of southeastern France. *Palaeogeography, Palaeoclimatology, Palaeoecology*, **123**, 273-287.

Orszag-Sperber, F., Rouchy, J. M. & Elion, P. (1989) The sedimentary expression of regional tectonic events during the Miocene-Pliocene transition in the southern Cyprus basin. *Geological Magazine*, **123**(3), 291-299.

Pantazis, M. (1967) The Geology and Mineral Resources of the Pharmakas-Kalavasos Area. *Geological Survey Department Cyprus*, **Memoir No. 8**, 190.

Pantazis, T. M. (1980) Ophiolites of Cyprus. In: *Tethyan Ophiolites Eastern area. Ofioliti special issue, Vol. 2* (Ed. by G. Rocci), pp. 239-279. Pitagora Editrice Bologna.

Payne, A. S. & Robertson, A. H. F. (1995) Neogene supra-subduction extension in the Polis graben system. *Journal of the Geological Society, London*, **152**, 613-628.

Pekar, S. & Miller, K. G. (1996) New Jersey Oligocene "Icehouse" sequences (ODP Leg 150X) correlates with global d18O and Exxon records. *Geology*, **24**(6), 567-570.

Perch-Nielsen, K. (1985) Cenozoic calcareous nannofossils. In: *Plankton Stratigraphy, Vol. 1* (Ed. by H. M. Bolli, J. B. Saunders and K. Perch-Nielsen), pp. 427-554. Cambridge University Press.

Pillans, B., Chappell, J. & Naish, T. R. (1998) A review of the Milankovitch climatic beat: template for Plio-Pleistocene sea-level changes and sequence stratigraphy. *Sedimentary Geology*, **122**(1-4), 5-21.

Plint, A. G., Eyles, N., Eyles, C. H. & Walker, R. G. (1992) Control of sea level change. In: *Facies Models: response to seal level change* (Ed. by R. G. Walker and N. P. James), pp. 15-25.

Poole, A. J. & Robertson, A. H. F. (1991) Quaternary uplift and sea-level change at an active plate boundary, Cyprus. *Journal of the Geological Society, London*, **148**, 909-921.

Priestley, M. B. (1981) *Spectral Analysis and time Series*. Academic Press, London.

Raffi, I. (1999) Precision and accuracy of nannofossil biostratigraphic correlation. *Philosphical Transactions of the Royal Society of London*, **357**(1557), 1975-1993.

Ramsey, A. T., Smart, C. W. & Zachos, J. C. (1998) A model of early to middle Miocene deep ocean circulation for the Atlantic and Indian Oceans. In: *Geological Evolution od Ocean Basins: Results from the Ocean Drilling Program., Vol. 131* (Ed. by A. Cramp, C. J. MacLeod, S. V. Lee and E. J. Jones). Geological Society, Special Publication, London.

Read, J. F. & Goldhammer, R. K. (1988) Use of Ficher plats to define third-order sea-level curves in Ordivician peritidal cyclic carbonates, Appalachians. *Geology*, **16**, 895-899.

Reading, H. G. & Levell, B. K. (1996) Controls on the sedimentary rock record. In: *Sedimentary Environments, Process, Facies and Stratigraphy* (Ed. by H. G. Reading), pp. 5-36. Blackwell Science Ltd.

Reading, H. G. & Richards, M. T. (1994) The classification of deep-water siliciclastic depositional systems by grainsize and feeder systems. *American Association of Petroleum Geologists*, **78**, 792-822.

Reinhardt, P. (1972) *Coccoliths*. Wittenberg, Federal Republic of Germany, 95 pp.

Richards, M., Bowman, M. & Reading, H. (1998) Submarine-fan systems: characterisation and stratigraphic prediction. *Marine and Petroleum Geology*, **15**, 689-717.

Roberston, A. H. F. & Dixon, J. E. (1984) Aspects of the geological evolution of the Eastern Mediterranean. In: *The Geological Evolution of the Eastern Mediterranean, Vol. 17* (Ed. by J. E. Dixon and A. H. F. Robertson), pp. 1-74. Geological Society of London Special Publication.

Robertson, A. H. F. & Hudson, J. D. (1974) Pelagic sediments in the Cretaceous and Tertiary history of Cyprus. In: *Pelagic sediments: on land and under the sea, Vol. 1* (Ed. by K. J. Hsu and H. C. Jenkyns), pp. 403-436. Special Publication of International Association of Sedimentologists.

Robertson, A. H. F. (1976) Pelagic chalks and calcturbidites from the Lower Tertiary of the Troods massif, Cyprus. *Journal of Sedimentary Petrology*, **46**(4), 1007-1016.

Robertson, A. H. F. (1977a) The Moni melange, Cyprus: and olistostrome formed at a destructive plate margin. *Journal of the Geological Society of London*, **133**, 447-446.

Robertson, A. H. F (1977b) Tertiary uplift of the Troodos massif, Cyprus. *Geological Society of American Bulletin*, **88**, 1763-1772.

Robertson, A. H F., Eaton, S., Follows, E.J., McCallum, J.E. (1991). The role of local tectonics versus global sea-level change in the Neogene evolution of the Cyprus active margin. Special Publication of the International Association of Sedimentologists, **12**, 331-369.

Robertson, A. H. F. & Xenophontos, C. (1993) Development of concepts concerning the Troodos ophiolite and adjacent units in Cyprus. In: *Magmatic Processes and Plate Tectonics, Vol. 76* (Ed. by H. M. Prichard, T. Alabaster, N. B. W. Harris and C. R. Neary), pp. 85-119. Geological Society Special Publication.

Robertson, A. H. F. & Grasso. M. (1995) Overview of the Late Tertiary-recent tectonic and paleo-environmental development of the Mediterranean region. *Terra Nova*, **7**(114-127).

Robertson, A. H. F. (1996a) Role of the Eratosthenes seamount in collisional process in the Eastern Mediterranean. *Proceedings of the Ocean Drilling Program, Initial Reports*, **160**, 513-520.

Robertson, A. H. F. (1998a) Late Miocene paleoenvironments and tectonic setting of the southern margin of Cyprus and the Eratosthenes seamount. In: *Proceedings of the Ocean Drilling Program, Scientific Results, Vol. 160* (Ed. by A. H. F. Robertson, K. C. Emeis, C. Richter and A. Camerlenghi), pp. 453-463.

Robertson, A. H. F. (1998b) Mesozoic-Tertiary tectonic evolution of the Easternmost Mediterranean area: Integration of marine and land evidence. In: *Proceedings of the Ocean Drilling Program, Scientific Results, Vol. 160* (Ed. by A. H. F. Robertson, K. C. Emeis, C. Richter and A. Camerlenghi), pp. 723-782.

Robertson, A. H. F., Eaton, S., Follows, E. J. & Payne, A. S. (1995) Depositional processes and basin analysis of Messinian evaporites in Cyprus. *Terra Nova*, **7**, 233-253.

Robertson, A. H. F. e. a. (1996b) Tectonic Introduction. *Proceedings of the Ocean Drilling Program, Initial Reports*, **160**, 5-19.

Sadler, P. M. (1981) Sediment accumulation rates and the completeness of stratigraphic sections. *Journal of Geology*, **89**(5), 569-584.

Sarg, J. F. (1988) Carbonate sequence stratigraphy. In: *Sea-level changes: An integrated Approach* (Ed. by B. S. Hastings, H. Posamentier, C. A. van Wagoner, Ross and C. G. St Kendall). Society of the Economic Palaeontologist and Mineralogists Special Publication 42.

Savin, S. M. (1977) The history of the Earth's surface temperature during the last 100 million years. *Annual review of Earth and Planetary Sciences*, **5**, 319-355.

Savin, S. M., Douglas, R. G. & Stehli, F. G. (1975) Tertiary marine palaeotemperatures. *Geological Society of America Bulletin*, **86**, 1499-1510.

Schirmer, W. (2000). Neogene submarine relief and Troodos uplift in southeastern Cyprus. In: Panayides, I., Xenophontos, C. & Malpas, J (eds.), *Proceedings of the Third International Conference on the Geology of the Eastern Mediterranean.*

Schoell, M., Schouten, S., Sinninghe Damste, J. S., de Leeuw, J. W. & Summons, R. E. (1994) A Molecular organic carbon isotope record of Miocene climate changes. *Science*, **263**, 1122-1125.

Scholle, P. A. & Arthur, M. (1980) Carbon isotope fluctuations in Cretaceous pelagic limestones: potential stratigraphic and petroleum exploration tool. *Bulletin of the American Association of Petroleum Geologists*, **64**, 67-87.

Schwarzacher, W. (2000) Repetitions and cycles in stratigraphy. *Earth-Science Reviews*, **50**, 51-75.

Seidler, L. (2000) Incised submarine canyons governing new evidence of Early Triassic rifting in East Greenland. *Palaeogeography, Palaeoclimatology, Palaeoecology*, **161**, 267-293.

Shackelton, N. J., Crowhurts, S. J., Weedon, G. P. & Laskar, J. (1999) Astronomical calibration of the Oligocene-Miocene time. *Philosophical Transactions of the Royal Society of London*, **537**(1757), 1907-1929.

Shackleton, N. J., Hall, M. A. & Pate, D. (1995) Pliocene stable isotope stratigraphy of ODP Site 846. In: *Proceedings of the Ocean Drilling Program, Scientific Results, Vol. 138* (Ed. by N. e. a. Pisias), pp. 73-101.

Shackleton, N. J. & Kennet, J. P. (1975) Palaeotemperature history of the Cenozoic and initiation of the Antarctic glaciation: oxygen and carbon isotope analysis in DSDP Sites 227, 279, and 281. *Initial Reports: Deep Sea Drilling Project*, **29**, 743-755.

Shackleton, N. J. & Opdyke, N. D. (1973) Oxygen isotope and paleomagnetic stratigraphy of equatorial Pacific core V 28-238: Oxygen isotope temperature and ice volumes on a 105 year and 106 year scale. *Quaternary Research*, **3**, 39-55.

Shelton, A. W. & Gass, I. G. (1980) Rotation of the Cyprus microplate. In: *Ophiolites; Proceedings, International ophiolite symposium* (Ed. by A. Panayiotou), pp. 61-65. Cyprus, Minist. Agric. Nat. Resour., Geol. Surv. Dep, Nicosia, Cyprus.

Siesser, W. G. & de Kaenel, E. P. (1999) Neogene calcareous nannofossils: Western Mediterranean Biostratigraphy and Paleoclimatology. In: *Proceedings of the Ocean Drilling Program, Scientific Results, Vol. 161* (Ed. by Z. R. Comas and M. C. Klaus), pp. 223-237.

Smith, A. G. & Briden, J. C. (1977) *Mesozoic and Cenozoic Palaeocontinental maps*. Cambridge University Press, 65 pp.

Stow, D. A. V., Braakenburg, N. E. & Xenophontos, C. (1995) The Pissouri Basin fan-delta complex, southwestern Cyprus. *Sedimentary Geology*, **98**, 245-262.

Stradner, H. (1959b) First report on the discoasters of the Tertiary of Austria and their stratigraphic use. In: *Proceedings - World Petroleum Congress*, pp. 1081-1095. John Wiley & Sons, Chichester.

Stradner, H. (1959a) First report on the discoasters of the Tertiary of Austria and their stratigraphic use. *Proceedings of the 5th World Petroleum Conference*, **1**, 1081-1095.

Tappan, H. (1980) *The paleobiology of plant protists*. W. H. Freeman and Co, San Francisco, 997 pp.

Taylor, J., Dowdeswell, J. A. & Kenyon, N. H. (2000) Canyons and late Quaternary sedimentation on the North Norwegian margin. *Marine Geology*, **166**, 1-9.

Thiede, J., Eldholm, O. & Taylor, E. (1989) Variability of Cenozoic Norwegian-Greenland Sea palaeoceanography and Northern Hemisphere palaeoclimate. In: *Proceeding of the ODP Scientific Results, Vol. 104* (Ed. by O. Eldholm, J. Thiede and E. Taylor), pp. 1067-1118.

Tiedemann, S., Sarnthein, M. & Shackleton, N. J. (1994) Astronomical time scales for the Pliocene Atlantic d18O and dust flux records of Ocean Drilling Program Site 659. *Palaeoceanography*, **9**, 613-638.

Tiwari, R. K. (1987) Higher-order eccentricity cycles of the middle and late Miocene climatic variations. *nature*, **327**, 219-221.

Turner, W. M. (1971) The Geology of the Polis-Kathikas area. *Geological Survey Department, Cyprus*, **Memoir No. 6**, 256.

Vail, P. R., Audemard, F., Bowman, S. A., Eisner, P. N. & Perez-Crus, C. (1991) The stratigraphic signatures of tectonics, eustacy and sedimentology - an overview. In: *Cycela and Events in Stratigraphy* (Ed. by E. e. al.), pp. 617-659. Springer-Verlag, Berlin Heidelberg.

Vail, P. R., Mitchum, R. M. & Thompson III, S. (1977) Seismic stratigraphy and global changes in sea-level. Part 4: Global cycles of relative changes in sea-level. In: *Seismic Stratigraphy - Applications to Hydrocarbon Exploration* (Ed. by C. W. Payton), pp. 83-97. *American Association of Petroleum Geologists' Memoir 26.*

Valdes, P. J. & Glover, R. W. (1999) Modelling the climate response to orbital forcing. *Philosophical Transactions of the Royal Society of London*, **357**(1757), 1837-1890.

van Wagoner, J. C., Posamentier, H. W., Mitchum, R. M., Vial, P. R., Sarg, J. F., Loutit, T. & Hardenbol, J. (1988) An overview of the fundamentals of sequence stratigraphy and key definition. In: *Sea-level changes: an integrated approach, Vol. 42* (Ed. by C. K. Wilgus, B. S. Hastings, J. Posamentier, C. A. van Wagoner, Ross and S. C. Kendall), pp. 39-45. Society of Economic Palaeontologists and Mineralogists Special Publication.

Vecsei, A. & Sanders, D. K. G. (1999) Facies analysis and sequence stratigraphy of a Miocene warm-temperature carbonate ramp, Montagna della Maiella, Italy. *Sedimentary Geology*, 103-127.

Vincent, E. & Berger, W. H. (1985) Carbon dioxide and polar cooling in the Miocene: The Monterey Hypothesis. In: *The carbon cycle and atmospheres CO2: Natural variations Archean to present* (Ed. by E. T. Sundquist and W. S. Broecker), pp. 455-468. American Geophysical Union, Washington D.C.

Vincent, E. & Killingley, J. S. (1985) Oxygen and Carbon isotope record for the early and middle Miocene in the central equatorial Pacific (Leg 85) and palaeoceanographic implications. In: *Initial Reports of the deep Sea Drilling Project* (Ed. by L. Mayer and F. Theyer), pp. 749-769. U.S. Government Printing Office, Washington D.C.

Vincent, E., Killingley, J. S. & Berger, W. H. (1985) Miocene oxygen and carbon isotope stratigraphy of the tropical Indian Ocean. *Geological Society of America*, Memoir **163**, 103-122.

Voigt, S. & Hilbrecht, H. (1997) Late Cretaceous carbon isotope stratigraphy in Europe: Correlation and relations with sea level and sediment stability. *Palaeogeography, Palaeoclimatology, Palaeoecology*, **134**, 39-59.

Volkova, V. S., Kul'kova, I. A. & Fradkina, A. F. (1986) Palynostratigraphy of the non-marine Neogene in North Asia. *Reviews in Palaeobotany and Palynology*, **48**, 415-424.

Walker, J. C. G. & Zahnle, K. J. (1986) Lunar nodal tide and distance to the Moon during the Precambrian. *Nature*, **320**(6064), 600-602.

Walker, R. G. (1978) Deep Water Sandstone facies and Ancient Sub-marine Fans: Models for Exploration for Stratigraphic Traps. *American Association of Petroleum Geologists*, **62**, 932-966.

Walker, R. G. & James, N. P. (1992) Facies Models: Response to Sea-level Change, pp. 454. Geological Association of Canada.

Weedon, G. P. (1985) Hemipelagic shelf sedimentation and climatic cycles: the basal Jurassic (Blue Lias) of South Britain. *Earth and Planetary Science Letters*, **76**, 321-335.

Weedon, G. P. (1991) The Spectral Analysis of Stratigraphic Time Series. In: *Cycles and Events in Stratigraphy* (Ed. by E. e. al.). Springer-Verlag, Berlin Heidelberg.

Weedon, G. P. (1993) The recognition and stratigraphic implications of orbital-forcing of climate and sedimentary cycles. In: *Sedimentology Review, Vol. 1*, pp. 31-50. Blackwell Scientific Publications.

Weedon, G. P., Jenkyns, H. C., Coe, A. L. & Hesselbo, S. P. (1999) Astronomical calibration of the Jurassic time-scale from cyclostratigraphy in British mudrock formations. *Philosophical Transactions of the Royal Society of London*, **357**(1757), 1787-1813.

Weimer, P. (1990) Sequence stratigraphy, facies geometries, and depositional history of the Mississippi Fan, Golf of Mexico. *American Association of Petroleum Geologists Bulletin*, **74**, 425-453.

Weissert, H. & Lini, A. (1991) Ice age interludes during the time of Cretaceous greenhouse climate. In: *Controversies in modern Geology* (Ed. by D. W. Muller, J. A. McKenzie and H. Weissert), pp. 173-191. London Academic Press.

Whiting, B. M. (1998) Subsidence Record of early-stage continental collision, Eratosthenes platform (Sites 966 and 967). In: *Proceedings of the Ocean Drilling Program, Scientific results, Vol. 160* (Ed. by A. H. F. Robertson, K. C. Emeis, C. Richter and A. Camerlenghi), pp. 509-708.

Wilson, R. A. M. (1959) *The geology of the Xeros-Troodos area*. Ministry of Agriculture and Natural Resources, 184 pp.

Wilson, R. C. L., Dury, S. A. & Chapman, J. L. (2000) *The Great Ice Age*. Routledge, London, 267 pp.

Wonham, J. P., Jayr, S., Mougamba, R. & Chuilon, P. (2000) 3D sedimentary evolution of a canyon fill (Lower Miocene-age) from the Mandorove Formation, offshore Gabon. *Marine and Petroleum Geology*, **17**, 175-197.

Woodruff, F. & Savin, S. (1991) Mid-Miocene isotope stratigraphy in the deep sea: high resolution correlations, palaeoclimatic cycles, and sediment preservation. *Palaeoceanography*, **6**, 755-806.

Worsley, T. W., Nance, D. & Moody, J. B. (1984) Global tectonics and eustacy for the past 2 billion years. *Marine Geology*, **58**, 373-400.

Wray, J. L. (1978) Calcareous microfossils; calcareous algae. In: *Introduction to marine micropaleontology* (Ed. by B. U. Haq and A. Boersma). Elsevier, North-Holland New York.

Wright, J. D. & Miller, K. G. (1992) Miocene stable isotope stratigraphy. site 747, Kerguelan Plateau. *Proceeding of the Ocean Drilling Program, Scientific Results*, **120**, 855-866.

Zweigel, J., Aigner, T. & Luterbacher, H. (1998) Eustatic versus tectonic controls on Alpine forland basin fill: sequence stratigraphy and subsidence analysis in the SE German Molasse. In: *Cenozoic Foreland Basins of Western Europe, Vol. 134* (Ed. by A. Mascle, C. Puigdefabre-Gas, H. P. Luterbacher and M. Fernandez), pp. 299-323. Geological Society Special Publications.

APPENDIX A

GRAPHIC LOGS

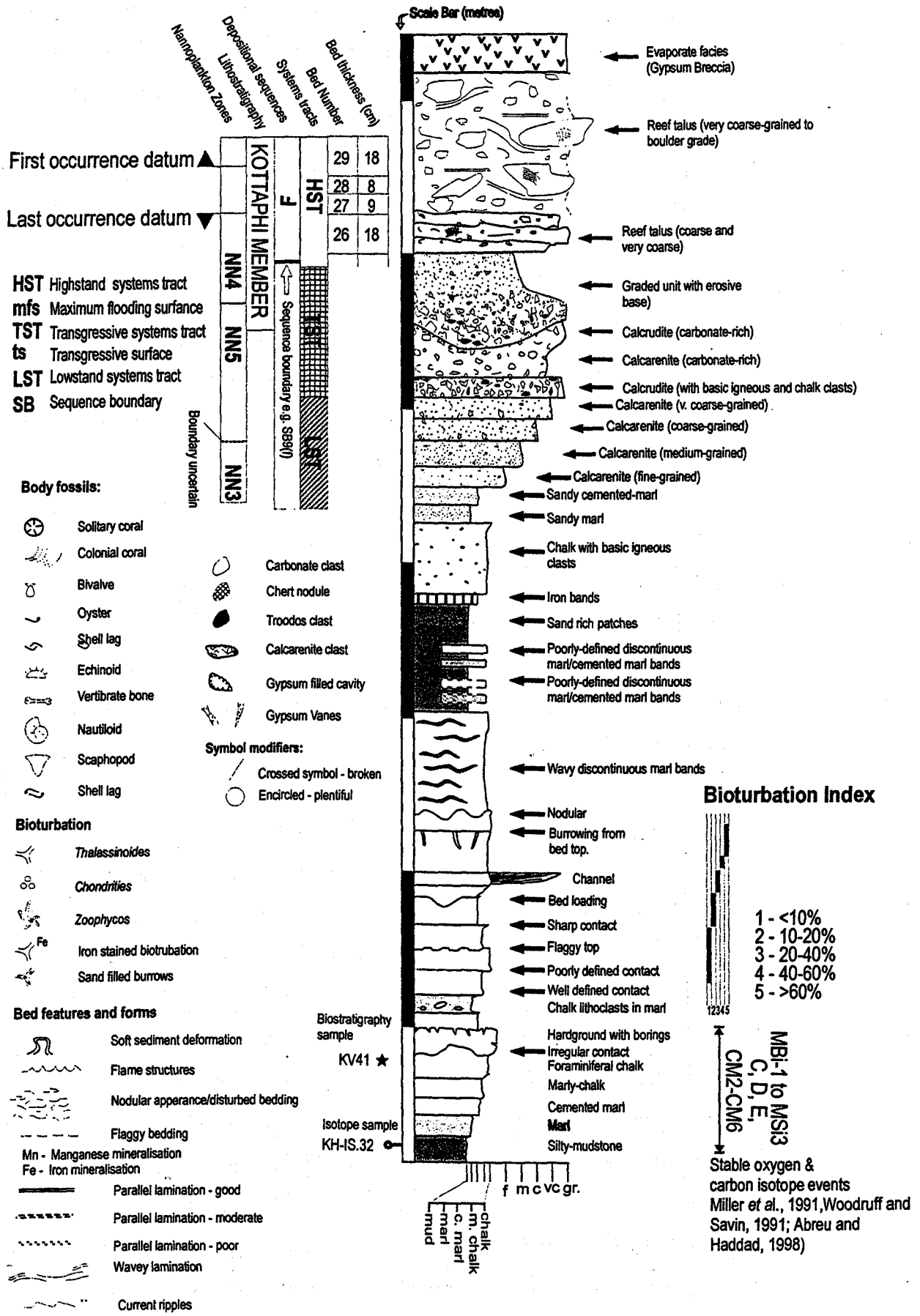
Scale Bar (metres)
Nannoplankton Zones
Depositional sequences
Lithostratigraphy
Systems tracks
Bed Number
Bed thickness (cm)
First occurrence datum
Last occurrence datum
KOTTAPHI MEMBER
NN4
NN5
NN3
HST
LST
29 18
28 8
27 9
26 18
Sequence boundary e.g. SB9(f)
Boundary uncertain
HST Highstand systems tract
mfs Maximum flooding surface
TST Transgressive systems tract
ts Transgressive surface
LST Lowstand systems tract
SB Sequence boundary
Body fossils:
Solitary coral
Colonial coral
Bivalve
Oyster
Shell lag
Echinoid
Vertibrate bone
Nautiloid
Scaphopod
Shell lag
Carbonate clast
Chert nodule
Troodos clast
Calcarenite clast
Gypsum filled cavity
Gypsum Vanes
Symbol modifiers:
Crossed symbol - broken
Encircled - plentiful
Bioturbation
Thalassinoides
Chondrites
Zoophycos
Fe
Iron stained biotrubation
Sand filled burrows
Bed features and forms
Soft sediment deformation
Flame structures
Nodular apperance/disturbed bedding
Flaggy bedding
Mn - Manganese mineralisation
Fe - Iron mineralisation
Parallel lamination - good
Parallel lamination - moderate
Parallel lamination - poor
Wavey lamination
Current ripples
Evaporate facies (Gypsum Breccia)
Reef talus (very coarse-grained to boulder grade)
Reef talus (coarse and very coarse)
Graded unit with erosive base)
Calcrudite (carbonate-rich)
Calcarenite (carbonate-rich)
Calcrudite (with basic igneous and chalk clasts)
Calcarenite (v. coarse-grained)
Calcarenite (coarse-grained)
Calcarenite (medium-grained)
Calcarenite (fine-grained)
Sandy cemented-marl
Sandy marl
Chalk with basic igneous clasts
Iron bands
Sand rich patches
Poorly-defined discontinuous marl/cemented marl bands
Poorly-defined discontinuous marl/cemented marl bands
Wavy discontinuous marl bands
Nodular
Burrowing from bed top.
Channel
Bed loading
Sharp contact
Flaggy top
Poorly defined contact
Well defined contact
Chalk lithoclasts in marl
Hardground with borings
Irregular contact
Foraminiferal chalk
Marly-chalk
Cemented marl
Marl
Silty-mudstone
Biostratigraphy sample
KV41
Isotope sample
KH-IS.32
f m c vc gr.
mud
marl
c. marl
m. chalk
chalk
Bioturbation Index
1 - <10%
2 - 10-20%
3 - 20-40%
4 - 40-60%
5 - >60%
12345
MBi-1 to MSi3
C, D, E,
CM2-CM6
Stable oxygen & carbon isotope events Miller et al., 1991,Woodruff and Savin, 1991; Abreu and Haddad, 1998)

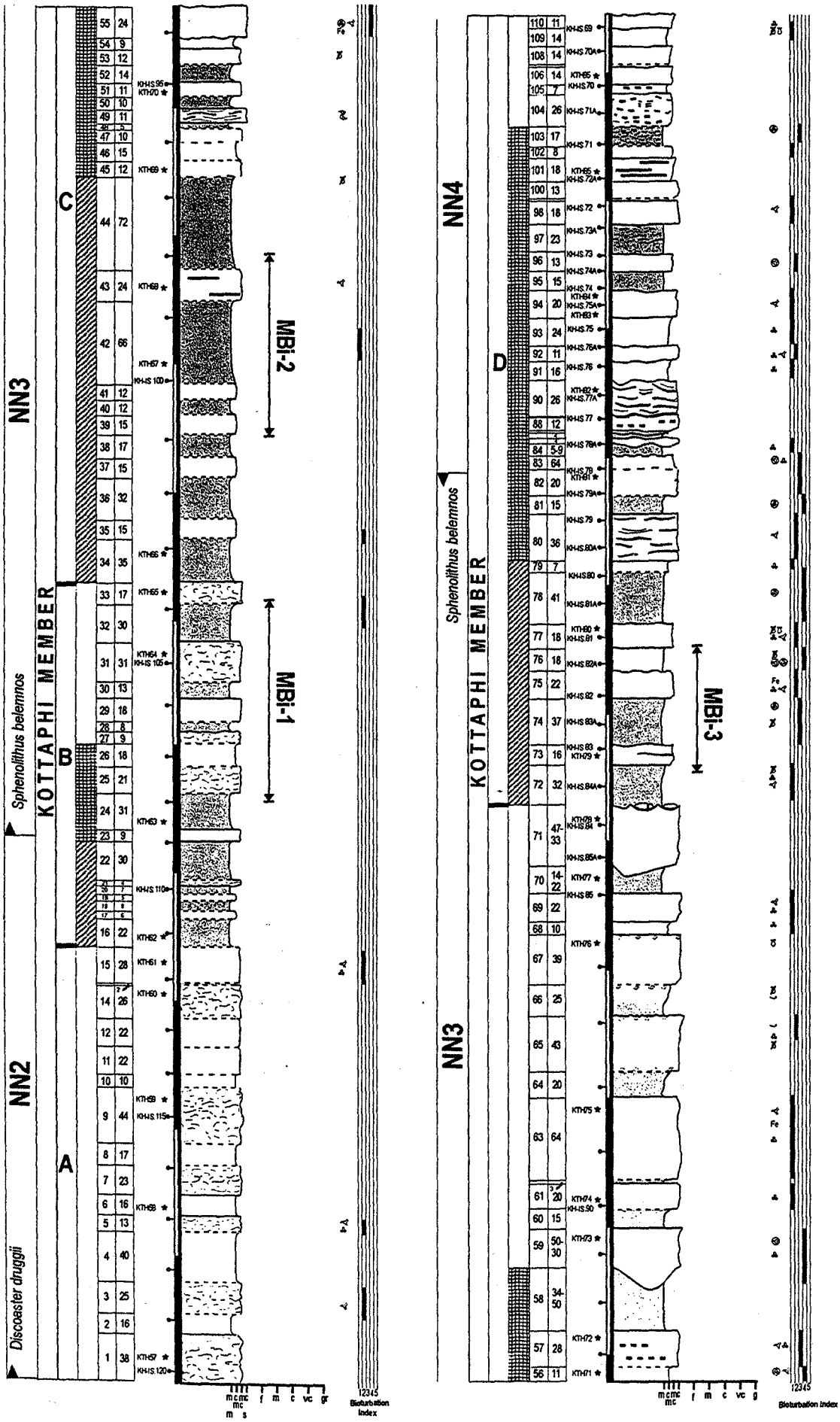
NN3
NN2
NN4
KOTTAPHI MEMBER
Sphenolithus belemnos
Discoaster druggii
A
B
C
D
MBi-1
MBi-2
MBi-3
Bioturbation Index

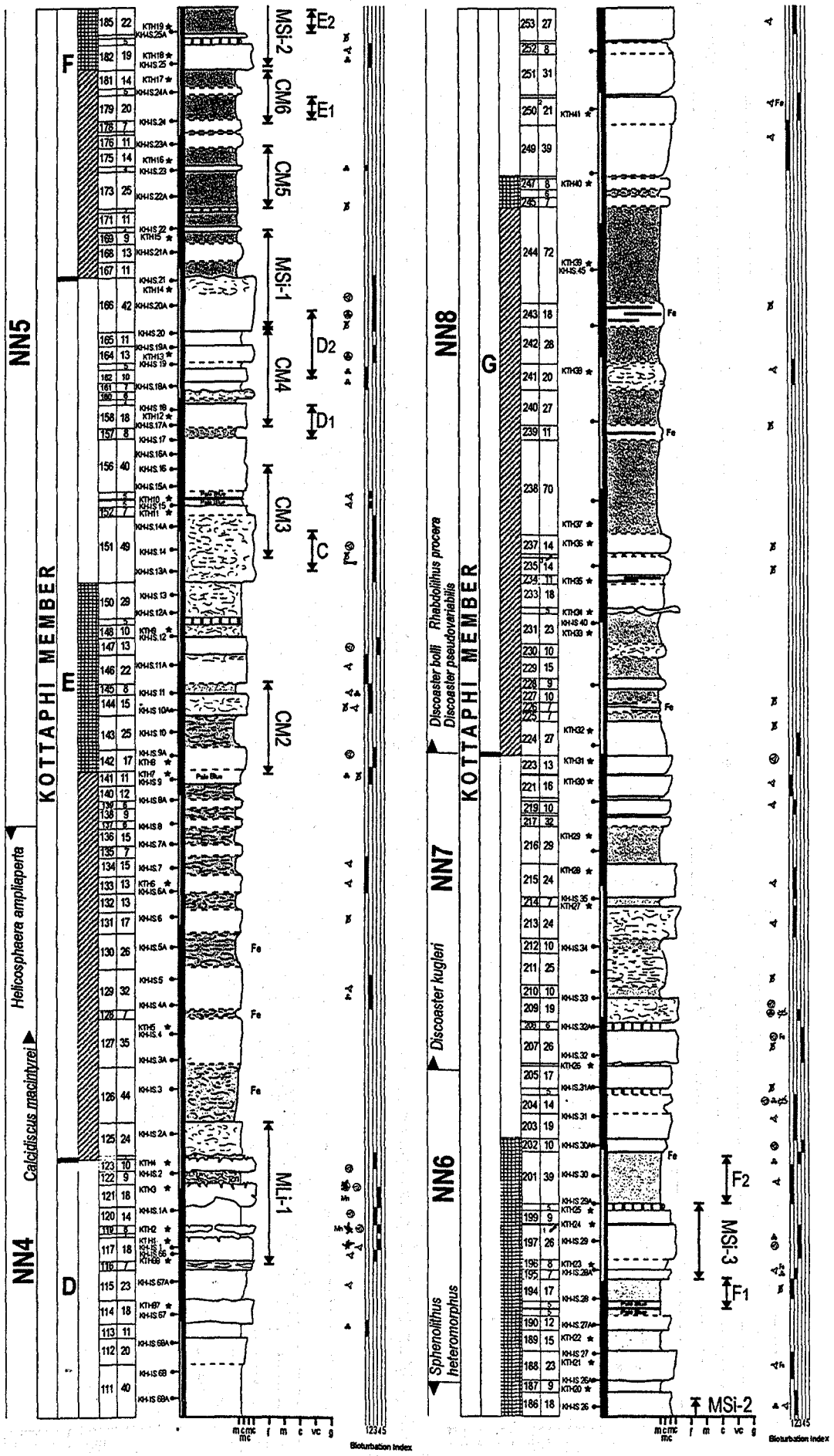
NN5
NN4
NN8
NN7
NN6
KOTTAPHI MEMBER
Helicosphaera ampliaperta
Calcidiscus macintyrei
Discoaster bolli
Rhabdolithus procera
Discoaster pseudovariabilis
Discoaster kugleri
Sphenolithus heteromorphus
F
D
G
MSi-2
CM6
CM5
MSi-1
CM4
CM3
CM2
MLi-1
E2
E1
D2
D1
C
F2
MSi-3
F1
Fe
mc mc mc f m c vc g
Bioturbation Index
1 2 3 4 5

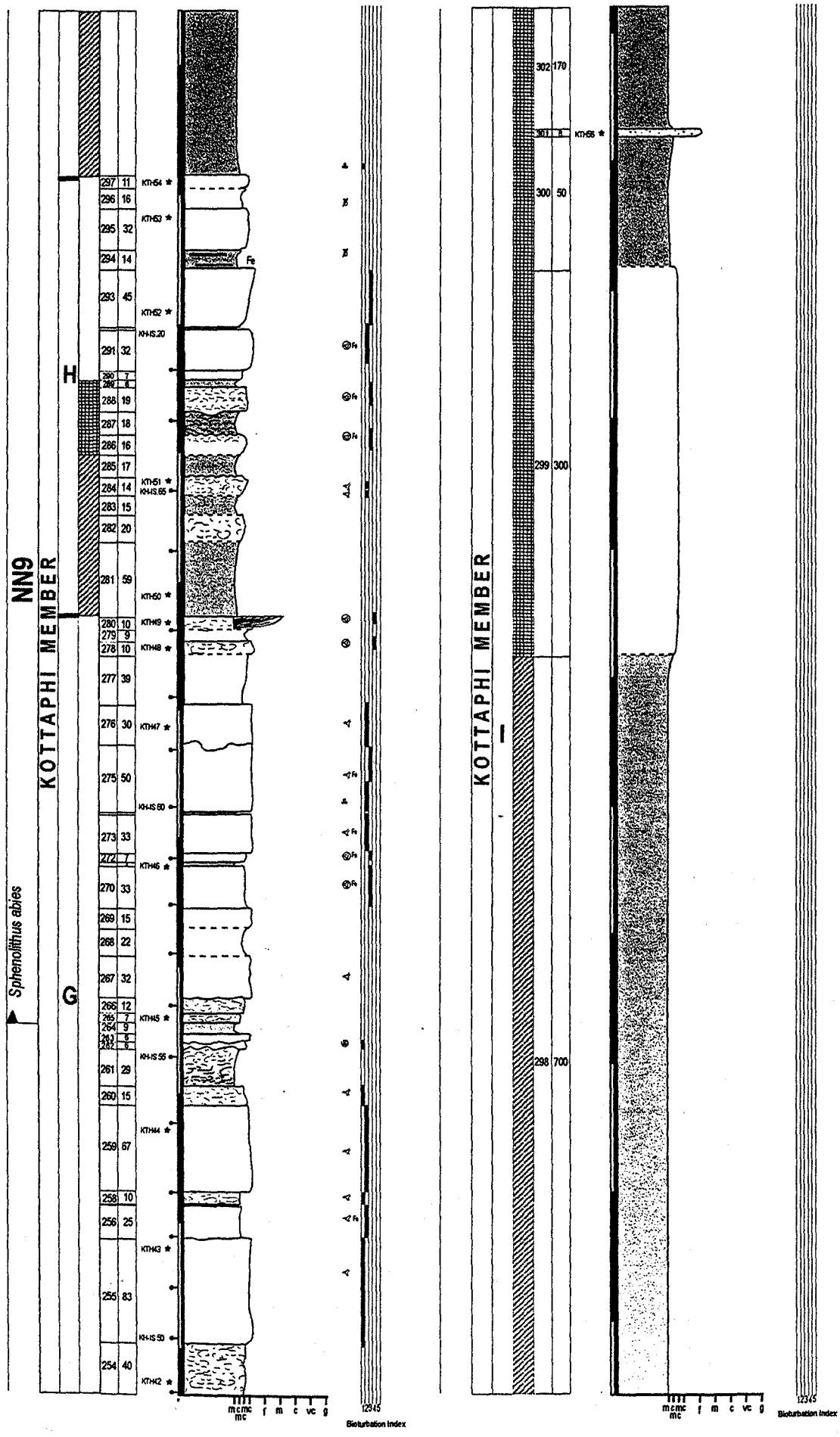
NN9
KOTTAPHI MEMBER
Sphenolithus abies
H
G
297 11
296 16
295 32
294 14
293 45
291 32
290 7
289 6
288 19
287 18
286 16
285 17
284 14
283 15
282 20
281 59
280 10
279 9
278 10
277 39
276 30
275 50
273 33
272 7
270 33
269 15
268 22
267 32
266 12
265 7
264 9
263 6
262 6
261 29
260 15
259 67
258 10
256 25
255 83
254 40
KTH64
KTH63
KTH62
KH-IS.20
KTH51
KH-IS.65
KTH50
KTH49
KTH48
KTH47
KH-IS 50
KTH46
KTH45
KH-IS 55
KTH44
KTH43
KH-IS 50
KTH42
Fe
m c mc mc f m c vc g
1 2 3 4 5
Bioturbation Index
KOTTAPHI MEMBER
302 170
301 8
300 50
299 300
298 700
KTH66
m c mc mc f m c vc g
1 2 3 4 5
Bioturbation Index

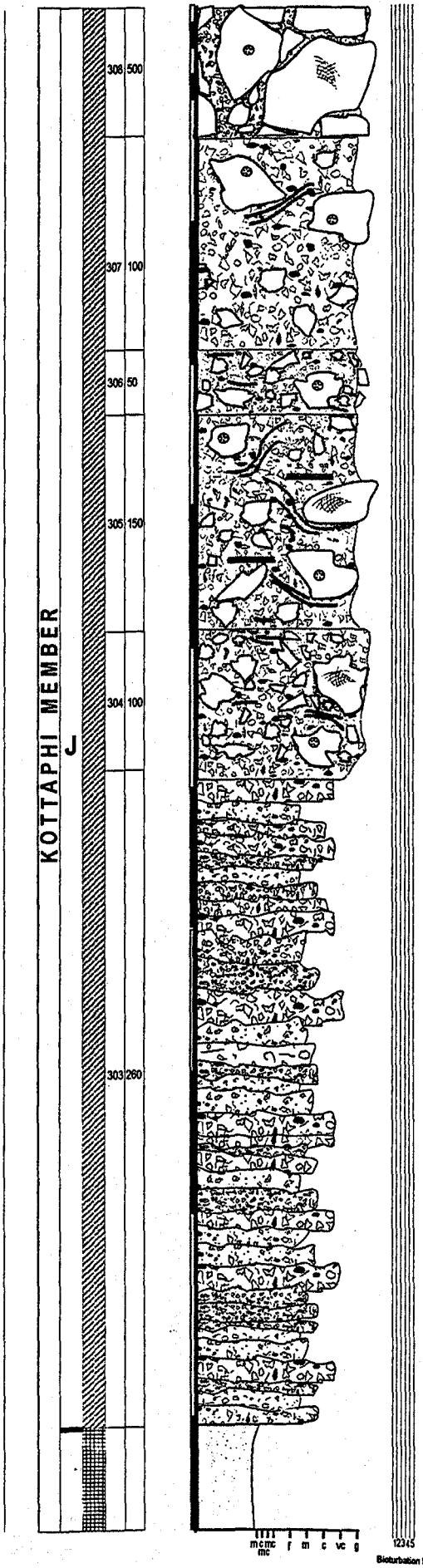
KOTTAPHI MEMBER
308 500
307 100
306 50
305 150
304 100
303 260
mc mc mc f m c vc g
12345
Bioturbation Index

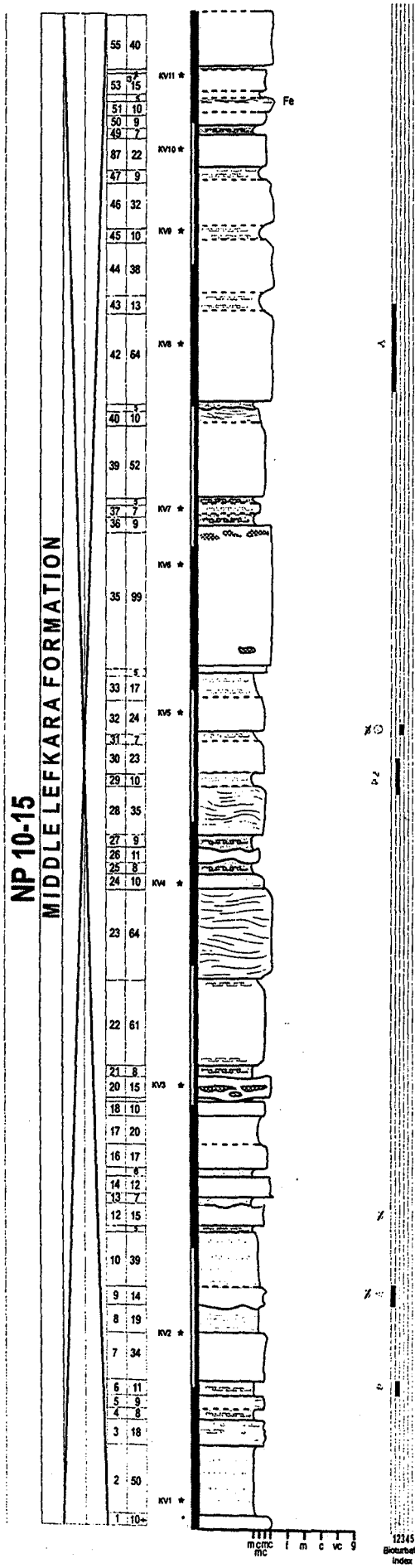
NP 10-15
MIDDLE LEFKARA FORMATION
KV11
KV10
KV9
KV8
KV7
KV6
KV5
KV4
KV3
KV2
KV1
Fe
m c mc mc f m c vc g
1 2 3 4 5
Bioturbation Index

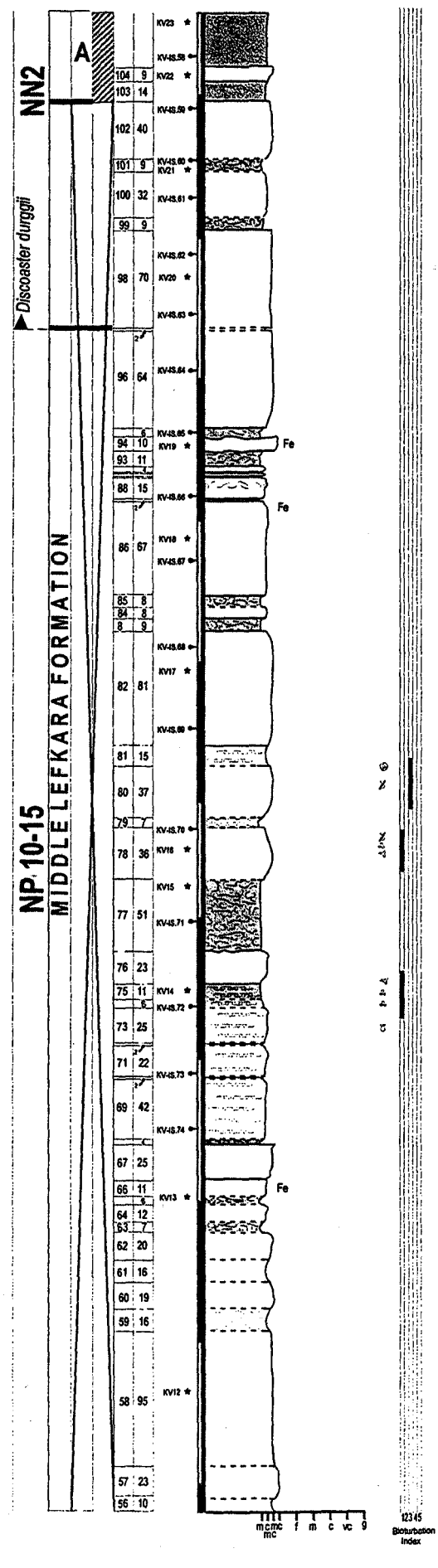
NN2
A
Discoaster durrgii
NP 10-15
MIDDLE LEFKARA FORMATION
KV23
KV22
KV21
KV20
KV19
KV18
KV17
KV16
KV15
KV14
KV13
KV12
Fe
Fe
Fe
m c mc mc f m c vc g
1 2 3 4 5
Bioturbation Index

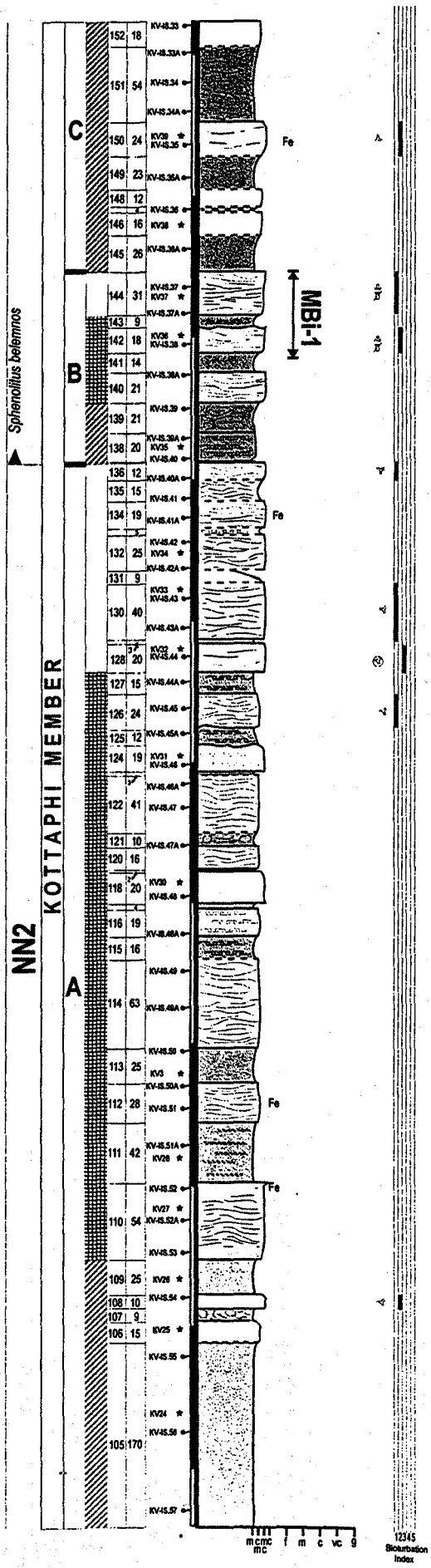
NN2
KOTTAPHI MEMBER
Sphenolithus belemnos
A
B
C
MBi-1
Fe
m cmc mc f m c vc g
12345
Bioturbation Index

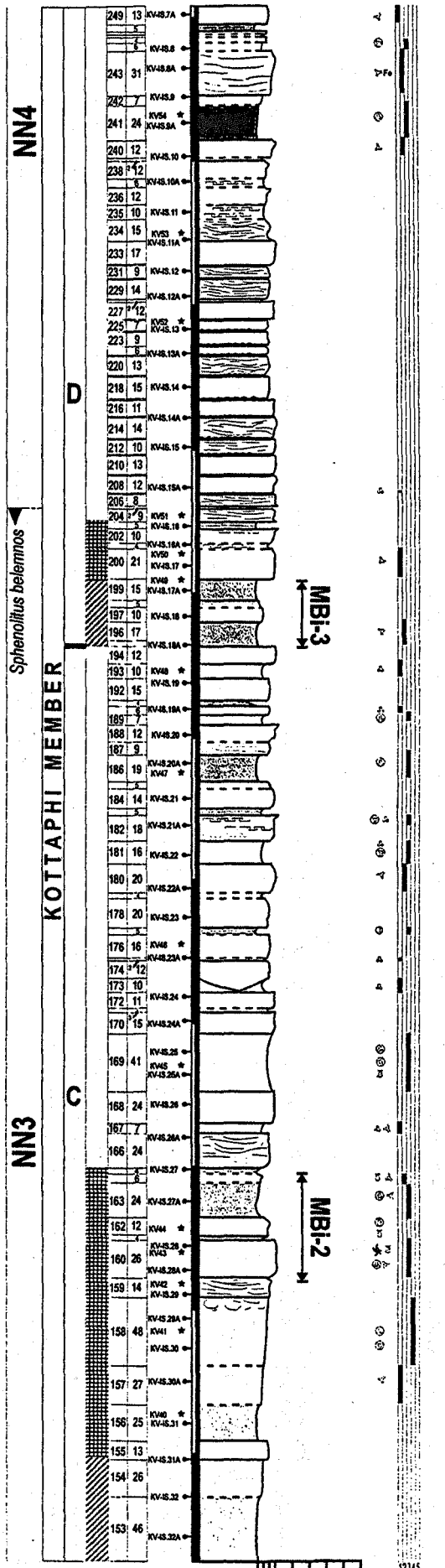
NN4
NN3
KOTTAPHI MEMBER
Sphenolithus belemnos
C
D
MBi-3
MBi-2
m cmc mc f m c vc g
12345
Bioturbation Index

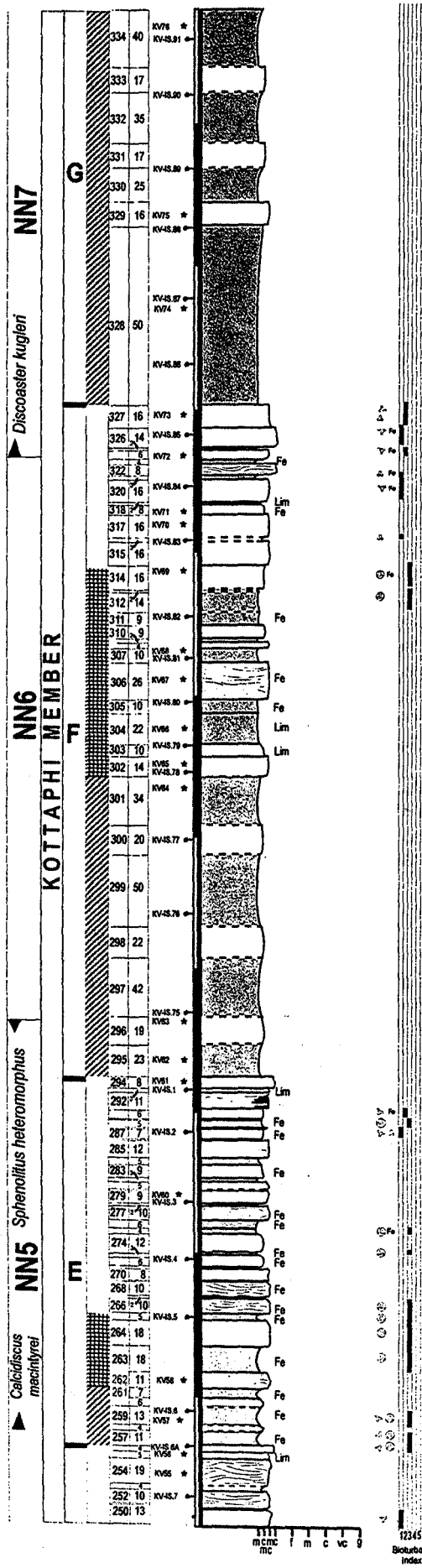
Discoaster kugleri
NN7
NN6
Sphenolithus heteromorphus
NN5
Calcidiscus macintyrei
KOTTAPHI MEMBER
G
F
E
Lim
Fe
mc mc mc f m c vc g
12345
Bioturbation Index

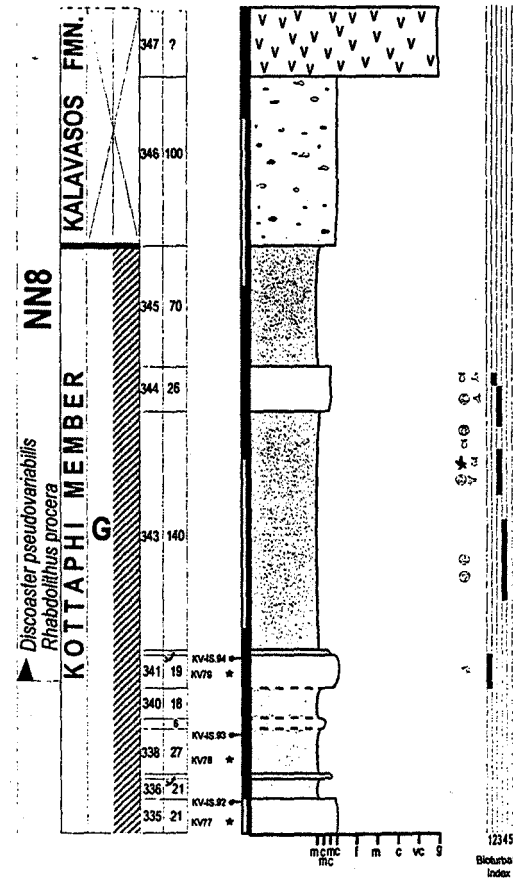
KALAVASOS FMN.
NN8
Discoaster pseudovariabilis
Rhabdolithus procera
KOTTAPHI MEMBER
G
mc mc mc f m c vc g
12345
Bioturbation Index

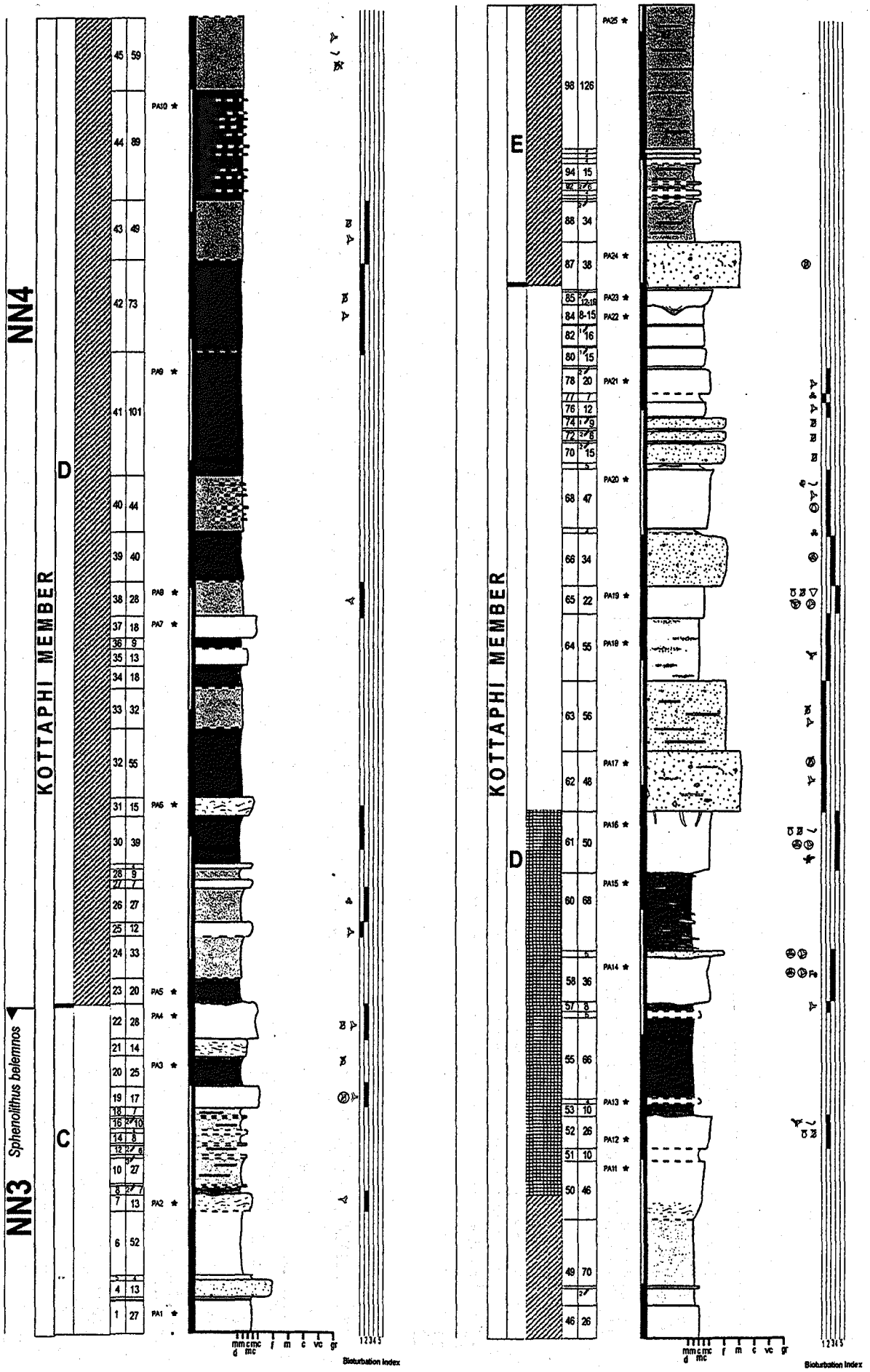
NN4
NN3
Sphenolithus belemnos
KOTTAPHI MEMBER
D
C
m
PA1
PA2
PA3
PA4
PA5
PA6
PA7
PA8
PA9
PA10
PA11
PA12
PA13
PA14
PA15
PA16
PA17
PA18
PA19
PA20
PA21
PA22
PA23
PA24
PA25
mm c mc f m c vc gr
d mc
Bioturbation Index
1 2 3 4 5

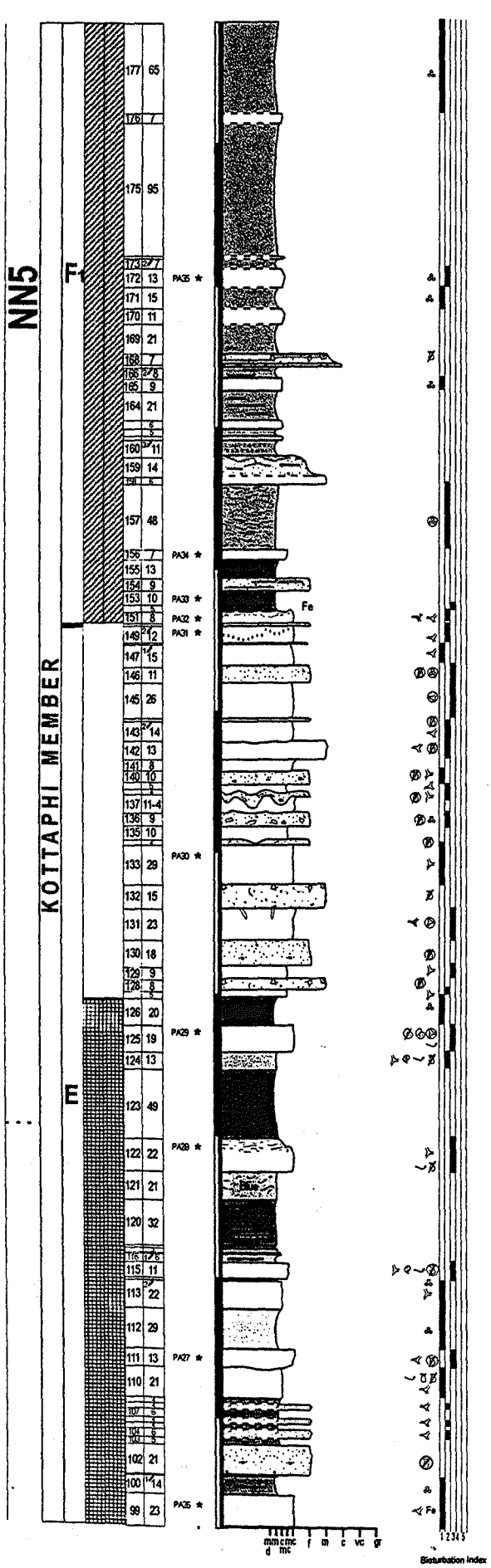
NN5
KOTTAPHI MEMBER
T
M
PA35
PA34
PA33
PA32
PA31
PA30
PA29
PA28
PA27
PA25
Fe
mm cmc f m c vc gr
d mc
1 2 3 4 5
Bioturbation Index

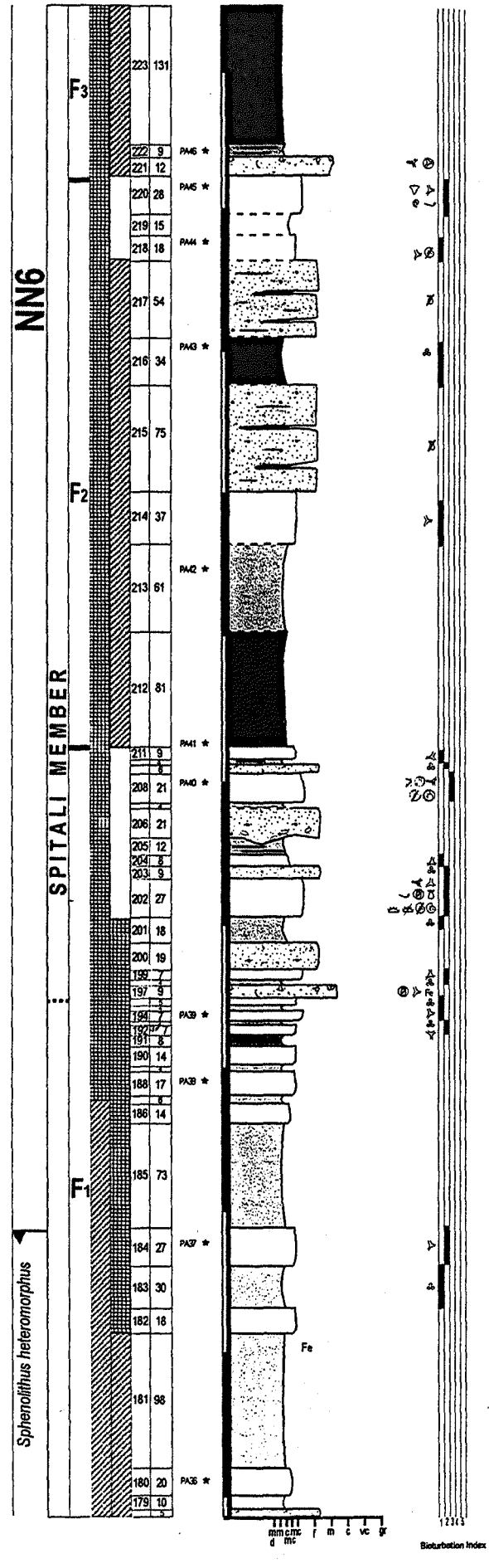
NN6
SPITALI MEMBER
F3
F2
F1
Sphenolithus heteromorphus
PA46
PA45
PA44
PA43
PA42
PA41
PA40
PA39
PA38
PA37
PA36
Fe
mm cmc f m c vc gr
d mc
1 2 3 4 5
Bioturbation Index

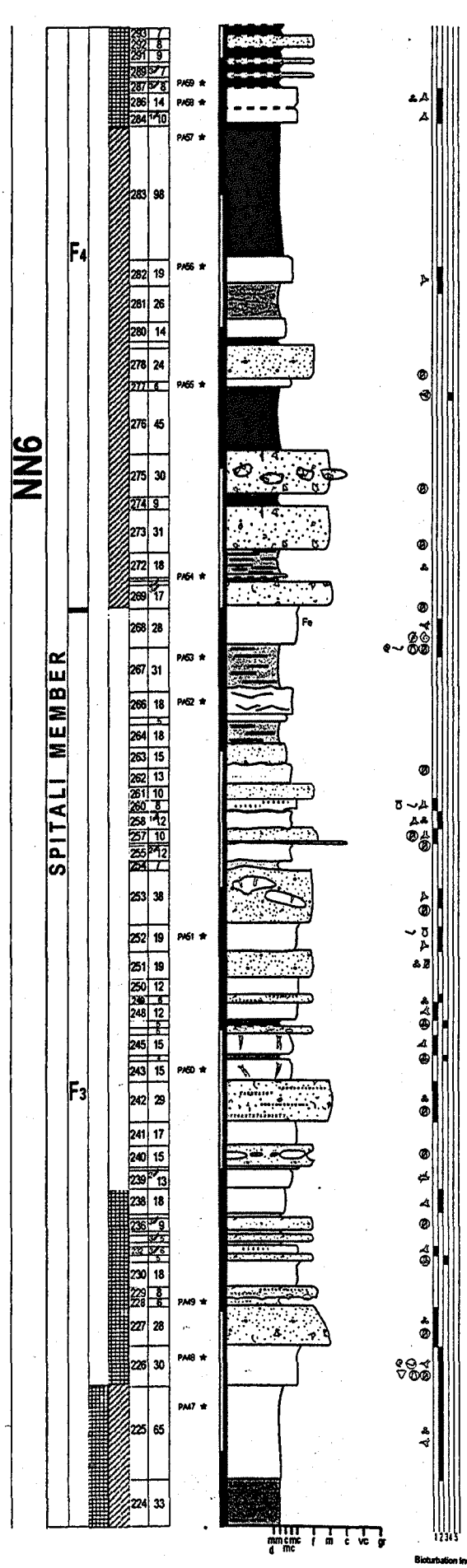
NN6
SPITALI MEMBER
F4
F3
PA69
PA58
PA57
PA56
PA55
PA54
PA53
PA52
PA51
PA50
PA49
PA48
PA47
Fe
mm cmc mc f m c vc gr
Bioturbation Index

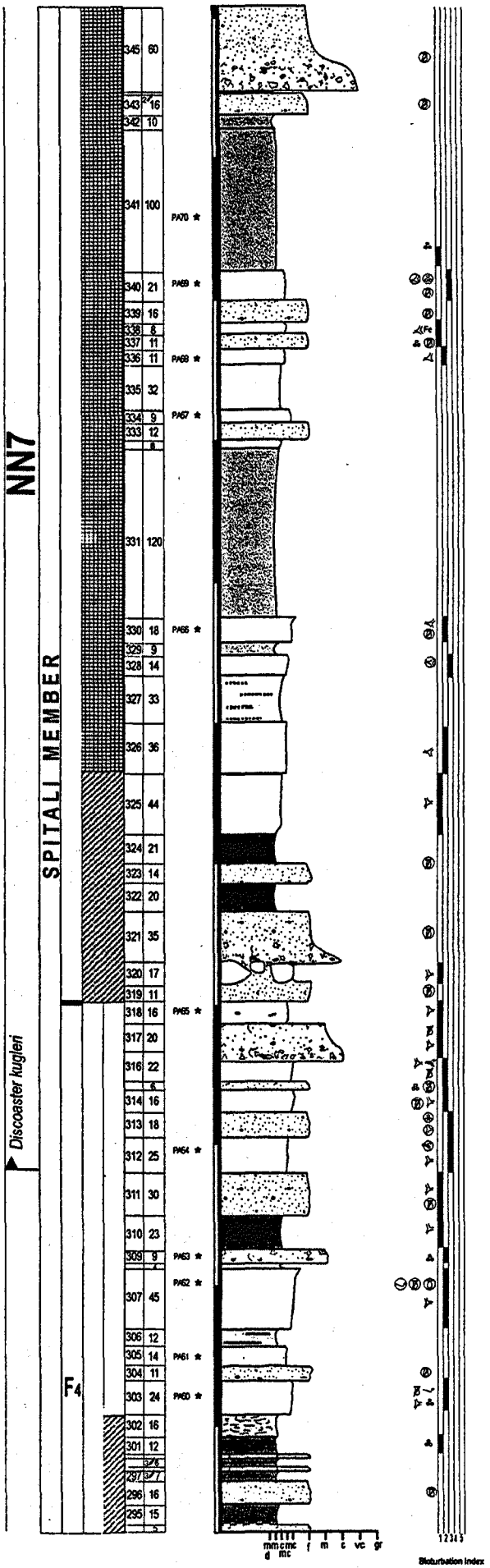
NN7
SPITALI MEMBER
Discoaster kugleri
F4
PA70
PA69
PA68
PA67
PA66
PA65
PA64
PA63
PA62
PA61
PA60
mm cmc mc f m c vc gr
Bioturbation Index

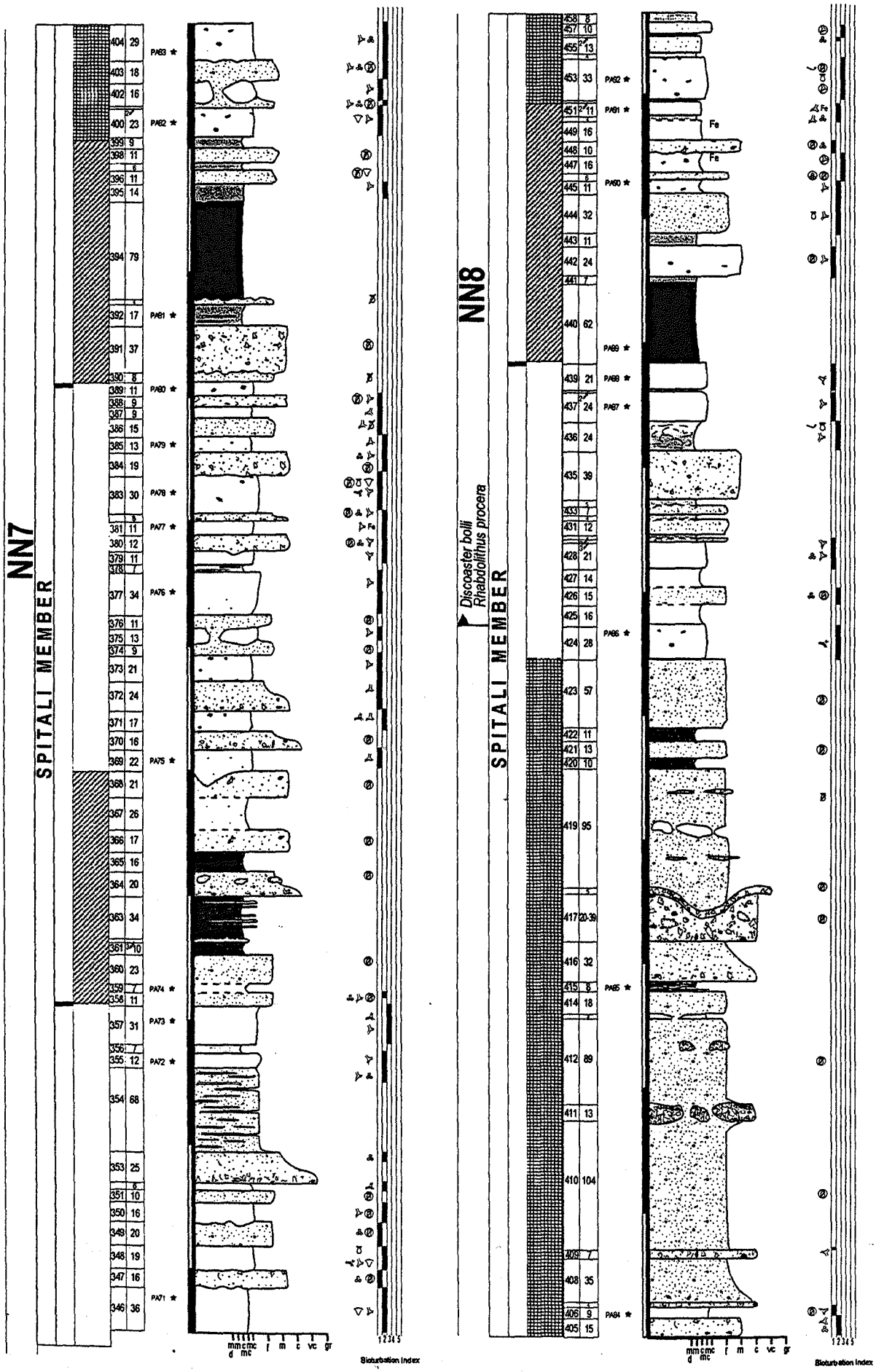
NN7
SPITALI MEMBER
NN8
SPITALI MEMBER
Discoaster bolli
Rhabdolithus procera
Fe
mm cmc f m c vc gr
d mc
Bioturbation Index
1 2 3 4 5

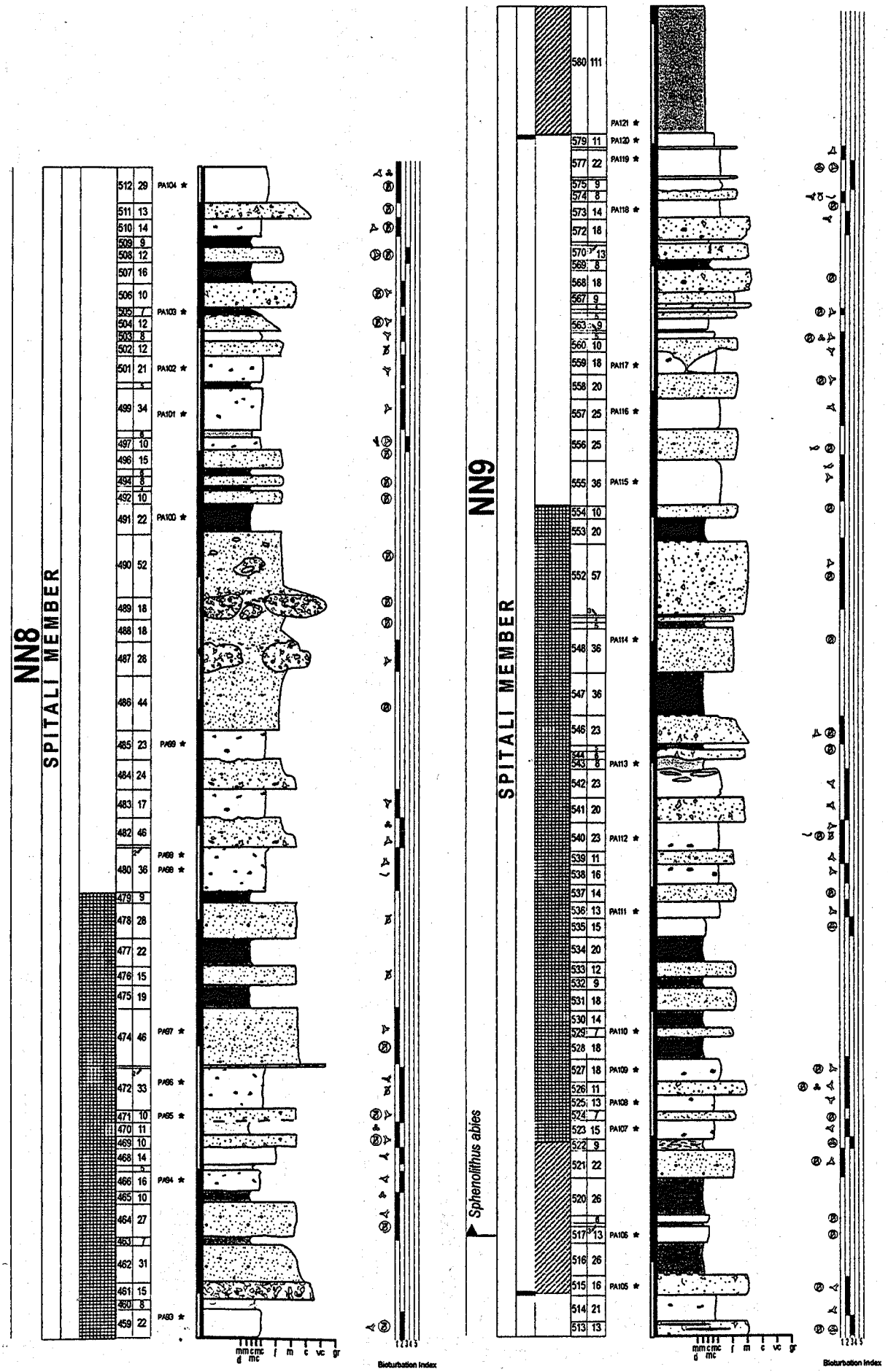
NN8
SPITALI MEMBER
512 29 PA104
511 13
510 14
509 9
508 12
507 16
506 10
505 7 PA103
504 12
503 8
502 12
501 21 PA102
499 34 PA101
497 10
496 15
494 8
492 10
491 22 PA100
490 52
489 18
488 18
487 28
486 44
485 23 PA99
484 24
483 17
482 46
PA99
480 36 PA98
479 9
478 28
477 22
476 15
475 19
474 46 PA97
472 33 PA96
471 10 PA95
470 11
469 10
468 14
466 16 PA94
465 10
464 27
463 7
462 31
461 15
460 8
459 22 PA93
mm c mc f m c vc gr
d mc
Bioturbation Index
1 2 3 4 5
NN9
SPITALI MEMBER
Sphenolithus abies
580 111
PA121
579 11 PA120
577 22 PA119
575 9
574 8
573 14 PA118
572 18
570 13
569 8
568 18
567 9
563 9
560 10
559 18 PA117
558 20
557 25 PA116
556 25
555 36 PA115
554 10
553 20
552 57
PA114
548 36
547 36
546 23
PA113
543 8
542 23
541 20
540 23 PA112
539 11
538 16
537 14
536 13 PA111
535 15
534 20
533 12
532 9
531 18
530 14
529 7 PA110
528 18
527 18 PA109
526 11
525 13 PA108
524 7
523 15 PA107
522 9
521 22
520 26
517 13 PA106
516 26
515 16 PA105
514 21
513 13
mm c mc f m c vc gr
d mc
Bioturbation Index
1 2 3 4 5

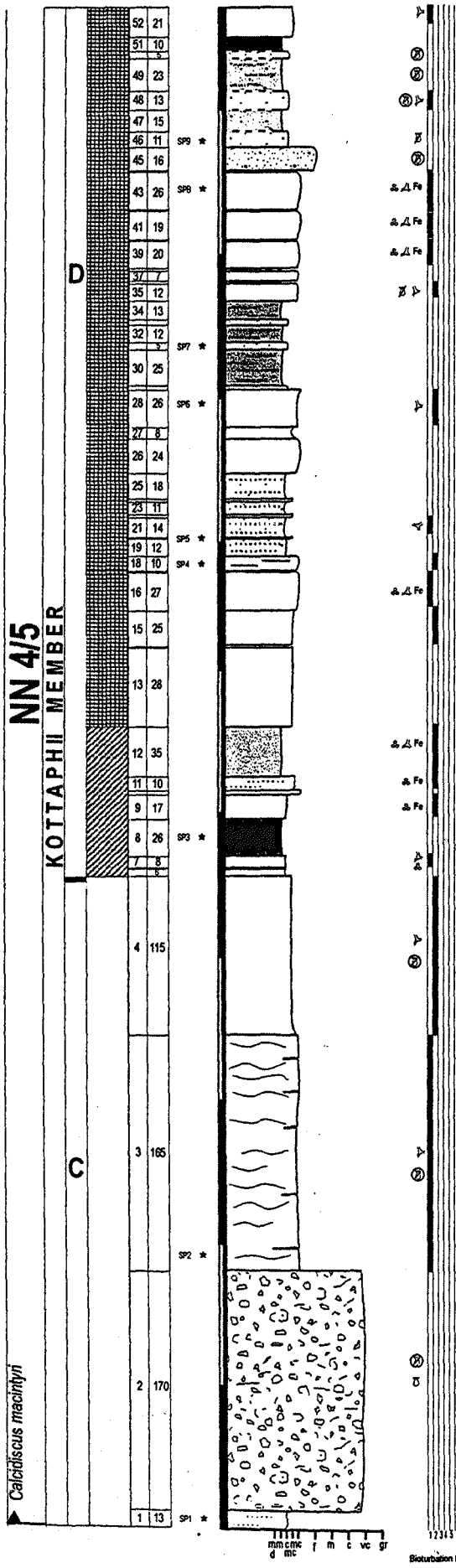
NN 4/5
KOTTAPHII MEMBER
D
C
Calcidiscus macintyri
52 21
51 10
49 23
48 13
47 15
46 11 SP9
45 16
43 26 SP8
41 19
39 20
37 7
35 12
34 13
32 12
30 25 SP7
28 26 SP6
27 8
26 24
25 18
23 11
21 14 SP5
19 12
18 10 SP4
16 27
15 25
13 28
12 35
11 10
9 17
8 26 SP3
7 8
4 115
3 165
SP2
2 170
1 13 SP1
mm c mc d mc f m c vc gr
Bioturbation Index
1 2 3 4 5

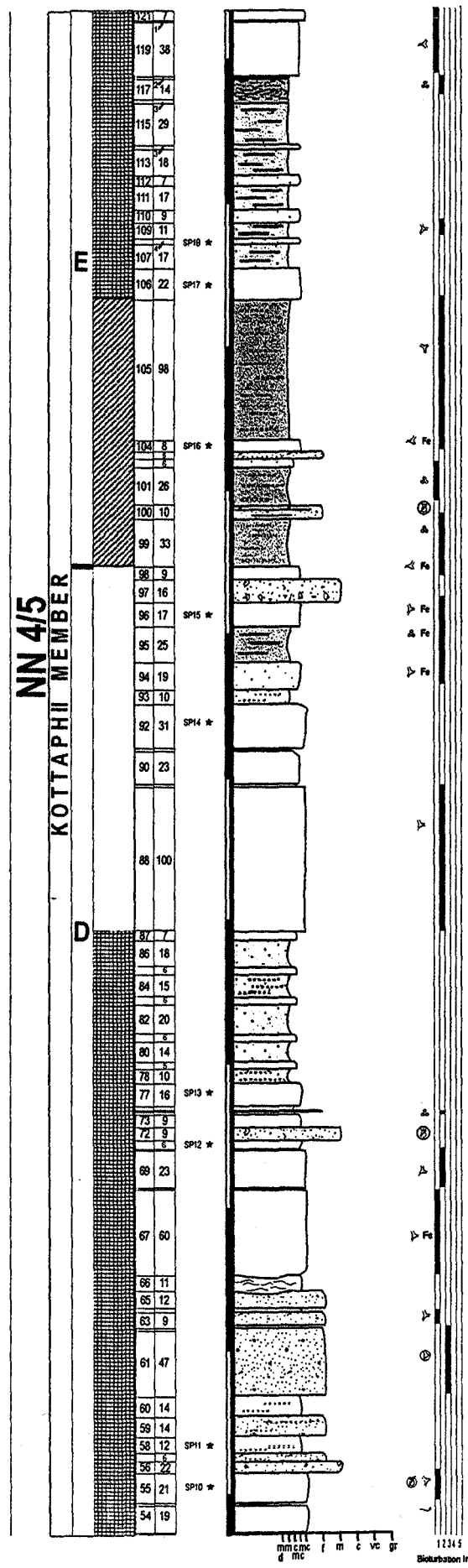
NN 4/5
KOTTAPHII MEMBER
m
D
121 7
119 38
117 14
115 29
113 18
112 7
111 17
110 9
109 11 SP18
107 17
106 22 SP17
105 98
104 8 SP16
101 26
100 10
99 33
98 9
97 16
96 17 SP15
95 25
94 19
93 10
92 31 SP14
90 23
88 100
87 7
86 18
84 15
82 20
80 14
78 10
77 16 SP13
73 9
72 9 SP12
69 23
67 60
66 11
65 12
63 9
61 47
60 14
59 14
58 12 SP11
56 22
55 21 SP10
54 19
mm c mc d mc f m c vc gr
Bioturbation Index
1 2 3 4 5

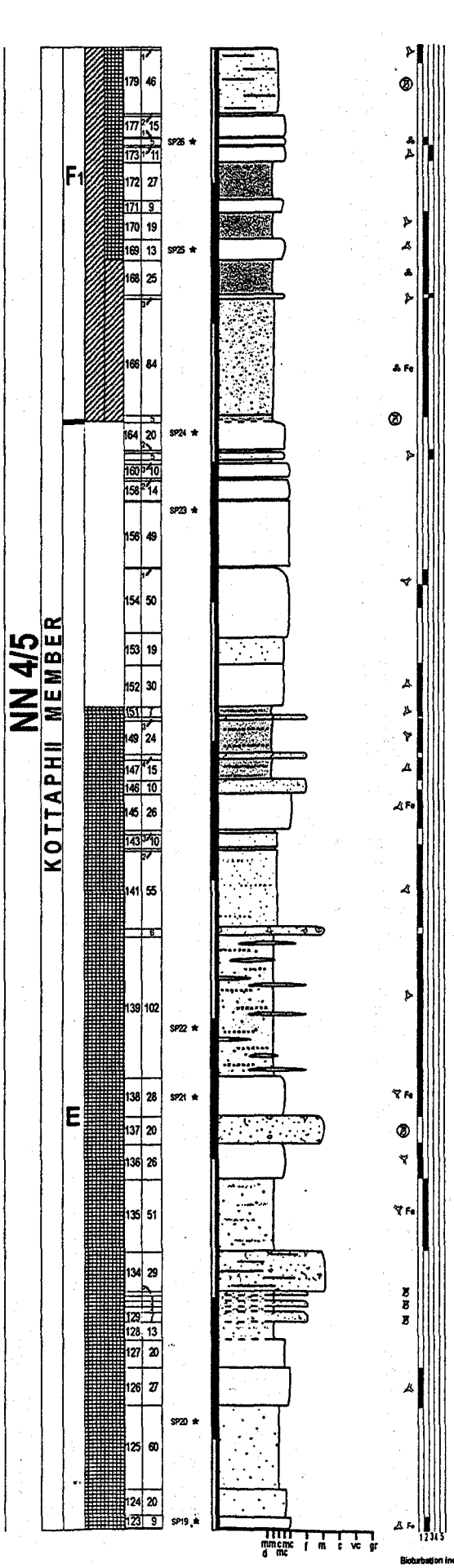
NN 4/5
KOTTAPHII MEMBER
F1
m
179 46
177 15
173 11
172 27
171 9
170 19
169 13
168 25
166 84
164 20
160 10
158 14
156 49
154 50
153 19
152 30
151 7
149 24
147 15
146 10
145 26
143 10
141 55
139 102
138 28
137 20
136 26
135 51
134 29
129 7
128 13
127 20
126 27
125 60
124 20
123 9
SP26 ★
SP25 ★
SP24 ★
SP23 ★
SP22 ★
SP21 ★
SP20 ★
SP19 ★
Fe
mm c mc f m c vc gr
d mc
1 2 3 4 5
Bioturbation Index

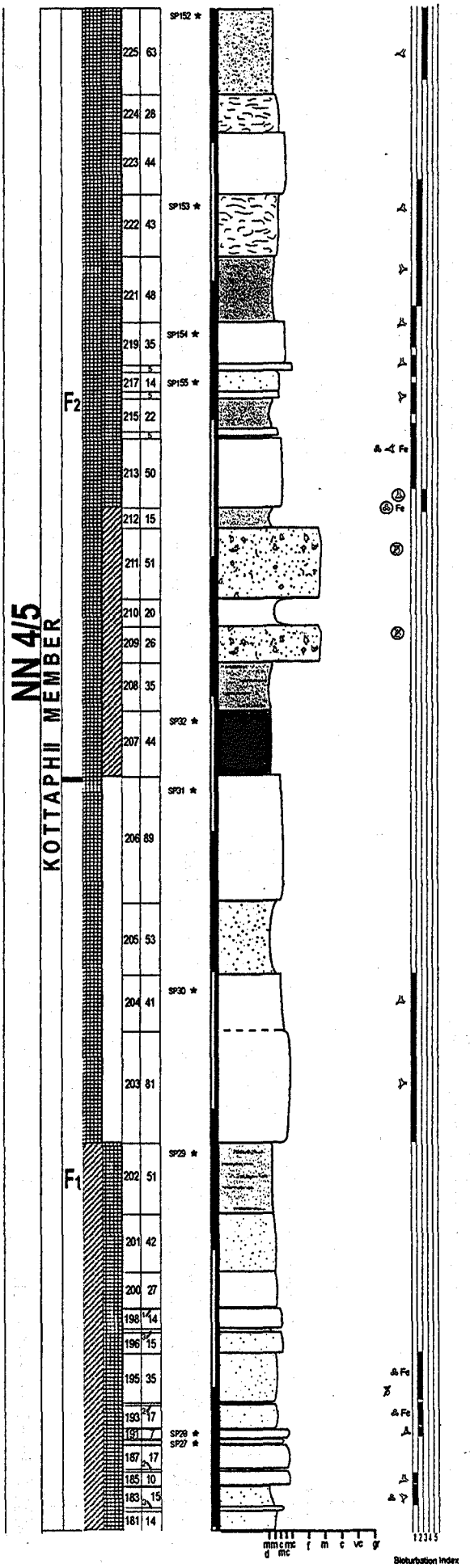
NN 4/5
KOTTAPHII MEMBER
F2
F1
225 63
224 28
223 44
222 43
221 48
219 35
217 14
215 22
213 50
212 15
211 51
210 20
209 26
208 35
207 44
206 89
205 53
204 41
203 81
202 51
201 42
200 27
198 14
196 15
195 35
193 17
191 7
187 17
185 10
183 15
181 14
SP152 ★
SP153 ★
SP154 ★
SP155 ★
SP32 ★
SP31 ★
SP30 ★
SP29 ★
SP28 ★
SP27 ★
Fe
mm c mc f m c vc gr
g mc
1 2 3 4 5
Bioturbation Index

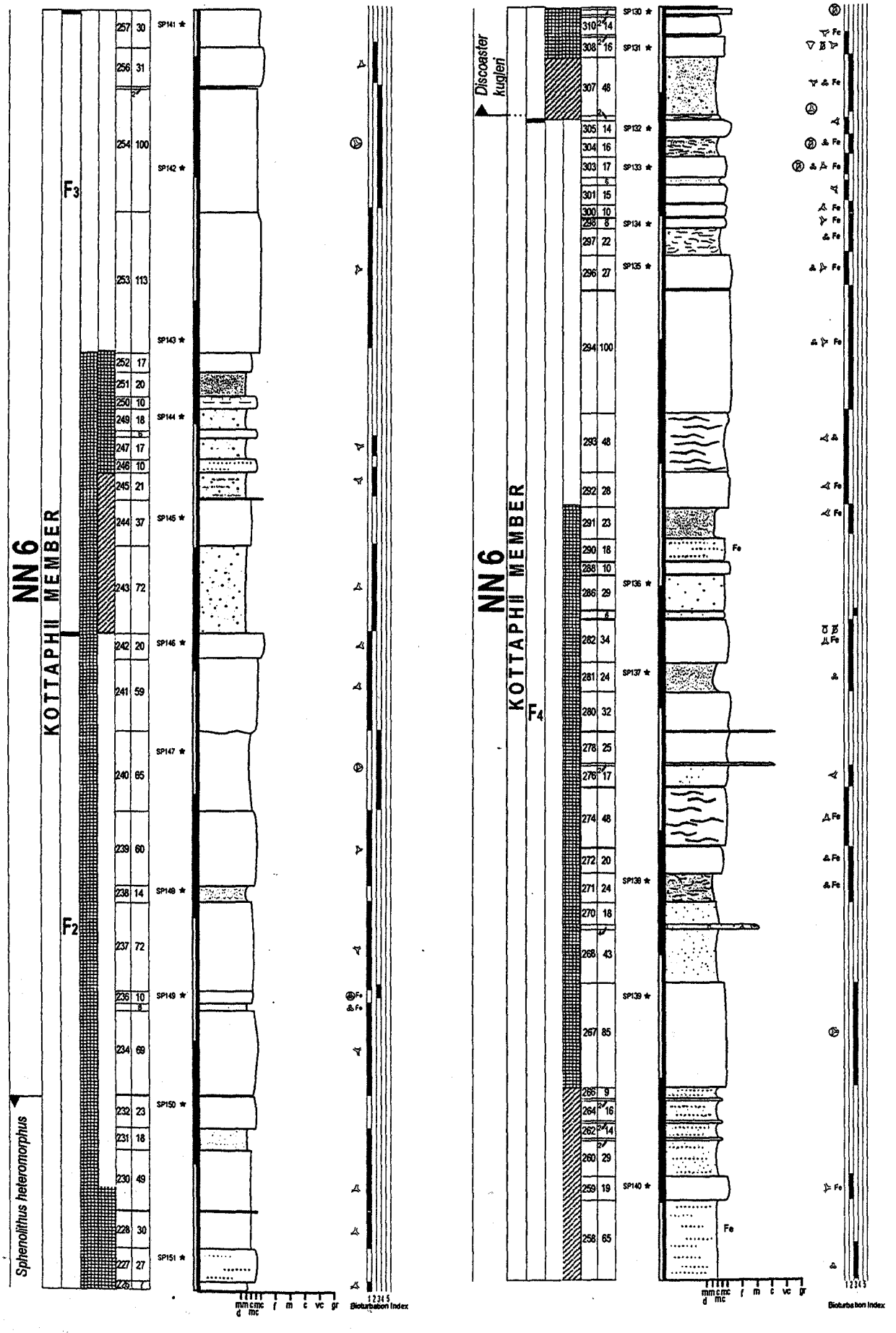
NN6
KOTTAPHII MEMBER
F3
F2
F4
Sphenolithus heteromorphus
Discoaster kugleri
Fe
mm c mc f m c vc gr
d mc
1 2 3 4 5
Bioturbation Index

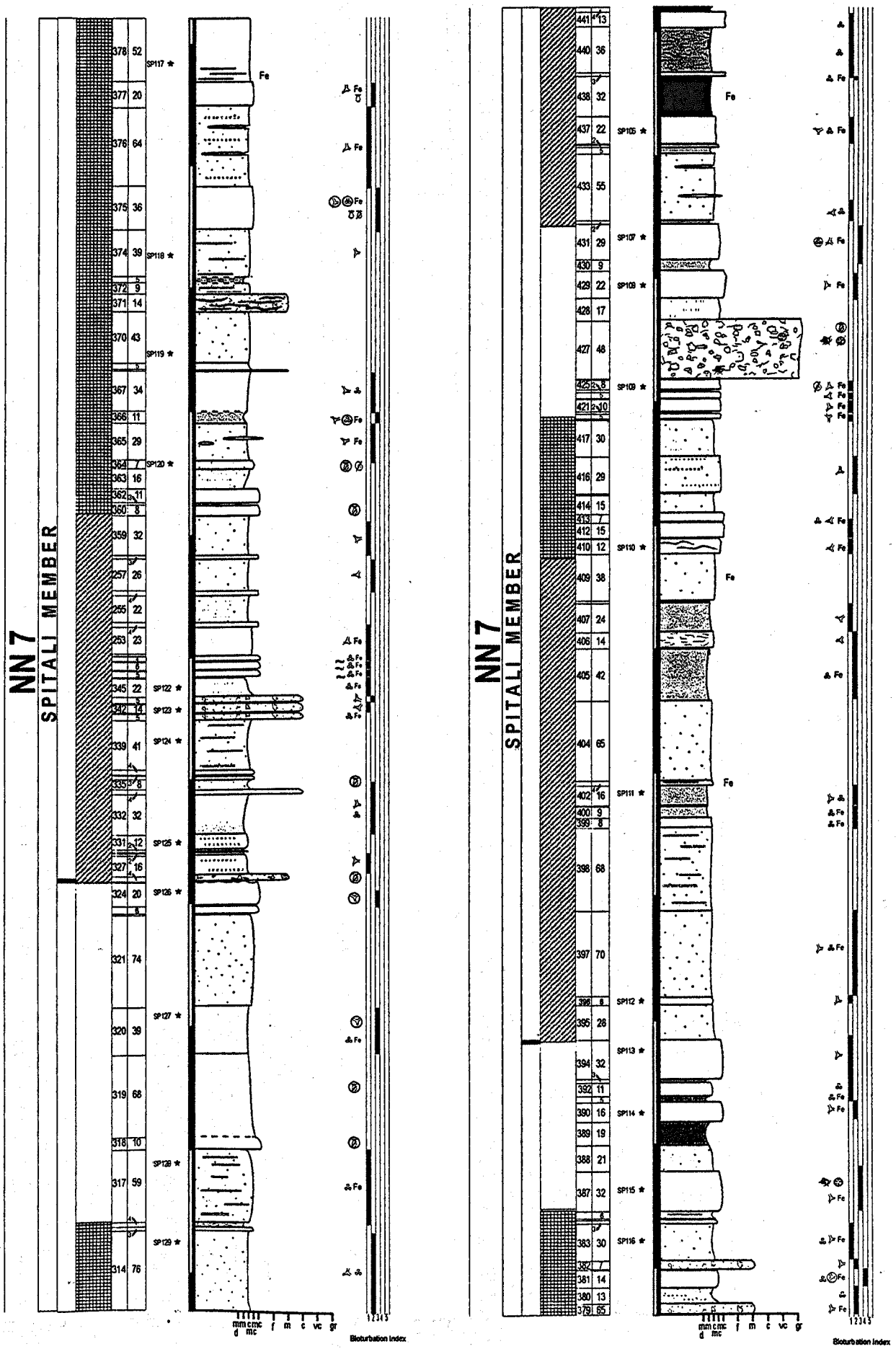
NN7
SPITALI MEMBER
mm c mc f m c vc gr
d mc
Bioturbation Index
1 2 3 4 5

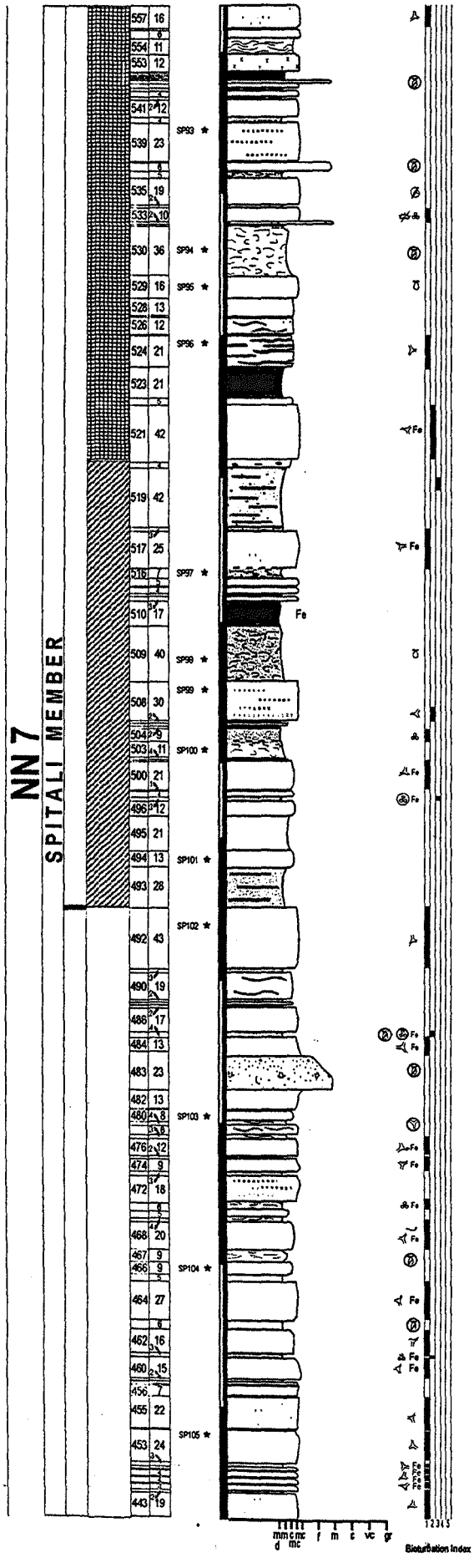
NN 7
SPITALI MEMBER
mm c mc f m c vc gr
d mc
Bioturbation Index

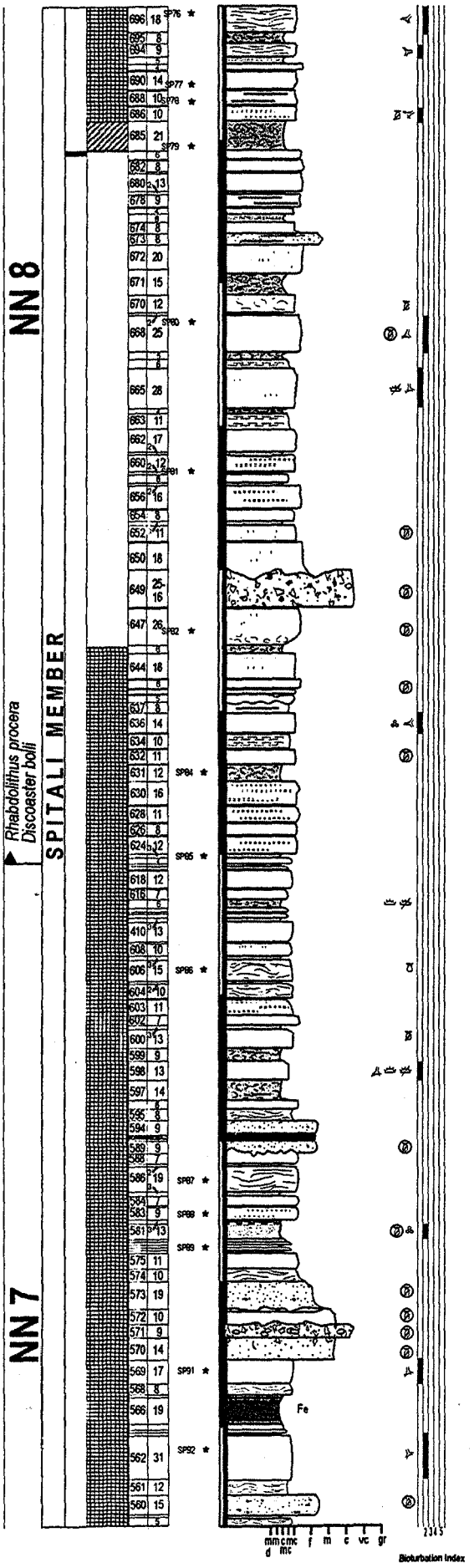
NN 8
NN 7
SPITALI MEMBER
Rhabdolithus procera
Discoaster bolii
Fe
mm c mc f m c vc gr
d mc
Bioturbation Index

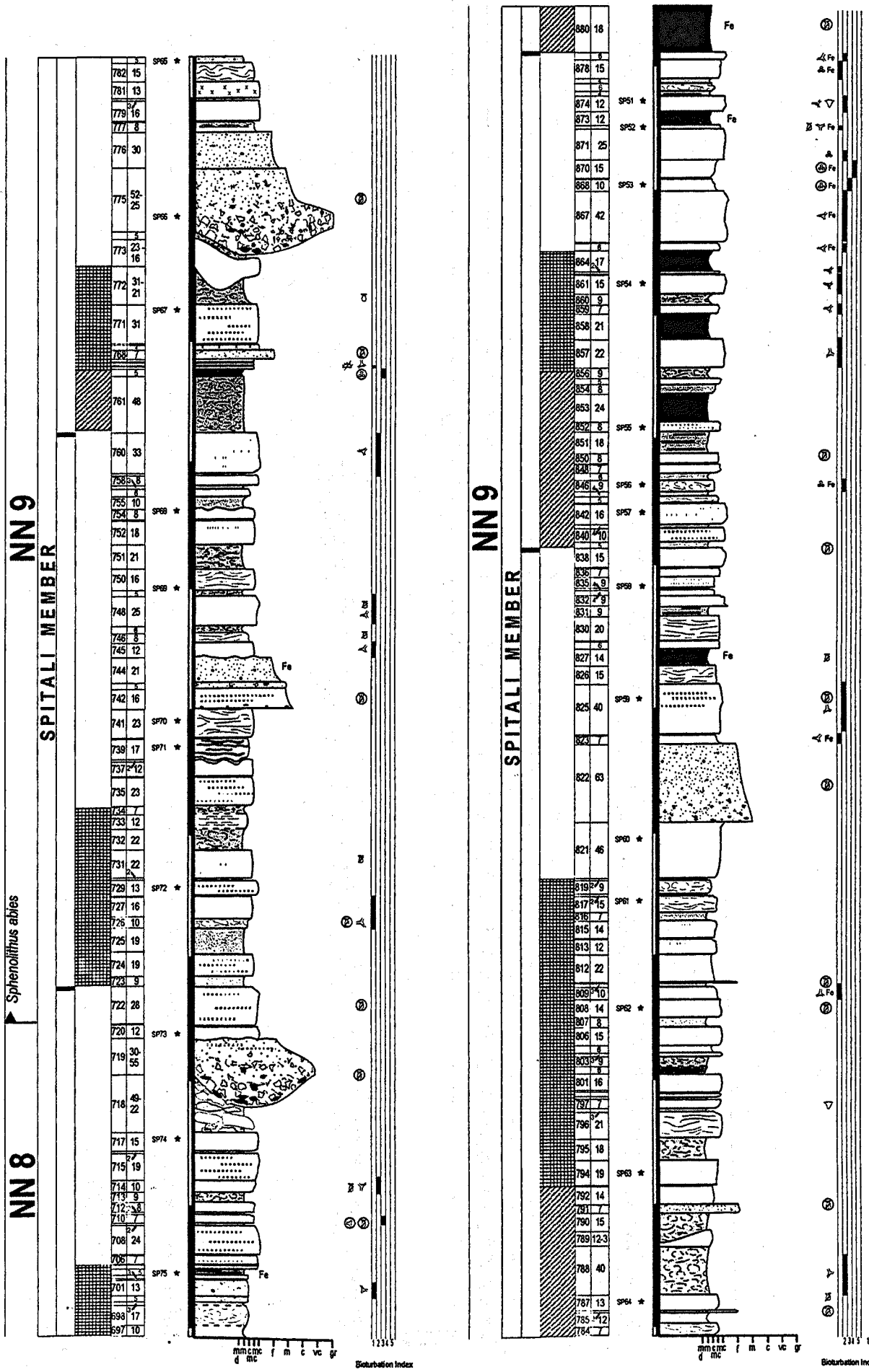
NN 8
NN 9
SPITALI MEMBER
Sphenolithus abies
SP65
SP66
SP67
SP68
SP69
SP70
SP71
SP72
SP73
SP74
SP75
SP51
SP52
SP53
SP54
SP55
SP56
SP57
SP58
SP59
SP60
SP61
SP62
SP63
SP64
Fe
mm c mc f m c vc gr
d mc
Bioturbation Index

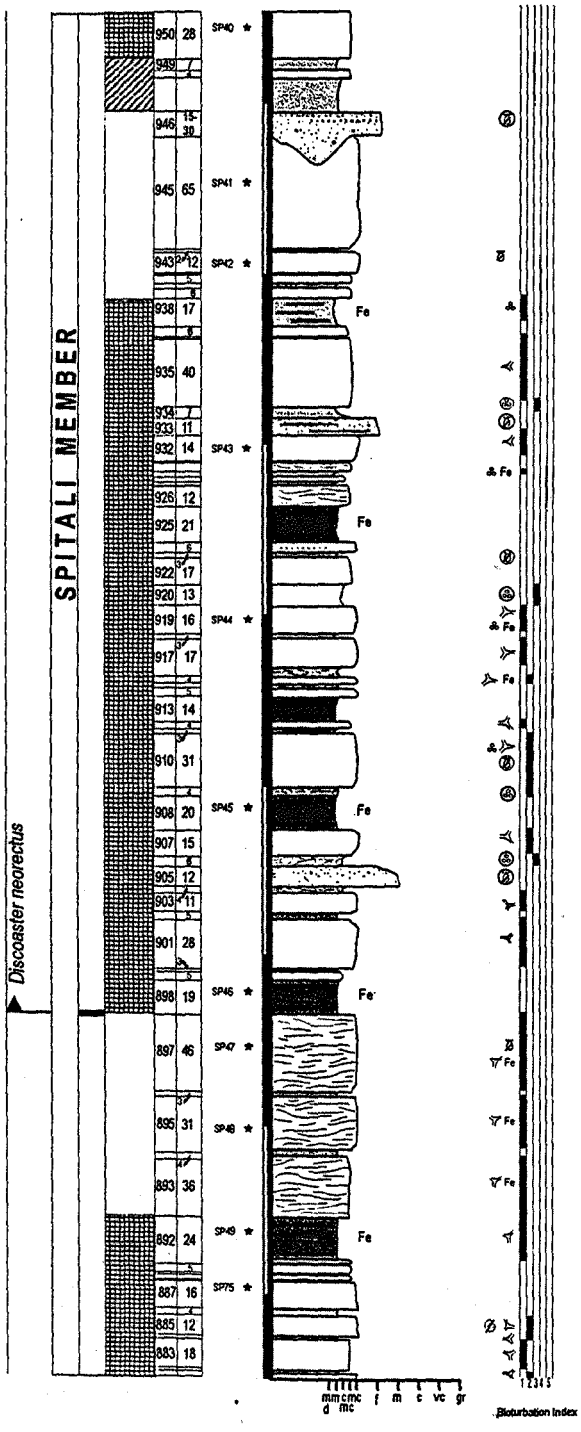
SPITALI MEMBER
Discoaster neorectus
950 28
949
946 15-30
945 65
943 12
938 17
935 40
934
933 11
932 14
926 12
925 21
922 17
920 13
919 16
917 17
913 14
910 31
908 20
907 15
905 12
903 11
901 28
898 19
897 46
895 31
893 36
892 24
887 16
885 12
883 18
SP40
SP41
SP42
SP43
SP44
SP45
SP46
SP47
SP48
SP49
SP75
Fe
mm c mc f m c vc gr
d mc
Bioturbation Index
1 2 3 4 5

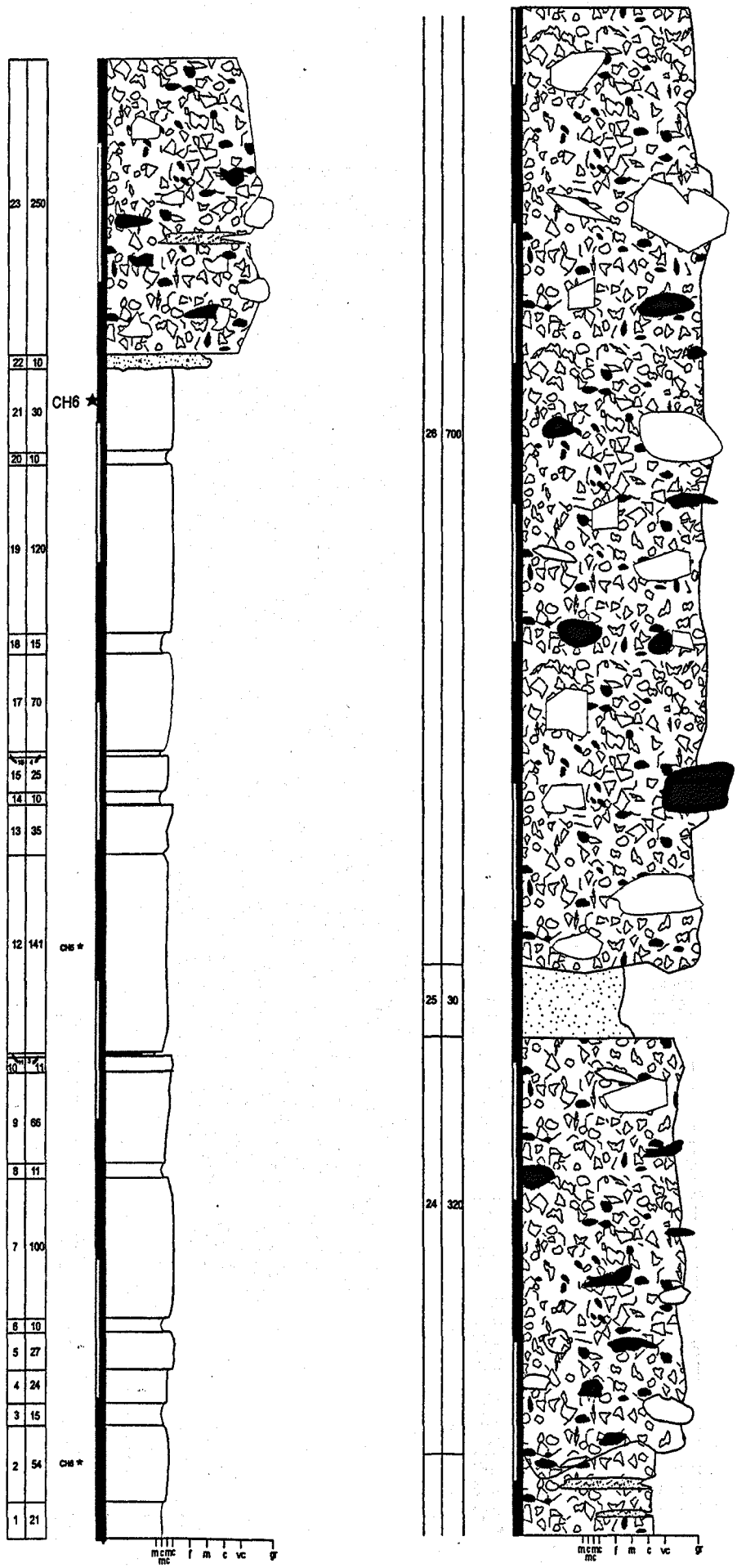
23 250
22 10
21 30
CH6
20 10
19 120
18 15
17 70
16 4
15 25
14 10
13 35
12 141
CH5
10 11
9 65
8 11
7 100
6 10
5 27
4 24
3 15
2 54
CH4
1 21
mc mc mc f m c vc gr
26 700
25 30
24 320
mc mc mc f m c vc gr

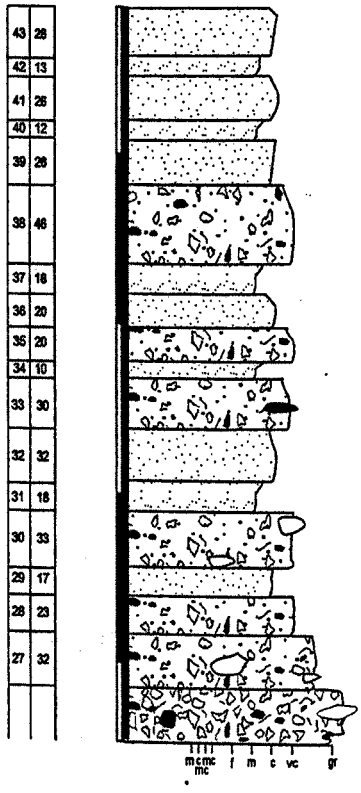
43 28
42 13
41 26
40 12
39 28
38 46
37 16
36 20
35 20
34 10
33 30
32 32
31 16
30 33
29 17
28 23
27 32
m c mc mc f m c vc gr

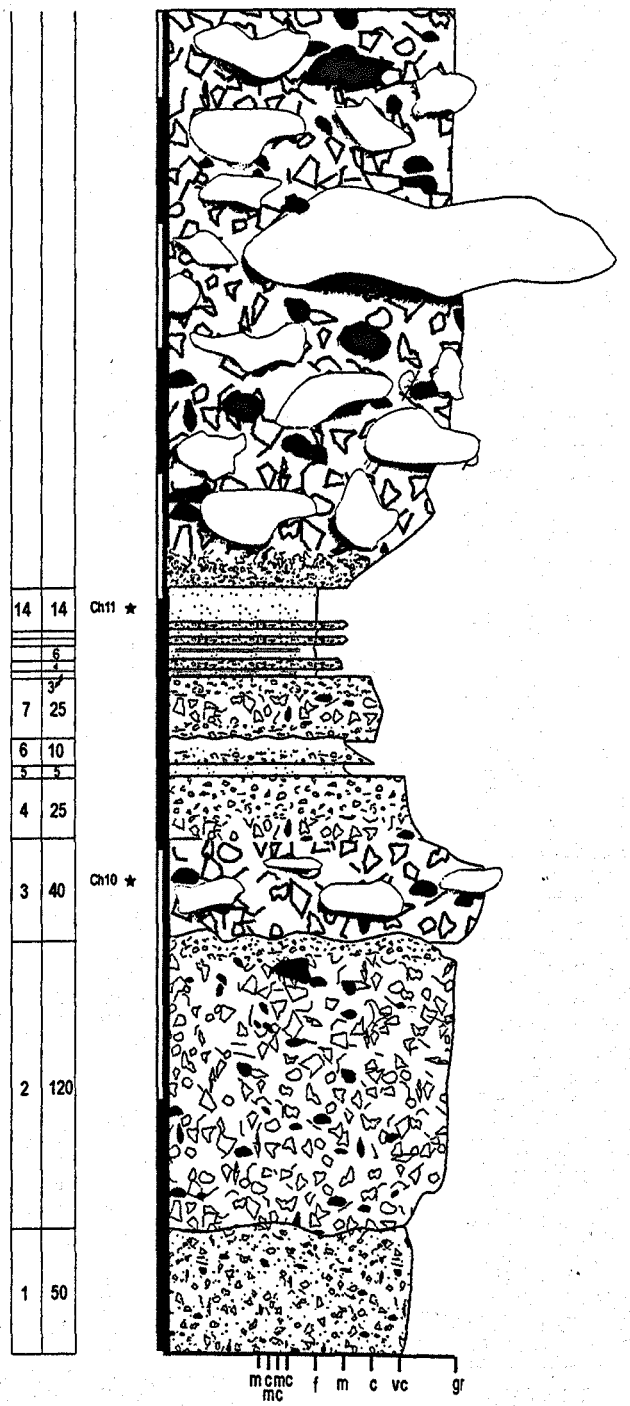
14
14
Ch11 ★
6
4
3
7
25
6
10
5
5
4
25
3
40
Ch10 ★
2
120
1
50
m c mc
mc
f
m
c
vc
gr

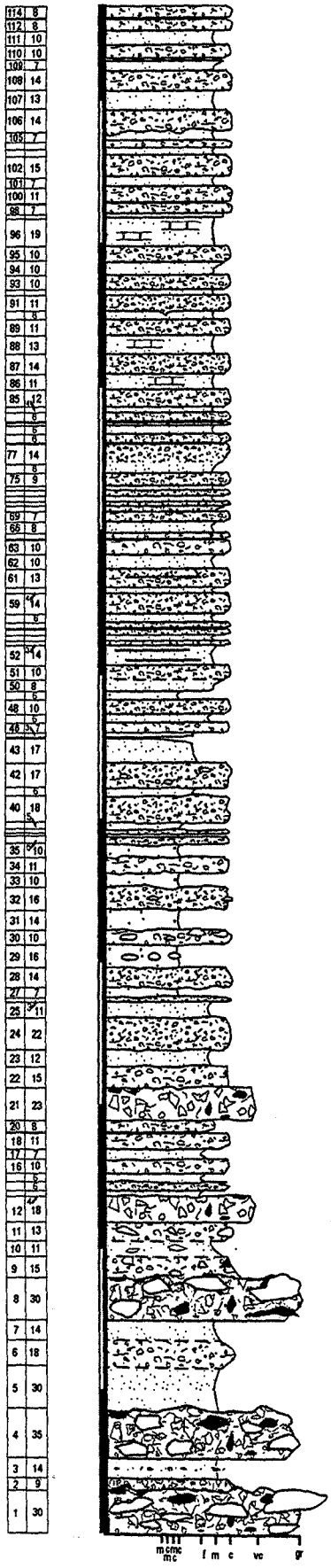
114 8
112 8
111 10
110 10
109 7
108 14
107 13
106 14
105 7
102 15
101 7
100 11
98 7
96 19
95 10
94 10
93 10
91 11
89 11
88 13
87 14
86 11
85 12
77 14
75 9
69 7
65 8
63 10
62 10
61 13
59 14
52 14
51 10
50 8
48 10
43 17
42 17
40 18
35 10
34 11
33 10
32 16
31 14
30 10
29 16
28 14
27 7
25 11
24 22
23 12
22 15
21 23
20 8
18 11
17 7
16 10
12 18
11 13
10 11
9 15
8 30
7 14
6 18
5 30
4 35
3 14
2 9
1 30
m c mc mc f m c vc gr

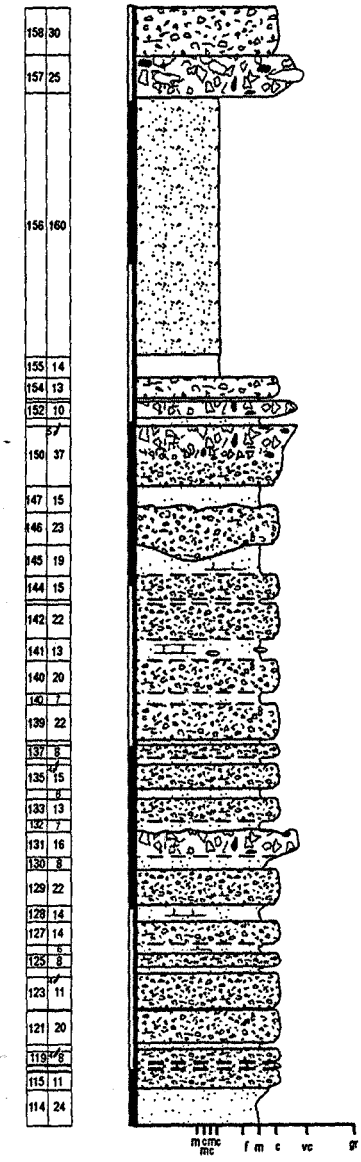
158 30
157 25
156 160
155 14
154 13
152 10
150 37
147 15
146 23
145 19
144 15
142 22
141 13
140 20
140 7
139 22
137 8
135 15
133 13
132 7
131 16
130 8
129 22
128 14
127 14
125 8
123 11
121 20
119 6
115 11
114 24
m c mc mc f m c vc gr

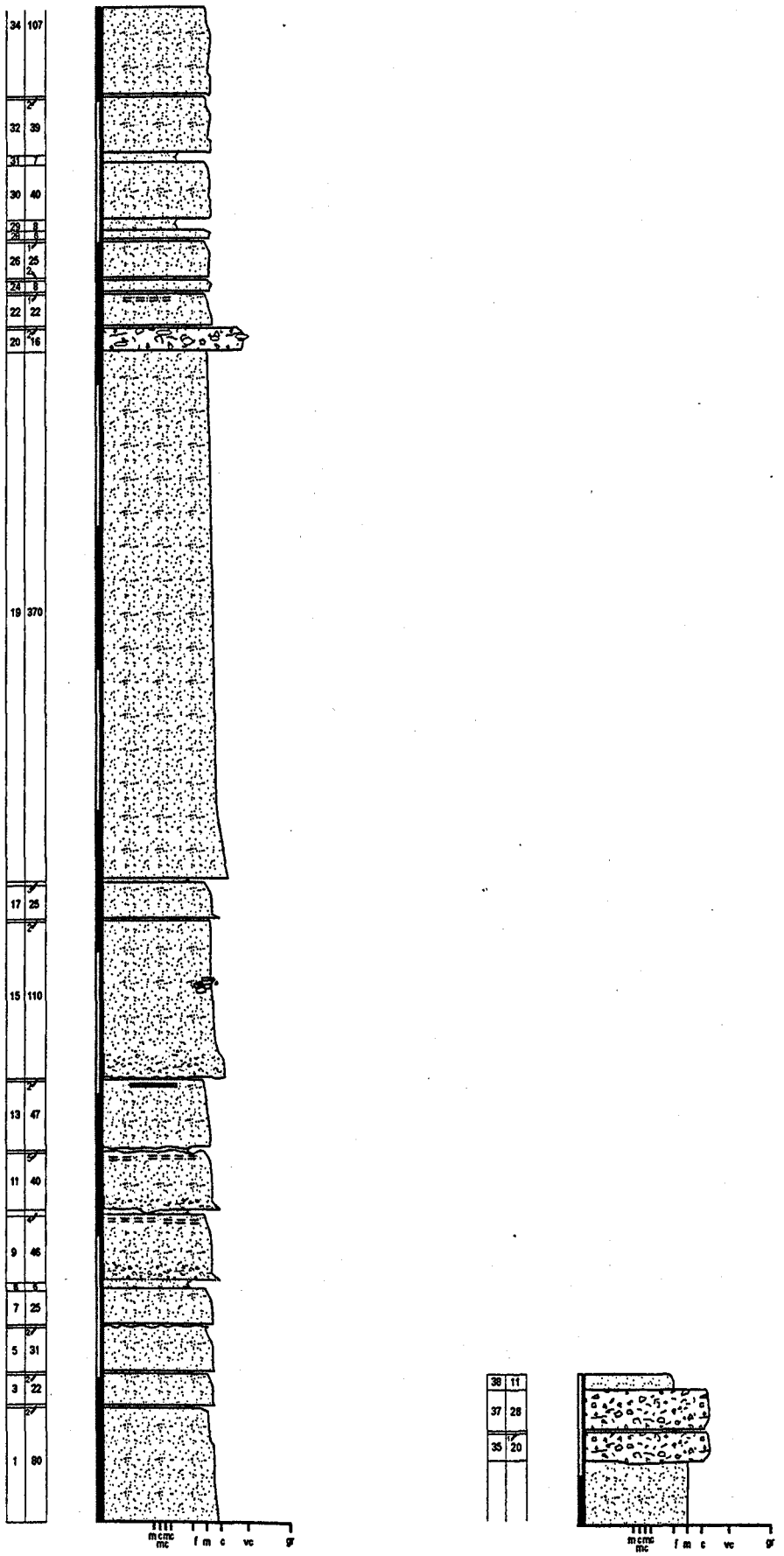
34 107
32 39
31 7
30 40
29 8
28 6
26 25
24 8
22 22
20 16
19 370
17 25
15 110
13 47
11 40
9 46
8 6
7 25
5 31
3 22
1 80
38 11
37 28
35 20
mc vc gr

APPENDIX B

ANALYTICAL TECHNIQUES AND RAW DATA

B.1 Raw data and technique for determining wt.% clay.

To determine wt. % clay (non-carbonate) dry and clean samples are broken in to ~1 cm^3 fragments to increase the surface area. The fragments were then accurately weighed and placed in a glass beaker in a fume cupboard. 40 % HCl acid is gradually poured in to the beakers, to avoid excessive froth due to carbonate dissolution. When frothing subsides add more HCl was added until all the carbonate is dissolved. Residues are then filtered (with the weight of the dry filter paper recorded for each sample). Residues should then be dried again, after which, the residue and the filter paper are weighed, minus the weight of the dry filter paper, previously recorded. The wt. % clay is then the percentage of the residue to the original sample.

Sample	Original weight (g)	Residue weight (g)	% Clay (non-carbonate)
Marl	59.651	17.322	29.0
Cemented-marl	57.492	11.633	20.2
Marly-chalk	56.08	7.3	13.0
Foraminiferal chalk	54.073	3.059	5.7
KHC-F	29.5	1.78	6.0
KHC-E	30.5	2.05	6.7
KHC-D	29.8	1.87	6.3
KHC-C	20.48	2.29	11.2
KHC-B	14.8	3.59	24.3
KHC-A	17.8	3.56	20.0
KHC-10	16.3	2.87	17.6
KHC-9	17.58	2.94	16.7
KHC-7	18.1	2.87	15.9
KHC-5	17.3	4.22	24.4
KHC-3	12	3.54	29.5
KHC-1	14.5	3.90	26.9

B.2 Sample preparation for nannoplankton biostratigraphy

For biostratigraphic analysis, smear-slides were prepared in the manner outlined by (Perch-Nielsen (1885). To prepare a smear-slide the outer layer of a section of the rock sample is scraped (with a scalpel) away, to avoid contamination. From a fresh surface more rock is scraped and the residue is collected on a filter paper. In order to remove the coarser fraction the residue is placed in a 5 ml sample vial with water, shaken vigorously and left to settle for about a minute. The suspended fraction is then drawn off using a disposable pipette into a second vial containing a few drops of cellulose, which acts as a dispersant, and shaken further to homogenise the sample. The suspended residue is then again draw off using a pipette and piped on to a standard glass cover slip, placed on a warm hotplate. Once dry, Canada balm/areldite is deposited on to the cover slip, which is transferred on to standard glass microscope slide. Once completely dry the slide is ready for analysis using an optical microscope.

B.3 Raw data for spectral analysis, and power spectra.

Raw data used for spectral analysis, based on bed thickness and lithology, for Kottaphi Hill. Positions of KOT SEC 1-8 are indicated on Figure 4.2, Chapter 4.

Lithology code	1 = Marl	2 = Cemented-Marl	3 = Marly-chalk	4 = Chalk

KOT SEC 1			KOT SEC 1 cont.			KOT SEC 3 cont.			KOT SEC 4 cont.		
Bed No.	Thick -ness (cm)	Litho. Code	Bed No.	Thick -ness (cm)	Litho. Code	Bed No.	Thick -ness (cm)	Litho. Code	Bed No.	Thick -ness (cm)	Litho. Code
56	11	2	9	44	3	114	18	4	129	32	2
55	24	4	8	17	2	113	11	2	128	7	1
54	9	2	7	23	3	112	20	3	127	35	2
53	12	3	6	16	2	111	40	2	126	44	1
52	14	1	5	13	3	110	11	3	125	24	2
51	11	3	4	40	2	109	14	2	124	3	2
50	10	1	3	25	3	108	14	3	KOT SEC 5		
49	11	4	2	16	2	107	2	2	213	10	1
48	5	1	1	38	3	106	14	3	212	25	2
47	10	3	KOT SEC 2			105	7	2	211	10	1
46	15	2	83	64	3	104	26	3	210	19	4
45	12	3	82	20	4	103	17	1	209	6	2
44	72	1	81	15	1	102	8	3	208	26	4
43	24	3	80	36	4	101	18	3	207	2	2
42	66	1	79	9	2	100	13	4	206	17	3
41	12	2	78	41	1	99	2	2	205	5	2
40	12	1	77	18	3	98	18	4	204	14	3
39	15	2	76	18	1	97	23	1	203	19	3
38	17	1	75	22	3	96	13	3	202	10	2
37	15	2	74	37	1	95	15	1	201	39	1
36	32	1	73	16	3	94	20	4	200	5	2
35	15	2	72	32	1	93	24	2	199	9	3
34	25	1	71	40	4	92	11	4	198	1	2
33	17	3	70	17	1	91	16	1	197	26	4
32	30	1	69	22	4	90	26	4	196	8	2
31	31	3	68	10	2	89	1	1	195	7	3
30	13	1	67	39	4	88	12	4	194	17	1
29	18	4	66	25	1	87	2	2	193	5	1
28	8	1	65	43	4	86	4	1	192	1	1
27	9	3	64	20	1	85	4	4	191	5	1
26	18	2	63	64	4	84	7	1	190	12	3
25	21	3	62	3	1	KOT SEC 4			189	15	1
24	31	1	61	20	4	144	15	3	188	23	4
23	9	4	60	15	1	143	25	1	187	9	1
22	30	1	59	40	4	142	17	3	186	18	3
21	4	3	58	43	1	141	11	2	185	22	1
20	7	1	57	28	3	140	12	1	184	2	3
19	5	2	KOT SEC 3			139	6	2	183	5	3
18	8	1	123	10	4	138	9	1	182	19	4
17	6	2	122	9	2	137	6	2	181	14	1
16	22	1	121	18	4	136	15	1	180	5	2
15	28	3	120	14	2	135	7	2	179	20	1
14	2	2	119	6	4	134	15	1	178	7	2
13	26	3	118	3	2	133	13	2	177	3	1
12	22	3	117	18	4	132	13	1	176	11	2
11	22	3	116	7	4	131	17	2	175	14	1
10	10	2	115	23	2	130	26	1	174	4	2

KOT SEC 5 cont.		
Bed No.	Thick-ness (cm)	Litho. Code
173	25	1
172	3	2
171	11	1
170	4	2
169	9	1
168	13	2
167	11	1
166	42	4
165	11	2
164	13	4
163	5	2
162	10	3
161	7	2
160	6	4
159	4	1
158	18	3
157	8	1
156	40	3
155	5	2
154	1	2
153	5	2
152	7	3
151	49	4
150	29	2
149	5	2
148	10	2
147	13	3
146	22	3
145	8	1
KOT SEC 6		
243	28	1
242	20	2
241	27	1
240	11	2
239	70	1
238	14	3
237	3	2
236	14	3
235	11	2
234	18	2
233	5	4
232	23	1
231	10	2
230	15	1
229	9	2
228	10	1
227	7	2

KOT SEC 6 cont.		
Bed No.	Thick -ness (cm)	Litho. Code
226	7	1
225	27	2
224	13	3
223	1	2
222	16	3
221	2	1
220	10	3
7	2	1
218	32	3
217	29	1
216	24	3
215	7	1
214	24	4
KOT SEC 7		
283	10	4
282	9	3
281	10	4
280	39	2
279	30	4
278	50	4
277	2	2
276	33	4
275	7	3
274	3	1
273	33	3
272	15	4
271	22	3
270	23	4
269	12	3
268	7	2
267	9	1
266	6	4
265	6	3
264	29	1
263	15	3
262	67	4
261	10	2
260	1	1
259	25	2
258	83	4
257	40	3
256	27	4
255	2	1
254	8	3
253	31	4
252	2	1
251	21	4

KOT SEC 7 cont.		
Bed No.	Thick-ness (cm)	Litho. Code
250	39	3
249	2	1
248	8	3
247	6	1
246	7	3
245	72	1
244	18	2
KOT SEC 8		
300	11	3
299	16	2
298	32	3
297	14	1
296	45	4
295	2	1
294	32	4
293	7	2
292	5	1
291	19	3
290	18	2
289	16	3
288	17	1
287	14	3
286	15	1
285	20	2
284	59	1

B.4 Stable oxygen and carbon isotope sample preparation, and analytical methodology

Sample Preparation

In order to retrieve foraminifera, samples were manually broken onto ~2 cm diameter fragments, and placed in an ultrasound bath, for up to 30 hours. A few more resistant samples required soaking in petroleum ether for 1 hour after which, adding boiling water caused further fragmentation, before being placed in the ultrasound bath. Residues were sieved to retrieve the 125-1000 μm fraction, which was returned again to the ultra sound bath for a further hour, before the samples were dried at 50°C ready for picking. The foraminifera showed no sign replacement when examined under an electron microscope, and were considered suitable for isotopic analysis. About 20 individual *G. altispira* were picked for each analytical sample.

Isotope analysis was conducted at NIGL Keyworth under the direction of Baruch Spriro. 0.4 μg of crushed (homogenised) form tests were required for each analysis on a Micromass Optima dual inlet, gas source mass spectrometer, with isocarb attached. Samples are loaded into carrousel with an acid bath containing anhydrous HP_3O_4 at 90°C attached. The whole system is evacuated each sample is then dropped into the acid , the resultant CO_2 is cryogenically cleaned (cold trap with acetone at -90°C) to remove water and any volatile organics. Clean CO_2 is then transferred to the mass spectrometer using liquid nitrogen and analysed against a reference gas.

Corrections made to raw data:

1) Craig (1953) correction for ^{17}O

$\delta^{13}C = 1.0676 \times \delta(45/44) - 0.0338 \times \delta^{18}O$ (approx 6% contribution to mass 45 from ^{17}O).

$\delta^{18}O$=1.0010 x δ(46/44) -0.0021 x $\delta^{13}C$ (0.2% contribution to mass 46 containing ^{13}C and ^{17}O but not ^{18}O)

2) Zero correction (the shift from the preferred value of the standard applied)

The offset derived from the preferred standard value and the mean $\delta^{13}C$ and $\delta^{18}O$ values from all standards in any single run is applied to all unknowns in that run.

3) Fractionation factor

Application of fractionation factor to derive the solid value from the gas value. On reaction with the acid $CaCo_3$ liberates 2 moles of CO_2, with 1 mole remaining in solution. The fractionation factors correct for the acid bath at 90°C with the following fractionation:

@ 1‰ / 30°C = 0.04 ‰ / °C = result + (90-25.2) x 0.04

R = result +2.6‰

To report stable isotope ratios to the standard PDB notation

$$\delta^{"}O \text{ PDB solid} = \left\{\frac{R + 1000}{1.01025}\right\} - 1000$$

Where **R** is the fractionation factor (3), and 1.01025 is the fractionation factor for calcite at 25.2°C

Stable oxygen and carbon isotope data

Kottaphi Hill

Age Ma	Sample	$\delta^{13}C$ ‰ PDB	$\delta^{18}O$ ‰ PDB
11.56	KH-IS-32A	1.96	-0.52
11.80	KH-IS.32	1.48	0.33
11.95	KH-IS-31A	1.66	-0.70
12.10	KH-IS.31	1.12	0.72
12.25	KH-IS-30A	1.49	0.10
12.40	KH-IS.30	1.35	0.51
12.55	KH-IS-29A	2.32	-0.55
12.70	KH-IS.29	1.38	0.668
12.85	KH-IS-28A	1.42	0.30
13.00	KH-IS.28	1.39	0.64
13.15	KH-IS-27A	1.09	0.56
13.30	KH-IS.27	1.19	0.1
13.45	KH-IS-26A	1.32	0.20
13.60	KH-IS.26	1.26	0.08
13.75	KH-IS-25A	1.17	0.28
13.90	KH-IS.25	1.81	-0.23
14.05	KH-IS-24A	1.78	-0.57
14.20	KH-IS.24	1.77	0.5
14.35	KH-IS-23A	1.91	-0.47
14.50	KH-IS.23	1.43	-0.01
14.65	KH-IS-22A	1.68	-0.27
14.80	KH-IS.22	1.62	-0.46
14.84	KH-IS.21	2.02	-0.29
14.88	KH-IS-20A	1.98	0.17
14.93	KH-IS.20	1.9	0.42
14.97	KH-IS-19A	1.59	0.10
15.01	KH-IS.19	2.4	-0.36
15.05	KH-IS-18A	1.78	-0.46
15.09	KH-IS.18	2.58	-0.46
15.14	KH-IS-17A	1.94	-0.10
15.18	KH-IS.17	1.17	-0.49
15.22	KH-IS-16A	2.00	-0.29
15.26	KH-IS.16	2.55	-0.84
15.31	KH-IS-15A	1.87	0.04
15.35	KH-IS.15	2.05	-0.71
15.39	KH-IS-14A	2.31	-0.39
15.43	KH-IS.14	2.15	-0.37
15.47	KH-IS-13A	1.97	-0.31
15.52	KH-IS.13	1.24	-1.02
15.56	KH-IS-12A	1.95	-0.58
15.60	KH-IS.12	1.94	-0.64
15.64	KH-IS-11A	2.02	-0.68
15.68	KH-IS.11	1.5	-0.36
15.73	KH-IS-10A	1.73	-0.50
15.77	KH-IS.10	1.82	-0.48
15.81	KH-IS-9A	1.76	-0.63
15.85	KH-IS.9	1.58	-0.5
15.89	KH-IS-8A	1.65	-0.10
15.94	KH-IS.8	1.7	-0.16
15.98	KH-IS-7A	1.82	-0.03
16.02	KH-IS.7	1.74	-0.04
16.06	KH-IS-6A	1.95	0.62
16.11	KH-IS.6	1.85	-0.5
16.15	KH-IS-5A	1.77	0.17
16.19	KH-IS.5	1.49	-0.65
16.23	KH-IS-4A	1.99	0.27
16.27	KH-IS.4	2.04	0.17
16.32	KH-IS-3A	1.88	0.36
16.36	KH-IS.3	1.62	-0.15
16.40	KH-IS-2A	2.04	-0.11
16.42	KH-IS.2	1.28	-0.74
16.45	KH-IS-1A	1.78	-0.29
16.47	KH-IS.1	2.23	-0.61
16.49	KH-IS-67A	0.77	0.05

Kalavasos

Age Ma	Sample	$\delta^{13}C$ ‰ PDB	$\delta^{18}O$ ‰ PDB
16.40	KV-IS.6	1.63	0.06
16.44	KV-IS.7	1.72	-0.17
16.48	KV-IS.8	1.8	-0.02
16.52	KV-IS.9	1.41	-0.78
16.56	KV-IS-9A	2.01	0.31
16.60	KV-IS.10	1.81	-0.105
16.65	KV-IS-10A	1.89	-0.06
16.69	KV-IS.11	1.52	-0.02
16.73	KV-IS-11A	1.79	-0.32
16.77	KV-IS.12	1.95	-0.02
16.81	KV-IS-12A	1.53	-0.18
16.85	KV-IS.13	1.5	0.24
16.89	KV-IS-13A	1.53	0.39
16.93	KV-IS.14	1.68	-0.14
16.97	KV-IS-14A	1.59	-0.02
17.01	KV-IS.15	1.57	0.07
17.05	KV-IS-ISA	1.36	0.18
17.10	KV-IS.16	1.37	0.18
17.14	KV-IS-16A	1.69	-0.36
17.18	KV-IS.17	1.73	-0.28
17.22	KV-IS-17A	1.37	0.44
17.26	KV-IS.18	0.96	0.01
17.30	KV-IS-18A	1.70	0.03
17.34	KV-IS.19	1.09	-0.18
17.38	KV-IS-19A	1.35	0.01
17.42	KV-IS.20	0.84	-0.8
17.46	KV-IS.20A	1.36	-0.34
17.49	KV-IS.21	1.55	-0.22
17.53	KV-IS-21A	0.96	0.07
17.57	KV-IS.22	0.87	-0.8
17.61	KV-IS-22A	1.46	-0.22
17.65	KV-IS.23	0.82	-0.4
17.69	KV-IS-23A	1.31	0.09
17.73	KV-IS.24	1.21	-0.93
17.77	KV-IS-24A	1.64	0.38
17.81	KV-IS.25	1.1	-0.6
17.84	KV-IS-25A	1.17	0.00
17.88	KV-IS.26	0.92	0.14
17.92	KV-IS-26A	1.28	-0.11
17.96	KV-IS.27	0.6	-0.34
18.00	KV-IS-27A	1.19	0.00
18.04	KV-IS.28	1.04	0.44
18.08	KV-IS-28A	1.08	0.27
18.12	KV-IS.29	0.77	-0.61
18.16	KV-IS-29A	1.28	0.20
18.19	KV-IS.30	0.55	-0.43
18.23	KV-IS-30A	1.05	0.25
18.27	KV-IS.31	0.52	-0.42
18.31	KV-IS-31A	0.86	0.02
18.35	KV-IS.32	0.77	-0.23
18.39	KV-IS-32A	0.63	0.04
18.43	KV-IS.33	1.09	1
18.47	KV-IS-33A	0.80	-0.06
18.51	KV-IS.34	0.95	0.82
18.54	KV-IS-34A	0.55	0.21
18.58	KV-IS.35	1.11	1.25
18.62	KV-IS-35A	1.19	0.19
18.66	KV-IS.36	1.23	0.8
18.70	KV-IS-36A	0.94	-0.28
18.78	KV-IS.37	1.6	1.53
18.87	KV-IS-37A	0.99	0.23
18.95	KV-IS.38	1.64	1.12
19.03	KV-IS-38A	1.12	0.21
19.12	KV-IS.39	1.42	0.74

16.52	KH-IS.67	0.95	-0.11
16.54	KH-IS-68A	1.16	0.46
16.57	KH-IS.68	1.57	-0.87
16.59	KH-IS-69A	1.55	-0.36
16.61	KH-IS.69	0.99	-0.99
16.64	KH-IS-70A	0.74	0.20
16.66	KH-IS.70	2.03	-0.94
16.68	KH-IS-71A	1.68	-0.48
16.71	KH-IS.71	1.41	-0.75
16.73	KH-IS-72A	1.27	-0.07
16.76	KH-IS.72	1.36	-1.22
16.78	KH-IS-73A	1.93	0.13
16.80	KH-IS.73	1.16	-0.7
16.83	KH-IS-74A	1.67	0.06
16.85	KH-IS.74	0.78	-0.42
16.87	KH-IS-75A	0.76	-0.33
16.90	KH-IS.75	0.75	-0.63
16.92	KH-IS-76A	1.34	-0.50
16.94	KH-IS.76	0.67	-0.48
16.97	KH-IS-77A	0.95	-0.18
16.99	KH-IS.77	0.48	-0.58
17.02	KH-IS-78A	1.02	-0.35
17.04	KH-IS.78	0.78	-0.41
17.06	KH-IS-79A	1.48	-0.58
17.09	KH-IS.79	1.06	-0.32
17.11	KH-IS-80A	1.50	-0.51
17.13	KH-IS.80	1.08	-0.56
17.16	KH-IS-81A	0.82	0.42
17.18	KH-IS.81	1.12	-0.15
17.21	KH-IS-82A	0.85	0.08
17.23	KH-IS.82	0.72	-0.32
17.25	KH-IS-83A	1.11	-0.02
17.28	KH-IS.83	0.67	-0.29
17.30	KH-IS-84A	1.06	-0.22
17.37	KH-IS.84	0.69	-0.32
17.43	KH-IS-85A	0.85	-0.33
17.50	KH-IS.85	0.88	0
17.57	KH-IS.86	0.65	-0.45
17.63	KH-IS.87	0.61	0.01
17.70	KH-IS.88	0.87	0.25
17.76	KH-IS-89	0.87	0.39
17.83	KH-IS-90	1.28	-0.67
17.90	KH-IS-91	0.78	-0.49
17.96	KH-IS-92	1.00	0.46
18.03	KH-IS-93	1.31	0.13
18.10	KH-IS-94	0.94	-0.22
18.16	KH-IS-95	1.70	-0.30
18.23	KH-IS-96	0.85	0.57
18.29	KH-IS-97	0.62	0.73
18.36	KH-IS-98	1.20	0.55
18.43	KH-IS-99	1.00	0.88
18.49	KH-IS-100	1.08	0.10
18.56	KH-IS-101	0.66	0.30
18.63	KH-IS-102	0.78	0.59
18.69	KH-IS-103	0.84	0.26
18.70	KH-IS-104	1.27	0.89
18.83	KH-IS-105	0.84	0.80
18.95	KH-IS-106	0.93	0.81
19.08	KH-IS-107	1.04	1.00
19.20	KH-IS-108	0.87	0.84
19.30	KH-IS-109	0.70	0.45
19.40	KH-IS-110	0.89	0.48
19.50	KH-IS-111	0.72	0.33
19.58	KH-IS-112	1.17	0.58
19.66	KH-IS-113	1.02	1.08
19.74	KH-IS-114	1.16	0.66
19.82	KH-IS-115	1.02	0.25
19.20	KV-IS-39A	1.09	-0.12
19.49	KV-IS.40	1.35	1
19.54	KV-IS-40A	1.12	0.44
19.60	KV-IS.41	1.14	0.05
19.65	KV-IS.42	0.99	0.12
19.71	KV-IS.43	1.5	0.82
19.76	KV-IS.44	1.36	0.87
19.82	KV-IS.45	0.99	-0.5
19.87	KV-IS.46	1.41	-0.07
19.92	KV-IS.47	1.77	0.4
19.98	KV-IS.48	1.29	-0.08
20.03	KV-IS.49	1.7	0.51
20.09	KV-IS.50	1.4	-0.36
20.14	KV-IS.51	1.21	-0.33
20.19	KV-IS.52	1.38	-0.2
20.25	KV-IS.53	1.27	-0.19

Raw stable isotope data for couplets

LST Couplet. Beds No. 130 + 131 (Kottaphi Hill)

Sample	$\delta^{13}C$ ‰ PDB	$\delta^{18}O$ ‰ PDB
KHC-10	2.15	-0.61
KHC-9	2.09	-0.43
KHC-8	2.26	-0.21
KHC-7	1.95	-0.09
KHC-6	1.57	-0.04
KHC-5	2.02	-0.33
KHC-4	1.77	-0.97
KHC-3	1.94	-0.35
KHC-2	1.75	-0.52
KHC-1	2.00	-0.33

HST Couplet. Beds No. 157 + 158 (Kottaphi Hill)

Sample	$\delta^{13}C$ ‰ PDB	$\delta^{18}O$ ‰ PDB
KHC-F	2.07	0.11
KHC-E	2.01	0.10
KHC-D	2.32	-0.01
KHC-C	1.78	0.20
KHC-B	2.48	-0.29
KHC-A	2.75	-0.30